



UNIVERSIDAD
DE MÁLAGA

Facultad de Ciencias

Departamento de Química Inorgánica,
Cristalografía y Mineralogía

**Active sulpho-belite cements.
Hydration mechanisms and mechanical
properties.**

Tesis Doctoral
por
Gema Álvarez Pinazo

Málaga, 2015



Publicaciones y
Divulgación Científica

AUTOR: Gema Álvarez Pinazo

 <http://orcid.org/0000-0003-1396-2156>

EDITA: Publicaciones y Divulgación Científica. Universidad de Málaga



Esta obra está sujeta a una licencia Creative Commons:

Reconocimiento - No comercial - SinObraDerivada (cc-by-nc-nd):

[Http://creativecommons.org/licenses/by-nc-nd/3.0/es](http://creativecommons.org/licenses/by-nc-nd/3.0/es)

Cualquier parte de esta obra se puede reproducir sin autorización
pero con el reconocimiento y atribución de los autores.

No se puede hacer uso comercial de la obra y no se puede alterar, transformar o hacer
obras derivadas.

Esta Tesis Doctoral está depositada en el Repositorio Institucional de la Universidad de
Málaga (RIUMA): riuma.uma.es

Active sulpho-belite cements. Hydration mechanisms and mechanical properties

MEMORIA presentada por la Ingeniera Química D^a Gema Álvarez Pinazo para optar al Grado de Doctora en Ciencias, Sección de Químicas, por la Universidad de Málaga.



Fdo.: Gema Álvarez Pinazo

Los Directores,



Fdo.:

Dr. Miguel Ángel García Aranda
Catedrático de la Universidad



Fdo.:

Dra. M^a Ángeles Gómez de la Torre
Profesora Titular de Universidad



Fdo.:

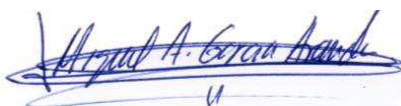
Dra. María Isabel Santacruz Cruz
Investigadora Ramón y Cajal

Dr. MIGUEL ÁNGEL GARCÍA ARANDA, Catedrático de la Universidad de Málaga, Dra. M^a ÁNGELES GÓMEZ DE LA TORRE, Profesora Titular de la Universidad de Málaga, y Dra. M^a ISABEL SANTACRUZ CRUZ, Investigadora Ramón y Cajal de la Universidad de Málaga, todos pertenecientes al Departamento de Química Inorgánica, Cristalografía y Mineralogía de la Facultad de Ciencias de la Universidad de Málaga,

CERTIFICAN:

Que la presente memoria realizada por D^a Gema Álvarez Pinazo, titulada: "ACTIVE SULPHO-BELITE CEMENTS. HYDRATION MECHANISMS AND MECHANICAL PROPERTIES", ha sido realizada bajo nuestra dirección en el Departamento de Química Inorgánica, Cristalografía y Mineralogía de la Facultad de Ciencias de la Universidad de Málaga. Este trabajo reúne, a nuestro juicio, contenido científico suficiente y las condiciones necesarias para ser presentado y defendido ante el tribunal correspondiente para optar al Grado de Doctora.

Málaga a 1 de Junio de 2015



Fdo.:

Dr. Miguel Ángel García Aranda
Catedrático de la Universidad



Fdo.:

Dra. M^a Ángeles Gómez de la Torre
Profesora Titular de Universidad



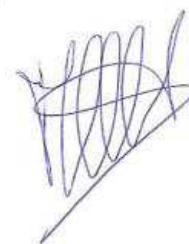
Fdo.:

Dra. María Isabel Santacruz Cruz
Investigadora Ramón y Cajal

Dr. PEDRO JESÚS MAIRELES TORRES, Catedrático de la Universidad de Málaga y Director del Departamento de Química Inorgánica, Cristalografía y Mineralogía de la Facultad de Ciencias de la misma universidad.

INFORMA:

Que la presente memoria realizada por D^a Gema Álvarez Pinazo, titulada: "ACTIVE SULPHO-BELITE CEMENTS. HYDRATION MECHANISMS AND MECHANICAL PROPERTIES", ha sido realizada bajo la dirección del Catedrático Miguel Ángel García Aranda, la Profesora Titular D^a M^a Ángeles Gómez De la Torre y la Investigadora Ramón y Cajal D^a. M^a Isabel Santacruz Cruz en el Departamento de Química Inorgánica, Cristalografía y Mineralogía de la Facultad de Ciencias de la Universidad de Málaga. Este trabajo constituye la Memoria de Tesis Doctoral de la interesada, cuya presentación autorizo en Málaga a 1 de Junio de 2015.



Fdo.: Dr. Pedro Jesús Maireles Torres.

ACKNOWLEDGEMENTS

My first thoughts are naturally given to the Department of Inorganic Chemistry, Crystallography and Mineralogy of University of Málaga to give me the opportunity to perform this Thesis, under the direction of Prof. Miguel Angel García Aranda, Dr. María de los Ángeles Gómez de la Torre, and Dr. María Isabel Santacruz Cruz. This memory is the result of efforts of many people who directly or indirectly have participated providing knowledge, giving their opinion, correcting and encouraging me, both in times of success and times of difficulty.

Firstly, I would like to thank my PhD supervisors. I express my sincere gratitude for their assistance, suggestions, support, and friendly counselling in both research and life. Thanks for the time spent on my learning and transmit me their knowledge and values. Without all of that this memory would not have been possible.

I also thank all the members of the Department of Inorganic Chemistry, Crystallography and Mineralogy. Countless memories accumulated during the last years are made by pieces of unforgettable experience with countless people; even every person that I crossed in my way has already earned his place in my esteem.

Institute of Material Science of Madrid (ICMM-CSIC), especially Dr. Jesús Sanz Lázaro and Dr. Isabel Sobrados de la Plaza, and the two technicians of the NMR laboratory, Dr. Virginia Díez and Verónica López. Thanks for your hospitality and help during my stay.

"Cementos Financiera y Minera (FYM)" cements factory, from Italcementi Group, in Málaga, is thanked.

My special appreciation to my parents, my siblings and, in particular, to my husband for their love and support during my studies.

Finally, I would like to acknowledge the financial contribution supported by Spanish MINECO through MAT2010-16213 research grant, which is co-funded by FEDER, and Junta de Andalucía through P11-FQM-07517.

AGRADECIMIENTOS

Llegado este momento, es para mí un placer poder utilizar este espacio para ser justa y consecuente con todas aquellas personas e instituciones que han facilitado y ayudado a que este trabajo llegue a su fin.

Quiero empezar agradeciendo al Departamento de Química Inorgánica, Cristalografía y Mineralogía de la Universidad de Málaga, por haberme dado la oportunidad de realizar esta tesis doctoral bajo la dirección del Dr. Miguel Ángel García Aranda, la Dra. María de los Ángeles Gómez De la Torre, y la Dra. María Isabel Santacruz Cruz. Destacar y agradecer también la aportación económica recibida mediante la ayuda FPI del Ministerio de Economía y Competitividad (MINECO) y fondos FEDER a través del proyecto MAT2010-16213.

Debo agradecer de una manera muy especial y sincera a mis directores de tesis: el Dr. Miguel Ángel García Aranda, la Dra. María de los Ángeles Gómez De la Torre y la Dra. María Isabel Santacruz Cruz, por aceptarme para realizar esta tesis doctoral bajo su dirección. Gracias por todo vuestro apoyo y confianza en mi trabajo, por el tiempo dedicado en mi aprendizaje y por transmitirme vuestros conocimientos y valores.

Vayan también mis más sinceros agradecimientos para todo el personal del Departamento de Química Inorgánica, Cristalografía y Mineralogía: profesores, doctorandos, posdocs, personal administrativo y estudiantes que pasaron para hacer sus proyectos de fin de grado, Erasmus,.... A pesar de haber tenido un excelente trato con todos, me gustaría resaltar mis agradecimientos para algunas personas. A Enrique Ramírez Losilla, porque nuestros "piques" (de carácter científico o personal) siempre se vieron compensados por tu atención y cariño. A Pascual y Toñi, porque vuestra compañía hizo más grata y llevadera mi estancia en la "4ª planta". Gracias por ser tan bellas personas. A Aurelio Cabeza, por su paciencia, disponibilidad y generosidad para compartir sus conocimientos siempre que se le ha necesitado. A Antonio Jiménez Morales, para el que guardo un enorme cariño, aunque no siempre se lo haya demostrado. Gracias porque, a pesar de todo, siempre has estado dispuesto a ayudarme.

A la Dra. Laura León Reina, es admirable tu capacidad de trabajo y entrega con todos los que hemos necesitado de ti. Gracias por hacer la DRX más

fácil. Sólo puedo expresarte mi gran admiración por ser tan increíble, no sólo en el terreno profesional, sino también como persona.

Agradezco también de manera especial al Dr. Jesús Sanz Lázaro y la Dra. Isabel Sobrados de la Plaza por su generosidad y disponibilidad durante mi estancia en el ICMM de Madrid. Gracias por todos los conocimientos transmitidos y la cercanía mostrada en todo momento. Muchas gracias también a las "chicas" del laboratorio, Virginia y Verónica, por vuestra acogida y ayuda en todo momento.

Al personal de la fábrica de Cementos Financiera y Minera, Italcementi Group, de Málaga, por recibirme siempre con tanta amabilidad.

Para mis compañer@s de la "sala de becarios" solo tengo palabras de agradecimiento. Echando la vista atrás, ha sido un largo y duro camino durante el cual he podido compartir grandes momentos. Algunos ya no estáis presentes en el departamento pero, me gustaría teneros aquí presentes para daros las gracias por vuestra amistad y todas los momentos vividos juntos (a M^a Carmen, Antonio, Rosario, "Compañía" y sobre todo a mi "Pollo"). También quiero agradecer a Jose porque siempre ha sido un compañero generoso y dispuesto como pocos. A Marta por ser compañera de batallas y por ayudarme y apoyarme en todo este tiempo, gracias por los momentos vividos y los que nos quedan por vivir. A Ana por su capacidad de trabajo y sus ganas de aprender. A Cristina por su enorme calidad personal, gracias por estar siempre ahí, en los buenos y malos momentos, no me olvido de esos mojitos pendientes... A Lucía porque para mí es una chica 10, trabajadora, servicial, buena compañera, siempre con una sonrisa y además buena cocinera... gracias por ponerle "sabor a nuestro departamento". Y al resto de compañeros, Montse, Diana, Mercedes, M^a José y el todos los compañeros de catálisis, gracias por haber formado parte de esta etapa de mi vida. Sin vosotros esto no hubiese sido igual.

A mi familia, a los que debo todo lo que soy, le expreso mi agradecimiento más profundo y sentido. A mis padres, Juanita y José, por ser un ejemplo a seguir en la vida. Gracias por haberme enseñado lo que es una familia. A mi hermana por tantos momentos vividos juntas y los que nos quedan, gracias por estar siempre ahí. A mi hermano por demostrarme que las personas con ilusión son las que marcan la diferencia y que muchas veces "todo parece imposible hasta que se hace". Gracias a todos por haber creído en mi, por vuestro apoyo y cariño.

Por último, pero no por ello menos importante, quiero agradecer a Raúl y a mis hijos, por ser mi mayor apoyo durante todo este tiempo. Raúl, muchas gracias por tu amor, comprensión, paciencia y fortaleza que han permitido que pudiese, no sólo trabajar, sino también llegar a buen puerto. Como en todo lo que escribo, estás presente en mi mente y en el alma de estas líneas. Quiero agradecer a mis hijos, Juan José y Paula, porque tuvieron que soportar largas horas (incluso días) sin la compañía de su mamá, sin poder entender, a su corta edad, el porqué. Gracias porque vuestras sonrisas me llenaban de ánimo y fuerzas para seguir adelante y porque vuestra existencia da todo el sentido a mi vida.

A mis padres

A mis hermanos

A Raúl

A mis hijos

INDEX

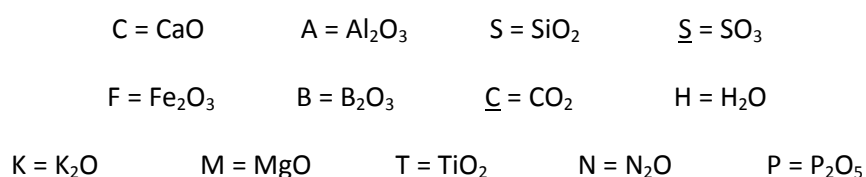
Acknowledgments	i
Agradecimientos	iii
Index	ix
Notations	xiii
Chemical Reactions	xvii
List of Tables	xix
List of Figures	xxi
ABSTRACT	3
RESUMEN	15
CHAPTER 1: INTRODUCTION	29
1.1. CLIMATE CHANGE. INDUSTRIAL CO ₂ EMISSIONS.	29
1.2. BELITE CEMENTS.	31
1.3. YE'ELIMITE -CONTAINING CEMENTS.	31
1.3.1. Classification.	32
1.3.2. Commercial ye'elimite -containing cements.	33
1.4. BELITE CALCIUM SULFOALUMINATE CEMENTS (BCSA).	35
1.4.1. Reduction of CO ₂ emissions.	36
1.4.2. Crystallochemistry of main anhydrous phases of BCSA cements.	38
1.4.3. Reactivity of principal constituents of BCSAF cements during hydration.	43
1.4.4. Crystallochemistry of main hydrated phases of BCSAF cements.	48
1.4.5. Properties of BCSA mortars and concretes. Durability.	52
1.4.5.1. Sulphate Resistance.	52
1.4.5.2. Corrosion Resistance.	52
1.4.5.3. Compressive Strength.	53
1.4.5.4. Dimensional Stability.	54

1.5. METHODOLOGY.	54
1.5.1. Cement (anhydrous and paste) characterisation.	54
1.5.1.1. LRPD and Rietveld method.	54
1.5.1.2. SXRPD (BL04 – MSPD, ALBA).	59
1.5.1.3. SEM.	59
1.5.1.4. Solid-state NMR spectroscopy.	60
1.5.1.5. Thermal measurements.	60
1.5.1.6. Isothermal conduction calorimetry.	61
1.5.1.7. MIP.	61
1.5.1.8. Rheological behaviour.	62
1.5.2. Mortars characterisation.	63
1.5.2.1. Compressive strength.	63
1.5.2.2. Shrinkage/Expansion properties (Length Changes).	64
1.5.2.3. Setting.	64
CHAPTER 2: OBJECTIVES	69
CHAPTER 3: ARTICLES SECTION	73
A#1. Rietveld quantitative phase analysis of Ye'elimite-containing cements.	75
A#2. In-situ early-age hydration study of sulfobelite cements by synchrotron powder diffraction.	89
A#3. Hydration reactions and mechanical strength developments of iron-rich sulfobelite eco-cements.	103
A#4. Rietveld quantitative phase analysis with molybdenum radiation.	125
A#5. Hydration of iron-rich BCSA cements with different calcium sulfate sources.	139
CHAPTER 4: RESULTS AND DISCUSSION	171
4.1. SYNTHESIS OF LABORATORY-PREPARED BCSAF CLINKERS: SCALE-UP.	173
4.1.1. Raw materials characterisation.	173
4.1.2. BCSAF clinkers preparation: optimisation of process.	174

4.1.3. Characterisation of the scaled-up BCSAF clinkers.	177
4.1.3.1. RQPA (normalized to 100% of crystalline phases).	177
4.1.3.2. Selective dissolutions.	178
4.1.3.3. SEM-EDS characterisation.	181
4.2. PHASE ANALYSIS OF YE'ELIMITE-CONTAINING CLINKERS AND CEMENTS.	182
4.2.1. RQPA (normalized to 100% of crystalline phases).	183
4.2.2. ACn content determination.	185
4.3. HYDRATION STUDY OF BCSAF CEMENTS.	186
4.3.1. Hydration of BCSAF cements with gypsum as setting regulator.	187
4.3.1.1. <i>In-situ</i> early hydration behaviour (< 24 h).	188
4.3.1.2. <i>Ex-situ</i> hydration behaviour at late ages (> 24 h), with different amounts of gypsum.	190
4.3.1.3. Elemental composition of ACn.	194
4.3.1.4. A comparative study of MoK α_1 and synchrotron radiations for selected samples.	201
4.3.2. Hydration of BCSAF cements with different calcium sulphate source.	204
4.3.2.1. Early hydration behaviour (< 24 h).	204
4.3.2.2. Hydration with different sulphate sources at later ages (> 24 h).	209
4.4. MECHANICAL PROPERTIES OF BCSAF MORTARS.	217
CHAPTER 5: CONCLUSIONS	227
CHAPTER 5: CONCLUSIONES (<i>In Spanish</i>)	233
CHAPTER 6: REFERENCES	239
ANNEX A: LICENSES AGREEMENTS	263
ANNEX B: OTHER PUBLICATIONS	269

NOTATIONS

A simplified notation is used when describing cement compounds or chemical formulations. The cement shorthand notation is found below:



This leads to the following abbreviations for anhydrous and hydrates phases:

Formula	Oxides	Cement nomenclature	Name
$\text{Ca}_2\text{Mg}(\text{Si}_2\text{O}_7)$	$2\text{CaO} \cdot \text{MgO} \cdot 2\text{SiO}_2$	C_2MS_2	Akermanite
Ca_3SiO_5	$3\text{CaO} \cdot \text{SiO}_2$	C_3S	Alite
$2\text{Al}(\text{OH})_3 \cdot n\text{H}_2\text{O}$	$\text{Al}_2\text{O}_3 \cdot (3+n)\text{H}_2\text{O}$	$\text{AH}_3 \cdot n\text{H}$	Amorphous aluminium hydroxide
CaSO_4	$\text{CaO} \cdot \text{SO}_3$	$\underline{\text{CS}}$	Anhydrite
$\text{CaSO}_4 \cdot 0.5\text{H}_2\text{O}$	$\text{CaO} \cdot \text{SO}_3 \cdot 0.5\text{H}_2\text{O}$	$\underline{\text{CS}}\text{H}_{0.5}$	Bassanite
Ca_2SiO_4	$2\text{CaO} \cdot \text{SiO}_2$	C_2S	Belite
CaCO_3	$\text{CaO} \cdot \text{CO}_2$	$\underline{\text{CC}}$	Calcite or vaterite
CaAl_2O_4	$\text{CaO} \cdot \text{Al}_2\text{O}_3$	CA	Calcium aluminate
$\text{Ca}_2\text{Al}(\text{OH})_6[\text{Al}(\text{OH})_4 \cdot 3\text{H}_2\text{O}]$	$2\text{CaO} \cdot \text{Al}_2\text{O}_3 \cdot 8\text{H}_2\text{O}$	C_2AH_8	Dicalcium aluminate hydrate
$\text{CaMg}(\text{CO}_3)_2$	$\text{CaO} \cdot \text{MgO} \cdot 2\text{CO}_2$	$\underline{\text{CMC}}_2$	Dolomite
$\text{Ca}_6\text{Al}_2(\text{OH})_{12}(\text{SO}_4)_3 \cdot 26\text{H}_2\text{O}$	$6\text{CaO} \cdot \text{Al}_2\text{O}_3 \cdot 3\text{SO}_3 \cdot 32\text{H}_2\text{O}$	$\text{C}_6\text{A}\underline{\text{S}}_3\text{H}_{32}$	Ettringite (AFt)
$\text{Ca}_4\text{Al}_2\text{Fe}_2\text{O}_{10}$	$4\text{CaO} \cdot \text{Al}_2\text{O}_3 \cdot \text{Fe}_2\text{O}_3$	C_4AF	Ferrite

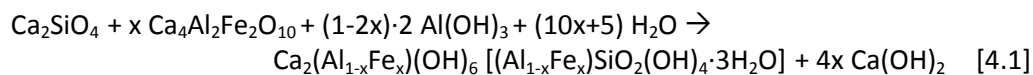
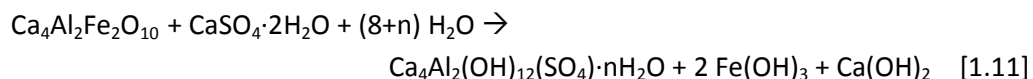
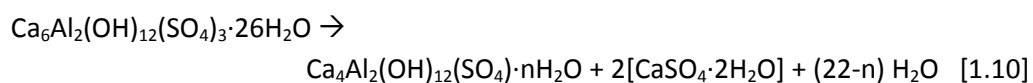
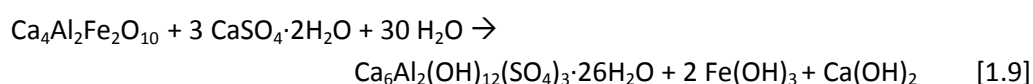
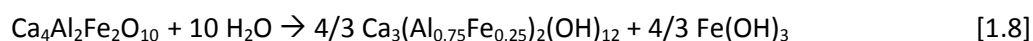
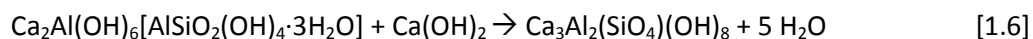
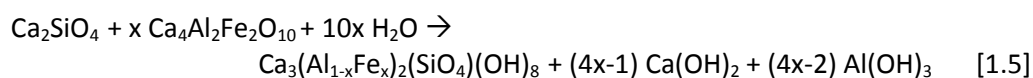
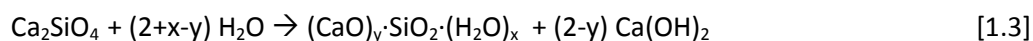
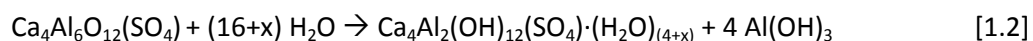
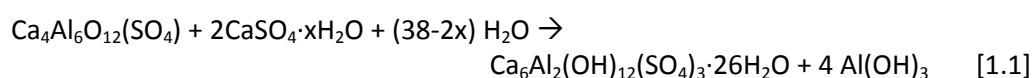
Formula	Oxides	Cement nomenclature	Name
$\text{Ca}_3\text{Al}_2(\text{SiO}_4)_3$	$3\text{CaO}\cdot\text{Al}_2\text{O}_3\cdot 3\text{SiO}_2$	C₃AS₃	Garnet
$\text{Ca}_2\text{Al}_2\text{SiO}_7$	$2\text{CaO}\cdot\text{Al}_2\text{O}_3\cdot\text{SiO}_2$	C₂AS	Gehlenite
$2\text{Al}(\text{OH})_3$	$\text{Al}_2\text{O}_3\cdot 3\text{H}_2\text{O}$	AH₃	Gibbsite
$\text{CaSO}_4\cdot 2\text{H}_2\text{O}$	$\text{CaO}\cdot\text{SO}_3\cdot 2\text{H}_2\text{O}$	CSH₂	Gypsum
$(\text{Ca}_4\text{Al}_2(\text{OH})_{12})[\text{OH}(\text{CO}_3)_{0.5}(\text{H}_2\text{O})_4]$	$4\text{CaO}\cdot\text{Al}_2\text{O}_3\cdot 10.5\text{H}_2\text{O}\cdot 0.5\text{CO}_2$	C₄AH_{10.5}C_{0.5}	Hemicarboaluminat
$\text{Ca}_3\text{Al}_2(\text{OH})_{12}$	$3\text{CaO}\cdot\text{Al}_2\text{O}_3\cdot 6\text{H}_2\text{O}$	C₃AH₆	Hidrogarnet or katoite
$\text{Ca}_3(\text{Al}_{0.5}\text{Fe}_{0.5})_2(\text{SiO}_4)(\text{OH})_8$	$3\text{CaO}\cdot 0.5\text{Al}_2\text{O}_3\cdot 0.5\text{Fe}_2\text{O}_3\cdot\text{SiO}_2\cdot 4\text{H}_2\text{O}$	C₃A_{0.5}F_{0.5}SH₄	Iron-hidrogarnet
$2\text{Fe}(\text{OH})_3$	$\text{Fe}_2\text{O}_3\cdot 3\text{H}_2\text{O}$	FH₃	Iron hydroxide
$\text{Ca}_{12}\text{Al}_{14}\text{O}_{33}$	$12\text{CaO}\cdot 7\text{Al}_2\text{O}_3$	C₁₂A₇	Mayenite
$\text{Ca}_3\text{Mg}(\text{SiO}_4)_2$	$3\text{CaO}\cdot\text{MgO}\cdot 2\text{SiO}_2$	C₃MS₂	Merwinite
$\text{Ca}_4\text{Al}_2(\text{OH})_{12}(\text{SO}_4)\cdot 6\text{H}_2\text{O}$	$4\text{CaO}\cdot\text{Al}_2\text{O}_3\cdot\text{SO}_3\cdot 12\text{H}_2\text{O}$	C₄ASH₁₂	Monosulphate (AFm)
CaTiO_3	$\text{CaO}\cdot\text{TiO}_2$	CT	Perovskite
$\text{Ca}(\text{OH})_2$	$\text{CaO}\cdot\text{H}_2\text{O}$	CH	Portlandite
$\text{Ca}_2\text{Al}(\text{OH})_6[\text{AlSiO}_2(\text{OH})_4\cdot 3\text{H}_2\text{O}]$	$2\text{CaO}\cdot\text{Al}_2\text{O}_3\cdot\text{SiO}_2\cdot 8\text{H}_2\text{O}$	C₂ASH₈	Stratlingite
$\text{Ca}_5(\text{SiO}_4)_2(\text{SO}_4)$	$5\text{CaO}\cdot 2\text{SiO}_2\cdot\text{SO}_3$	C₅S₂S	Ternesite
$\text{Ca}_3\text{Al}_2\text{O}_6$	$3\text{CaO}\cdot\text{Al}_2\text{O}_3$	C₃A	Tricalcium aluminat

Abbreviated names or initials have also been used to refer to some terms:

- A#x: Article number x.
- aBCSA: active Belite Calcium Sulpho-Aluminat.
- ACn: Amorphous and Crystalline non-quantified.
- ACSA: Alite Calcium Sulpho-Aluminat.
- BACSA: Belite Alite Calcium Sulpho-Aluminat.
- BCSA: Belite Calcium Sulpho-Aluminat.

- BCSAA: Aluminum-rich Belite Calcium Sulpho-Aluminate.
- BCSAF: Iron-rich Belite Calcium Sulpho-Aluminate.
- CSA: Calcium Sulpho-Aluminate.
- DIBt: Deutsches Institut für Bautechnik.
- DTA: Differential Thermal Analysis.
- EDS: Energy Dispersive X-ray Spectroscopy.
- ETA: European Technical Approval.
- FW: Free Water.
- FWHM: Full-width at the half-maximum.
- GHGs: Greenhouse gases.
- ICSD: Inorganic Crystal Structure Database.
- Lol: Loss of Ignition.
- LXRPD: Laboratory X-Ray Powder Diffraction.
- MIP: Mercury Intrusion Porosimetry.
- MSPD: Materials Science and Powder Diffraction.
- NMR: Nuclear Magnetic Resonance.
- OPC: Ordinary Portland Cement.
- PTFE: Polytetrafluoroethylene.
- RMCO₂: Raw material CO₂.
- RQPA: Rietveld Quantitative Phase Analysis.
- SCMs: Supplementary Cementitious Materials.
- SEM: Scanning Electron Microscopy.
- SRM: Standard Reference Material.
- SXRPD: Synchrotron X-ray Powder Diffraction.
- TGA: Thermogravimetric Analysis.
- w/c: water to cement ratio.
- XRF: X-Ray Fluorescence.
- XRPD: X-Ray Powder Diffraction.

CHEMICAL REACTIONS



LIST OF TABLES

Coding of Tables: **Table X.Y.** means the Yst Table mentioned in Chapter X.

Table 1.1. Lime content for different cement phases	35
Table 1.2. Crystallographic data of dicalcium silicate polymorphs	39
Table 1.3. Crystallographic data of Klein's salt polymorphs	41
Table 1.4. Crystallographic data of ferrite phase polymorphs ($\text{Ca}_2\text{Al}_x\text{Fe}_{2-x}\text{O}_5$)	43
Table 4.1. Elemental composition of raw materials determined by XRF and expressed as oxide wt%	173
Table 4.2. Raw materials dosages in wt% and elemental composition of raw mixtures except for water or CO_2 (expressed as oxide in wt%)	174
Table 4.3. Direct RQPA for BCSAF_BO clinker prepared following different clinkering cycles	176
Table 4.4. Direct RQPA results (wt%) for the two BCSAF clinkers normalised to 100% of crystalline phases. Numbers between brackets are the standard deviations of three independent measurements. Rietveld disagreement factors are also given	177
Table 4.5. Direct RQPA results (wt%) for the aluminate and silicate residues of two BCSAF clinkers normalised to 100% of crystalline phases. Rietveld disagreement factors are also given	180
Table 4.6. Direct RQPA results (wt%) for the ye'elimite-containing cements normalized to 100% of crystalline phases. Numbers between brackets are the standard deviations of three independent measurements	183
Table 4.7. Direct Rietveld quantitative phase analysis results (wt%) for G10B2 sample as a function of hydration time. Numbers between brackets are mathematical errors from Rietveld calculations	205
Table 4.8. Direct Rietveld quantitative phase analysis results (wt%) for A10B2 sample as a function of hydration time. Numbers between brackets are mathematical errors from Rietveld calculations	206
Table 4.9. Direct Rietveld quantitative phase analysis results (wt%) for B10B2 sample as a function of hydration time. Numbers between brackets are mathematical errors from Rietveld calculations	206

Table 4.10. RQPA results for G10B0 cement paste, as a function of hydration time, including ACn content calculated with G-method and free water content. Numbers between brackets are mathematical errors from Rietveld calculations 211

Table 4.11. RQPA results for G10B2 cement paste, as a function of hydration time, including ACn content calculated with G-method and free water content. Numbers between brackets are mathematical errors from Rietveld calculations 212

Table 4.12. RQPA results for A10B0 cement paste, as a function of hydration time, including ACn content calculated with G-method and free water content. Numbers between brackets are mathematical errors from Rietveld calculations 212

Table 4.13. RQPA results for A10B2 cement paste, as a function of hydration time, including ACn content calculated with G-method and free water content. Numbers between brackets are mathematical errors from Rietveld calculations 213

Table 4.14. RQPA results for B10B0 cement paste, as a function of hydration time, including ACn content calculated with G-method and free water content. Numbers between brackets are mathematical errors from Rietveld calculations 213

Table 4.15. RQPA results for B10B2 cement paste, as a function of hydration time, including ACn content calculated with G-method and free water content. Numbers between brackets are mathematical errors from Rietveld calculations 214

Table 4.16. Initial and final setting times of different G-mortars 219

LIST OF FIGURES

Coding of Figures: **Figure X.Y.** means the Yst Figure mentioned in Chapter X.

Figure 1.1.	<i>World cement production evolution (million tonnes) by region</i>	<i>30</i>
Figure 1.2.	<i>Comparison of OPC and BCSAF production CO₂ footprint</i>	<i>37</i>
Figure 1.3.	<i>Dicalcium silicate polymorphic transformations with temperature</i>	<i>38</i>
Figure 1.4.	<i>Range from 29 to 35° (2θ) of the theoretical diffractograms. (a) α-C₂S at RT; (b) α'_F-C₂S at RT; (c) β-C₂S at RT and (d) γ-C₂S at RT</i>	<i>40</i>
Figure 1.5.	<i>Region 15° to 35° (2θ) of the theoretical diffractograms, (a) stoichiometric (orthorhombic) C₄A₃S; (b) doped (pseudo-cubic) C₄A₃S</i>	<i>42</i>
Figure 1.6.	<i>Cryo-SEM photographs of BCSAF cement pastes after 4 h of hydration for (a) 20 wt % of gypsum and (b) 5 wt % of gypsum</i>	<i>45</i>
Figure 1.7.	<i>Hexagonal ettringite unit cell of the revised structure projected down c</i>	<i>48</i>
Figure 1.8.	<i>Layered crystal structure of stratlingite</i>	<i>50</i>
Figure 1.9.	<i>Octahedral and tetrahedral connections of hydrogarnet structure</i>	<i>51</i>
Figure 1.10.	<i>Nomenclature of minerals of the hydrogarnet group Ca₃(Al_xFe_{1-x})₂(SiO₄)_y(OH)_{4(3-y)}</i>	<i>51</i>
Figure 1.11.	<i>Schematic phase diagram of ternary system representing BCSA cement; slow, normal and rapid refer to hardening rates</i>	<i>53</i>
Figure 1.12.	<i>Examples of a) flow curve and b) viscosity curve of CSA cement paste (A25CSA; w/c=0.5)</i>	<i>63</i>
Figure 4.1.	<i>(a) BCSAF raw mixture pellet; (b) Pt/Rh crucible use for clinkering</i>	<i>175</i>
Figure 4.2.	<i>Selected region of patterns of BCSAF_B0 clinker after heating at (a) 1300°C for 15 min, (b) 1325°C for 30 min, and (c) 1350°C for 30 min; and ● highlights free lime (CaO)</i>	<i>176</i>
Figure 4.3.	<i>Selected range of Rietveld plots for (a) BCSAF_B0, and (b) BCSAF_B2 clinkers. Peaks due to a given phase are labelled</i>	<i>178</i>
Figure 4.4.	<i>Selected range of the Rietveld plots for: (a) BCSAF_B0 aluminate residue and (b) BCSAF_B0 silicate residue</i>	<i>179</i>

Figure 4.5. Selected range of the Rietveld plots for: (a) BCSAF_B2 aluminate residue and (b) BCSAF_B2 silicate residue	181
Figure 4.6. SEM micrographs of (a) and (b) anhydrous non-active-BCSAF clinker (BCSAF_B0), and (c) and (d) anhydrous active-BCSAF clinker (BCSAF_B2)	182
Figure 4.7. Cement paste in sealed capillary placed in the sample holder in the XRPD end station of MSPD beamline of ALBA synchrotron	188
Figure 4.8. Selected ranges of SXPDP raw patterns for (a) and (b) G10B0; and (c) and (d) G10B2 cement paste at different ages of hydration ($\lambda = 0.61984 \text{ \AA}$)	189
Figure 4.9. Hydration degree, α (%), for GgB0 and GgB2 pastes as a function of curing time and amount of gypsum added of (a) C_2S ; (b) $C_4A_3\bar{S}$; and (c) C_4AF . Solid lines are just guide to the eyes	191
Figure 4.10. Selected range of Rietveld plots for two pastes, (a) G15B0 and (b) G15B2, cured for 120 days	193
Figure 4.11. Values of the cell parameter (a) for katoite vs values of x (moles of Fe_2O_3 in formula $C_3A_{1-x}F_xSH_4$) for different GgBx pastes. Dotted line stands for theoretical dependence of a as function of x	194
Figure 4.12. Hydration and crystallization rate of sulphate groups for (a) G10B0 and (b) G10B2 pastes. Dashed lines represent the maximum values of dissolved sulphate group	195
Figure 4.13. Hydration and crystallisation rate of silicate groups for (a) G10B0 and (b) G10B2 pastes. Dashed lines represent the maximum values of dissolved silicate group	196
Figure 4.14. ^{29}Si NMR MAS spectra for G10B0 cement, (a) anhydrous, and hydrated at different curing times: (b) 7 days, (c) 28 days, and (d) 180 days	198
Figure 4.15. ^{29}Si NMR MAS spectra for G10B2 cement, (a) anhydrous, and hydrated at different curing times: (b) 7 days, (c) 28 days, and (d) 180 days	200
Figure 4.16. ^{27}Al NMR MAS spectra at 28 days of hydration for (a) G10B0, and (b) G10B2 cement paste	201
Figure 4.17. Irradiated volume for flat sample holder in the transmission mode using (a) Mo radiation and (b) Cu radiation and (c) reflection mode using Cu radiation ..	202
Figure 4.18. Rietveld plots for G10B0 hydrated sample patterns (a) strictly monochromatic $MoK\alpha_1$ radiation in transmission (flat sample), (b) synchrotron radiation in transmission (capillary)	203
Figure 4.19. Degree of reaction $[\alpha]$ of ye'elimite, sulphate source and Aft as a function of time for (a) G10B2, (b) A10B2 and (c) B10B2. Solid lines are just guide to the eyes	207

Figure 4.20. Normalised direct RQPA results and the calorimetric heat flow curve (dashed line) for (a) G10B2, (b) A10B2 and (c) B10B2. Solid lines are just guide to the eyes	208
Figure 4.21. Viscosity curves of G10B2, A10B2, B10B2 and B10B2 with 0.05 wt% superplasticizer pastes	210
Figure 4.22. DTA-TGA curves for: (a) G10B0, and (b) G10B2 pastes after stopping hydration at 3, 7, 28, 120, 180 and 365 days	215
Figure 4.23. SEM micrographs of A10B2 stopped-hydration paste at different hydration time: (a) 7 days and (b) 120 days	216
Figure 4.24. Compressive strength development at different hydration times for (a) non-active, and (b) active BCSAF mortars	219
Figure 4.25. Open porosity percentage of X10B2 pastes at 120 days	220
Figure 4.26. SEM micrographs of polished (a) G10B2, (b) A10B2 and (c) B10B2_0.05%SP, pastes at 120 days of hydration time. The inset of figure (c) shows the B10B2 paste at a lower magnification	221
Figure 4.27. Length change measurements for mortars prepared with active and non-active BCSAF cement. Corresponding values for OPC and CSA mortars are also given for the sake of comparison	223

ABSTRACT

The threat of climate change is considered to be one of the major environmental challenges for our society, where carbon dioxide (CO₂) is one of the major GHGs. Anthropogenic sources of CO₂ are the combustion of fossil fuels, deforestation, unsustainable combustion of biomass, and decomposition of mineral sources such as limestone.

Cement manufacturing is considered as one of the main sources of carbon dioxide emissions among industrial activities. Every ton of OPC produces about one ton of carbon dioxide. Consequently, OPC production accounts for 5-7% of the global CO₂ emissions resulting from human activity, and for 4% of total global warming, making the cement industry an important sector for CO₂-emission mitigation strategies. CO₂ is emitted from the calcination process of limestone, from combustion of fuels in the kiln, as well as from power generation.

Due to these environmental problems the industry of building materials is under increasing pressure to reduce the energy used in the production of Portland cement clinker and mainly the associated with GHGs emissions. Therefore, the design of new formulations of cements, such as belite or/and ye'elimite based cements, has many advantages and promises to be a viable solution. One of the most interesting alternatives is the BCSA cement.

BCSA cement was first put into industrial production in China under the name "Third Cement Series" in the 1970s, and are considered environmentally friendly cements for several reasons, including the low amount of limestone required to achieve the desired composition. The substitution of alite (main phase in OPC) by belite reduces the limestone demand and temperature of cement manufacturing, thereby reducing CO₂ emissions and energy consumption while maintaining satisfying long-term properties. However, that substitution compromises the early-age strength development because C₂S reacts slower than C₃S. This renders the high-C₂S cement unusable in nearly any field related to structural applications. However, this is partially compensated by the presence of a fast reacting calcium sulphoaluminate phase (ye'elimite) in these BCSA cements. Thus, BCSA cements arise from clinkers containing belite (C₂S) as main phase (40-50 wt%) and intermediate contents (20-30 wt%) of calcium sulphoaluminate, also called Klein's salt, ye'elimite or tetracalcium trialuminate sulphate (C₄A₃S). These cements, also known as sulphobelite, are an emerging type of ye'elimite-containing cements due to their environmental benefits. The most common formulation of BCSA clinkers consists on β-C₂S, orthorhombic-C₄A₃S and C₄AF. Due to the presence of the latter, these cements are usually called iron-rich BCSA (BCSAF). BCSAF cements might also contain minor phases such as calcium aluminates (C₁₂A₇ and CA), gehlenite (C₂AS), and calcium sulphosilicate (C₅S₂S). The clinkering temperature is around 1250-1300°C, ~200°C lower than that

Abstract

for OPC production. The lower synthesis temperature not only reduces the energy consumption and CO₂ emissions from cement manufacturing but also the resulting clinker is more friable (due to high porosity), which reduces the energy needed for grinding (indirect emissions). These cements also show rapid hardening, excellent durability, and, depending on the amount of gypsum added, self-stressing and volume stability. The properties and applications of this type of cements are strongly influenced by many factors: i) chemical and mineralogical composition of the clinker, ii) sulphate source (amount and type), iii) water to cement ratio (w/c); iv) the presence of other binders such as SCMs or even OPC.

Carbon dioxide emissions in the cement industry can be classified in two main categories: those coming from raw materials and those from the operation processes. Raw materials and products obtained during the clinkering process are well known. On the one hand, the production of one ton of OPC clinker composed of 65 wt% of C₃S, 15 wt% of C₂S, 10 wt% of C₃A and 10 wt% of C₄AF released 0.54 tons of carbon dioxide. However one ton of BCSAF clinker composed by 50 wt% of C₂S, 30 wt% of C₄A₃S₂, and 20 wt% of C₄AF releases 0.39 tons of CO₂. It implies a reduction of 0.15 tons of CO₂ for BCSAF due to raw material decomposition. On the other hand, the reduction in CO₂ emissions coming from operation processes are directly related to the type of processing equipment and the specific chosen fuel. Cement production is a high energy demanding process, so it is important to consider emissions from fuel consumption to achieve high clinkering temperatures in the kiln and thus quantify CO₂ emissions. Several studies estimate an emission of ~0.30 t of CO₂ per ton of clinker produced assuming that good quality of bituminous coal is used and taking into account energy efficiency of modern kilns. The reduction in CO₂ emissions coming from the burning of the fuel can be achieved by the reduction of clinkering temperature. This is the case of BCSAF clinker production where the operating temperature can be reduced in ~200°C with a concomitant reduction of up to 0.04 t of CO₂ per ton of BCSAF clinker produced. Moreover, emissions derived from electricity consumption are about 0.09 t of CO₂ per ton of OPC. The lower firing temperatures needed for BCSAF clinkering made it easier to be ground. Therefore, reduction on the electricity consumption yields a depletion of up to 0.02 t of CO₂ emissions. Considering all emissions together, the production of one ton of OPC clinker releases a maximum of 0.97 tons of CO₂; thus, the production of one ton of BCSAF clinker leads to a reduction of ~22% CO₂ emissions compared to OPC. That reduction depends on the composition.

In the last few years, BCSAF cements have emerged with the initial aim to substitute OPC. An industrial trial, ~2500 tons of BCSAF, was carried out in 2011 by Lafarge under the AETHER™ project (<http://www.aether-cement.eu/>). Clinkering was performed in a Portland industrial kiln but using lower operating temperatures (1225-1300°C), reducing CO₂ emissions by 25-30% in comparison with CEM (I) type

OPC cement. The temperature in the clinkering zone resulted to be a key parameter, as too high temperatures may give kiln blockage, loss of grindability and C_4A_3S decomposition with high SO_2 emissions, and too low temperatures gave under burnt binder with high free lime and $C_{12}A_7$ contents. The optimum clinkering temperature resulted much lower in NO_x emissions than those for OPC, due to the lower burning temperature, and SO_2 emissions resulted at the same level than for OPC production.

As mentioned before, the main technological disadvantage of these cements is related to the low mechanical strengths developed at very-early ages due to the slow hydration of belite. However, this problem may be overcome by the activation of belite and the presence of high amounts of ye'elimite. The production of active BCSAF cements involves the stabilisation of highly reactive C_2S polymorphs, i.e. β -modified form and α -forms, as they react faster with water. Active-BCSAF cements have been patented by Lafarge and they contain Klein's salt and α -forms of belite as main phases. The latter was stabilised due to addition of minor elements, such as B_2O_3 and Na_2O . Active-BCSAF with 2.0 wt% of B_2O_3 , added as borax, developed comparable compressive strengths to those of OPC.

For these reasons, BCSAF cements are considered, nowadays, as one of the most promising alternatives to OPC. This is supported by both the environmental benefits (lower CO_2 emissions) and industrial interest. However, before to be implanted in Europe, all the steps evolved in the process need to be under control, including clinkering (activation/composition and temperature), hydration (rheological behaviour and phase assemblage), and final performances (mechanical strength and dimensional stability). This PhD Thesis is focused on the study and optimisation of those parameters to improve the final performances of BCSAF mortars.

One of the main objectives of this Thesis has been to perform the "medium scale" synthesis (~2 kg) of two BCSAF clinkers in our laboratory with the expected phase composition of 50 wt% of C_2S , 30 wt% of C_4A_3S and 20 wt% of C_4AF . One of the clinkers was "activated" through the addition of borax, 2 wt% expressed as B_2O_3 , to the raw material mixture. The aim of the activation has been obtaining clinkers with different belite (β - C_2S or α'_H - C_2S) and ye'elimite (orthorhombic or pseudo-cubic) polymorphs to understand the effect of the polymorphism on the paste hydration mechanism and mechanical performances of the corresponding mortars. These clinkers were named as BCSAF_B0 (non-active) and BCSAF_B2 (active), for boron-free and boron-containing clinkers, respectively. The optimised two-step clinkering process consisted on: heating at 900°C during 30 min and further heating to 1350°C during 30 min. The clinker was rapidly quenched by forced air flow. The two obtained BCSAF clinkers were characterised through LRPD, including the analysis of selective dissolutions, and SEM-EDS.

Abstract

The quantitative phase analysis of BCSAF clinkers and cement pastes is an essential part of this Thesis needed to better understand their hydration behaviour and thus how their performances can be modified for any given application. X-ray diffraction coupled with Rietveld analysis is a suitable methodology to obtain quantitative phase analysis of these materials in the laboratory. The application of RQPA to characterise clinkers/cements/pastes is not an easy task due to the presence of appreciable amounts of amorphous/sub-cooled and/or non-crystalline phases. However, the quantification of the amorphous phases is a very important issue to understand hydration mechanisms. The final phase assemblage obtained by LRPD and Rietveld method for the two laboratory-scaled-up prepared clinkers confirmed that BCSAF_B0 clinker contains β -C₂S and both orthorhombic and pseudo-cubic ye'elimite as main phases, meanwhile α' -C₂S and pseudo-cubic ye'elimite are stabilised in BCSAF_B2.

The quantification of the ACn content was also performed. For that, the following two approaches have been used: i) external standard procedure (G-factor method) with reflection geometry; ii) internal standard procedure (spiking method with ZnO) with transmission geometry, using CuK $\alpha_{1,2}$ radiations. Several conclusions drawn from a comparative study using the two approaches were: on the one hand, the G-factor method allows the quantifications of both crystalline phases and ACn contents in these materials, where the latter reaches ~25 wt% in BCSAF clinkers. On the other hand, the amount of ACn calculated showed the same trend independently on the used methodology.

Moreover, the microstructural characterisation of both clinkers revealed that the average particle size of ye'elimite (with angular shaped particles) and belite (with typical rounded shape) particles present in BCSAF_B0 were smaller than those found in BCSAF_B2. In addition, ye'elimite particles in the active clinker contain small amounts of Si, Fe and Na.

Other important objective of this Thesis has been to understand the influence of calcium sulphate (type and amount) on the hydration of active and non-active BCSAF cements. BCSAF clinkers were mixed with different types and amounts of calcium sulphate sources (gypsum (G), anhydrite (A) and bassanite (B)). Cements prepared with gypsum are labelled hereafter as GgBx, where g stands for 5, 10 or 15 wt% of gypsum, and x for 0 or 2 (for non-active or active clinkers, respectively). Cements prepared with different sulphate sources are labelled hereafter as G10Bx, A10Bx and B10Bx, for 10 wt% of gypsum, anhydrite or bassanite, respectively. Bassanite, C₂H_{0.5}, and anhydrite, C₂S, were previously synthesized by heating commercial gypsum. All the cement pastes were prepared, at a w/c = 0.55, by mixing both BCSAF clinkers (BCSAF_B0 and BCSAF_B2) with the corresponding sulphate source. Two studies were carried out to better understand the hydration behaviour.

On the one hand, an *in-situ* SXRPD study for the first hours of hydration was carried out in the SXRPD station of MSPD beamline at ALBA synchrotron (Barcelona, Spain). On the other hand, *ex-situ* studies at later ages of hydration were performed to determine the influence of the amount and type of calcium sulphate added to BCSAF cements on hydration behaviour through LXRPD (CuK α_1 radiation). In addition, a comparative study of MoK α_1 and synchrotron radiations for selected hydrated samples was also performed.

The *in-situ* study, in GgBx cements, showed important differences in the hydration process, such as different dissolution kinetic of gypsum and ye'elimite. For instance in G10B0, gypsum is completely dissolved after 5 h of hydration and ye'elimite dissolves at a higher pace than in active BCSAF. However, in G10B2, gypsum is dissolved after 11 h and ye'elimite is still present after 51 h of hydration. In addition, the crystallisation rate of AFt is also different in both cements. At 1 h of hydration G10B0 contains 14.2(2) wt% of AFt while at the same hydration time, only 1.9(1) wt% was quantified for G10B2. The fast sulphate consumption by crystalline ettringite precipitation in G10B0 paste is responsible of its higher pH value, 12.4 ± 0.1 , when compared to 10.3 ± 0.1 for G10B2. The second most important difference between both hydration behaviours takes place after 1 day of hydration. On the one hand, in G10B0, the dissolution of β -C₂S and C₄AF starts after 24 h of hydration, with the consequent crystallisation of layered AFm type phases, such as stratlingite. On the other hand, for G10B2, α'_H -C₂S percentage remains constant up to 51 h of hydration and C₄AF dissolves very slowly after 14 h. The difference in reactivity of both belite polymorphs is in disagreement with the general accepted idea in the cement field: α -forms of belite present faster hydration kinetics than β -forms. But under our studied experimental conditions, β -C₂S reacts faster than α'_H -C₂S to yield stratlingite, and this behaviour may well be justified with the formation of high amounts of ettringite at early hours which implies a concomitant large quantity of amorphous aluminium hydroxide. The availability of amorphous AH₃ promotes the precipitation of stratlingite, C₂ASH₈, from belite reaction. Then, the hydration behaviour of C₂S is more dependent on the chemical environment than on its polymorphism.

The influence of the amount of added gypsum in BCSAF cements at late ages of hydration (> 24 h) was also tested in GgBx cements. One of the main conclusions obtained in this part of the study was the astonishing behaviour of β -belite in non-active clinkers since it reacts at a higher pace than α'_H -belite in BCSAF_B2, as mentioned before. Moreover, ye'elimite reacts at a different pace for BCSAF_B0 and BCSAF_B2. Orthorhombic ye'elimite, in non-active cements, is completely hydrated after 3 days of hydration in GgB0, while pseudo-cubic ye'elimite in GgB2 reacts at slightly slower pace for the same gypsum content and age of hydration. This effect was also previously observed in the hydration study at early hours.

Other conclusion has been that ye'elimite reaction kinetics showed a small dependence on the amount of added gypsum, as there was a slight increase in hydration rate by increasing the gypsum content. This behaviour seems to be slightly more marked for the pseudo-cubic ye'elimite. Moreover, the final reaction degree of both polymorphs of dicalcium silicate is affected by the increment of gypsum. On the one hand, β -C₂S reactivity (given by the degree of reaction, α) was enhanced by increasing the gypsum content (α rises from 65% to 75% by the addition from 5 to 15 wt% of gypsum). On the other hand, α' -C₂S reaction degree decreased from 62% to 42% for addition of 5 to 15 wt% of gypsum, respectively. Finally, the hydration of the ferrite phase was strongly retarded by increasing the gypsum content in both GgB0 and GgB2 cements.

In all cases the main crystalline hydrated compounds were ettringite, stratlingite and katoite. The amount of crystallised ettringite in GgB2 cements resulted higher than that in GgB0 cements, irrespective of gypsum content. Moreover, the crystallisation process of stratlingite is strongly affected by the amount of added gypsum; in fact, the amount of stratlingite decreases by increasing the gypsum content.

It is not only important to quantify the amorphous content, but also to try to characterise and estimate its elemental composition and correlate it with the cement hydration behaviour and mechanical properties. It is not possible to determine the chemical composition of ACn directly by LXRPD, but an attempt to find it out (sulphate, silicate, aluminate and iron-bearing groups) has been performed through RQPA and Rietveld methodology combined with G-factor. For this purpose, the evolution of different ions-containing groups was studied with time. Since the amount of sulphates crystallised in GxB2 was higher than that in GxB0 pastes, it means that a bigger amount of sulphate groups were dissolved, but not crystallised in the last one; then, they were mainly incorporated into ACn phase(s) and/or in pore solution of the GxB0 cement pastes. The amount of crystallised silicate is higher in GxB0 than in GxB2, where higher amounts of stratlingite were found. Thus, a higher amount of hydrated silicate remains in the amorphous phase(s) for GxB2 cement paste. The amount of crystallised aluminium-bearing phases was higher in GgB0 than in GgB2 cement pastes, matching in some cases the maximum, whereas more than 30 wt% of the aluminate content remained in the ACn phase(s) for GgB2 pastes, and/or to a minor extent in pore solution.

A hydration study of BCSAF cements with different calcium sulphate source [gypsum (G), bassanite (B) and anhydrite (A)] was also performed. First, an *in-situ* SXRPD study was carried out to determine the role of the type of calcium sulphate source (with 10 wt%) in the first hours of hydration. The reaction degree of both ye'elimite and ettringite in G10B2, A10B2 and B10B2 at early ages was determined.

The direct RQPA results were normalised taking into account the theoretical data of the sample at 0.0 h of hydration. Comparing the theoretical results with the direct RQPA data, we can conclude that, for G10B2 sample, the AFt crystallisation process is parallel to ye'elimite dissolution, and the gypsum dissolution is very fast. In addition, G10B2 presented an induction period close to 6 h, when the dissolution and crystallisation of phases become significant. For A10B2, the RQPA results showed that the dissolution kinetic of anhydrite is much slower than that for gypsum or bassanite, as expected. For A10B2 paste, the precipitation of ettringite is limited by C₃S dissolution, which starts to be significant up to 7 h. Using these results we can also state that the predicted reactivity of ye'elimite with water to form AFm as main hydrated phase has not taken place within the first 6 h of hydration. Our results state that ye'elimite dissolution yields ettringite in spite of the fact that anhydrite is not dissolved until 6 h. B10B2 paste was also analysed. Due to experimental requirements (sample loading in the capillaries, alignment and so on), it was not possible to measure the first ~40 min of hydration. Since the dissolution of bassanite and precipitation of gypsum are very fast processes, bassanite was almost absent and gypsum had crystallised just after 1 h of hydration. Subsequent hydration reactions are similar to those already described for the gypsum-regulated cement, G10B2. The very fast dissolution of bassanite with precipitation of gypsum, as well as the low dissolution rate of anhydrite was quantified, confirming the accurateness of the methodology used.

Since bassanite in contact with water suffers from a fast grain decay (intergranular attack) which produces an increasing of the surface area of the sulphate carrier, and as a consequence, a high water demand (and high viscosity). In addition, a primary gypsum precipitation occurs, which will also affect the rheological behaviour of the paste. Thus, both parameters the high water demand and the gypsum precipitation increase the viscosity of bassanite-pastes. Since our objective is to study the effect of the calcium sulphate source (including compressive strengths of the corresponding mortars) similar rheological behaviour, and in particular, similar viscosity values at very early hydration ages are desired. In this case a small amount of a commercial polycarboxylate-based superplasticizer (SP) (0.05 wt% of active matter referred to total solids content), was added to water to prepare bassanite-containing pastes. It exhibited a considerable diminishing in viscosity and a similar rheological behaviour to those prepared with gypsum or anhydrite. The main conclusions obtained of this hydration study at late ages are below.

In all cases, the sulphate source was consumed before 3 days of hydration to form ettringite as the main crystalline hydrated phase. AFm and stratlingite were also found in all the studied pastes but in variable amounts. Independently of the sulphate source, ettringite seems to be more stable in active cements (X10B2), which contained $\alpha'_H\text{-C}_2\text{S}$ and pseudo-cubic ye'elimite, as it is almost constant with time of

Abstract

hydration. On the other hand, AFt contents decrease with time for X10B0 to give AFm phases. Consequently at later ages the amount of AFt is much larger in X10B2 and this is very likely the responsible of the improved mechanical properties of this family when compared to the poorer data for X10B0. Focusing on the belite reactivity, β -C₂S (present in X10B0) dissolves faster than α' -C₂S (present in X10B2) within the first 28 days, independently of the sulphate source, as described before. Moreover, crystalline stratlingite is quantified in X10B0 just after 3 days of hydration, but it is not detected until 28 days in X10B2 pastes. DTA and TG analysis for G10Bx, A10Bx and B10Bx pastes at different curing ages were also carried out. As an example, G10B2 has a higher degree of reaction at 365 hydration days with a higher overall weight loss (~32 wt%) than the corresponding value for G10B0 (~26 wt%). Therefore, X10B2 families showed lower amounts of FW at curing ages over 28 days, indicating higher degree of reaction. At latter ages, the analysis of the data indicates that the phase assemblage is slightly sensitive to the initial sulphate source. AFt, stratlingite, katoite and AFm contents between 120 and 365 days are very similar for G10B2 and A10B2. When comparing the results for G10B0 and A10B0, some (minor) differences are detected, for instance larger amounts of AFm in G10B0 than in A10B0 were found.

A SEM-EDS study was performed in the X10B2 pastes to better characterise the chemical composition of each phase, especially for amorphous/ill-crystalline phases. This type of study helped to estimate the elemental composition (especially Si, Al and Fe) of new crystalline or amorphous phases with time of hydration, since this may affect the mechanical properties. SEM-EDS analyses of these hydrated pastes reveal that the chemical composition of amorphous phase(s) in G10B2 and B10B2 at 120 days is very similar, but slightly richer in silicon and iron in A10B2. The chemical composition evolution with time generates interesting information. Al/Ca vs. Si/Ca atomic ratios, for A10B2 paste at 7 and 120 days of hydration, show that particles without a defined shape, which may be amorphous phases, are rich in aluminium at 7 days, while they are enriched in silicon with time (120 days). The former is related to early hydration products (AFt and amorphous aluminium hydroxide) formed in these cements from the dissolution of ye'elimite and calcium sulphate; the latter, with the reactivity of belite. Moreover, hydration products which contain iron are difficult to be identified by LXRPD. The Al-Fe atomic ratio for A10B2 pastes at different ages (7 and 120 days) was also studied. When analyzing particles with a needle shape, which are identified as ettringite, some amounts of iron were found. These results may indicate that iron is incorporating in AFt crystal structure, but more research is needed to confirm this item. In addition, A10B2 hydrated during 7 days shows some small bright particles with a chemical composition similar to stratlingite. However these particles seem to have low crystallinity degree, and they were not detected by LXRPD at that hydration age, but the DTA thermograph of this sample showed a small shoulder at ~170°C, which is related to stratlingite.

Mechanical properties of standard mortars (from active and non-active cements) were prepared with a cement/sand/water ratio of 1/3/0.55. In order to use the minimum amount of sample (laboratory studies), moulds with dimensions of 30 x 30 x 30 mm³ were used. To compare the results with those obtained using the moulds that fulfil the normative, a conversion factor is used, and the results are multiplied by 1.78.

The most important result is that all mortars prepared with the active BCSAF cement developed higher compressive strengths than non-active mortars, independently of the type and amount of sulphate source. In addition, by increasing the gypsum content from 5 to 10 wt%, the compressive strength increased in both systems. Furthermore, the addition of 15 wt% gypsum produced a slight decrease in the compressive strength, likely due to the slowdown of belite hydration rate. Within the non-active mortars, A10B0 presented the highest values. This behaviour may be explained/justified by the higher BET area value and the slightly higher stability of Aft present in that paste when compared to G10B0. Bassanite cement reacts very quickly with water showing a short setting time which leads to mortars with low degree of homogeneity. Due to this fact, the compressive strength values for B10B0 mortars were not measured. For B10B2, although the addition of a small amount of SP improved the workability of the mortar, the delay in the setting time was not enough to develop comparable mechanical strength values to gypsum and anhydrite mortars.

At 120 days, G10B2 mortar developed the highest mechanical strength value (68±1 MPa), even when the amount of ettringite in A-paste was slightly larger than that for G-paste. Therefore, we are forced to conclude that the amorphous contents are playing a key role for the strength development at late ages. Moreover, G10B2 cement has the highest BET area value (1.8109 ± 0.0241 m²/g) of all the studied cements and this may also justify this behaviour. The reaction degree of $\alpha'_H\text{-C}_2\text{S}$ in G10B2 (74%) is slightly higher than that in A10B2 (65%), which could help in improving the mechanical strengths. The porosity of the three X10B2 cement pastes at 120 days of hydration was measured by mercury intrusion porosimetry (MIP), which could be extrapolated to the mortars. Bassanite-paste showed the highest percentage of porosity (16%), and the gypsum one showed the lowest value (10%); this behaviour also helps to justify the measured mechanical strengths. In conclusion, the **optimum amount and type of sulphate source** in these systems seems to be quite close to **10 wt% of gypsum**, as higher mechanical strengths are obtained.

Finally, the expansion/shrinkage data of BCSAF mortars revealed the effect of gypsum content in dimensional stability of BCSAF mortars. The addition of 15 wt% of gypsum caused the highest expansion values for both systems. In addition, G5B2 and G10B2 mortars showed a length variation roughly from -0.01% to 0.04% within 180 days. The effect of the sulphate source on dimensional stability was also studied.

Abstract

Mortars prepared with anhydrite presented high expansion in early hydration ages, similar to that in CSA mortars. However, the B10B2 mortar showed very low expansion values, similar to mortars prepared with 5 wt% of gypsum, in agreement with the results obtained in the hydrating behaviour study, as bassanite is completely dissolved before the first 45 minutes of hydration and gypsum precipitates. Consequently, bassanite-mortars behave similar to those made with gypsum at very early ages.

Finally, I would say that I am a member of a working group which has a vast experience in anhydrous cements and clinkers characterisation by X-Ray powder diffraction combined with Rietveld methodology, and in the processing of (ceramic) materials. So, I would like to highlight my contribution in the scaled-up synthesis and characterisation of BCSAF clinkers and cement pastes, including the quantification and “chemical analysis” of ACn content, and the measurement of mechanical properties (compressive strength and length change) of the corresponding mortars.

RESUMEN

La amenaza del cambio climático es considerada como uno de los principales retos ambientales de nuestra sociedad, donde el dióxido de carbono (CO_2) es uno de los principales gases de efecto invernadero. Las principales fuentes antropogénicas de CO_2 son la combustión de combustibles fósiles, la deforestación, la insostenible combustión de la biomasa, y la descomposición de las fuentes de minerales tales como la caliza.

La fabricación del cemento se considera como una de las principales fuentes de emisiones de dióxido de carbono entre las actividades industriales. Cada tonelada de cemento Portland ordinario (OPC, *del inglés Ordinary Portland Cement*) produce alrededor de una tonelada de dióxido de carbono. En consecuencia, la producción del OPC representa el 5-7% de las emisiones globales de CO_2 resultantes de la actividad humana, y el 4% del total del calentamiento global, haciendo que la industria del cemento sea un sector importante para las estrategias de mitigación de emisiones de CO_2 . El CO_2 procede del proceso de calcinación de la piedra caliza, de la combustión de los combustibles en el horno, así como de la generación de energía.

Debido a estos problemas ambientales, la industria de los materiales de construcción se encuentra bajo una creciente presión para reducir la energía utilizada en la producción del clínker del cemento Portland y sobre todo de las emisiones asociadas a los gases de efecto invernadero (GHGs, *del inglés Greenhouse Gases*). Por lo tanto, el diseño de nuevas formulaciones de cementos, como los cementos basados en belita y/o ye'elimita, tienen muchas ventajas y prometen ser una solución viable. Una de las alternativas más interesantes son los llamados cementos belíticos de sulfoaluminato de calcio (BCSA, *del inglés Belite Calcium Sulpho-Aluminate*).

Los cementos BCSA se produjeron por primera vez de forma industrial en China bajo el nombre "Tercera Serie de Cementos" en la década de 1970, y se consideran cementos ecológicos por varias razones, entre ellas la baja cantidad de piedra caliza necesaria para lograr la composición deseada. La sustitución de alita (fase principal en el OPC) por belita reduce la demanda de caliza y la temperatura de fabricación del cemento, reduciendo así las emisiones de CO_2 y el consumo de energía, manteniendo sus propiedades a largo plazo. Sin embargo, esta sustitución compromete el desarrollo de la resistencia a edades tempranas porque el C_2S reacciona más lento que el C_3S . Esto hace que el cemento con altos contenidos de C_2S sea inutilizable en casi cualquier campo relacionado con aplicaciones estructurales. Sin embargo, esto se compensa parcialmente por la presencia de una fase de sulfoaluminato de calcio de reacción rápida (ye'elimita) en estos cementos BCSA. Así, estos cementos BCSA se forman a partir de clínkeres que contienen belita (C_2S) como fase principal (de 40 a 50% en peso) y contenidos intermedios (de 20 a 30% en peso) de sulfoaluminato de calcio, también llamado sal de Klein o ye'elimita ($\text{C}_4\text{A}_3\text{S}$). Estos cementos, también conocidos como sulfobelíticos, son un tipo emergente de

cementos que contienen β -C₂S, C₄A₃S₂ ortorrómbica y C₄AF. Debido a la presencia de esta última fase, estos cementos se llaman generalmente cementos BCSA ricos en hierro (BCSAF). Los cementos BCSAF también pueden contener fases minoritarias tales como aluminatos de calcio (C₁₂A₇ y CA), gehlenita (C₂AS) y sulfosilicato de calcio (C₅S₂S). La temperatura de clinkerización de estos clínteres está en torno a 1250-1300°C, ~200°C más baja que la de producción del OPC. Esta temperatura de síntesis inferior no sólo reduce el consumo de energía y las emisiones de CO₂ procedentes de la fabricación de cemento, sino que también da lugar a un clínter más friable (debido a la alta porosidad), lo que reduce la energía necesaria para la molienda (emisiones indirectas). Estos cementos también muestran un endurecimiento rápido, una excelente durabilidad, y, dependiendo de la cantidad de yeso añadida, una buena estabilidad de volumen. Las propiedades y aplicaciones de este tipo de cementos están fuertemente influenciadas por muchos factores: i) la composición química y mineralógica del clínter, ii) la fuente de sulfato (cantidad y tipo), iii) la relación agua/cemento; iv) la presencia de otros aglutinantes tales como materiales suplementarios (SCMs, *del inglés Supplementary Cementitious Materials*) o incluso OPC.

Las emisiones de dióxido de carbono en la industria del cemento se pueden clasificar en dos categorías principales: las que vienen de las materias primas y las de los procesos de operación. Las materias primas y los productos obtenidos durante el proceso de clinkerización se conocen bien. Por un lado, la producción de una tonelada de clínter OPC formado por un 65% en peso de C₃S, 15% en peso de C₂S, 10% en peso de C₃A y 10% en peso de C₄AF, libera 0.54 toneladas de dióxido de carbono. Sin embargo una tonelada de clínter BCSAF compuesta por 50% en peso de C₂S, 30% en peso de C₄A₃S₂, y 20% en peso de C₄AF libera 0.39 toneladas de CO₂. Esto implica una reducción de 0.15 toneladas de CO₂ para el BCSAF debido a la descomposición de materia prima. Por otro lado, la reducción en las emisiones de CO₂ procedentes de los procesos de operación está directamente relacionada con el tipo de equipo de procesamiento y el combustible específico elegido. La producción de cemento es un proceso de alta demanda energética, por lo que es importante tener en cuenta las emisiones procedentes del consumo de combustible necesario para alcanzar las altas temperaturas de clinkerización en el horno, y así cuantificar las emisiones de CO₂. Diversos estudios estiman una emisión de ~0.30 t de CO₂ por tonelada de clínter producido, asumiendo una buena calidad del carbón bituminoso usado y teniendo en cuenta la eficiencia energética de los hornos modernos. La reducción en las emisiones de CO₂ procedentes de la quema del combustible se puede lograr mediante la reducción de la temperatura de clinkerización. Este es el caso de la producción de clínter BCSAF donde la temperatura de operación se puede reducir en ~200°C con una reducción asociada de hasta 0.04 t de CO₂ por tonelada de clínter BCSAF producido. Por otra parte, las emisiones derivadas del consumo de

electricidad son aproximadamente 0.09 toneladas de CO₂ por tonelada de OPC. Las temperaturas de cocción más bajas necesarias para la clinkerización del BCSAF hacen que sea más fácil a moler. Por lo tanto, la reducción en el consumo de electricidad produce un descenso de las emisiones de CO₂ de hasta 0.02 toneladas. Teniendo en cuenta todas las emisiones en conjunto, la producción de una tonelada de clinker OPC libera un máximo de 0.97 toneladas de CO₂; sin embargo, la producción de una tonelada de clinker BCSAF conduce a una reducción de ~22%, dependiendo de la composición.

En los últimos años, los cementos BCSAF han surgido con el objetivo inicial de sustituir al OPC. Una prueba industrial, de ~2500 toneladas de BCSAF, se llevó a cabo en 2011 por Lafarge en el marco del proyecto AETHER™ (<http://www.aether-cement.eu/>). La clinkerización se llevó a cabo en un horno de Portland industrial pero utilizando temperaturas menores (1225-1300°C), reduciendo las emisiones de CO₂ en un 25-30% en comparación con el cemento OPC tipo CEM (I). La temperatura en la zona de clinkerización resultó ser un parámetro clave, ya que temperaturas demasiado altas podían provocar el bloqueo del horno, la pérdida de la capacidad de molienda y la descomposición del C₄A₃S̄ con altas emisiones de SO₂, y temperaturas demasiado bajas daba un ligante poco quemado con altos contenidos de cal libre y C₁₂A₇. La temperatura óptima de clinkerización resultó dar menores emisiones de NO_x que los OPC, debido a la temperatura de combustión inferior, y emisiones de SO₂ del mismo nivel que para la producción de OPC.

Como se mencionó anteriormente, la principal desventaja tecnológica de estos cementos está relacionada con sus bajas resistencias mecánicas a edades tempranas, debido a la lenta hidratación de la belita. Sin embargo, este problema puede superarse mediante la activación de la belita y la presencia de altas cantidades de ye'elimita. La producción de cementos BCSAF activados implica la estabilización de los polimorfos de C₂S altamente reactivos, es decir, la forma β-modificada y las formas α, ya que estas reaccionan más rápidamente con el agua. Los cementos BCSAF activados han sido patentados por Lafarge y contienen sal de Klein y formas α de la belita como fases principales. Esta última fue estabilizada debido a la adición de elementos minoritarios, como B₂O₃ y Na₂O. Cementos BCSAF activados con 2% en peso de B₂O₃, añadido como bórax, han desarrollado resistencias a la compresión comparables a los OPC.

Por estas razones, los cementos BCSAF se consideran, hoy en día, como una de las alternativas más prometedoras a los OPC. Esto es apoyado por los beneficios ambientales (emisiones de CO₂) y el interés industrial. Sin embargo, antes de ser implantados en Europa, deben de controlarse todos los pasos envueltos en el proceso, incluyendo la clinkerización (activación/composición y temperatura), la hidratación (comportamiento reológico y ensamblaje de fase), y las propiedades

finales (resistencias mecánicas y estabilidad dimensional). Esta tesis doctoral se centra en el estudio y optimización de estos parámetros para mejorar las propiedades finales de los morteros BCSAF.

Uno de los principales objetivos de esta tesis ha sido llevar a cabo la síntesis a "mediana escala" (para obtener ~2 kg) de dos clínkeres BCSAF en nuestro laboratorio con una composición de fases esperada de 50% en peso de C_2S , 30% en peso de C_4A_3S y 20% en peso de C_4AF . Uno de los clínkeres fue "activado" mediante la adición de bórax, 2% en peso expresado como B_2O_3 , a la mezcla de materia prima. El objetivo de la activación fue obtener clínkeres con diferentes polimorfos de la belita (β - C_2S o α'_H - C_2S) y de la ye'elimita (ortorrómbica o pseudo-cúbica), para comprender el efecto del polimorfismo en el mecanismo de hidratación de las pastas y en las propiedades mecánicas de los morteros correspondientes. Estos clínkeres se llamaron como BCSAF_B0 (no activo) y BCSAF_B2 (activo), para el libre de boro y el que contiene boro, respectivamente. El proceso de óptimo de clínkerización fue el siguiente: calentamiento hasta 900°C manteniendo 30 min a esa temperatura, y calentamiento posterior hasta 1350°C manteniendo durante 30 min. El clínker resultante fue enfriado rápidamente mediante un flujo de aire forzado. Los dos clínkeres BCSAF obtenidos se caracterizaron a través LXRPD, incluyendo el análisis de disoluciones selectivas y microscopía electrónica de barrido (SEM-EDS).

El análisis cuantitativo de fases de los clínkeres BCSAF es una parte esencial de esta tesis necesaria para comprender mejor su comportamiento de hidratación y por tanto cómo sus propiedades mecánicas pueden modificarse para cualquier aplicación dada. La difracción de rayos X junto con el análisis de Rietveld es una metodología adecuada para obtener el análisis de fase cuantitativo de estos materiales en el laboratorio. La aplicación de RQPA para caracterizar clínkeres/cementos/pastas no es una tarea fácil debido a la presencia de fases amorfas y/o no cristalinas en las muestras. Por eso, la cuantificación de las fases amorfas es un tema muy importante para entender los mecanismos de hidratación. El ensamblaje final de fases obtenido por LXRPD y el método Rietveld para los dos clínkeres preparados en el laboratorio confirma que el clínker BCSAF_B0 contiene β - C_2S y ye'elimita (ortorrómbica y pseudo-cúbica) como fases principales, mientras que la α'_H - C_2S y la ye'elimita pseudo-cúbica se estabilizaron en el clínker BCSAF_B2.

La cuantificación del contenido amorfo (ACn, *del inglés Amorphous and Crystalline non-quantified*) también se llevó a cabo. Para ello, dos métodos se han utilizado en esta Tesis doctoral: i) el procedimiento del estándar externo (Factor G) con la geometría de reflexión; ii) el procedimiento del estándar interno ("spiking" método con ZnO) con la geometría de transmisión, utilizando radiaciones $CuK\alpha_{1,2}$. Varias conclusiones se han extraído del estudio comparativo usando los dos métodos: por un lado, el método del factor G permite la cuantificación tanto de fases

cristalinas como del ACn en estos materiales, siendo este último de ~25% en peso en los clínkeres BCSAF. Por otro lado, la cantidad de ACn calculado mostró la misma tendencia independientemente de la metodología utilizada.

Además, una caracterización micro estructural de ambos clínkeres reveló que los tamaños medios de partícula para la ye'elimita (partículas con forma angular) y la belita (con típica forma redondeada) presentes en BCSAF_B0 eran ligeramente menores que en BCSAF_B2. Por otra parte, las partículas de ye'elimita en el clínker activado contienen pequeñas cantidades de Si, Fe y Na.

Otro objetivo importante de esta Tesis ha sido comprender la influencia del sulfato de calcio (tipo y cantidad) en la hidratación de los cementos BCSAF (activos y no activos). Para ello, ambos clínkeres se mezclaron con diferentes tipos y cantidades de fuentes de sulfato de calcio [yeso (G), anhidrita (A) y basanita (B)]. Los cementos preparados con yeso se van a nombrar a partir de ahora como GgBx, donde g representa 5, 10 o 15% en peso de yeso, y x será 0 o 2 (para el clínker no activo o activo, respectivamente). Los cementos preparados con diferentes fuentes de sulfato se nombrarán en lo sucesivo como G10Bx, A10Bx y B10Bx, para el 10% en peso de yeso, anhidrita o basanita, respectivamente. La basanita, $C_2SH_{0.5}$, y anhidrita, CS_2 , fueron sintetizadas previamente por calentamiento del yeso comercial. Se prepararon todas las pastas de cemento, con una relación agua/cemento = 0.55, mezclando ambos clínkeres (BCSAF_B0 y BCSAF_B2) con la fuente de sulfato correspondiente. Se llevaron a cabo dos estudios para comprender mejor el comportamiento de hidratación. Por un lado, un estudio *in-situ* para las primeras horas de hidratación, se llevó a cabo mediante SXRPD en la línea MSPD del sincrotrón ALBA (Barcelona, España). Por otra parte, se realizaron estudios *ex-situ* a edades posteriores de hidratación, para determinar la influencia de la cantidad y el tipo de sulfato de calcio añadido al cemento BCSAF a través de LXRPD (radiación $CuK\alpha_1$). Además, también se ha llevado a cabo un estudio comparativo radiaciones de $MoK\alpha_1$ y sincrotrón para muestras hidratadas seleccionados.

El estudio *in-situ*, de los cementos GgBx, mostró importantes diferencias durante la hidratación, como la diferente cinética de disolución del yeso y la ye'elimita. Por ejemplo, en G10B0, el yeso se disolvió completamente después de 5 h de hidratación y la ye'elimita se disolvió a un ritmo mayor que en el cemento BCSAF activo. Sin embargo, en G10B2, el yeso se disolvió después de 11 h y la ye'elimita todavía estaba presente después de 51h de hidratación. Además, la velocidad de cristalización del AFt también es diferente en ambos cementos. A 1 h de hidratación, G10B0 contiene 14.2(2)% en peso de AFt mientras que para el G10B2 solamente se cuantificó 1.9(1)% en peso de AFt. El rápido consumo del sulfato debido a la precipitación de etringita cristalina en la pasta de G10B0 es responsable del mayor valor de pH, 12.4 ± 0.1 , en comparación con 10.3 ± 0.1 para la pasta G10B2. La

segunda diferencia más importante entre ambos comportamientos de hidratación tiene lugar después de 1 día. Por un lado, en G10B0, la disolución de β -C₂S y C₄AF comienza después de 24 h, con la consiguiente cristalización de fases tipo AFm, tales como la stratlingita. Mientras que para G10B2, el porcentaje de α' -C₂S permanece constante hasta las 51 h de hidratación y el C₄AF se disuelve muy lentamente a partir de las 14 h. La diferencia en la reactividad de ambos polimorfos de la belita está en desacuerdo con la idea general aceptada en el campo del cemento: las formas α de la belita presentan cinéticas de hidratación más rápidas que las formas β . Aún así, bajo nuestras condiciones experimentales estudiadas, β -C₂S reacciona más rápidamente que α' -C₂S, para producir stratlingita, y este comportamiento puede estar bien justificado con la formación de altas cantidades de etringita en las primeras horas lo que implica una gran cantidad de hidróxido de aluminio amorfo. La disponibilidad de AH₃ amorfo promueve la precipitación de la stratlingita, C₂ASH₈, a partir de la reacción de la belita. En conclusión, el comportamiento de hidratación del C₂S es más dependiente del ambiente químico que de su polimorfismo.

La influencia de la cantidad de yeso añadida en los cementos BCSAF a edades tardías de hidratación (>24h) también fue estudiado. Una de las principales conclusiones obtenidas en esta parte del estudio fue de nuevo el sorprendente comportamiento de la β -belita en el clínker no activo, ya que reaccionó a un ritmo más alto que la α' -belita en BCSAF_B2, como se mencionó antes. Además, la ye'elimita reaccionó a un ritmo diferente para BCSAF_B0 y para BCSAF_B2. La forma ortorrómbica de la ye'elimita, en los cementos no activos, se disuelve por completo después de 3 días de hidratación, mientras que la ye'elimita pseudo-cúbica presente en GgB2 se disuelve ligeramente más lenta para el mismo contenido de yeso y la misma edad de hidratación. Este efecto también se observó anteriormente en el estudio de hidratación en las primeras horas.

Otra conclusión de este estudio fue que la cinética de reacción de la ye'elimita mostró una pequeña dependencia con la cantidad de yeso añadido, ya que la velocidad de hidratación aumentó ligeramente al aumentar el contenido de yeso. Este comportamiento parece un poco más marcado para la ye'elimita pseudo-cúbica. Por otro lado, el grado final de reacción de ambos polimorfos del silicato dicálcico se ve afectada por el incremento de yeso. Por un lado, la reactividad de β -C₂S (dada por el grado de reacción, α) se mejoró al aumentar el contenido de yeso (α aumenta del 65% al 75% mediante la adición de 5 a 15% en peso de yeso). Por otro lado, el grado de reacción de α' -C₂S se redujo de 62% a 42% para la adición de 5 a 15% en peso de yeso, respectivamente. Por último, la hidratación de la fase de ferrita está fuertemente retardada por el aumento del contenido de yeso en ambos cementos (GgB0 y GgB2).

En todos los casos los principales compuestos cristalinos hidratados obtenidos fueron etringita, stratlingita y katoita. La cantidad de etringita cristalizada en los cementos GgB2 resultó más elevada que en los cementos GgB0, independientemente del contenido de yeso. Por otra parte, la cristalización de la stratlingita está fuertemente afectada por la cantidad de yeso añadido; de hecho, la cantidad de stratlingita disminuye al aumentar el contenido de yeso.

No sólo es importante poder cuantificar el contenido amorfo de estos materiales, sino también tratar de caracterizar y estimar su composición elemental y correlacionarla con el comportamiento de hidratación del cemento y sus propiedades mecánicas. No es posible determinar la composición química de ACn directamente por LRPD, pero se ha llevado a cabo un intento mediante RQPA y la metodología de Rietveld combinado con el factor G para descubrir la posible composición de la ACn (grupos sulfatos, silicatos, aluminatos y grupos que contienen hierro). Para este fin, se ha estudiado la evolución de los diferentes grupos de iones con el tiempo. Puesto que la cantidad de sulfatos cristalizadas en GxB2 fue mayor que en las pastas de GxB0, esto significaba que una mayor cantidad de grupos sulfatos se disolvieron, pero no cristalizaron en la última; entonces, se incorporaron principalmente en la fase (s) ACn y/o en los poros de las pastas de cemento GxB0. La cantidad de silicatos cristalizados fue mayor en GxB0 que en GxB2, donde se encontraron mayores cantidades de stratlingita. Por lo tanto, una mayor cantidad de silicatos hidratado permanecen en la fase amorfa (s) para las pastas de cementos GxB2. La cantidad de fases que contienen aluminio cristalizadas en GgB0 fue mayor que en las pastas de cemento GgB2, igualando en algunos casos el máximo, mientras que más del 30% en peso del contenido de aluminato permaneció en la fase de ACn (s) para pastas GgB2, y/o en menor medida en los poros.

Un estudio de hidratación de cementos BCSAF con diferentes fuentes de sulfato de calcio [yeso (G), basanita (B) y anhidrita (A)] también se ha llevado a cabo. En primer lugar, un estudio *in-situ* con SXPDP, se realizó para determinar el papel del tipo de sulfato de calcio (con 10% en peso) en las primeras horas de hidratación. Se determinó el grado de reacción de la ye'elimita y la etringita en G10B2, A10B2 y B10B2 a edades tempranas. Los resultados directos de RQPA se normalizaron teniendo en cuenta los datos teóricos de la muestra a 0.0 h de hidratación. Comparando los resultados teóricos con los datos RQPA directos, se puede concluir que, para la muestra G10B2, el proceso de cristalización del AFt es paralelo a la disolución de la ye'elimita, y la disolución de yeso es muy rápida. Además, G10B2 presentó un período de inducción cercano a 6 h, a partir del cual la disolución y cristalización de las fases se vuelven significativas. Para A10B2, los resultados RQPA mostraron que la cinética de disolución de la anhidrita es mucho más lenta que la del yeso o la basanita, como se esperaba. Para A10B2, la precipitación de la etringita está limitada por la disolución de la CS₂, que empieza a ser significativo a partir de 7 h.

Usando estos resultados podemos afirmar que la reactividad prevista de la ye'elimita con agua para formar AFm como principal fase hidratada no ha tenido lugar dentro de las primeras 6 h de hidratación. Nuestros resultados muestran que la disolución de la ye'elimita da etringita a pesar del hecho de que la anhidrita no se disuelve hasta 6 h. También se analizó la pasta B10B2. Debido a los requisitos experimentales (relleno de la muestra en los capilares, alineación,...), no fue posible medir los primeros ~40 min de hidratación. Debido a que la disolución de la basanita y la precipitación de yeso son procesos muy rápidos, la basanita está casi ausente y el yeso se ha cristalizado justo después de 1 h de hidratación. Las reacciones de hidratación posteriores son similares a las ya descritos para los cementos con yeso. La rápida disolución de la basanita con la precipitación de yeso, así como la lenta velocidad de disolución de la anhidrita fue cuantificada, confirmando la exactitud de la metodología utilizada.

Debido a que la basanita en contacto con agua sufre un rápido deterioro de grano (ataque intergranular) se produce un aumento del área superficial de la fuente de sulfato, y como consecuencia, una alta demanda de agua (y una alta viscosidad). Además, la precipitación de yeso primario también afectará al comportamiento reológico de la pasta. Por lo tanto, ambos parámetros, la alta demanda de agua y la precipitación de yeso aumentan la viscosidad de las pastas con basanita. Dado que nuestro objetivo es estudiar el efecto de la fuente de sulfato de calcio (incluyendo resistencias a compresión de los correspondientes morteros) es necesario tener similares comportamientos reológicos, y, en particular, similares valores de viscosidad a edades muy tempranas de hidratación. En este caso una pequeña cantidad de un superplastificante comercial (SP), basado en policarboxilato, (0,05% en peso de materia activa, referida al total de contenido de sólidos), se añadió al agua para preparar pastas que contienen basanita. Se observó una disminución considerable de la viscosidad y un comportamiento reológico similar a los preparados con yeso o anhidrita. Las principales conclusiones obtenidas de este estudio de hidratación a edades más tardías se encuentran a continuación.

En todos los casos, la fuente de sulfato se consumió antes de los 3 días de hidratación para formar etringita como principal fase cristalina hidratada. AFm y stratlingita también se encontraron en todas las pastas estudiadas pero en cantidades variables. Independientemente de la fuente de sulfato, la etringita parece ser más estable en los cementos activos (X10B2), los cuales contienen $\alpha'_H\text{-C}_2\text{S}$ y ye'elimita pseudo-cúbica, y además es casi se mantiene casi constante con el tiempo de hidratación. Por otro lado, el contenido de AFt disminuye con el tiempo en los cementos X10B0 para dar AFm. En consecuencia, a altas edades la cantidad de AFt es mucho mayor en X10B2, lo que probablemente sea responsable de las mejores propiedades mecánicas encontradas en esta familia, en comparación con los datos obtenidos para X10B0. Centrándose en la reactividad de la belita, $\beta\text{-C}_2\text{S}$

(presente en X10B0) se disuelve más rápido que $\alpha^1_{\text{H}}\text{-C}_2\text{S}$ (presente en X10B2) durante los primeros 28 días, independientemente de la fuente de sulfato, como se ha descrito anteriormente. Por otra parte, se cuantifica stratlingita cristalina en X10B0 justo después de 3 días de hidratación, pero no se detecta hasta los 28 días en las pastas de X10B2. Los análisis térmicos (DTA y TG) para las pastas G10Bx, A10Bx y B10Bx a diferentes edades de hidratación también se llevaron a cabo. A modo de ejemplo, G10B2 presenta un mayor grado de reacción a 365 días de hidratación con una mayor pérdida de peso global (~32% en peso) comparado con el valor correspondiente para G10B0 (~26% en peso). Por lo tanto, las familias X10B2 mostraron menores cantidades de agua libre (FW, *del inglés Free Water*) a edades por encima de 28 días, lo que indica un mayor grado de reacción. El análisis de los datos, a altas edades, indica que el ensamblaje de fase es poco sensible a la fuente de sulfato inicial. Los contenidos de AFt, stratlingita, katoita y AFm, entre 120 y 365 días son muy similares para G10B2 y A10B2. Comparando los resultados para G10B0 y A10B0, se detectan algunas diferencias (menores), por ejemplo, se encontraron mayores cantidades de AFm en G10B0 que en A10B0.

Un estudio SEM-EDS se realizó en las pastas X10B2 para caracterizar mejor la composición química de cada fase, especialmente para las fases amorfas/mal cristalizadas. Este tipo de estudio ayuda a estimar la composición elemental (especialmente para los átomos de Si, Al y Fe) de las nuevas fases cristalinas o amorfas que aparecen con el tiempo de hidratación, y que pueden afectar a las propiedades mecánicas. Los análisis de estas pastas hidratadas revelaron que la composición química de la fase amorfa(s) en G10B2 y B10B2 a los 120 días era muy similar, pero ligeramente más rica en silicio y hierro en A10B2. La evolución de la composición química con el tiempo puede generar información interesante. La representación de las relaciones atómicas, Al/Ca vs. Si/Ca, para la pasta A10B2 a 7 y 120 días de hidratación, muestra que partículas sin una forma definida, que podrían ser fases amorfas, son ricas en aluminio a 7 días, mientras que se enriquecen en silicio con el tiempo (120 días). El primer resultado está relacionado con los primeros productos de hidratación (AFt e hidróxido de aluminio amorfo) formados a partir de la disolución de la ye'elimita y el sulfato de calcio; el segundo con la reactividad de la belita. Por otro lado, los productos de hidratación que contienen hierro son difíciles de identificar por LXRPD. La relación atómica Al/Ca vs. Fe/Ca para la pasta A10B2 a diferentes edades (7 y 120 días) fue también estudiada. Analizando partículas con forma de aguja, que se identificaron como etringita, se encontró pequeñas cantidades de hierro. Estos resultados podrían indicar que el hierro se incorpora en la estructura cristalina de la etringita, pero se necesita más investigación para poder confirmar este hecho. Además, a 7 días la muestra presenta algunas pequeñas partículas brillantes con una composición química similar a la de la stratlingita. Sin embargo, estas partículas parecen tener un bajo grado de cristalinidad, por lo que no fueron detectadas por LXRPD a esa edad de hidratación, pero mediante el análisis

térmico, el ATD de esta muestra mostró un pequeño hombro a $\sim 170^{\circ}\text{C}$, que está relacionado con la stratlingita.

Las propiedades mecánicas de morteros estándar (de cementos activados y no activados) se prepararon con una relación cemento/arena/agua de 1/3/0.55. Para utilizar la mínima cantidad de muestra (estudios de laboratorio), se utilizaron moldes con dimensiones de $30 \times 30 \times 30 \text{ mm}^3$. Para comparar los resultados con los obtenidos utilizando los moldes que cumplen la normativa, se utilizó un factor de conversión, y los resultados se multiplicaron por 1.78.

El resultado más importante es que todos los morteros preparados con el cemento BCSAF activado desarrollaron mayores resistencias a la compresión que los morteros no activados, independientemente del tipo y la cantidad de fuente de sulfato usado. Además, aumentando el contenido de yeso de 5 a 10% en peso, la resistencia aumentó en ambos sistemas. La adición de 15% en peso de yeso produce una ligera disminución en la resistencia a la compresión, probablemente debido a la disminución de la velocidad de hidratación de la belita. Dentro de los morteros preparados con los cementos no activados, el A10B0 presentó los valores más altos. Este comportamiento puede explicarse/justificarse debido a su mayor valor de área específica y la mayor estabilidad del Aft presente en esa pasta en comparación con G10B0. Los cementos con basanita reaccionan muy rápidamente con el agua mostrando un tiempo de fraguado corto, esto conduce a morteros con bajo grado de homogeneidad. Debido a este hecho, no se midieron los valores de resistencia de los morteros B10B0. Para B10B2, aunque la adición de una pequeña cantidad de SP mejora la trabajabilidad del mortero, el retraso en el tiempo de fraguado no es suficiente para desarrollar valores de resistencia comparables con los morteros de yeso y de anhidrita.

A los 120 días, el mortero G10B2 desarrolló el valor de resistencia mecánica más alta ($68 \pm 1 \text{ MPa}$), incluso cuando la cantidad de etringita en la pasta con anhidrita era ligeramente mayor que en la pasta con yeso. Este comportamiento nos obliga a concluir que el contenido amorfo está jugando un papel clave para el desarrollo de las resistencias a edades más tardías. Además, el cemento G10B2, presentó el mayor valor de área específica ($1.8109 \pm 0.0241 \text{ m}^2/\text{g}$) de todos los cementos estudiados y esto también puede justificar los resultados obtenidos. El grado de reacción de la $\alpha'_H\text{-C}_2\text{S}$ en G10B2 (74%) es ligeramente mayor que en A10B2 (65%), que podría ayudar en la mejora de las resistencias mecánicas. La porosidad de las tres pastas de cemento activado (X10B2) a 120 días de hidratación medidas mediante porosimetría de intrusión de mercurio (MIP, *del inglés Mercury Intrusion Porosimetry*), se pueden extrapolar a los morteros. La pasta con basanita mostró el mayor porcentaje de porosidad (16%), y la de yeso el valor más bajo (10%); este comportamiento ayuda a justificar las resistencias mecánicas medidas. En conclusión,

podemos decir que **la cantidad y el tipo de sulfato óptimos** en estos sistemas parece estar cercanos al **10% en peso de yeso**, ya que es con los que se obtienen resistencias mecánicas más altas.

Finalmente, también se midió la expansión/contracción de los morteros BCSAF a diferentes edades de hidratación. El primer resultado revelado de este estudio ha sido el efecto del contenido de yeso en la estabilidad dimensional de los morteros BCSAF. La adición de 15% en peso de yeso dio los valores de expansión más altos para ambos sistemas. Los morteros G5B2 y G10B2 mostraron una variación de longitud de entre -0.01% y 0.04% en el plazo de 180 días. En segundo lugar, también se estudió el efecto de la fuente de sulfato en la estabilidad dimensional. Los morteros preparados con anhidrita presentaron los valores más altos de expansión a edades tempranas, de forma similar a los morteros de sulfoaluminato de calcio (CSA, *del inglés Calcium Sulpho-Aluminate*). Sin embargo, el mortero B10B2 mostró valores de expansión muy bajos, similares a los morteros preparados con un 5% en peso de yeso, de acuerdo con los resultados obtenidos en el estudio de hidratación, en el que la basanita se disuelve completamente antes de los primeros 45 minutos de hidratación para dar la precipitación de yeso. En consecuencia, los morteros con basanita se comportan de manera similar a los realizados con yeso a edades muy tempranas.

Por último, me gustaría resaltar que pertenezco a un grupo de trabajo que tiene una amplia experiencia en la caracterización de clínkeres y cementos anhidros por difracción de polvo de rayos X combinada con la metodología Rietveld, y en el procesamiento de materiales (cerámicos). En este punto me gustaría destacar mi contribución en la síntesis (a mayor escala) y la caracterización de clínkeres BCSAF y pastas de cemento, incluyendo la cuantificación del contenido ACn, y la medida de las propiedades mecánicas (resistencia a la compresión y cambio longitudinal) de los correspondientes morteros preparados.

CHAPTER 1

INTRODUCTION

1.1. CLIMATE CHANGE. INDUSTRIAL CO₂ EMISSIONS.

It is world widely accepted that global warming is indeed the major environmental and economic threat in our time. Mahlia (2002) and Zhang et al. (2012) confirmed that global warming is mainly caused by the emissions of GHGs connected to human activities which will result in catastrophic consequences if it is not controlled or mitigated. Progressive emissions of GHGs related to rapid industrial extension and dramatic increase of public and individual transportation have reached to an alarming level and are expected to be enlarged even at a faster rate.

Carbon dioxide is the most important and abundant GHG, where almost 61% of global CO₂ emissions are caused by industrial activities (electricity, heat generation and other industries) (IEA statistics, 2010) showing the significant impact of such processes on climate change. Although the urgent request for energy and emissions reduction is globally admitted, global industrial GHGs emissions are being rapidly increased and it is expected to be 14 Gt CO₂ by 2030 (Walsh and Thornley, 2012). Thus finding approaches to mitigate CO₂ emissions is the priority of many studies focused on reducing the threat of climate change.

Cement manufacturing has been always ranked in the list of the main sources of carbon dioxide emissions among industrial activities. The process emits around 0.9 tons of CO₂ per ton of cement produced (Hasanbeigi et al., 2010) which constitutes approximately 5-7% of the global anthropogenic carbon dioxide emissions (Chen et al., 2010). In this process carbon dioxide is mainly generated by two sources: 1) Combustion of huge amounts of mainly fossil fuels; 2) Decomposition of CaCO₃ to CaO and CO₂ as initial chemical reaction (Benhelal et al., 2012).

Portland cement concrete is the most used manufactured material in the world, and it is made primarily from water, mineral aggregates, and OPC. Nowadays annual worldwide Portland cement production is approaching 4 Gt (U.S. Geological Survey, 2014). Figure 1.1 shows the OPC production in the period 2001-2013. (www.cembureau.be). Due to the expected growth in population and global demand for concrete as the major material for construction, cement production is also anticipated to be annually enhanced by 0.8-1.2%, reaching 3.7-4.4 billion tons in 2050 (IDB, 2010). As a consequence of such significant growth in cement production, CO₂ emissions will be sharply risen up. In addition, small quantities of solid particles, SO₂, NO_x, CO, and in less percentage, chlorides, organic compounds and heavy metals are also emitted.

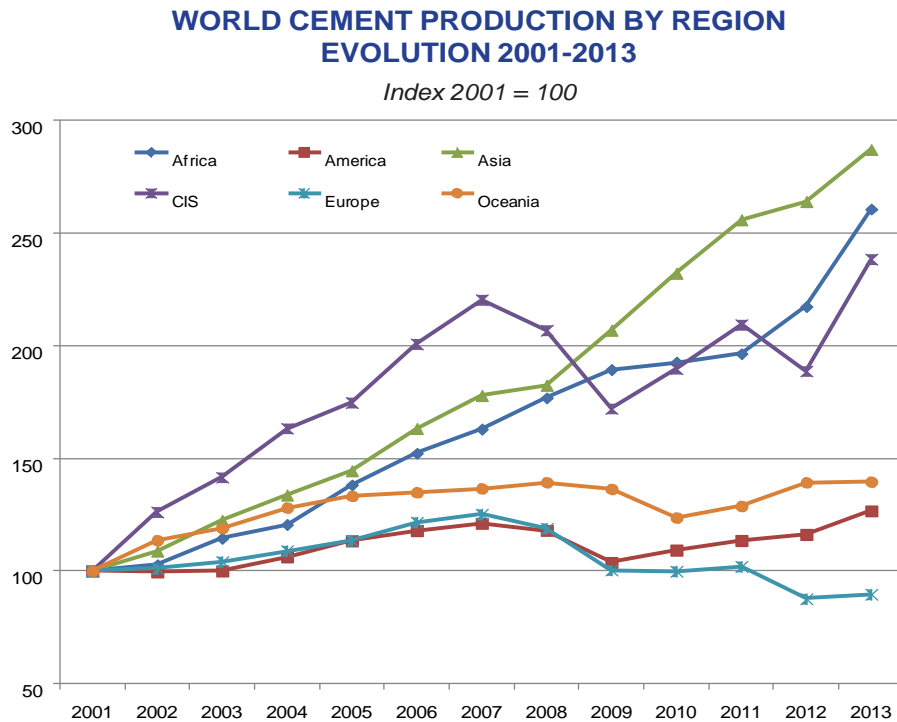


Figure 1.1. World cement production evolution (million tonnes) by region.

Due to these environmental problems, the industry of building materials is under increasing pressure to reduce the energy used in production of Portland cement clinker and mainly the associated with GHGs emissions. Moreover, Portland cement is not the ideal binder for all construction applications, as it suffers durability problems in particularly aggressive environments. Several studies have been carried out and there is a growing interest in the development, characterisation, and implementation of alternatives to Portland cements.

The design of new formulations of cements, such as belite or/and ye'elinite based cements, has some advantages and promise to be viable solutions. This will be explained below.

1.2. BELITE CEMENTS.

Belite cements contain, as main phase, belite (C_2S) in ~60 wt%, and, alite (C_3S), tricalcium aluminate (C_3A) and ferrite (C_4AF) as minor phases (Chatterjee, 2002). Belite based cements have a theoretical formation heat of ~150 kJ/kg lower than that for OPC (Stark et al., 1981). Moreover, raw materials with lower lime content can be used. Thus it helps to reduce CO_2 emissions from the decomposition of $CaCO_3$. In particular, approximately 0.50 t of CO_2 are released in the production of a ton of belite Portland cement. This means a reduction in carbon dioxide emissions of ~7% when compared to OPC (~0.97 tons of CO_2). Moreover, it is possible obtaining belite clinker at lower temperature by the additions of mineralisers (as NaF and Fe_2O_3) that contribute to the improvement of the clinker properties (Kacimi et al., 2009). This reduction in the synthesis temperature leads to additional diminutions of CO_2 emissions from fuel oxidation and lower heat loss in the kiln during cooling (Locher, 1986). In addition, belite cements give more durable concretes than OPC due to the lower alkalinity of the pastes. However, they are more difficult to grind and their hydration kinetic is slower.

1.3. YE'ELIMITE-CONTAINING CEMENTS.

Commercial ye'elimites-containing cements have been manufactured and used at large scale in China since 1970s (Zhang et al., 1999). These binders may have quite variable compositions, but all of them contain ye'elimites, also called Klein's salt, calcium sulphoaluminate or tetracalcium trialuminate sulphate (C_4A_3S) (Odler, 2000). The properties and applications of this type of binder are strongly influenced by many factors: i) chemical and mineralogical composition of the cement; ii) sulphate source (amount and type); iii) water to cement ratio (w/c); or iv) blending with other binders, for instance, OPC. Some special applications of ye'elimites-containing cements are: high strength developments at early-ages to be used in precast concrete and at moderate curing temperatures (Quillin, 2001; Glasser and Zhang, 2001), self-stressing materials (Péra and Ambroise, 2004; Georgin et al., 2008), expansive properties for shrinkage compensating concrete (Klein, 1963; Chen et al., 2012) or for radioactive element encapsulation in high-density cement pastes (Zhou et al., 2006; Cau Dit Coumes et al., 2009; Sun et al., 2011).

The interest in ye'elimites-containing cements is increasing as are eco-friendly materials because their manufacture process releases less CO_2 into atmosphere than ordinary Portland cement (Sharp et al., 1999; Gartner, 2004; Barcelo et al., 2014). This reduction depends on the composition, but it can release up to 40% less CO_2 emissions. This is described below.

1.3.1. Classification.

Although ye'elimate-containing cements are very promising, their use is limited in Europe by the few standards concerning special cements derived from non-Portland clinkers. At the present state of European standard regulations, binders based on ye'elimate-containing cements cannot be used in structural concrete according to the EN 206–1; only three formulations of CSA cements, produced by Buzzi Unicemin Trino (Italy), obtained in June 2013 a CE mark based on an ETA procedure, released by DIBt, allowing their use for structural applications (Paul et al., 2015).

There are very wide ranges of phase assemblages in ye'elimate-containing cements (Zhang et al., 1999; Quillin, 2001). These eco-cements can be classified according to the content of their main crystalline phase. Aranda and De la Torre (2013) unified the terminology used for these cements, and gathered them in three mains groups:

i) CSA: CSA cements are prepared from clinkers containing a high amount of C_4A_3S (50-80 wt%) (Sahu and Majling, 1993; Zhang et al., 1999; Older, 2000; Glasser and Zhang, 2001). These clinkers may also have minor phases such as C_2S , CT, C_4AF , CS and others. The calcium sulphate addition is very important as it may strongly affect the properties of the resulting binder (Winnefeld and Barlag, 2010; Marchi and Costa, 2011; Berger et al., 2011a; Chen et al., 2012; Bizzozero et al., 2014; García-Maté et al., 2015a). Due to the high amount of expensive aluminium source needed in their productions, CSA clinkers cannot replace OPC in massive constructions. Therefore, CSA clinkers can be prepared or partially substituted by different industrial by-products or waste materials as source of aluminium, calcium and silica (Viani and Gualtieri, 2013; García-Maté et al., 2013; Shen et al., 2014) to reduce cost but maintaining their performances. CSA clinkers show a reduction of ~37% of the CO₂ emission footprint when compared to OPC.

ii) BCSA: this term is reserved to the cements arising from clinkers containing C_2S as main phase (40-50 wt%) and intermediate C_4A_3S contents (20-30 wt%). These cements, also known as sulphobelite are a new emerging type of ye'elimate-containing cements due to their environmental benefits. The most common formulation of BCSA clinkers consists on β - C_2S , C_4A_3S and C_4AF (Janotka and Krajci, 1999; Janotka et al., 2007; Adolfsson et al., 2007). These cements are called **BCSAF**. The clinkering temperature of these clinkers is 1250-1300°C, ~200°C lower than that for OPC. In addition, BCSAF clinkers are porous, because of that can be easily ground. These cements also show a rapid hardening, excellent durability, self-stressing and volume stability, depending on the amount of gypsum added (Pera and Ambrose, 2004). These cements are being studied with the final aim of replacing OPC as the

aluminium demand is much smaller when compared to that of CSA. In addition, the production of BCSAF clinker shows a relative reduction of ~22% of the CO₂ footprint when compared to OPC manufacturing.

Other type of BCSA cements are the **BCSAA**. They have C₂S, C₄A₃S, C₁₂A₇ and CA as main phases (Martín-Sedeño et al., 2010) and they are prepared in order to further enhance mechanical strengths at very early ages. Nevertheless, the clinkering temperature should be increased (around ~100°C higher than that of BCSAF) and moreover, higher amounts of expensive bauxite (or another aluminium-rich source) are needed. Recently, a new formulation of BCSA cement which contains alite jointly with ye'elimite has been published (Liu et al., 2013). These cements are known as **BACSA** cements. Their manufacture may produce 15% less CO₂ than OPC. The reaction of alite and ye'elimite with water will develop cements with higher mechanical strengths at early ages, while belite will contribute to later values (Liu and Li, 2005; Lili et al., 2009; Liu et al., 2002; 2009; 2013). BACSA cements may contain ~40 wt% of belite, ~20 wt% of ye'elimite and ~20 wt% of alite. BACSA would overcome the problems of BCSA cements since the basicity of the pastes should be higher due to the presence of alite, and therefore, the pozzolanic effect with fly ash or slag will be promoted.

iii) **ACSA**: ACSA cements are characterized by the simultaneous presence of C₃S and C₄A₃S phases. In this special case, ye'elimite phase content may be even higher than that of alite (Li et al., 2007b). Other phases which may appear in these clinkers, in smaller amounts, are C₂S, C₄AF and C₃A (Abdul-Maula and Odler, 1992; Odler and Zhang, 1996; Zhang and Odler, 1996). However, there are inherent difficulties in the production of this type of clinker due to the differences between the optimum formation temperatures of the main phases. On the one hand, alite formation is favoured by the presence of melted phases (De la Torre et al., 2007) and at least a temperature of 1350°C is required. On the other hand, decomposition or melting of ye'elimite takes place above 1350°C (De la Torre et al., 2011a, b). However, the addition of minor quantities of fluorite (Ma et al., 2006) and other minor elements such as Mg (Liu and Li, 2005), Cu (Ma et al., 2006), Mn (Lili et al., 2009), Ti (Liu et al., 2009) or Zn (Pérez-Bravo et al., 2014) to raw materials will yield to the coexistence of these two phases by using clinkering temperatures of ~1300°C. Recently, a new (different) strategy to produce cements with alite and ye'elimite has been published (Ma et al., 2013), which consists on a two-step clinkering cycle, one to form alite at 1450°C and a second one to re-crystallise ye'elimite at 1250°C.

1.3.2. Commercial ye'elimite-containing cements.

Nowadays, there are some commercial ye'elimite-containing clinkers/cements being marketed and used *for special applications* in Europe, e.g.

S.A. Cement from Buzzi-Unicem, ALIPRE® 2009 from Italcementi Group, or CSA cement (model number 62.5, 72.5, 82.5, 92.5) from Tangshan Polar Bear Building Materials, China, among others.

An industrial trial of low energy belite-based cements was reported by Popescu et al. (2003), highlighting environmental profits of belite-rich materials and even concluded that these cements developed higher mechanical strengths than OPC at very large hydration ages (after 90 days). However, mechanical strengths at early ages resulted much lower than those of a typical OPC due to the low C_4A_3S content (~12 wt%).

In the last few years, BCSAF cements have emerged with the initial aim to substitute OPC. An industrial trial, ~2500 tons of BCSAF, was carried out in 2011 by Lafarge under the AETHER™ project (<http://www.aether-cement.eu/>) (Walenta and Comparet, 2011). Clinkering was performed in a Portland industrial kiln but using lower operating temperatures (1225-1300°C), reducing CO₂ emissions by 25-30% in comparison with CEM (I) type OPC cement. The temperature in the clinkering zone resulted to be a key parameter, as too high temperatures may give kiln blockage, loss of grindability and C_4A_3S decomposition with high SO₂ emissions, and too low temperatures gave under burnt binder with high free lime and $C_{12}A_7$ contents. The optimum clinkering temperature resulted much lower in NO_x emissions than those for OPC, due to the lower burning temperature, and SO₂ emissions resulted at the same level than for OPC production.

The main technological disadvantage of these cements is related to their low mechanical strengths developed at very-early ages due to the slow hydration of belite. However, this problem is being overcome by the activation of belite and the presence of high amounts of ye'elite (Gartner and Li, 2006; Cuberos et al., 2010; Morin et al., 2011). The production of aBCSAF cements involves the stabilization of highly reactive C_2S polymorphs, i.e. β -modified form and α -forms, as they react faster with water. aBCSAF cements have been patented by Lafarge (Gartner and Li, 2006; Morin et al., 2011). They show ~20-30 wt% of Klein's salt and α -forms of belite, the latter due to addition of minor elements, such as B₂O₃ and Na₂O. These minor elements promoted the stabilisation of α' -forms of belite and the distortion of β -form. aBCSAF with 2.0 wt% of B₂O₃, added as borax, developed comparable compressive strengths to those of OPC. The role of belite polymorphs is explained in detail in section 1.4.3. This material developed mechanical strengths of 25 MPa at one hydration day and the strengths were even better than those developed by type I 52.5 OPC after 7 days (Walenta and Comparet, 2011).

1.4. BELITE CALCIUM SULPHOALUMINATE CEMENTS (BCSA).

Belite calcium sulphoaluminate cements are environmentally friendly cements for several reasons, including the low amount of limestone required to achieve the desired composition. Table 1.1 shows the lime contents of the main phases present in BCSAF clinkers and C_3S , present in OPC. C_3S shows the highest lime amount and requires the highest formation temperature. The substitution of alite by belite reduces the limestone demand and temperature of cement manufacturing, thereby reducing CO_2 emissions and energy consumption while maintaining satisfying long-term properties. However, that substitution compromises the early-age strength development because C_2S reacts slower than C_3S . This renders the high- C_2S cement unusable in nearly any field related to structural applications. However, this is partially compensated by the presence of a fast reacting calcium sulphoaluminate phase (ye'elimate) in these BCSA cements (Mehta, 1980). This phase, that was described by Alexander Klein in 1963 as an additive to Portland cement to make expansive cements, has the lowest lime content of any of the cement phases reported in Table 1.1.

Table 1.1. Lime content for different cement phases (Mehta, 1980).

Cement Phase	Lime Content (wt%)
C_2S	65.1
C_4A_3S	36.7
C_4AF	46.2
C_3S	73.7

Raw meal formulations for BCSA clinkers have been discussed extensively in the literature (Gartner and Li, 2006; Idrissi et al., 2010, 2012; Martín-Sedeño et al., 2010; Cuberos et al., 2010). However, due to environmental and cost concerns, BCSA cements are mostly produced by combining natural and industrial waste materials to provide the necessary CaO , SiO_2 , Al_2O_3 and SO_3 amounts required for each phase formation. The addition of waste materials in the raw mixtures to produce BCSA clinkers also has been investigated (Arjunan et al., 1999; Katsioti et al., 2006; Phair, 2006; Seluck et al., 2010; Yang et al., 2013; Ma et al., 2014a). For example, Yang et al. (2013) studied the use of the phosphate fertilizer industry waste products as raw materials to prepare BCSAF cements with similar performances to those obtained by using common grade raw materials. This material is not only an iron source but also supplies silicon, aluminium and sulphur to reduce burning temperature.

Other authors (Strigac et al., 2000) studied the composition of ferrite phase in BCSA cement and showed that this phase formed a solid solution and accommodated some SiO_2 . It is also known that the actual composition of the ferrite phase solid solution can range from C_4AF to C_6AF_2 . $\text{C}_4\text{A}_3\text{S}$ accommodated some SiO_2 and up to 2% of Fe_2O_3 . C_2S can accommodate minor elements such as sulphur or alkaline (Ghosh et al., 1979) and on the other hand, CS forms more homogenous compositions with minor substitute ions.

In the last decade, the research in the preparation of BCSAF clinkers has increased (De la Torre et al., 2011a, b; Chen et al., 2011). A recent study (Bullerjahn et al., 2014) proved that iron-rich BCSA contains ye'elimite with significant amounts of iron stabilizing the cubic form and enhancing its hydration rates. Moreover, they stated that ternesite ($\text{C}_5\text{S}_2\text{S}$) was formed under certain clinkering conditions and it was found to be hydraulically active. In addition, stoichiometric $\text{C}_4\text{A}_3\text{S}$ is orthorhombic at room temperature (RT) (Calos et al., 1995; Cuesta et al., 2013). However, it can form solid solution with Na^+ , B^{3+} , Si^{4+} and/or Fe^{3+} , among other elements, to restore the pseudo-cubic symmetry (Saalfeld and Depmeier, 1972; Cuesta et al., 2014c).

Sokol et al. (2014) have recently reported natural ye'elimite-larnite rocks found in the Hatrurim formation of Negev Desert, Israel, which mineralogical compositions are similar to BCSA clinkers. Their mineralogy consists on 35-50 wt% β - C_2S , 15-20 wt% $\text{C}_4\text{A}_3\text{S}$, 7-15 wt% ferrites, and 15–20 wt% fluorapatite and/or fluorellestadite. This study concludes that chalky and/or marly sediments with randomly distributed clay, phosphorite, and gypsum may be used as cheap naturally homogenised and pulverised mixtures for industrial production of BCSA cement clinkers.

1.4.1. Reduction of CO_2 emissions.

Carbon dioxide emissions in the cement industry can be classified in two main categories: those coming from raw materials and those from the operation processes. Figure 1.2 depicts in detail the CO_2 emissions released during the manufacturing of both a typical BCSAF clinker (50 wt% of C_2S , 30 wt% of $\text{C}_4\text{A}_3\text{S}$, and 20 wt% C_4AF) and OPC (65 wt% of C_3S , 15 wt% of C_2S , 10 wt% of C_3A and 10 wt% of C_4AF). Considering all emissions together, the production of one ton of OPC clinker releases a maximum of 0.97 t of CO_2 ; however the production of one ton of BCSAF clinker leads to a reduction of ~22%, which will depend on the composition.

On the one hand, the generation of CO_2 from decarbonation of raw materials for different minerals was calculated by Gartner (2004). For example, RMCO_2 values for $\text{C}_4\text{A}_3\text{S}$, C_2S and C_4AF resulted to be 0.216, 0.511 and 0.362, respectively. However,

the value for C_3S (major phase of OPC), is much higher, 0.578 (Gartner, 2004). According to these values, CO_2 emissions released during clinkering of 1 ton of BCSAF and OPC are 0.54 t and 0.39 t, respectively (figure 1.2). It implies a reduction of 0.15 tons of CO_2 for BCSAF due to raw material decomposition.

On the other hand, CO_2 emissions derived from operation processes are directly related to the type of processing equipment and the specific chosen fuel. Gartner in 2004 estimated 0.30 t of CO_2 per ton of clinker produced assuming that good quality of bituminous coal is used and taking into account energy efficiency of modern kilns. The reduction in CO_2 emissions coming from fuel burning can be achieved by different strategies (Gartner, 2004; Juenger et al., 2011) including the reduction of clinkering temperature. This is the case of BCSAF clinkers where the operating temperature can be reduced down to $150^\circ C$ with a concomitant reduction of up to 0.04 t of CO_2 per ton of BCSAF clinker produced. Moreover, emissions derived from electricity consumption are about 0.09 t of CO_2 per ton of OPC (McCaffrey, 2002). The lower firing temperatures needed for BCSAF clinkering make it easier to be ground, hence it yields a depletion of up to 0.02 t of CO_2 emissions.

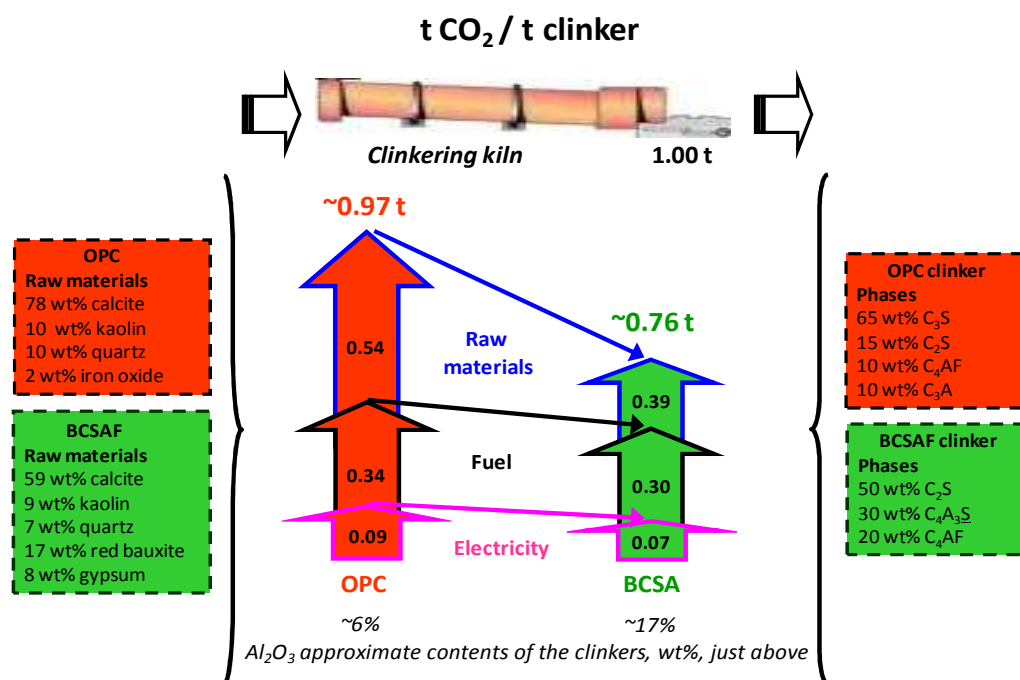


Figure 1.2. Comparison of OPC and BCSAF production CO_2 footprint.

1.4.2. Crystallochemistry of main anhydrous phases of BCSAF cements.

The crystallography of the main anhydrous phases present in BCSAF cements (belite, ye'elinite and ferrite) is described.

i) Belite or dicalcium silicate [Ca_2SiO_4 , C_2S].

Belite is of great interest in BCSAA and BCSAF cements as it is their main component (~60 wt%). Stoichiometric dicalcium silicate presents five forms (Mumme et al., 1996) γ , β , α'_L , α'_H and α . On the other hand, element substitutions stabilize different structures of dicalcium silicate and β - C_2S is the form that commonly prevails in OPC, BCSAF and BCSAA without any activation. All the structures are built from Ca^{2+} and SiO_4^{4-} ions. The arrangements of these ions are closely similar in α , α'_L , α'_H and β polymorphs, but that in γ - C_2S is somewhat different. γ - C_2S is much less dense than the other polymorphs. These polymorphic transformations, as a function of temperature, are shown in Figure 1.3. The physical and chemical properties of these phases can be altered by introducing defects or strains in their crystalline structures. Moreover, these defects can even stabilize high-temperature forms of C_2S at room temperature (Ghosh et al., 1979; Nettleship et al., 1992). The different type of defects can be produced by the addition of foreign elements to form solid solutions (Jelenic et al., 1978) or by specific thermal treatments (Fukuda and Ito, 1999). There are many studies concerning the chemical-stabilization of β - C_2S by foreign ions such as SO_3 , B_2O_3 , Cr_2O_3 , Na_2O , K_2O , BaO , MnO_2 and Al_2O_3 (Pritts and Daugherty, 1976; Kantro and Weise, 1979; Matkovic et al., 1981; Fierens and Tirlocq, 1983; Ziemer et al., 1984; Benarchid et al., 2004; Cuesta et al., 2014b).

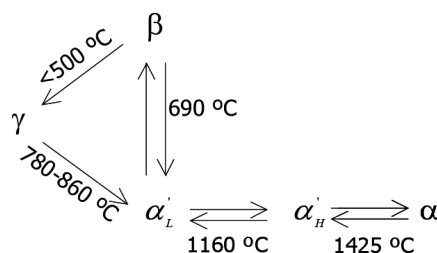


Figure 1.3. Dicalcium silicate polymorphic transformations with temperature.

These investigations showed that the hydration reactivity of stabilized β - C_2S depends on the preparation parameters that influence particle and crystallite size. These parameters include temperature, type and amount of stabilizer, and fineness of the final ground. The stabilization of α' -forms through the introduction of foreign

oxides, such as MgO, P₂O₅, K₂O, BaO, Na₂O, B₂O and SO₃ has also been studied (Bensted, 1979; Fukuda et al., 2001; Park, 2001; Morsli et al., 2007a, b; Li et al., 2007a; Wesselsky and Jensen, 2009; Cuberos et al., 2010; Morin et al., 2011; Cuesta et al., 2012). These works stated that hydraulic properties were increased when compared to the materials without foreign ions.

Table 1.2 shows the crystallographic information of dicalcium silicate polymorphs. The crystal structures of α'_H , α'_L and β phases are derived from that α form by progressive decreases in symmetry, which arise from changes in the orientations of the SiO₄⁴⁻ tetrahedral and small movements of Ca²⁺ ions (Taylor, 1997). Such structures belong to the family of the glaserite, K₃Na(SO₄)₂ (Moore, 1973). However, the γ -C₂S framework belongs to the olivine type structure (O'Daniel and Tescheischwili, 1942).

Tabla 1.2. Crystallographic data of dicalcium silicate polymorphs.

Polymorph	Space Group	Unit cell parameters			β (g)	V/Z (Å ³)	T(°C)/ Stabilizer	ICSD
		a (Å)	b (Å)	c (Å)				
α	P6 ₃ /mmc ^a	5.420	5.420	7.027	90.0	89.4	-	81099
	P6 ₃ /mmc ^b	5.532(9)	5.532(9)	7.327(11)	90.0	97.1	1545/-	82998
	P-3m1 ^b	5.532(9)	5.532(9)	7.327(11)	90.0	97.1	1545/-	82999
α'_H	Pnma ^a	6.7673(4)	5.5191(4)	9.3031(6)	90.0	86.9	-/5% (molar) Ca ₃ (PO ₄) ₂	81097
	Pnma ^b	6.871(0)	5.601(0)	9.556(1)	90.0	92.0	1250/-	82997
	Pmnb ^c	5.647(1)	7.037(1)	9.644(2)	90.0	95.8	-	49662
	Pnma ^d	6.8263(3)	5.4684(3)	9.2658(4)	90.0	86.5	/Ca _{1.8} Sr _{0.2} SiO ₄ RT/ B ₂ O ₃ and Na ₂ O	-
α'_L	Pna2 ₁ ^b	20.527(2)	9.496(1)	5.590(1)	90.0	90.8	1060/-	82996
	Pna2 ₁ ^d	20.863(2)	9.5000(8)	5.6005(5)	90.0	92.5	-/ Ca _{0.84} Sr _{1.16} SiO ₄	39203
	P2 ₁ cn ^e	5.566	9.355	20.569	90.0	89.3	-	39100
β	P2 ₁ /n ^a	5.512(0)	6.758(0)	9.314(0)	94.6	86.5	-/0.5 wt% Cr ₂ O ₃	81096
	P2 ₁ /n ^f	5.48(2)	6.76(2)	9.28(2)	85.5	85.7	-	24640
	P2 ₁ /n ^g	5.502(1)	6.745(1)	9.297(1)	94.6	86.0	-	963
	P2 ₁ /n ⁱ	5.5127(1)	6.7586(1)	9.3266(2)	94.5	86.6	RT/Al ₂ O ₃	-
γ	Pbnm ^a	5.082(0)	11.224(0)	6.764(0)	90.0	96.5	-	81095
	Pbnm ^h	5.081(2)	11.224(5)	6.778(10)	90.0	96.6	-	200707

(a) Mumme et al., 1995; (b) Mumme et al., 1996; (c) Catti et al., 1984; (d) Cuesta et al., 2012; (e) Il'inets and Bikbau, 1990; (f) Udagawa et al., 1979; (g) Midgley, 1952; (h) Jost et al., 1977 ; (i) Cuesta et al., 2014b; (j) Udagawa et al., 1980.

Figure 1.4 shows the simulated diffractograms of different C_2S polymorphs. The presence of ions in the structure stabilizes the high temperature forms at RT. The stabilization of the high temperature polymorph is due to both ionic substitutions and quenching. It has been found the existence of α and α'_H forms in clinkers (Regourd and Guinier, 1974; Morsli et al., 2007a, b).

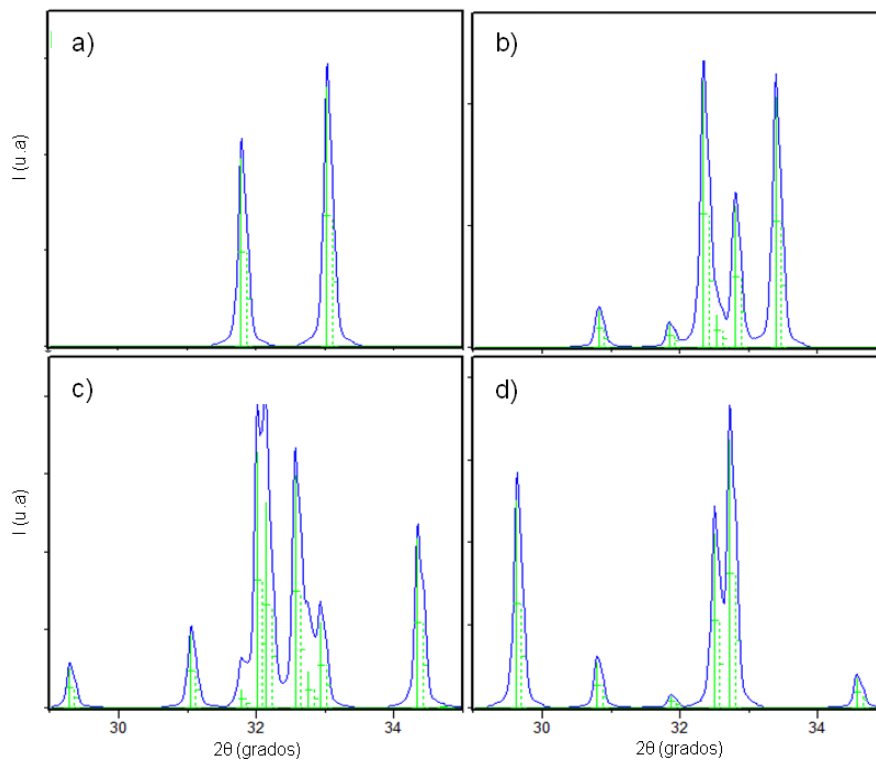


Figure 1.4. Range from 29 to 35° (2θ) of the theoretical diffractograms. (a) α - C_2S at RT (Mumme et al., 1995); (b) α'_H - C_2S at RT (Cuesta et al., 2012); (c) β - C_2S at RT (Mumme et al., 1995) and (d) γ - C_2S at RT (Udagawa et al., 1980).

ii) Ye'elimite, also named Klein's salt or calcium sulphoaluminate, $[Ca_4Al_6O_{12}(SO_4)_2C_4A_3S]$.

Ye'elimite is the major mineralogical compound in CSA cements. It is liable for high mechanical strengths at early hydration ages. Stoichiometric calcium sulphoaluminate or ye'elimite, can be described as a sodalite ($M_4[T_6O_{12}]X$) where $M=Ca$, $T=Al$, and $X=SO_4$, and crystallizes as a tectoaluminosilicate sodalite structure

(Cuesta et al., 2013). This structure was first analyzed by Hanstead and Moore (1962) using X-ray powder diffraction. Wang et al. (1990) and Saalfeld and Depmeier (1972) reported atomic parameters for a cubic crystal structure with space group I-43m and $a=9.195 \text{ \AA}$. In 1995, Calos published an orthorhombic crystal structure, Pcc2 space group, which has been revised by joint neutron and X-ray powder diffraction, Rietveld refinement and atomistic calculations (Cuesta et al., 2013). Recently, the disordered crystal structure of cubic stoichiometric ye'elimite at 800°C has been satisfactorily studied in the I-43m space group using a split-atom model (Kurokawa et al., 2014). In a recent study (Bullerjahn et al., 2014) the existence of two polymorphs of ye'elimite (pseudo-cubic and orthorhombic) was observed in BCSA cements. Published crystallographic data for the Klein's salt are shown in Table 1.3. Fe-Si-doped ye'elimite shows a pseudo-cubic structure at room temperature and suffers a phase transition on heating (Cuesta et al., 2014c).

Table 1.3. Crystallographic data of Klein's salt polymorphs.

Polymorph	Space Group	Unit cell parameters				V/Z (\AA^3)	Ref. bibl.	ICSD
		a (\AA)	b (\AA)	c (\AA)	β ($^\circ$)			
Cubic	I-43m	9.205	9.205	9.205	90.0	390	(a)	9560
Orthorhombic	Pcc2	13.028	13.037	9.161	90.0	389	(b)	80361
Tetragonal	P-4c2	13.031	13.031	9.163	90.0	389	(c)	-
Cubic	I-43m	9.197	9.197	9.197	90.0	389	(d)	-
Orthorhombic	Pcc2	13.036	13.035	9.168	90.0	346	(e)	-
Cubic at 1073 K	I-43m	9.253	9.253	9.253	90.0	396	(d)	-
Cubic at 1073 K	I-43m	9.243	9.243	9.243	90.0	395	(f)	-

(a) Saalfeld y Depmeier, 1972; (b) Calos et al., 1995; (c) Zhang et al., 1992; (d) Cuesta et al., 2014c; (e) Cuesta et al., 2013; (f) Kurokawa et al., 2014.

Figure 1.5 shows the simulated patterns of two of the $\text{C}_4\text{A}_3\text{S}$ polymorphs (orthorhombic and pseudo-cubic). As seen in this figure, all the peaks of the pseudo-cubic structure are also present in the orthorhombic form. We highlight that the RT pseudo-cubic form is not a strict ye'elimite polymorph as it required the presence of dopants within the crystal structure.

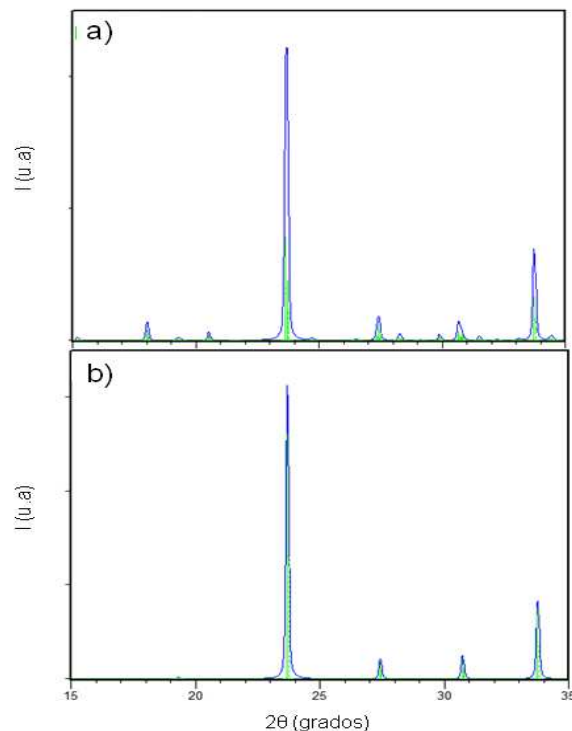


Figure 1.5. Region 15° to 35° (2θ) of the theoretical diffractograms, (a) stoichiometric (orthorhombic) C_4A_3S (Cuesta et al., 2013); (b) doped (pseudo-cubic) C_4A_3S (Cuesta et al., 2014c).

iii) Brownmillerite or tetracalcium aluminoferrite, $[Ca_2(AlFe)O_5, C_4AF]$.

The term “ferrite” usually refers to a solid solution with a wide range of compositions of the general formula $Ca_2(Al_xFe_{2-x})O_5$, where x can vary from 0 to about 1.33. The compound C_2F has an orthorhombic primitive lattice, with space group $Pnma$ (Taylor, 1997). This symmetry is preserved when aluminium substitutes iron up to $x \sim 0.4$ – 0.6 . The insertion of additional aluminium leads to a modification of the structure to an orthorhombic, body-centred phase termed brownmillerite with space group $Ibm2$. The solid solution is complete when x is up to ~ 1.4 at 1250 – $1300^\circ C$, although, as the substitution of Fe(III) by Al is not ideal, gradual symmetry changes occur. Four compositions are generally taken as reference points in this extensive solid solution, namely C_2F , C_6AF_2 , C_4AF (brownmillerite) and C_6A_2F , corresponding to $x = 0$, $2/3$, 1 and $4/3$, respectively. Typical elemental composition of this phase in a clinker is: 46.1 wt% of CaO , 21 wt% of Al_2O_3 and 32.9 wt% of Fe_2O_3 , it is equivalent to $x \sim 1$. In cement chemistry the ideal composition C_4AF

($4\text{CaO}\cdot\text{Al}_2\text{O}_3\cdot\text{Fe}_2\text{O}_3$), is used to describe the ferrite phase in Portland cement, in full awareness that other elements may be present and that the A/F ratio is commonly not unity (Ectors et al., 2013). Table 1.4 gives the crystallographic data of C_4AF structures.

Table 1.4. Crystallographic data of ferrite phase polymorphs ($\text{Ca}_2\text{Al}_x\text{Fe}_{2-x}\text{O}_5$).

Space Group	Z	Unit cell parameters			V/Z (\AA^3)	x	ICSD
		a (\AA)	b (\AA)	c (\AA)			
Pcmn ^a	4	5.559	14.771	5.429	111.5	0.0	14296
Ibm2 ^b	4	5.584	14.600	5.374	109.5	1.0	9197

(a) Colville, 1970 y (b) Colville y Geller, 1971

The coexistence of $\text{C}_4\text{A}_3\text{S}$ and ferrite solid solution was investigated (Juenger and Chen, 2011; Touzo et al., 2013) and some iron content, up to 4.3 mol% (=8.8 wt%), was found in the $\text{C}_4\text{A}_3\text{S}$ phase which coexists with melt and ferrite phase. However, at high overall iron contents, it is difficult to avoid (i) formation of excessive amounts of liquid phase, (ii) rather rapid development of a very fluid melt over a short range of temperatures, (iii) formation of other iron bearing phases such as monocalcium ferrite in iron-rich compositions, (iv) progressive replacement with increasing iron content of $\text{C}_4\text{A}_3\text{S}$ by CaSO_4 as sulphate-containing solid. These factors, taken together, suggest that the control of the Al/Fe ratio may well be a key parameter in optimising sulphoaluminate clinker production.

1.4.3. Reactivity of principal constituents of BCSAF cements during hydration.

Once the main anhydrous phases present in BCSAF cements are described, it is essential to know the evolution of those phases during the hydration, and the properties of the new formed phases. During the hydration process (Sahu et al., 1991), three main issues take place: (i) the dissolution of crystalline anhydrous phases; (ii) the appearance of new phases; and (iii) the consumption of free water.

Overall, the hydration of BCSAF cements can be summarized as follow. During early age hydration, ettringite is the main crystalline hydration product together with aluminium oxide hydrate gel, commonly reported as amorphous gibbsite (AH_3 , although its stoichiometry is still not well described). Ettringite is formed in these cements from the dissolution of ye'elimite and calcium sulphate. Once the sulphate source is depleted and there is enough water available, monosulphate (AFm) is formed (Winnefeld and Lothenbach, 2010). However, there are some contradictory results concerning the reactivity of ye'elimite with water in

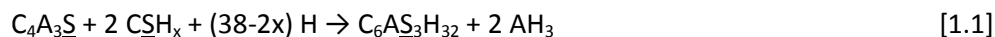
absence of sulphate. In addition, hydration kinetics not only depend on the water-cement (w/c) ratio and the solubility of the additional sulphate source, but also on the polymorphism of ye'elimite and the presence of foreign ions incorporated into the ye'elimite crystal structure (Cuesta et al., 2014a). It should be noted that the hydration of a phase within the cement matrix, does not have to exhibit the same behaviour as when hydration of an isolated phase is studied.

Furthermore, and independently of the kinetic of the reaction, C₂S may yield stratlingite (C₂ASH₈) or amorphous C-S-H gel and portlandite (CH). Finally, the reactivity of ferrite (C₄AF) during hydration in these cements is slower than that of C₄A₃S and it is not well understood. If the calcium concentration increases as a consequence of C₂S hydration, ferrite can take part of the formation of katoite or siliceous hydrogarnet.

In the cement, all the anhydrous phases do not have the same reactivity. The hydration of phases of interest in BCSAF cements is discussed just below:

C₄A₃S (Ye'elimite):

It is considered the most reactive phase of BCSA cements (Palou and Majling, 1996, 1997; Canonico and Bernardo, 2006; Zhang and Li, 2007). As soon as water is added to the cement, both ye'elimite and the sulphate source (gypsum, bassanite and/or anhydrite) start to get dissolved. Immediately after wetting, the following reaction takes place:



This reaction [1.1] corresponds to the formation of ettringite (C₆AS₃H₃₂), as main crystalline hydration product, and amorphous AH₃; the former contributes to the early-age strength development. The formation of ettringite will continue while calcium sulphate is present. Once the sulphate source is depleted and there is enough free water available, monosulphate also known as AFm (C₄ASH₁₂) (Glasser and Zhang, 2001; Winnefeld and Lothenbach, 2010) is formed according to equation [1.2].



These two reactions may take place in the early hydration of CSA and BCSA cements. However, there are some contradictory results concerning the reactivity of ye'elimite with water in the absence of another sulphate source. Some authors stated that only reaction [1.2] takes place (Winnefeld and Barlag, 2010), while others

have published that mixture of AFt and AFm phases are produced (Berger et al., 2011a).

As an example, Figure 1.6 shows the cryo-scanning electron microscopy micrographs of BCSAF pastes. BCSAF cement pastes with 20 wt% of gypsum (Figure 1.6.a) showed acicular-hexagonal AFt crystals even at very early hydration ages, reaction [1.1]. Conversely, BCSAF cement pastes with (only) 5 wt% of gypsum (Figure 1.6.b) showed, in addition to AFt crystals, thin-layered AFm crystals, due to reaction [1.2].

The influence of the polymorphism of C_4A_3S on hydration was recently studied by Cuesta et al. (2014a). In the absence of additional sulphate sources, stoichiometric-ye'elimite (orthorhombic) reacts slower than doped-ye'elimite (pseudo-cubic), and AFm-type phases are the main hydrated crystalline phases. Moreover, doped-ye'elimite produces higher amounts of ettringite than stoichiometric-ye'elimite. However, in the presence of additional sulphates, stoichiometric-ye'elimite reacts faster than doped-ye'elimite.

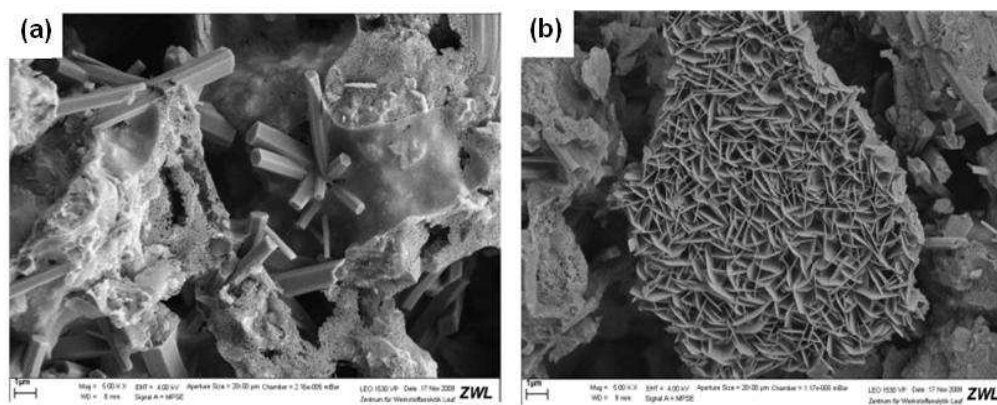


Figure 1.6. Cryo-SEM photographs of BCSAF cement pastes after 4 h of hydration for (a) 20 wt % of gypsum and (b) 5 wt % of gypsum (Cuberos et al., 2010).

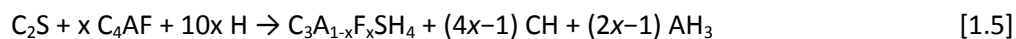
Hargis et al. (2014b) studied the influence of gypsum, calcite, and vaterite during the ye'elimite hydration in six calcium sulphoaluminate-based cementitious systems. Moreover, vaterite was more effective than calcite in mitigating the compressive strength loss. The expansion was reduced by calcite and vaterite, irrespective of the presence of gypsum.

C₂S (Belite):

C₂S hydration is of special interest in BCSA cements and its hydration kinetics seems to depend on its type of polymorph. Thus, α-forms of belite are considered more reactive than β-C₂S (Jelenic et al., 1978; Chatterjee, 1996). Nevertheless, it should be noted that the presence of sulphate in the belite structure or the chemical environment (high or low available amorphous aluminum hydroxide content) may enhance its reactivity due to the enlargement of its specific surface and/or occurrence of crystal distortions (Gies and Knofel, 1987; Martín-Sedeño et al., 2010). Different hydration products, C-S-H gel (Odler, 2003) and stratlingite (Andac and Glasser, 1999) have been identified during the hydration of this phase. According to the distinct hydrates, two chemical reactions (equations [1.3] and [1.4]) are proposed. The hydration of belite to form both amorphous gel C_vSH_x and portlandite corresponds to reaction [1.3]. However in BCSA pastes, belite coexists with aluminium rich amorphous hydrates and the formation of an AFm-type phase called stratlingite is favoured (Palou et al., 2005; Cuberos et al., 2010; Gartner and Macphee, 2011; Santacruz et al., 2015) (reaction [1.4]). Then, C₂S consumes the amorphous AH₃ formed by the hydration reactions of aluminium-rich phases. The presence of stratlingite was confirmed by XRPD and DTA techniques by several researchers (Cuberos et al., 2010; Aranda et al., 2011; Morin et al., 2011), and likely play an important role in the advanced-ages mechanical strengths as it is produced at a larger pace when high temperature polymorphs of belite are present.



Other reactions need to be taken into account. Some studies have confirmed the presence of katoite phases, also known as siliceous hydrogarnet. When the calcium concentration increases, ferrite phase can take part of the formation of this katoite by the following equation:



Reaction [1.5] justifies the formation of portlandite, which is not detected by XRPD or DTA, through the consumption of ferrite. Consequently, this portlandite may be consumed by stratlingite as follows, producing larger quantities of katoite:



Katoite may provide with durability to these corresponding mortars and concretes as portlandite is consumed.

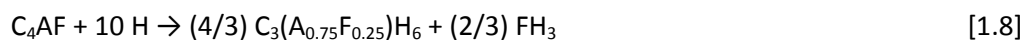
C₄AF (Ferrite phase):

Ferrite phases present in sulphaaluminate cements show many compositions (different concentrations of Si, Ti and Mg) (Drabik et al, 1987). C₄AF was found "more reactive" in BCSAF during hydration than that present in OPC (Sharp et al., 1999), likely due to the lower clinkering temperature. However, the hydration of ferrite in CSA cements was found much slower than C₄A₃S̄ (Kasselouri et al., 1995).

In the absence of any other phases, the hydration of brownmillerite appears to be similar to the hydration of the iron-free C₃A, in which a C-A-H gel first coats the C₃A grains from which metastable hexagonal C-A-H plates develop within 10 min (Jupe et al., 1996; Meredith et al., 2004). However, the hydration products are (quite often) assumed to incorporate some iron (Rogers and Aldridge, 1977; Fukuhara et al., 1981; Older, 1998; Meller et al., 2004b). The hydration of pure brownmillerite with water initially forms metastable C-(A,F)-H hydrates (hydroxy-AFm), possibly in a C-(A,F)-H gel (Meredith et al., 2004). These metastable C-(A,F)-H hydrates eventually convert to a hydrogarnet-type phase C₃(A,F)H₆ (katoite) over time (Ectors et al., 2013). The exact Al/Fe ratios of the hydrogarnets are as yet under debate but it is generally accepted that the Al/Fe ratio of the crystalline products is greater than in C₄AF itself (Meller et al., 2004a). The hydration of brownmillerite (Meller et al., 2004b) could be written formally as:



In this equation, FH₃ denotes a hydrated amorphous Fe-containing gel. If iron is incorporated into the hydrogarnet product by consumption of the CH produced, then the reaction could be expressed as:



The addition of calcium sulphates to C₄AF inhibits the direct hydration of C₄AF to hydroxy-AFm or C₃(A,F)H₆. In this case, ettringite is the most commonly hydration product observed. There are some theories about the exact mechanism governing the retardation process (Ectors et al., 2013). In the presence of sulphate the simplest (i.e. no Fe-solid solution) scheme is:



In turn, ettringite could decompose to an AFm monosulfoaluminate hydrate as stated next:



The gypsum released can react with any remaining C_4AF to form further AFm (C_4ASH_n) with overall stoichiometry:



However, the hydration process involving iron-containing phases may be more complex, as the formation of solid solutions between Fe- and Al-containing hydrates may stabilize mixed solids, such as Fe-AFt (Möschner et al., 2009) and Fe-AFm (Dilnesa et al., 2012).

1.4.4. Crystallochemistry of main hydrated phases of BCSAF cements.

i) Ettringite or AFt phase.

AFt is the abbreviation for "alumina, ferric oxide, tri-sulfate" or (Al_2O_3 - Fe_2O_3 -tri). It represents a group of calcium sulfoaluminate hydrates and has the general formula $[Ca_3(Al,Fe)(OH)_6 \cdot 12H_2O]_2 \cdot X_3 \cdot nH_2O$, where X represents a doubly charged anion or, sometimes, two singly charged anions. Ettringite is the most common and important member of the AFt group and, in this case, X denoting sulfate ($X=SO_4^{2-}$). The crystal structure of ettringite can be described as compact columns of $[Ca_3Al(OH)_6 \cdot 24H_2O]^{3+}$, running parallel to the c-axis, with $3SO_4^{2-}$ and H_2O molecules in the intervening channels. Figure 1.7 shows a revised structure model of ettringite presented by Goetz-Neunhoeffer and Neubauer (2006).

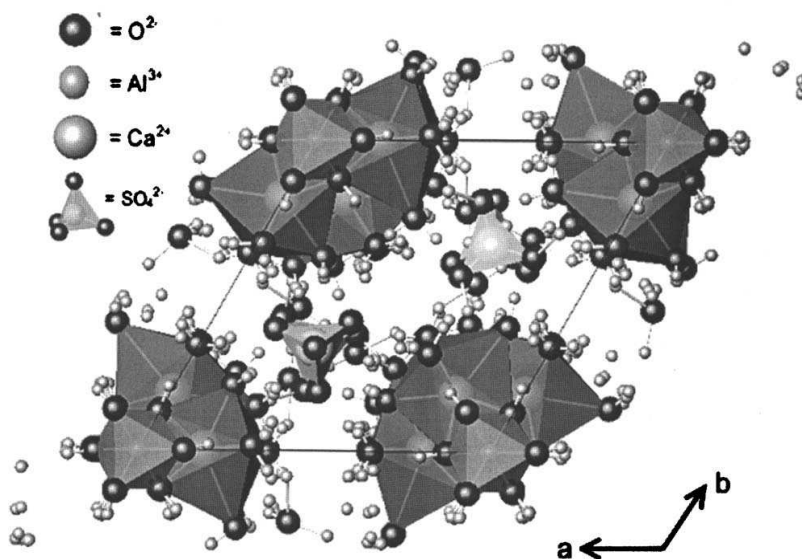


Figure 1.7. Hexagonal ettringite unit cell of the revised structure projected down c. (Goetz-Neunhoeffer and Neubauer, 2006).

ii) AFm phases.

Phases in this family ($\text{Al}_2\text{O}_3\text{-Fe}_2\text{O}_3\text{-mono}$) are comprised of a layer structure with the general formula $[\text{Ca}_2\text{Al}(\text{OH})_6]\text{X}\cdot x\text{H}_2\text{O}$ where X denotes one formula unit of a singly charged anion, (for instance OH^- or $[\text{SiAlO}_2(\text{OH})_4]^-$ in the case of stratlingite, or half a formula unit of a doubly charged anion (for instance SO_4^{2-}) placed in the interlayer space jointly with water molecules. These compounds crystallize in hexagonal planes and are very relevant to cement hydration. AFm are formed from aluminium rich phases, such as $\text{C}_4\text{A}_3\text{S}$, when the sulphate source (gypsum, bassanite or anhydrite) is depleted and there is enough free water available (Winnefeld and Lothenbach, 2010). The presence of AFm-phases with different layer spacing is justified twofold: i) by the partial anion replacement $\text{OH}^-/\text{SO}_4^{2-}$ within the layers; and ii) by the progressive release of the water molecules as a consequence of the hydration of other phases. Stratlingite (Rinaldi et al., 1990), kuzelite (Allmann, 1977) or C_2AH_8 are AFm-type phases. There are other AFm-type phases such as monocarbonates (François et al., 1998) or monochlorides (Renaudin et al., 1999) that usually appear in chemically aggressive environments.

Stratlingite:

$\text{Ca}_4\text{Al}_2(\text{OH})_{12}[\text{AlSiO}_2(\text{OH})_4]_2\cdot 2\text{H}_2\text{O}$, is an AFm phase which appears as hydration product of aluminium-rich cements, such as calcium aluminate, calcium sulfoaluminate and also belite calcium sulfoaluminate cements. The structure of stratlingite is known from single crystal studies of mineral fragments from Mayern and Montalto di Castro (Rinaldi et al., 1990). It is formed by a principal octahedral or brucite-type layer, $[\text{Ca}_2\text{Al}(\text{OH})_6\cdot 2\text{H}_2\text{O}]^+$ with a full occupancy, and a double tetrahedral layer, $[(\text{T},\square)_4(\text{OH},\text{O})_8\cdot 0.25\text{H}_2\text{O}]^-$, with a 45% of vacancies. The symmetry of stratlingite is R3m. The structure analysis (Rinaldi et al., 1990; Kwan et al., 1995) indicates that the octahedral layer shows an ordered scheme where each Al-octahedron is linked to 6 edge-sharing Ca^{VII} polyhedra (2 out 3 positions are then occupied by the seven coordinated Ca-type cation). Figure 1.8 shows the crystal structure of stratlingite where selected atoms are labelled (Santacruz et al., 2015).

It is known that the structural and microstructural models have important implications for a correct quantitative phase analysis of stratlingite in cement pastes and it is highly dependent on the hydration conditions (for instance, in pastes of BCSA cements) (Santacruz et al., 2015).

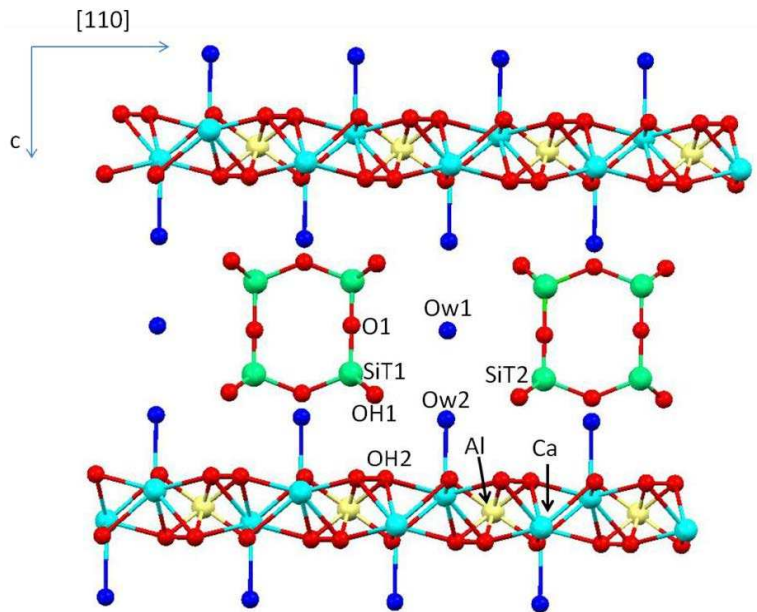


Figure 1.8. Layered crystal structure of stratlingite (Santacruz et al., 2015).

iii) Katoite.

Katoite has a structure related to the grossular or garnet. Garnet minerals have a cubic structure with the general formula $X_3Y_2(SiO_4)_3$. The X site is usually occupied by divalent cations (Ca^{2+} , Mg^{2+} and Fe^{2+}) and the Y site by trivalent cations (Al^{3+} , Fe^{3+} and Cr^{3+}) in an octahedral/tetrahedral framework with $[SiO_4]^{4-}$ occupying the tetrahedral positions (see Figure 1.9). The anhydrous end members of the $Ca_3(Al,Fe)_2(SiO_4)_3$ series are grossular ($Ca_3Al_2(SiO_4)_3$) and andradite ($Ca_3Fe_2(SiO_4)_3$). Hydrogarnet ($Ca_3(Al,Fe)_2(SiO_4)_y(OH)_{4(3-y)}$; $0 < y < 3$) includes a group of minerals where the $[SiO_4]^{4-}$ tetrahedra are partially or completely replaced by OH^- . The Al-containing hydrogarnet includes hydrogrossular ($Ca_3Al_2(SiO_4)_y(OH)_{4(3-y)}$; $0 < y < 3$) with the end member katoite ($Ca_3Al_2(OH)_{12}$ or C_3AH_6).

The nomenclature of minerals of the hydrogarnet group $Ca_3(Al_xFe_{1-x})_2(SiO_4)_y(OH)_{4(3-y)}$ as recommended by Passaglia and Rinaldi (1984) is given in Figure 1.10. The formation of siliceous hydrogarnet was reported for cements hydrated at high temperatures (Collier et al., 2009; Le Saout et al., 2006; Lothenbach et al., 2008; Neuvill et al., 2009) or in the presence of excess of $Fe(OH)_3$ (Collier et al., 2006).

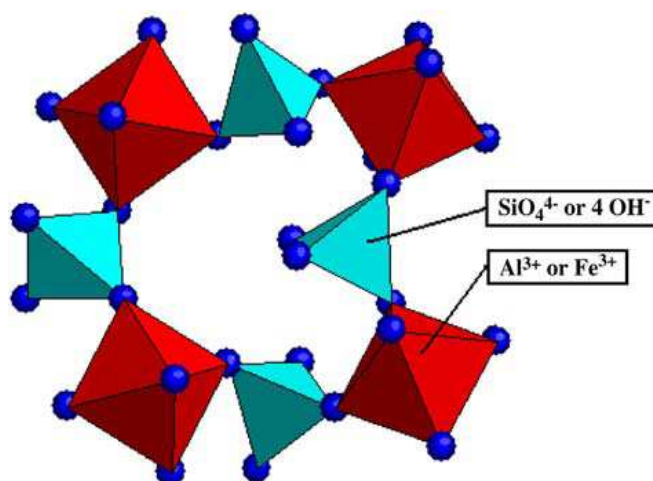


Figure 1.9. Octahedral and tetrahedral connections of hydrogarnet structure (Dilnesa et al., 2014).

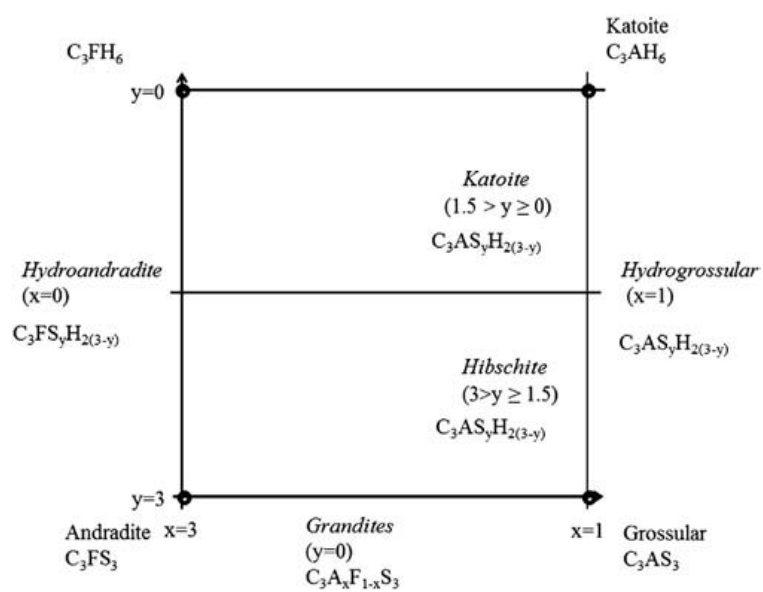


Figure 1.10. Nomenclature of minerals of the hydrogarnet group $\text{Ca}_3(\text{Al}_x\text{Fe}_{1-x})_2(\text{SiO}_4)_y(\text{OH})_{4(3-y)}$ (Passaglia and Rinaldi, 1984).

1.4.5. Properties of BCSA mortars and concretes. Durability.

Ye'elinite-containing cements and their corresponding mortars and concretes are considered as durable binders. Nevertheless, degradation processes should be taken into account, depending on the environment on which these mortars or concretes are serving. There are different ways of cement degradation e.g. carbonation, sulphate attack or chlorine diffusion. All these effects need ions diffusion through the porous microstructure. In CSA and BCSAF cements, the resistance to diffusion is enhanced due to the quick water consumption during the hydration process. Moreover, porosity decreases during hydration due to the large amount of hydration products generated at very early ages (Bernardo et al., 2006).

1.4.5.1. Sulphate Resistance.

Cementitious building materials are damaged by sulphate attack at moderate temperatures due to delayed ettringite formation. In OPC, when insufficient gypsum is added, ettringite reacts with the aluminium containing phases (C_3A and C_4AF) to form AFm (C_4ASH_{12}) (Mindess et al., 2003). Calcium monosulphoaluminate is subject to transform back to ettringite in the presence of environmental sulphate, causing cracking due to the enlargement of volume. However, BCSA cement generally shows good sulphate resistance (Quillin, 2001; Dan and Janotka, 2003) even for insufficient amounts of calcium sulphate in the system. The durability of these materials is usually studied through XRPD (Paglia et al., 2001), microscopy, linear expansion and compressive strengths.

1.4.5.2. Corrosion Resistance.

Atmospheric carbon dioxide can be dissolved in the pore solution of cement pastes and react with the hydration products increasing the carbonate concentration. This phenomenon will cause three effects: i) lowering pH value, ii) precipitation of $CaCO_3$ by the reaction of carbonate ions with Ca^{2+} ions and iii) possible damaging of ettringite. Porosity and water/cement (w/c) ratio determine the degree of resistance to carbonation. Carbonation happens quicker in CSA than in Portland concretes, leading to partial decomposition of ettringite, which may cause a moderate strength loss (Sharp et al., 1999; Mechling et al., 2013). In addition, decreasing w/c ratio (high-strength concrete) increases resistance to carbonation as there is not free water available to dissolve CO_2 .

The pH of the pore solution in BCSA cements is generally lower than that in OPC due to the lower amount of CH formed in BCSA cements (Kalogridis et al., 2000). Furthermore, ettringite, the main hydration product in BCSA cements, is susceptible to carbonation, which further reduces the pore solution pH at later ages (Quillin,

2001). In steel reinforced concrete, a passivated oxide layer is formed on the reinforcement steel surface and protects it from corrosion when the pH of the surrounding pore solution is high (Jones, 1996). However, this passivated layer breaks down when the surrounding pore solution pH is below ~ 11.5 . The low pH of the pore solution in BCSA cement might not be high enough to protect the reinforcement steel, leading to corrosion in the reinforcement steel if cracking is developed in the concrete.

1.4.5.3. Compressive Strength.

BCSA cements can be produced with a wide range of properties from rapid to slow hardening and good to poor durability depending on their phase assemblage (Mehta, 1980), as it is shown in Figure 1.11. The hydration reactions of the fast-reacting C_4A_3S and C_4AF with CS to form ettringite and AH_3 resulted in rapid setting and contributed to the high early-age strength development, while the hydration reaction of the slow-reacting C_2S to form C-S-H contributed to the long-term strength development. However, mortars made from BCSAF cements that contain 10 wt% C_4A_3S , 50-65 wt% C_2S , 10 wt% CS and 15-30 wt% C_4AF with a water-to-cement ratio of 0.4 show slow hardening, poor early-age and long-term compressive strengths likely due to their low C_4A_3S , C_4AF and CS contents and high C_2S contents.

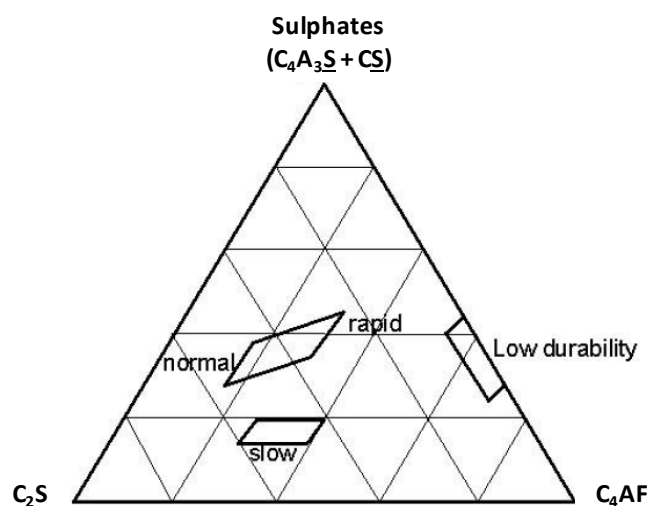


Figure 1.11. Schematic phase diagram of ternary system representing BCSA cement; slow, normal and rapid refer to hardening rates (adapted from Mehta, 1980).

1.4.5.4. Dimensional Stability.

Other problem related to durability is the expansion of concrete during hydration. Differences in dimensional stability are observed in BCSA systems by different factors: i) C_4A_3S content (Kasselouri et al., 1995; Beretka et al., 1996; Janotka et al., 2007; Chen et al., 2012); ii) amount of gypsum available in the system (Glasser and Zhang, 2001; Bizzozero et al., 2014); iii) w/c ratio and curing conditions (humidity degree) (Beretka et al., 1996; Odler and Colan-Subauste, 1999; Chen et al., 2012).

The sulphate diffusion into the mortar matrix may delay the ettringite formation and cause expansion (Chen et al., 2012). When most of the ettringite is formed before the paste hardens, non-expansive and rapid hardening BCSA cements can be achieved. However, the formation of a significant amount of ettringite after hardening may cause expansion and cracking (Ogawa and Roy, 1982). However, after some days of hydration water may be exhausted and, unless there is another deterioration mechanism (as leaching) (Berger et al., 2011b), the expansion due to the delayed formation of ettringite is not significant (Glasser and Zhang, 2001).

For the reasons discussed above, BCSAF cements are considered, nowadays, as one of the most promising alternatives to OPC. This is supported by the environmental benefits (lower CO_2 emissions) and industrial interest. However, before been implanted in Europe, all the steps involved in the process need to be under control, including synthesis (activation, clinkering conditions and composition), hydration (rheological behaviour and phase assemblage), and final performances (mechanical strength, durability, and dimensional stability). This PhD Thesis is focused on the study and optimisation of most of those parameters to improve the final performances of BCSAF mortars.

1.5. METHODOLOGY.

The most important characterisation techniques used in this work are described in this section. They are gathered in two mains groups: those used for cements and those for pastes and mortars.

1.5.1. Cement (anhydrous and paste) characterisation.

1.5.1.1. LRPD and Rietveld method.

XRPD can reveal the mineralogical nature of phases present in the solid. Principle is that a beam of X-ray penetrates the sample, and a constructive interference occurs between the X-rays and the crystals in the sample. The angle and the intensity of diffraction are characteristic of a crystalline structure. All lines of diffraction are used to identify the nature of crystals.

LXRPD studies can be performed using different radiations (Mo and Cu) and setups: i) Transmission geometry (Debye-Scherrer), and ii) Reflection geometry (Bragg-Brentano).

The irradiated volume in diffraction is a key issue since higher volume yields enhanced particle statistics. For a given sample, several methods can be used to increase the number of crystallites contributing to the diffraction pattern, including: i) rotate the sample about the normal to the sample surface for a flat plate sample or the sample axis for a capillary sample-holder; ii) oscillate the sample about the incident angle axis, this motion removes the exact Bragg-Brentano theta/2theta relationship between sample and receiving slit and may lead to aberrations in the peak intensities; iii) repack the sample, recollect and reanalyze the diffraction data, averaging the results from each analysis will produce more meaningful parameter values, iv) reduce the average crystallite size(s) by milling, however, caution must be exercised in the choice of mill since many grinding techniques introduce peak broadening (amorphization or inducing crystal strains) and some phases can undergo solid-solid phase transitions or dehydration during grinding; and v) enhancing particle statistic by the increasing the diffracting volume. The irradiated volume for Mo-radiation (transmission with flat sample) is higher than the volume for Cu-radiation (reflection). This larger irradiated volume for Mo-radiation should show several benefits that will be demonstrated in the results section.

The experimental set-up details for different diffractometers used for this Thesis were the following:

- X'Pert MPD PRO diffractometer (PANalytical B.V.) with strictly monochromatic $\text{CuK}\alpha_1$ radiation ($\lambda=1.54059 \text{ \AA}$) and primary monochromator Ge (111). The optics configuration was a fixed divergence slit ($1/2^\circ$), a fixed incident antiscatter slit (1°), a fixed diffracted antiscatter slit ($1/2^\circ$) and X'Celerator RTMS (Real Time Multiple Strip) detector, working in scanning mode with maximum active length. Data were collected from 5° to 70° (2θ) for $\sim 2\text{h}$. The samples were rotated during data collection at 16 rpm in order to enhance particle statistics.

- EMPYREAN diffractometer (PANalytical B.V.): used to recorded in flat-sample transmission geometry the patterns studied by the internal standard method. It has equipped with a θ/θ goniometer, $\text{CuK}\alpha_{1,2}$ radiation ($\lambda=1.542 \text{ \AA}$) and a focusing

mirror. This PreFIX optical component is capable of converting the divergent beam into a convergent radiation focused on the goniometer circle. The EMPYREAN diffractometer was equipped with fixed incident and diffracted beam anti-scatter slits of $\frac{1}{4}^\circ$ and 5 mm, respectively. The detector was PIXCEL 3D RTMS, which comprises more than 65,000 pixels, each $55 \times 55 \mu\text{m}$ in size; each having its own circuitry. The overall measurement time was $\sim 3\text{h}$ per pattern to have very good statistic over the 2θ range of $5\text{--}70^\circ$ with 0.0131° step size (2θ). The samples were spun at 16 rpm.

- D8 ADVANCE DaVinci diffractometer (Bruker AXS), (250 mm of diameter) with Mo radiation equipped with a primary Johansson monochromator Ge (220), which gives a strictly monochromatic radiation ($\lambda = 0.7093 \text{ \AA}$), $\text{MoK}\alpha_1$. The X-ray tube worked at 50 kV and 45 mA. The optics configuration was a fixed divergence slit (2°) and a fixed diffracted anti-scatter slit (9°) and the energy-dispersive linear detector LYNXEYE XE $500 \mu\text{m}$, specific for high energetic radiation, was used with the maximum opening angle. Using this conditions the samples were measured between $3\text{--}30^\circ$ (2θ) with a step size of 0.009° and with a measurement total time of 2 hours and 30 minutes. The samples were spun at 10 rpm.

Hugo Rietveld in the late sixties (Rietveld, 1967; 1969) devised “The Rietveld method” for the deeper characterisation of polycrystalline compounds. It consisted in the use of measured powder pattern intensities instead of reflection (peak) intensities, and supposed a conceptual breakthrough. This methodology, together with the coming of new technologies (computers), allowed to properly dealing with strongly overlapping reflections. Rietveld method is currently the most effective procedure for analysing powder diffraction data. This method can be used to carry out the QPA in crystalline samples.

To obtain a successful RQPA, a properly prepared sample, a well aligned and maintained diffractometer and good structural descriptions for each crystalline phase are needed. Under these pre-requisites, a good powder diffraction pattern may be collected and RQPA can be carried out. Furthermore, every crystalline phase in the sample should be identified. This is easy to say but sometimes quite complex to fulfil because sometimes there are strong peak overlapping in the diffraction patterns and does not allow to conclusively determining all present phases. Finally, the RQPA needs to be to carry out with the appropriate software. In our case GSAS (Larson and Von Dreele, 2000; Toby, 2001) was the software package used. In addition to the raw data, any Rietveld program needs a control file to execute the refinements. In this control file, the crystal structures of the different components must be included. The fit is carried out by optimising all appropriate variables such as: i) scale factor of every crystalline phase; ii) background parameters for the chosen function; iii) unit cell parameters for every crystalline phase; iv) peak shape parameters for every

computed phase; and finally, v) correction parameters which may be phase-dependent (such as preferred orientation, extinction, etc.) or pattern-dependent (zero-shift, absorption correction when working in transmission geometry, etc.). Usually, for RQPA, the structural descriptions (atomic positional parameters, atomic displacement parameters and occupation factors) are not optimised but kept as reported in bibliography.

The application of RQPA to clinkers/cements/pastes is not an easy task for the following reasons (Aranda et al., 2012; Aranda et al., 2015): i) there are many phases, usually more than five, which increases the diffraction peak overlapping and so the correlations; ii) each phase has its own mass absorption coefficient which may yield the micro-absorption problem; iii) the small irradiated volume ($\sim 2 \text{ mm}^3$) for Cu $K\alpha$, which may lead to poor particle statistics; iv) some phases, for instance alite or gypsum, crystallise as plaques which show preferred orientation, increasing the errors; v) phases can crystallise as several polymorphs that must be identified a priori; vi) the diffraction peak broadening for some phases may be anisotropic and it must be properly modelled; and vii) the atomic impurities inside each phase are not known and their scale factors are usually computed for ideal/stoichiometric phases. In any case, RQPA shows several advantages over other methods based on powder diffraction and other technologies (microscopy, thermal analysis, etc.).

As stated above, conventional RQPA requires all crystal structures to be known. Aranda et al (2012) reported the main hydrated and anhydrous cement standard phases. There are alternative whole-pattern quantitative phase analysis methods for crystalline phases with unknown structures (Smith et al., 1987; Taylor and Zhu, 1992; Scarlett and Madsen, 2006; Snellings et al., 2014). Currently, three ways to derive the phase content, W_{α} , from the Rietveld refined scale factor, S_{α} , can be used to determine the RQPA (Madsen et al., 2011; Gualtieri et al., 2014):

i) Normalization to full crystalline phase content method. The simplest approach is the approximation that the sample is composed only of crystalline phases with known structures. This method normalises the sum of the analysed weight fractions to 1.0. Thus, if the sample contains amorphous phases, and/or some amounts of unaccounted crystalline phases, the analysed weight fractions will be overestimated.

This approach is by far the most widely used method in RQPA. However, it must be highlighted that the resulting weight fractions are only accurate if the amount of unaccounted crystalline phases and amorphous content are very small (negligible) which may not be the case in anhydrous cements and for sure, is not the case in cement pastes.

ii) *Internal standard method*. A second, more experimentally-demanding, approach is to mix the sample with a crystalline standard in a known amount, W_{st} (also known as *spiking method*) (Cline et al., 2011). This standard must be free of amorphous content or at least its non-diffracting content must be known. This (artificial) mixture must be well homogenised as the particles should be randomly arranged. The addition of the standard dilutes the crystalline phases within the sample. This may be quite problematic for low-content phases.

This method allows the determination of an overall unaccounted content which is composed by amorphous phase(s), misfitting problems of the analysed crystalline phases, and some crystalline phases which may not be included in the control file due to several reasons (its crystal structure is not known, the phase was not identified, and so on). This overall content is hereinafter named AC_n, which stands for Amorphous and Crystalline non-quantified, to highlight that not only an amorphous fraction but also any non-computed crystalline phase and any misfit problem (for instance the lack of an adequate structural description for a given phase) may contribute to this number. The method derives the (overall) AC_n content of the sample from the small overestimation of an internal crystalline standard (De la Torre et al., 2001a). The errors associated to this approach and the optimum amount of standard have been discussed (Westphal et al., 2009). Several standards can be used as an internal standard. In this work ZnO was used as internal standard.

This methodology has been applied to anhydrous cement and also to pastes. However, the addition of an internal standard may alter the cement hydration reactions, dilutes the phases in the pastes, microabsorption problems, and so on.

iii) *External standard method (G-factor approach)*. To avoid complications that may arise from mixing an internal standard with the sample, it is possible to use an external standard method. This approach requires the recording of two patterns in identical diffractometer configuration/conditions for Bragg-Brentano $\theta/2\theta$ reflection geometry. The method was proposed sometime ago (O'Connor and Raven, 1988) and very recently applied to anhydrous cements (Jansen et al., 2011b), to OPC pastes (Jansen et al., 2011a, b) and organic mixtures (Schreyer et al., 2011). This method consists on determining the diffractometer constant, K_e (also called G), with an appropriate standard (for instance silicon powder from Si-single crystal). This methodology is also known as G-method since the standard allows calculating the G-factor of the diffractometer in the operating conditions. This calculated G-factor represents a calibration factor for the whole experimental setup and comprises the used diffractometer, radiation, optics, and all data acquisition conditions (f.i. detector configuration, integration time, etc.). It is experimentally more time demanding but it does not interfere with the hydration reactions.

1.5.1.2.SXRPD (BL04 – MSPD, ALBA).

In SXRPD, X-rays are generated by a synchrotron facility and are thus at least 5 orders of magnitude more intense than the best X-ray laboratory source. The *high brilliance* of the synchrotron radiation drastically improves the structural characterisation and level of detection of mixture components. The speed of the measurement makes possible to perform kinetic studies on structural changes during chemical reactions or under temperature and pressure ramps.

In this PhD. Thesis, SXRPD patterns have been collected in MSPD (BL04) beamline of ALBA, the Spanish Synchrotron Radiation Facility (Barcelona, Spain) (Fauth et al., 2013). Debye–Scherrer (transmission) mode was used (Knapp et al., 2011) with a wavelength of 0.61984(3) Å. The diffractometer is equipped with a so called MYTHEN detector system especially suited for time-resolved experiments. Raw SXRPD patterns were normalised taking into account the loss of X-ray beam flux with time due to the electron beam current decline in the storage ring. Normalised SXRPD patterns were analysed by using the Rietveld methodology in order to obtain RQPA.

1.5.1.3.SEM.

SEM is a type of electron microscope that images the sample surface by scanning it with a high-energy beam of electrons in a raster scan pattern. The electrons interact with the atoms that make up the sample producing signals that contain information about the sample surface topography, composition and other properties such as electrical conductivity.

SEM is used to study the microstructure of cement and cementitious materials and in combination with EDS to characterize the chemical (elemental) composition of the different phases and their spatial distribution of polished cement pastes (Gobbo et al., 2004; Crumbie et al., 2006). Both optical and electron microscopes are good complementary techniques to RQPA of clinkers and cements (Campbell and Galehouse, 1991; Stutzman and Leigh, 2002; Suherman et al., 2002; Stutzman, 2011).

Microstructural characterisation of anhydrous and hydrated samples was performed in a JEOL JSM-6490LV scanning electron microscope. EDS measurements were carried out (on samples coated with graphite) with the OXFORD INCA Energy 350 attachment. This unit has a Si(Li) detector with a super atmospheric thin window.

1.5.1.4. Solid-state NMR spectroscopy.

NMR spectroscopy is a powerful characterisation method capable of providing information about the structure of materials. The method exploits the interaction of nonzero spin nuclei and an external magnetic field to gain information about the local atomic environment of a specific nucleus. In cementitious materials, the ^{29}Si and ^{27}Al nuclei are the most widely studied nuclei. Different nuclei have different natural abundances and spin which affect the clarity of the resulting spectra. The natural abundance of a nucleus affects the time required for an experiment to achieve an acceptable signal/noise ratio. A higher natural abundance requires less experimental time.

Much information can be gained from the ^{29}Si nucleus in cementitious materials. The presentation of structural information obtained from ^{29}Si NMR in silicates often uses Q notation: $Q_n(m\text{Al})$, where Q indicates a silica tetrahedron forming bridges through n oxygen atoms with adjacent tetrahedra, of which m are alumina tetrahedra, where n and m range from 0 to 4. The information gained from ^{27}Al NMR is much more limited due to the quadrupolar interaction of the 5/2 spin nucleus. The quadrupolar interaction causes extreme line broadening that makes difficult the fine distinctions in the local atomic environment. An increase in the magnetic field used greatly reduces these effects. The basic ^{27}Al NMR experiment only gives information about the coordination of the aluminum nucleus, and not information on specific local bonding to the nucleus.

NMR techniques have been increasingly employed in studies of cementitious materials mainly for quantification and characterization of anhydrous and hydrated cement phases (Andersen et al., 2003; Poulsen et al., 2009; Florian et al., 2012; García-Lodeiro et al., 2012; Cuesta et al., 2014c;) and to understand the hydration reactions in OPC cements (Skibsted et al., 2002; Rawal et al., 2010) or blended OPC cements (Dyson et al., 2007).

The (independent) use of RQPA and NMR methods for characterising anhydrous cements and hydration reaction products can be used (Skibsted and Hall, 2008; Stark, 2011; Brunet et al., 2010).

NMR spectra for selected samples were conducted in a Bruker Avance-400 spectrometer with a 9.39 T widebore superconducting magnet.

1.5.1.5. Thermal measurements.

DTA-TGA have been used to quantify phases in cements and pastes, including the free water content. DTA-TGA measurements were performed in a SDT-Q600

analyzer from TA Instruments (New Castle, DE). The temperature was varied from room temperature to 1000°C at a heating rate of 10 °C/min. Measurements were carried out in open platinum crucibles under nitrogen flow.

Although the use of this analysis is straightforward, it allows the determination of different phases (f.i. calcium silicate hydrate, ettringite, gypsum, monosulphate, aluminium hydroxide and calcium hydroxide in a CSA cement paste) through the corresponding dehydration endothermic peaks (Winnefeld and Barlag, 2010; Telesca et al., 2014; Song et al., 2015). In addition, the overall calcite content (700-800°C) or portlandite (~450°C) can be determined from their decomposition temperatures (Scrivener et al., 2004; Puertas et al., 2010). DTA-TGA also allows distinguishing between gypsum and bassanite under the appropriate experimental conditions (Blaine, 1995), and verify the gypsum/bassanite ratio obtained from RQPA (Leon-Reina et al., 2009). Furthermore, DTA-TGA and RQPA have been carried out to monitor the long-term hydration behaviour of cement monoliths containing organic waste (Leoni et al., 2007), and to investigate long-term leaching in concretes (Marinoni et al., 2008).

1.5.1.6. Isothermal conduction calorimetry.

The rate of reaction with water in cements can be evaluated using an isothermal conduction calorimetry. The heat produced by cementitious materials in exothermic hydration reactions is a good indicator of their early-age hydration behaviour (Gartner et al., 2002). This methodology allows understanding the chemical origin of different regions/features (hydration reactions), the changes in reaction kinetics (Winnefeld and Barlag, 2010; Jansen et al., 2012b; Hargis et al., 2014b) and also supports the accuracy of RQPA (Hesse et al., 2011; Jansen et al., 2011b; Jansen et al., 2012a).

The isothermal calorimetric study was performed for selected samples in an eight channel Thermal Activity Monitor (TAM) instrument using glass ampoules. Pastes were prepared by mixing ~6 g of each sample with the appropriated water and the heat flow was collected up to 168 h at 20°C.

1.5.1.7. MIP.

Mercury intrusion porosimetry is based on the principle that the intrusion volume of mercury into a porous medium depends on the applied pressure. If the pore geometry is assumed to be cylindrical the pore diameter (size) can be related to the applied pressure. Open porosity was measurement through mercury porosimetry using a Quantachrome (Autoscan 33, Boynton Beach, Florida, US) porosimeter.

BCSA cement hardens quicker than OPC due to the fast formation of ettringite and AH_3 . The initial hydration products quickly reduce the internal pore space at first hours of hydration, and smaller pores (~25 nm) dominate over the capillary pores (~200 nm) and the system develops a bimodal pore structure, which generally correlates to a disconnected pore structure and a denser microstructure (Bernardo et al., 2006).

1.5.1.8. Rheological behaviour.

Rheology is the science that studies the flow and deformation of the matter under the influence of a mechanical force. It is concerned particularly with the material behaviour which cannot be described by the simple linear models of hydrodynamics and elasticity. When cement is mixed with water, each phase dissolves at least partially, leading to the establishment of supersaturated solution with respect to different hydrates, which can precipitate. As all chemical reactions, they obey the laws of thermodynamics and kinetics (Roussel, 2012).

Rheological measurements of the cement pastes were carried out using a viscometer (Model VT550, Thermo Haake, Karlsruhe, Germany) with a serrated coaxial cylinder sensor, SV2P, provided with a solvent trap to reduce evaporation. Flow curves were obtained with controlled rate (CR) measurements using a three-stage measuring program with a linear increase in the shear rate from 0 to 100 s^{-1} in 60 s, a plateau at 100 s^{-1} for 30 s, and a further decrease to zero shear rate in 60 s. Before starting the rheological measurement, the pastes were presheared for 30 s at 60 s^{-1} .

In rheology the graph representation of the correlation between shear stress and shear rate defining the flow behaviour of a liquid is called the “Flow Curve” (see figure 1.12.a). Other way to show the flow behaviour is through the “Viscosity curve”, the correlation between viscosity and shear rate (see figure 1.12.b). Once the cement is rheologically characterised, it is possible to improve the workability/flowability of mortars/pastes (Banfill, 2006) by the addition of additives to obtain more homogeneous mixtures and hence, improved mechanical properties (García-Maté, 2015). Moreover, the setting evolution of cement pastes can be also followed at very early hydration times by following their viscosity values with time at a fixed shear rate, or even through oscillatory measurements.

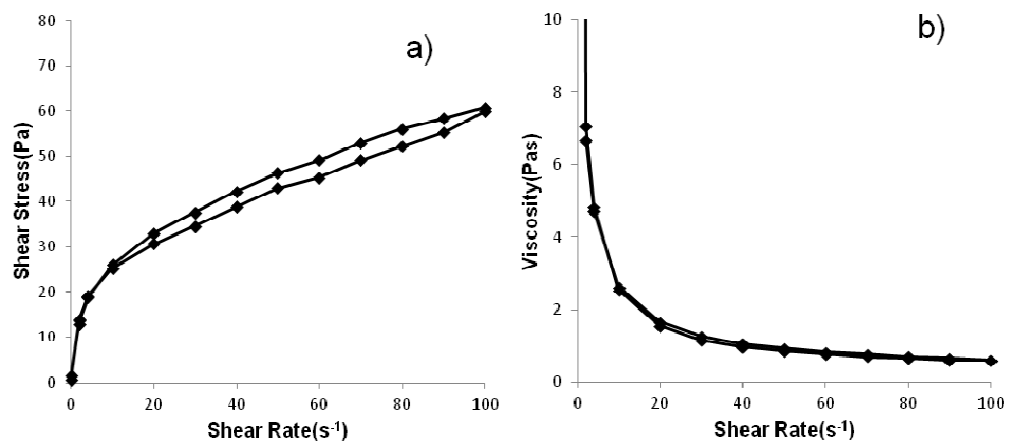


Figure 1.12. Examples of a) flow curve and b) viscosity curve of CSA cement paste (A25CSA; w/c=0.5) (García-Maté, 2015).

1.5.2. Mortar characterisation.

1.5.2.1. Compressive strength.

The compressive strength is defined as the capacity of a material or structure to withstand loads tending to reduce size. It can be measured in a testing machine by checking the deformation of the material by applying pressure. At their compressive strength limit, some materials fracture and others deform irreversibly. So a given amount of deformation may be considered as the limit for compressive load. In cement based materials (mortars) high values of compressive strength are desired. In this PhD Thesis, moulds of 30 x 30 x 30 mm³ have been used to measurement the compressive strength values under compression machine (Model Autotest 200/10 W, Ibertest, Madrid, Spain). Standard mortars were prepared and mechanically homogenized according to the standard EN196-1. A factor of 1.78 was used in order to obtain values comparable to those determined by use of standard prisms (40 × 40 × 160 mm³).

Factors determining the compressive strength of a cement paste (Taylor, 1997) include: i) characteristics of the cement, such as clinker composition and microstructure, gypsum content and particle size distribution; ii) w/c ratio and contents of air and of any admixtures present in the mix; iii) mixing conditions; iv) curing conditions (temperature and relative humidity); v) curing age; vi) the manner of testing, including the water content of the specimen. The factors listed determine

the degree of hydration of the clinker phases, the phase composition and the microstructure of the hardened paste, which in turn determine its physical properties, including strength.

1.5.2.2. Shrinkage/Expansion properties (Length Changes).

During the cement hydration, length changes can occur. The expansion (or shrinkage) experienced in mortars is mainly related to the nature of the pore structure, which affects the mobility of ions and the available space to accommodate new phases. Both adequate deformability and strength values are required to allow expansion without the formation of cracks. The dimensional stability of all the mortars prepared was measured with an analogic length comparator (mod. E077, MATEST) in standard prismatic samples (40× 40×160 mm) by applying the equation $\Delta L(\%) = [(L_f - L_0)/L_0] \times 100$. In this equation, L_f is the measured length at a given time and L_0 is the initial length (taken just after demolding and prior to immersion in water).

The hydration of OPC cement causes a reduction in the absolute volume of the paste. In CSA and BCSA cement systems the expansive behaviour associated with ettringite formation has been widely studied (Mehta, 1973; Cohen, 1983a, b; Andac et al., 1999; Scherer, 1999; Scherer, 2004; Flatt and Scherer, 2008; Winnefeld and Lothenbach, 2010; Chen et al., 2012) but the mechanisms of expansion are still not fully understood. Calcium, sulphate or hydroxyl ions promote, when present in elevated amounts, the formation of fine ettringite crystals on the surface of $C_4A_3\bar{S}$ particles; in addition, they can combine, if their concentration is relatively low, with enough $Al(OH)_4^-$ ions to produce large ettringite crystals in the bulk solution. Various mechanisms implicated in external sulphate attack of cementitious materials were well reviewed by Brown and Taylor (1999). Most of their arguments have a general validity to systems in which expansion is related to ettringite formation (Bizzozero et al., 2014). The two head theories about the origin of expansion associated with ettringite are: the “crystal growth” and “swelling”. First one concludes that expansion is caused by the growth of ettringite crystals and the related crystallization pressure (Bentur and Ish-Shalom, 1974; Ogawa and Roy, 1981; Herrick et al., 1992; Deng and Tang, 1994); but according to the last theory (Mehta, 1973; Mehta and Hu, 1975; Mehta and Wang, 1982), the expansion is due to the adsorption of water molecules on ettringite, resulting in interparticle repulsion and swelling.

1.5.2.3. Setting.

The setting and hardening of cement is a continuous process, but two points are distinguished for test purposes:

i) The initial setting time, which is the interval between the mixing of the cement with water and the time when the mix has lost plasticity, stiffening to a certain degree. It marks roughly the end of the period when the wet mix can be moulded into shape. It is determined by monitoring the repeated penetration of a needle into a fresh cement paste of standard consistence (using the Vicat apparatus), and the time of initial setting is taken when the distance between the needle and the base plate is of 6 ± 3 mm according to UNE-EN 196-3.

ii) The final setting time, which is the point at which the set cement has acquired a sufficient firmness to resist a certain defined pressure and according to UNE-EN 196-3 corresponds to a penetration of the needle of only 0.5 mm in the cement paste specimen.

There are several parameters which affects initial and final setting times such as water/solid ratio, fineness, sulphate source, solubility and so on. For example Pelletier-Chaignat et al. (2012) measured the setting times of samples containing calcium sulphotoaluminate clinker and gypsum combined with quartz filler or limestone filler. The results show that the use of limestone filler instead of quartz filler accelerates the early hydration of the cement, thus shortening the initial setting time.

In this Thesis, paste setting times were determined using the Vicat test method according to UNE-EN 196-3, in VICATRONIC continuous penetration equipment (mod. E044N, MATEST).

CHAPTER 2

OBJETIVES

2. OBJECTIVES

The general aim of this PhD Thesis is to better understand the hydration mechanism of BCSAF cements to correlate it with the mechanical properties of the corresponding mortars. The specific objectives established in this work are described below:

i) To scale up the synthesis of two iron-rich belite sulphoaluminate clinkers (BCSAF) in the laboratory at "medium scale" (~2 kg) that contain different polymorphs of belite and ye'elimite.

ii) To perform an accurate full mineralogical analysis of anhydrous BCSAF clinker and other related materials, including the quantification of amorphous and crystalline non-quantified (ACn) contents by LXRPD and Rietveld method.

iii) To understand the hydration of BCSAF cement pastes at different curing ages through the quantification of the phase assemblage including ACn contents. To estimate the elemental composition of ACn phase(s) through LXRPD (indirectly) and SEM-EDS studies (directly).

iv) To determine the effect of different parameters in the phase assemblage of the cement during hydration, such as the type of polymorphs present in the clinker composition, and the amount and type of sulphate source in the cement.

v) To correlate the phase assemblage of BCSAF cement pastes with the mechanical properties, mainly compressive strength values and shrinkage/expansion of the corresponding mortars.

CHAPTER 3

ARTICLES SECTION

ARTICLE

A#1



Contents lists available at SciVerse ScienceDirect

Cement and Concrete Research

journal homepage: <http://ees.elsevier.com/CEMCON/default.asp>

Rietveld quantitative phase analysis of Yeelimite-containing cements

G. Álvarez-Pinazo^a, A. Cuesta^a, M. García-Maté^a, I. Santacruz^a, E.R. Losilla^a,
A.G. De la Torre^a, L. León-Reina^b, M.A.G. Aranda^{a,*}^a Departamento de Química Inorgánica, Cristalografía y Mineralogía, Universidad de Málaga, 29071 Málaga, Spain^b Servicios Centrales de Apoyo a la Investigación, Universidad de Málaga, 29071 Málaga, Spain

ARTICLE INFO

Article history:

Received 6 December 2011

Accepted 26 March 2012

Keywords:

4CaO·3Al₂O₃·CaSO₄ (D)
Calcium sulfoaluminate (D)
X-ray diffraction analysis (B)
Rietveld method (B)
Amorphous material (B)

ABSTRACT

Yeelimite-containing cements are attracting attention for their tailored properties. Calcium sulfoaluminate, CSA, cements have high contents of Yeelimite and they are used for special applications. Belite calcium sulfoaluminate, BCSA or sulfobelite, cements have high contents of belite and intermediate contents of Yeelimite, and they may become an alternative to OPC. Here, we report Rietveld quantitative phase analyses for three commercially available CSA clinkers, one CSA cement, and two laboratory-prepared iron-rich BCSA clinkers. The crystalline phases are reported and quantified. Selective dissolutions are employed for BCSA clinkers to firmly establish their phases. Finally, the overall unaccounted contents (amorphous plus crystalline not quantified) have been determined by two approaches: i) external standard procedure (G-method) with reflection data; ii) internal standard procedure (spiking method with ZnO) with transmission data. The overall unaccounted contents for CSA clinkers were ~10 wt.%. Conversely, the unaccounted contents for BCSA clinkers were higher, ~25 wt.%.

© 2012 Elsevier Ltd. All rights reserved.

1. Introduction

Calcium sulfoaluminate (CSA) cements have been applied worldwide from the 60s as expansive binders mixed with Portland cements [1]. These cements are characterized by containing high amounts of Yeelimite, also called Klein's salt or tetracalcium trialuminate sulfate (C₄A₃S). Hereafter, cement nomenclature will be used, i.e. C = CaO, S = SiO₂, A = Al₂O₃, F = Fe₂O₃, M = MgO, S = SO₃, C = CO₂, H = H₂O, K = K₂O and N = Na₂O. Therefore, C₄A₃S corresponds to Ca₄Al₆O₁₂(SO₄). During the 70s, CSA cements were introduced into the Chinese market as high performance and dimensionally stable cementitious matrices developed by the China Building Materials Academy [2]. In Europe, the use of CSA cements is strongly limited by the lack of standards concerning special cements derived from non-Portland clinkers. Nevertheless, their manufacture has recently been started by several companies. The main use of these CSA cements, or blends with Portland cements, is for quick repairs and pre-cast products or floor concrete applications.

Moreover, Yeelimite-containing cements have become highly popular over the last few years for research. The driving force for these investigations is the much lower CO₂ emissions in their manufacture when compared to those of Portland cement production due to the following main reasons [3,4]: i) Yeelimite releases during its synthesis only a third part of the CO₂ released by the production of

alite, ii) firing temperature is about 200 °C lower than that of OPC clinker, iii) various industrial by-products can be used in the kiln feed, and iv) Yeelimite-containing clinkers are easier to grind than OPC clinkers. The improvement of cement performances and the reduction of the environmental impact related to its manufacture are most likely the main areas of innovation for the cement industry [5]. It must be highlighted that CSA cements may have important special applications such radioactive element encapsulation in high-density cement pastes [6]. Other interesting properties of Yeelimite-containing cements are high early strengths, short setting times, low solution alkalinity as well as high impermeability and chemical resistance against several aggressive media [7].

However, while the composition of Portland cement is defined by long-standing codes and standards, there is no corresponding compositional framework for Yeelimite-containing cements. These clinkers may show very variable phase assemblage. The raw mix composition can be based on conventional raw materials (limestone, clay, bauxite and iron ores); in addition, industrial by-products and wastes can also be added [8,9]. Yeelimite-containing cements could be classified according to their C₄A₃S contents as:

- I) Calcium sulfo-aluminate (CSA) cements which would refer to those with high C₄A₃S contents. They may be prepared from CSA clinkers containing C₄A₃S as the main phase ranging between 50 and 90 wt.% [10]. The calcium sulfate addition is very important as it may profoundly affect the properties of the resulting binder [11–13]. The calcium sulfate source and content have to be customized for a given application. These

* Corresponding author. Tel.: +34 952131874; fax: +34 952132000.
E-mail address: g.aranda@uma.es (M.A.G. Aranda).

ARTICLE

A#2



In-situ early-age hydration study of sulfobelite cements by synchrotron powder diffraction



G. Álvarez-Pinazo ^a, A. Cuesta ^a, M. García-Maté ^a, I. Santacruz ^a, E.R. Losilla ^a, S.G. Sanfélix ^b, F. Fauth ^c, M.A.G. Aranda ^{a,c}, A.G. De la Torre ^{a,*}

^a Departamento de Química Inorgánica, Universidad de Málaga, Campus Teatinos S/N, 29071 Málaga, Spain

^b Unidad Técnica de Investigación de Materiales, AIDICO, Avda. Benjamín Franklin, 17 Paterna, Valencia, Spain

^c CELLS-Alba synchrotron, Carretera BP 1413, Km. 3.3, E-08290 Cerdanyola, Barcelona, Spain

ARTICLE INFO

Article history:

Received 11 July 2013

Accepted 24 October 2013

Available online xxx

Keywords:

Hydration (A)

X-ray diffraction (B)

Kinetics (A)

Sulfoaluminate (D)

Ca₂SiO₄ (D)

ABSTRACT

Eco-friendly belite calcium sulfoaluminate (BCSA) cement hydration behavior is not yet well understood. Here, we report an *in-situ* synchrotron X-ray powder diffraction study for the first hours of hydration of BCSA cements. Rietveld quantitative phase analysis has been used to establish the degree of reaction (α). The hydration of a mixture of ye'elimite and gypsum revealed that ettringite formation ($\alpha \sim 70\%$ at 50 h) is limited by ye'elimite dissolution. Two laboratory-prepared BCSA cements were also studied: non-active-BCSA and active-BCSA cements, with β - and α' -belite as main phases, respectively. Ye'elimite, in the non-active-BCSA system, dissolves at higher pace ($\alpha \sim 25\%$ at 1 h) than in the active-BCSA one ($\alpha \sim 10\%$ at 1 h), with differences in the crystallization of ettringite ($\alpha \sim 30\%$ and $\alpha \sim 5\%$, respectively). This behavior has strongly affected subsequent belite and ferrite reactivities, yielding stratingite and other layered phases in non-active-BCSA. The dissolution and crystallization processes are reported and discussed in detail.

© 2013 Elsevier Ltd. All rights reserved.

1. Introduction

Concrete is the most used artificial material, 6 km³/year or more than 2.5 tones per person yearly. This is due to many interesting features including low price, high versatility, remarkable change in mechanical properties during setting and chemical durability. The hydration of cements, to yield concrete, is a very complex process in which some crystalline phases are dissolved in free water. Pore solution becomes saturated in some ions, and after oversaturation, some crystalline and amorphous hydrated phases start to precipitate [1,2]. These processes are responsible for the development of a given microstructure (type, amount and distribution of the constituent phases, usually with chemical substitutions on the crystalline phases, and porous distribution) which is the fundamental link between chemical processes and final properties/performances. Many factors may affect the equilibrium between hydrous phases, pore solution, gel/amorphous phases and clinker phases, and their kinetics of dissolution and formation. Because of that, it is essential to understand (and at later stage to control) the hydration processes, in particular within the first few hours of hydration, named in the field as early hydration [2].

However, the complexity and heterogeneity of cementitious materials make difficult the understanding of the process–microstructure–properties relationship. Furthermore, there are only a few rapid, reliable and accurate techniques to quantify the amounts of the different phases

present in the hydrated cements (pastes), including amorphous contents and porous (micro) structure [3–6]. Due to these difficulties, the details of the hydration process of cements are still not completely clarified, even when the cement chemistry is well known in its most important features, as it is the case for ordinary Portland cement (OPC) [2]. These problems are enhanced for novel cementitious materials. Scientific community is searching for new cements with improved performances, such as high strengths and good workability of their corresponding concretes and/or environmentally friendly binders [7]. However, prior to the reliable use of any new binder, the hydration chemistry and durability of the mortars and concretes must be profoundly studied and characterized, as the safety and wealth of people are very much related to building industry.

Belite calcium sulfoaluminate [8], BCSA or sulfobelite, cements are considered environmentally friendly building materials, as their production may have up to 35% lower CO₂ footprint than OPC fabrication. They are prepared by mixing the clinker with different amounts of a calcium sulfate set regulator such as gypsum, bassanite or anhydrite. Hereafter cement nomenclature will be used: C = CaO, S = SiO₂, A = Al₂O₃, F = Fe₂O₃, S = SO₃, T = TiO₂ and H = H₂O. BCSA cements are based on belite (C₂S), ye'elimite (also called Klein's salt or tetracalcium trialuminate sulfate (C₄A₃S)) and other minor phases, such as ferrite (C₄AF) [9–13] or calcium aluminates (C₁₂A₇) [14] and calcium sulfate (CSH_x) as set retarder. The hydration of BCSA cements strongly depends on the amount and reactivity of the added calcium sulfate [15] and the presence of minor phases. Most of the hydration heat is released within the first 12–24 h of hydration [11,16,17]. The

* Corresponding author. Tel.: +34 952131877; fax: +34 952132000.
E-mail address: mgd@uma.es (A.G. De la Torre).

ARTICLE

A#3

Hydration Reactions and Mechanical Strength Developments of Iron-Rich Sulfolbelite Eco-cements

Gema Álvarez-Pinazo,[†] Isabel Santacruz,[†] Laura León-Reina,[‡] Miguel A. G. Aranda,^{†,§} and Angeles G. De la Torre^{*,†}

[†]Departamento de Química Inorgánica and [‡]Servicios Centrales de Apoyo a la Investigación, Universidad de Málaga, Campus Teatinos S/N, 29071 Málaga, Spain

[§]Consortium for the Exploitation of the Synchrotron Light Laboratory ALBA Synchrotron, Carretera BP 1413, km 3.3, E-08290 Cerdanyola, Barcelona, Spain

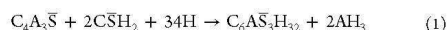
Supporting Information

ABSTRACT: Belite calcium sulfoaluminate (BCSA) cements are low-CO₂ building materials. However, their hydration behavior and its effect on mechanical properties have still to be clarified. Here, we report a full multitechnique study of the hydration behavior up to 120 days of nonactivated and activated BCSA laboratory-prepared clinkers, with β - or α' -belite as main phase, respectively. The effects of the amount of gypsum added were also studied. The hydration and crystallization processes are reported and discussed in detail. Finally, shrinkage/expansion data are also given. The optimum amount of gypsum was close to 10 wt %. Our study has demonstrated that β -belite reacts at a higher pace than α' -belite, irrespective of the gypsum content. The hydration mechanism of belite determines the development of the mechanical strengths. These are much higher for activated BCSA cement, ~65 MPa at 120 days, against ~20 MPa for nonactivated BCSA cement, with the latter having larger amounts of stratlingite.

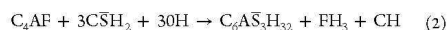
INTRODUCTION

Concrete based on ordinary Portland cement (OPC) is the most important building material. Its production is regarded as the third largest source of CO₂ emission, after combustion of fossil fuels and deforestation. CO₂ emissions emanating from cement kilns are associated with burning of carbon-based fuels (~40%) and decarbonation of limestone (~60%).¹ It is estimated that the global cement industry produces around 1.4 billion metric tons of CO₂ per year, or about 6% of worldwide man-made CO₂ emissions.² There are several possibilities to reduce the environmental impact of cement production, such as blending Portland clinker/cement with, for instance, fly ashes or slags, using alternative fuels in the cement kiln, or developing low-carbon binders, such as pozzoland-based, sulfate-based, or low-calcite-demanding cements.³ The latter binders are based on belite (C₂S)⁴ or ye'elimite (C₄A₃S).^{5–7} Ye'elimite-rich cements, also called calcium sulfoaluminate (CSA) cements, are mainly manufactured in China and their production, when compared to that of OPC, may reduce CO₂ emissions up to 40%. However, CSA cements are commonly used for niche applications⁸ due to their high prices, associated with the high demand for expensive bauxite. Belite calcium sulfoaluminate⁶ (BCSA) or sulfolbelite cements have belite as the main phase, with ye'elimite as a second component, and require much lower amounts of bauxite compared to CSA cements. The CO₂ footprint of sulfolbelite cements is about 30% lower than that of OPC. Compared to low-cost (and low-performance) belite-rich cements⁴ and high-cost (and high-performance) CSA cements, sulfolbelite cements are expected to show in-between behavior. The most common composition of BCSA clinkers includes β -C₂S, C₄A₃S, and C₄AF;^{6,9,10} being iron-rich sulfolbelite materials, they are

hereafter named as BCSAF. They are produced at ~1300 °C and show rapid hardening, good durability, self-stressing ability, and volume stability, depending on the amount of added gypsum; furthermore, they can be easily ground due to their high porosity, caused by lower clinkering temperature.⁶ Recently, a new class of BCSAF cements has been patented by Lafarge,^{9,11} to which stabilization of high-temperature belite polymorphs (α -forms) is given (for instance with borax) together with high early mechanical strength. However, the hydration chemistry and durability of mortars derived from these eco-cements must be profoundly studied. Ye'elimite and calcium sulfate (in the form of anhydrite or gypsum) govern the initial reactions and give early strengths. The hydration of ye'elimite in the presence of calcium sulfate provokes the precipitation of crystalline ettringite (C₆A₃S₃H₃₂), also called AFt, and amorphous aluminum hydroxide according to the following reaction:



Phases coming from hydration of brownmillerite and gypsum (see reaction 2) are identified as AFt, CH, and an iron-rich amorphous phase with a stoichiometry close to FH₃,¹² which slightly contributes to later strength development.



Received: July 31, 2013

Revised: October 18, 2013

Accepted: October 28, 2013

Published: October 28, 2013

ARTICLE

A#4

TECHNICAL ARTICLE

Rietveld quantitative phase analysis with molybdenum radiation

Ana Cuesta,¹ Gema Álvarez-Pinazo,¹ Marta García-Maté,¹ Isabel Santacruz,¹ Miguel A. G. Aranda,^{1,2} Angeles G. De la Torre,¹ and Laura León-Reina^{3a)}

¹Departamento de Química Inorgánica, Universidad de Málaga, Campus Teatinos S/N, 29071 Málaga, Spain

²ALBA-CELLS Synchrotron, Carretera BP 1413, Km. 3.3, E-08290 Cerdanyola, Barcelona, Spain

³Servicios Centrales de Investigación SCAI, Universidad de Málaga, 29071 Málaga, Spain

(Received 16 May 2014; accepted 31 August 2014)

Building materials are very complex samples of worldwide importance; hence quantitative knowledge of their mineralogical composition is necessary to predict performances. Rietveld quantitative phase analysis (RQPA) allows a direct measurement of the crystalline phase contents of cements. We highlight in this paper the use of laboratory X-ray powder diffraction (LXRPD) employing high-energy radiation, molybdenum (Mo), for attaining the RQPA of cements. Firstly, we evaluate the accuracy of RQPA employing a commercial calcium sulfoaluminate clinker with gypsum. In addition to $\text{MoK}\alpha_1$ and $\text{MoK}\alpha_{1,2}$ radiations, Cu and synchrotron patterns are also analyzed for the sake of comparison. Secondly, the assessment of the accuracy of RQPA results obtained using different radiations (synchrotron, Mo, and Cu) and geometries (reflection and transmission) is performed by analyzing two well-known commercial samples. As expected, for LXRPD data, accuracy in the RQPA results improves as the irradiated volume increases. Finally, three very complex aged hydrated cements have been analyzed using $\text{MoK}\alpha_1$ -LXRPD and Synchrotron-XRPD. The main overall outcome of this work is the benefit for RQPA of using strictly monochromatic $\text{MoK}\alpha_1$ radiation. Best laboratory results arise from $\text{MoK}\alpha_1$ data as the effective tested volume is much increased but peak overlapping is not swelled. © 2014 International Centre for Diffraction Data. [doi:10.1017/S0885715614000785]

Key words: Mo and Cu radiations, synchrotron radiation, irradiated volume, cement, accuracy

I. INTRODUCTION

In a standard laboratory instrument, the X-rays are produced in a sealed-tube source, in the same way as they were produced in the original tube discovered by W. C. Röntgen in 1895, where electrons accelerated by a potential difference of up to 60 kV bombard a metal anode inside a vacuum tube. Such sources differ only in the intensity of the radiation produced. The most common target elements are Cu for powder diffraction and molybdenum (Mo) for single-crystal studies. Alternative radiations, both with lower (Cr, Fe, and Co) and higher (Ag and W) energies, are employed for very special applications. For routine powder diffraction work, a Cu tube is the most common choice, giving the wavelength 1.5406 Å. Heavier elements are believed to give too short wavelengths for most practical use in the laboratory, as they exacerbate the peak overlapping, although they become important for total scattering, pair distribution function (PDF) studies and in order to avoid fluorescence from samples containing elements excited by Cu radiation (Dinnebier and Billinge, 2008). On the other hand, the advantages of high-energy penetrating laboratory X-ray sources are: (i) larger irradiated volumes, (ii) lower absorption effects, and (iii) more accessible Bragg reflections. However, to keep the angular resolution in powder diffraction is a key point since high-energy patterns are squeezed and therefore, if the appropriate optic elements

are not present, peak overlap may become an important drawback.

For powder diffraction-based quantitative phase analysis procedures, it is generally accepted that the peak intensities need to be measured to an accuracy of about ± 1 –2% relative (Dinnebier and Billinge, 2008). The ability to achieve this goal is strongly influenced by the size of the crystallites in the sample and their number contributing to the Debye-Scherrer cone (Smith, 2001). Reproducible diffraction intensities in zero-dimensional (0D) or 1D detectors require smooth cones which are obtained from samples containing small crystallite size(s) and high-enough number of crystallites per phase. Elton and Salt (1996) estimated the number of crystallites diffracting in a sample. Fluctuations in peak intensity between replicate samples arise largely from statistical variation in the number of particles contributing to the diffraction process. It was shown that small changes to the instrumental and sample configurations can significantly improve the sample particle statistics. For a given sample, several methods can be used to increase the number of crystallites contributing to the diffraction pattern, including: (i) rotate the sample about the normal to the sample surface for a flat plate sample or the sample axis for a capillary sample; (ii) oscillate the sample about the incident angle axis, this motion removes the exact Bragg-Brentano $\theta/2\theta$ relationship between sample and receiving slit and may lead to aberrations in the peak intensities; (iii) repack the sample, recollect, and reanalyze the diffraction data, averaging the results from each analysis will produce more meaningful parameter values, (iv) reduce the average crystallite size(s) by milling (Buhrke *et al.*, 1998),

^{a)}Author to whom correspondence should be addressed. Electronic mail: lauralr@uma.es

ARTICLE

A#5

Hydration of iron-rich BCSA cements with different calcium sulfate sources

G. Álvarez-Pinazo^a, I. Santacruz^a, M. A. G. Aranda^{a,b}, A. G. De la Torre^{a,*}

^a Departamento de Química Inorgánica, Universidad de Málaga, Campus Teatinos S/N. 29071-Málaga, Spain.

^b CELLS-ALBA Synchrotron Light Facility, 08290 Cerdanyola, Barcelona, Spain.

* Corresponding author. Tel.: +34952131877; fax: +34952132000.

E-mail address: mqd@uma.es (A.G. De la Torre)

Abstract

Iron-rich Belite Calcium SulfoAluminate cements, BCSAF, are a sustainable alternative to OPC to reduce CO₂ emissions. Their most common composition includes belite, ye'elinite and ferrite. The hydration of BCSAF-pastes is affected by the presence of different sulfate sources, water-to-cement (w/c) ratio, and the polymorphs of ye'elinite and belite. The aim of this research is to understand the influence of the sulfate source on the hydration of two laboratory-prepared BCSAF-cements. One studied clinker contained β -belite and orthorhombic-ye'elinite (non-active), and the other one α'_H -belite and pseudo-cubic-ye'elinite (activated with borax during clinking). Pastes were mainly characterized through Rietveld-quantitative-phase-analysis of powder patterns, thermal analysis and scanning-electron-microscopy. Active-mortars developed higher compressive strengths than non-active-mortars, independently of the sulfate source. The highest values for active-mortars (w/c=0.55) were 40±1MPa (28d) with anhydrite, and 68±1MPa (120d) with gypsum. Ettringite content and stability and hydration of belite are key issues that justify the reported mechanical strengths.

Keywords: Hydration (A), Rietveld Method (B), Backscattered Electron Imaging (B), Compressive Strength (C), Sulfobelite (D).

CHAPTER 4

RESULTS AND DISCUSSIONS

4.1. SYNTHESIS OF LABORATORY-PREPARED BCSAF CLINKERS: SCALE-UP.

One of the main objectives of this Thesis has been to perform the "medium-scale" synthesis of two BCSAF clinkers in our laboratory. The term "medium-scale" has been used in this work because the amount prepared from each of them has been about 2 kg, much higher than that used until now in the laboratory (a few grams).

4.1.1. Raw material characterisation.

In the preparation of the clinkers, the same raw materials commonly used in cement plants were used. Their characterisation was carried out by XRF chemical analysis, RQPA and DTA-TG studies. The raw materials used here were: **limestone**, as a source of calcium (from the cement factory *Financiera y Minera*, in Málaga); **kaolin**, as source of aluminium and silicon (from the company *Caolines Vimianzo, S.A.U., CAVISA*, La Coruña, ref. NC-35); **gypsum**, as a sulphur source (from the cement factory *Financiera y Minera*, in Málaga); **a red bauxite**, as a source of iron and aluminium, supplied by *Cementos Molins*; **marl**, a sand supplied by *Financiera y Minera* (in Málaga) was used as a silicon corrector; and finally **borax** (Prolabo, 97% min.), $\text{Na}_2\text{B}_4\text{O}_7 \cdot 10\text{H}_2\text{O}$, was used as an activator of clinker. The chemical composition of raw materials was determined by XRF and is given in Table 4.1.

Table 4.1. Elemental composition of raw materials determined by XRF and expressed as oxide wt%.

	Limestone	Sand	Kaolin	Bauxite
Al_2O_3	0.18	1.85	35.17	54.5
CaO	54.02	3.10	0.029	1.90
SiO_2	0.80	85.0	47.48	2.27
Fe_2O_3	0.09	2.45	1.14	25.3
K_2O		0.46	1.88	0.096
SO_3			0.027	0.175
Na_2O			0.08	0.015
MgO	0.50	1.95	0.16	
TiO_2			0.053	2.58
MnO			0.016	0.037
P_2O_5			0.095	0.061
ZrO_2			0.008	0.054
LoI*	44.41	5.19	13.8	12.89

LoI* : Loss on ignition at 1000°C

4.1.2. BCSAF clinkers preparation: optimisation of process.

Two BCSAF clinkers with the expected phase composition of 50 wt% of C_2S , 30 wt% of C_4A_3S and 20 wt% of C_4AF (Cuberos et al., 2010) were prepared. One of the clinkers was “activated” through the addition of borax, 2 wt% expressed as B_2O_3 , to the raw material mixture. The aim of the activation has been obtaining clinkers with different belite (β - C_2S or α'_H - C_2S) and ye'elite (orthorhombic or pseudo-cubic) polymorphs to understand the effect of the polymorphs on the pastes hydration mechanism and mechanical performances. Hereafter, these clinkers will be named as BCSAF_B0 (non-active) and BCSAF_B2 (active), for boron-free and boron-containing clinker, respectively. Table 4.2 depicts dosage of raw materials used to prepare both clinkers and the corresponding elemental composition of the raw mixtures. The clinkering process was optimised to obtain about 2 kg of clinker.

Table 4.2. Raw materials dosages in wt% and elemental composition of raw mixtures except for water or CO_2 (expressed as oxide in wt%).

	BCSAF_B0	BCSAF_B2
Limestone	59.2	56.9
Bauxite	17.1	16.5
Kaolin	9.3	8.9
Gypsum	7.5	7.2
Marl	6.9	6.6
Borax	-	3.9
CaO	52.7	51.3
SiO ₂	17.5	17.0
Al ₂ O ₃	19.2	18.6
Fe ₂ O ₃	6.6	6.4
SO ₃	4.0	3.8
B ₂ O ₃	-	2.0
Na ₂ O	-	0.9

In both cases, the raw mixture (~3 kg) was pre-homogenized in plastic bags for a few minutes. Then, the sample was mixed for 15 min in a micro-Deval machine (A0655, Proeti S.A., Spain) at 100±5 rpm with steel balls (9 balls of 30 mm of diameter, 21 balls of 18 mm of diameter and balls of 10 mm of diameter up to a total ball weight of 2500±4 g). A small amount of grinding additive was used to prevent the sticking of the material to the balls. The resulting mixture was pressed into pellets of about 40 g (55 mm of diameter and ~5 mm of height, see figure 4.1.a). Pellets were placed in a large Pt/Rh crucible of 325 cm³ of volume (figure 4.1.b).

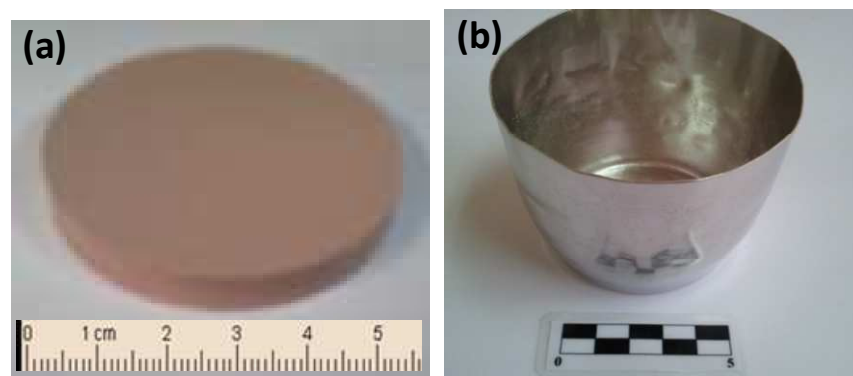


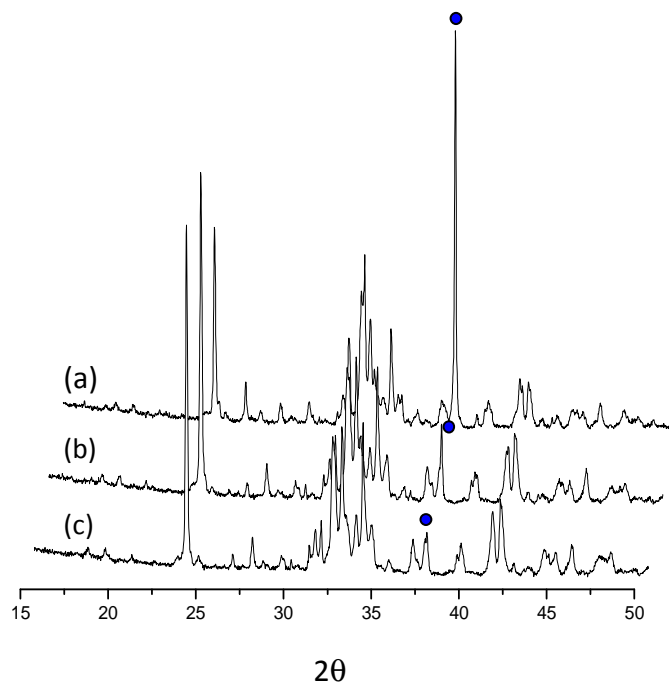
Figure 4.1. (a) BCSAF raw mixture pellet; (b) Pt/Rh crucible use for clinkering.

A two-step clinkering cycle was previously optimised for 5 g of BCSAF clinkers (dye-pressed samples with 10 mm of diameter) with different boron contents, (Cuberos et al., 2010). In that study, the best results were found when samples were heated at 900°C during 30 min (heating rate of 5 °C/min) and further heated at 1300°C for 15 min; all samples were quenched with air flow.

The same clinkering process was followed to start our study but keeping the sample at 1300°C for 15 min resulted not enough for the scaling up; hence, the process had to be optimised. Table 4.3 gives RQPA for BCSAF_B0 clinker prepared under different thermal cycles. Two main parameters were controlled to determine both the optimum temperature and time of dwelling at high temperature: i) the targeted phase assemblage and ii) the minimum free lime content. It can be seen that 1350°C is the temperature with the lowest percentage of free lime (< 1 wt%) indicating the success of the clinkering process. In addition the content of non-hydraulically active phases, such as gehlenite (C_2AS) and $\gamma-C_2S$, is the lowest when heating the samples at this temperature. Figure 4.2 shows, as an example, a selected region of three patterns of BCSAF_B0 clinker after different heating cycles. From all these results, we concluded that **1350°C (and 30 min of dwelling)** was the optimum clinkering cycle for our two scaled-up clinkers.

Table 4.3. Direct RQPA for BCSAF_B0 clinker prepared following different clinkering cycles.

	1300°C		1325°C		1350°C
	15 min	45 min	30 min	45 min	30 min
β -C ₂ S	41.5(4)	38.3(4)	46.7(3)	45.6(3)	46.8(3)
o-C ₄ A ₃ S	16.2(2)	17.1(2)	13.6(6)	16.1(6)	13.8(5)
c-C ₄ A ₃ S	-	-	13.0(6)	11.3(6)	12.8(5)
C ₄ AF	9.9(3)	10.1(3)	11.0(2)	11.7(3)	15.9(2)
C ₂ AS	12.2(2)	18.3(2)	6.4(2)	6.5(2)	4.9(2)
C ₃ A	-	-	4.6(3)	4.3(2)	3.3(2)
γ -C ₂ S	1.7(1)	2.2(2)	2.9(2)	3.1(2)	1.8(1)
CS	2.9(1)	1.0(1)	-	-	-
CaO	15.6(1)	13.1(1)	1.8(1)	1.3(1)	0.8(1)

**Figure 4.2.** Selected region of patterns of BCSAF_B0 clinker after heating at (a) 1300°C for 15 min , (b) 1325°C for 30 min, and (c) 1350°C for 30 min; and ● highlights free lime (CaO).

Once the heating cycle was optimised, ~3 kg of raw material was clinkered to obtain ~2 kg of each clinker (BCSAF_B0 and BCSAF_B2). For that, six pellets (~40 g each) were placed into the Pt/Rh crucible, heated (900°C/30 min and 1350°C/30 min with heating rates of 5 °C/min) and quenched with air flow. Since only ~200 g of raw mixture can be clinkered at the same time, the process was repeated several times. The as-clinkered pellets were grinded in a micro-Deval mill at 100 rpm for 1 h in batches of ~700 g; the obtained powder was sieved through a 250 µm mesh and characterised to verify the viability of the methodology.

4.1.3. Characterisation of the scaled-up BCSAF clinkers.

Once the clinkering process was optimised, the two obtained clinkers were characterised through LRPD, including the analysis of selective dissolutions, and SEM-EDS.

4.1.3.1. RQPA (normalised to 100% of crystalline phases).

Both scaled-up BCSAF_B0 and BCSAF_B2 clinkers were studied by LRPD (CuK α_1 radiation) to identify, characterise and quantify the crystalline phases (by the Rietveld method), as described in A#1. Table 4.4 reports the direct RQPA results (wt%), normalised to 100% of crystalline phases, obtained for these two clinkers.

Table 4.4. Direct RQPA results (wt%) for the two BCSAF clinkers normalised to 100% of crystalline phases. Numbers between brackets are the standard deviations of three independent measurements. Rietveld disagreement factors are also given.

Phase	BCSAF_B0	BCSAF_B2
α_H' -C ₂ S	-	57(2)
β -C ₂ S	48.7(6)	-
γ -C ₂ S	2.6(5)	-
o-C ₄ A ₃ S	15(1)	-
c-C ₄ A ₃ S	14(1)	31(2)
C ₄ AF	14.9(2)	10.1(6)
C ₂ AS	4.4(2)	
CT	1.3(2)	2.1(1)
R_{WP}/%	3.7	4.3

Figure 4.3 shows a selected range of Rietveld plots for both clinkers, where the main phases are labelled. The final phase assemblage obtained for the two laboratory-scaled-up prepared clinkers confirms that BCSAF_B0 clinker contains β -C₂S and both orthorhombic and pseudo-cubic ye'elite as main phases, meanwhile α' -C₂S and pseudo-cubic ye'elite are stabilised in BCSAF_B2.

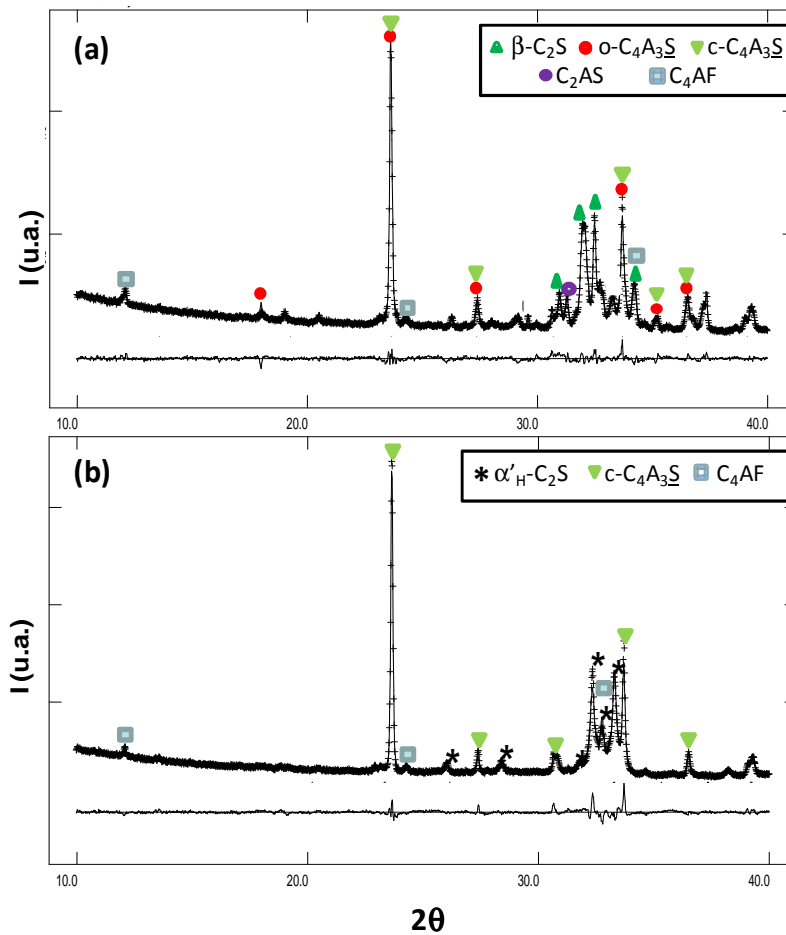


Figure 4.3. Selected range of Rietveld plots for (a) BCSAF_B0, and (b) BCSAF_B2 clinkers. Peaks due to a given phase are labelled.

4.1.3.2. Selective dissolutions.

Selective dissolutions of BCSAF_B0 and BCSAF_B2 clinkers were carried out for a better characterisation (see A#1). Since main peaks of CT, C₃A and merwinite,

$\text{Ca}_3\text{Mg}(\text{SiO}_4)_2$, are overlapped, their identification/quantification by LRPD and RQPA is a very rough task. Figures 4.4 and 4.5 show a small selected region of the Rietveld plots for the aluminate and silicate residues of BCSAF_B0 and BCSAF_B2 clinkers, respectively. It should be noted that the silicate residue is obtained when aluminate phases are removed. In similar way, the aluminate residue is achieved when the silicate phases were dissolved.

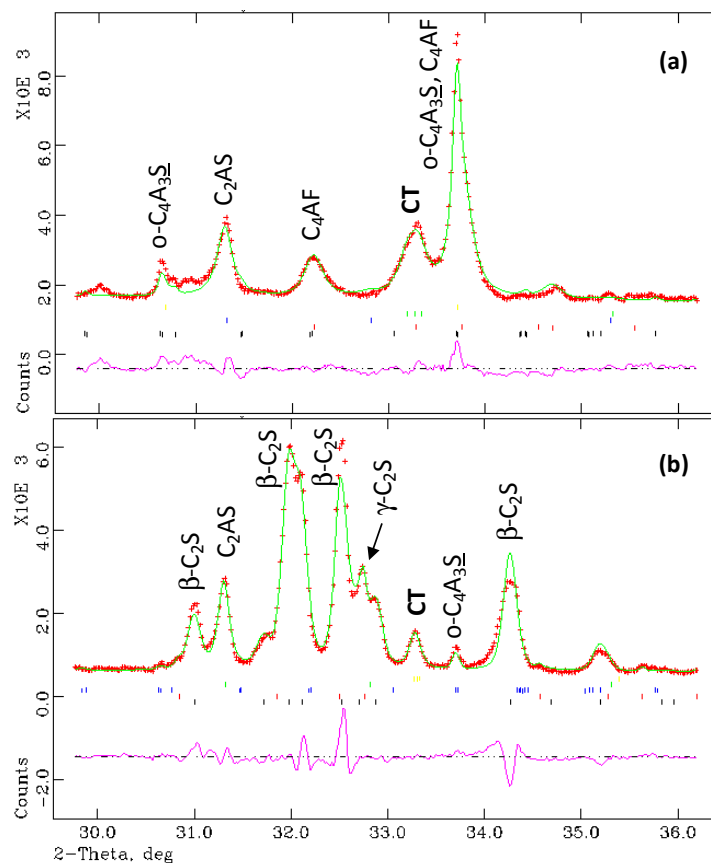


Figure 4.4. Selected range of the Rietveld plots for: (a) BCSAF_B0 aluminate residue and (b) BCSAF_B0 silicate residue.

In Table 4.5 is reported the direct RQPA results (wt%), normalised to 100% of crystalline phases, obtained for both aluminate and silicate residues of BCSAF_B0 and BCSAF_B2 clinkers. The results of this table show that aluminium containing phases have not been completely removed from the silicate residue (e.g. little amounts of $\text{C}_4\text{A}_3\text{S}$ and C_4AF is still present in BCSAF_B2 clinker). Moreover, it also can be

observed the existence of a small amount of C_2AS in both aluminate and silicate residue of BCSAF_B2, that it was not quantified in the original clinker.

Table 4.5. Direct RQPA results (wt%) for the aluminate and silicate residues of two BCSAF clinkers normalised to 100% of crystalline phases. Rietveld disagreement factors are also given.

Phase	Silicate residue		Aluminate residue	
	BCSAF_B0	BCSAF_B2	BCSAF_B0	BCSAF_B2
α'_H-C_2S	-	82.8(1)	-	-
$\beta-C_2S$	78.1(1)	-	-	-
$\gamma-C_2S$	4.9(2)	-	-	-
$o-C_4A_3S$	3.5(1)	-	20.1(6)	-
$c-C_4A_3S$	-	7.1(1)	26.8(5)	66.4(1)
C_4AF	-	3.1(1)	33.9(3)	22.2(3)
C_2AS	10.6(2)	2.8(2)	15.6(3)	4.6(4)
CT	2.8(1)	4.1(1)	3.7(2)	6.8(2)
$R_{WP}/\%$	5.5	4.8	4.3	3.9

The Rietveld plot for the silicate residue of BCSAF_B0 is very informative as the diffraction peaks from C_4AF disappear but the diffraction peak at $\sim 33.3^\circ$ (2θ) is still present (arrows in Figure 4.4 and 4.5). Hence, this phase may be perovskite or merwinite but not C_3A . The Rietveld refinements of the silicate residue indicated that the fit with perovskite was better (lower R-factors) than that with merwinite. A deep analysis of the Rietveld plots of the residues indicates that the peak widths in the BCSAF_B2 are narrower than those in BCSAF_B0. For instance, the diffraction peaks from CT and C_4A_3S in BCSAF_B2 aluminate fraction are narrower than those in the BCSAF_B0 aluminate fraction; see Figures 4.5.a and 4.4.a, respectively. This behaviour is likely due to a better particle growth when borax is added. In fact, scanning electron microscopy data (figure 4.6 in the next section) indicate that the average particle sizes for BCSAF_B2 are larger than those of BCSAF_B0.

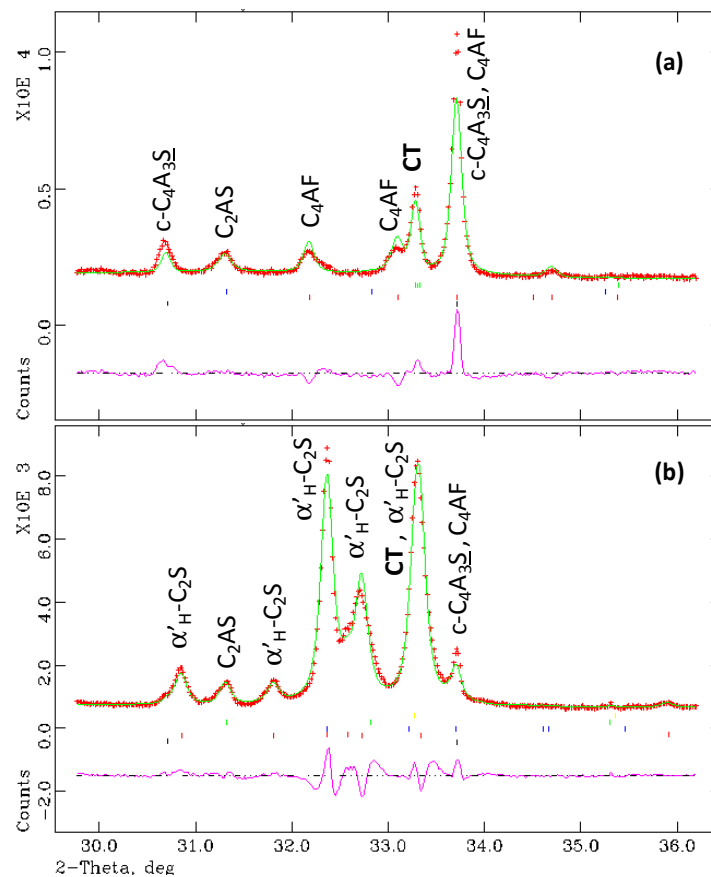


Figure 4.5. Selected range of the Rietveld plots for: (a) BCSAF_B2 aluminate residue and (b) BCSAF_B2 silicate residue.

4.1.3.3. SEM-EDS characterisation.

Size, morphology and composition of particles of both clinkers were studied through SEM-EDS (in A#2). Figures 4.6.a and 4.6.b show SEM micrographs of the polished anhydrous BCSAF_B0 clinker at different magnifications. Figures 4.6.c and 4.6.d show the equivalent micrographs for the polished anhydrous BCSAF_B2 clinker. Figures 4.6.a and 4.6.c show ye'elimite angular shaped particles, as previously described (Pérez-Bravo et al., 2014). The identification of these particles was confirmed by EDS analysis, showing semi-quantitative average Al/Ca and S/Ca ratios of 1.4 and 0.10, respectively, which are relatively close to the theoretical values, 1.5 and 0.25, respectively. Moreover, this study revealed that the average particle size of ye'elimite in BCSAF_B0 was slightly smaller than that in BCSAF_B2; this is marked with arrows in Figures 4.6.a and 4.6.c. In addition, belite particle size was also studied

by SEM, being also smaller in BCSAF_B0 than in BCSAF_B2 clinker; in both cases these particles show a typical rounded shape.

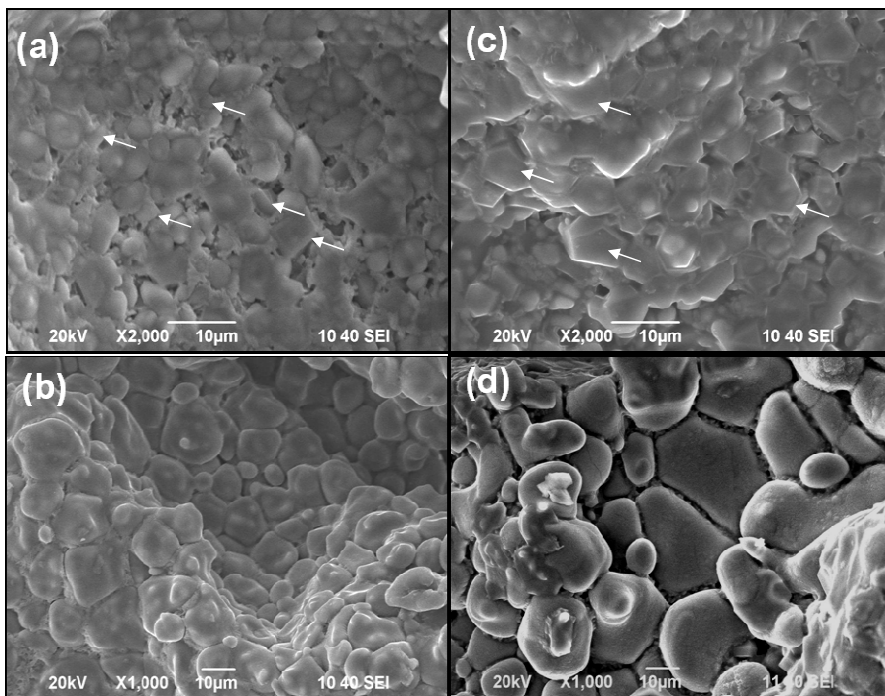


Figure 4.6. SEM micrographs of (a) and (b) anhydrous non-active-BCSAF clinker (BCSAF_B0), and (c) and (d) anhydrous active-BCSAF clinker (BCSAF_B2) (Figure 4 in A#2).

4.2. PHASE ANALYSIS OF DIFFERENT YE'ELIMITE-CONTAINING CLINKERS AND CEMENTS.

In general, ye'elimites-containing cements are complex materials due to the presence of many crystalline phases, some of them also displaying polymorphism. LXRPD is the most appropriate technique to identify, characterise and quantify the crystalline phases within these samples. Therefore, if the mixture has an appreciable amount of amorphous and/or non-crystalline phases, this method may be considered as semi-quantitative. To overcome this problem, two approaches have been used in this PhD Thesis, the internal and the external standard methods (see Introduction section).

In this section we discuss the most relevant results described in A#1 concerning the characterisation of these anhydrous materials through RQPA. The

research was aimed to: i) identify and quantify the crystalline phases present in several ye'elimite-containing clinkers and cements and ii) quantify their ACn content through two methodologies (external standard in reflection geometry and internal standard in transmission geometry). In order to do so, three commercial CSA clinkers (ALIPRE®, BELITH_CS10 and S.A.cement), one CSA cement (CSA_trial) and two laboratory-prepared BCSAF clinkers (BCSAF_B0 and BCSAF_B2) were analysed through LXRPD.

4.2.1. RQPA (normalized to 100% of crystalline phases).

Firstly, direct RQPA of these samples, normalised to 100% of crystalline phases, was performed, and they are shown in Tables 4.4 and 4.6. These values were obtained from the approach described in section 1.5.1.1., and hence, the presence of an ACn fraction was not considered. Note that standard deviations in these tables are those derived from three independent measurements (they are not the mathematical errors from the Rietveld refinements). These three analyses were carried out to different portions of the samples for better averaging (i.e. not recording three patterns for the same sample). Figures 1 to 6, in A#1, show a selected range of the Rietveld plots for the six studied ye'elimite-containing materials, showing the good fit of the analysis. The major peaks for each phase are labelled. Several conclusions can be obtained from this analysis, as described below:

Table 4.6. Direct RQPA results (wt%) for the ye'elimite-containing cements normalized to 100% of crystalline phases. Numbers between brackets are the standard deviations of three independent measurements.

	α -C ₄ A ₃ S	c-C ₄ A ₃ S	α' -C ₂ S	β -C ₂ S	C ₄ AF	CT	M	C ₃ S ₂ S	C ₂ SH ₂	C ₂ S	C ₃ S
ALIPRE® ^a	51.0(7)	18.5(6)	9.4(3)	7.7(1)		3.5(1)	0.52(2)			9.0(4)	
BELITH-CS10 ^b	40.1(9)	25.5(6)		16.0(2)	2.4(1)	9.3(1)	2.2(2)				
S.A.cement ^c	27.5(5)	28.7(6)	21.4(9)	9.7(4)		3.5(4)	1.1(1)			6.3(1)	
CSA_trial ^d	17(1)	23.6(7)		9.0(9)		4.8(2)		16.2(5)	13.7(4)	8.5(2)	5.9(5)

^aAlso contains 0.5(1) wt% of Na₂Si₂O₅. ^bAlso contains 4.6(1) wt% of akermanite. ^cAlso contains 1.9(1) wt% of CA. ^dAlso contains 1.8(7) wt% of dolomite.

i) The good accuracy of the analyses was confirmed by comparing the amount of magnesium oxide obtained by RQPA and the obtained by XRF (Tables 2 and 5 in A#1). Magnesium oxide contents were chosen because magnesium is little soluble in the ye'elimite or belite structures. For example, RQPA showed the highest amount of periclase (MgO) for BELITH_CS10, 2.2(2) wt%, and this is in full agreement with elemental analysis determined by XRF. Furthermore, S.A.cement (the second

sample with the highest magnesium content determined by XRF, 1.5 wt%) showed the second highest periclase content, 1.1 wt%, calculated by RQPA.

ii) Five out of six studied samples contained a mixture of orthorhombic and pseudo-cubic sodalite type-structures of ye'elimite. Only, BCSAF_B2 clinker showed just pseudo-cubic ye'elimite (Cuesta et al., 2014c). Stoichiometric ye'elimite at room temperature is orthorhombic $Pcc2$. However, the substitutions of Ca^{2+} by Na^+ and Al^{3+} by B^{3+} , Si^{4+} or Fe^{3+} seem to restore the cubic symmetry (Hargis et al., 2014a). The SEM-EDS study performed on BCSAF_B0 and BCSAF_B2 clinkers (see previous section 4.1.3.3.) shows that the ye'elimite particles in BCSAF_B2 containing little amount of Si, Fe and Na. The crystal structure of a doped (disordered) ye'elimite ($Ca_{3.8}Na_{0.2}Al_{5.6}Fe_{0.2}Si_{0.2}O_{12}SO_4$) has been studied at room temperature (Cuesta et al., 2014c). These authors established that the addition of SiO_2 , Na_2O , and Fe_2O_3 stabilized the high temperature pseudo-cubic form of ye'elimite at room temperature. Bullerjahn et al. (2014) also found a mixture of pseudo-cubic and orthorhombic ye'elimite in their cements, and the pseudo-cubic polymorph increased at the expense of the orthorhombic one with increasing the iron content. A reverse correlation between the amount of ye'elimite and tetracalcium aluminoferrite (C_4AF) was found, which agrees with the incorporation of iron into the ye'elimite framework.

iii) Different belite polymorphs have been identify and quantify. Borax addition fully transforms β -belite in BCSAF_B0 to α'_H -belite in BCSAF_B2. The mechanism for the borax activation of belite has been very recently unraveled as a solid solution, $Ca_{2-x}Na_x(SiO_4)_{1-x}(BO_3)_x$, and the crystal structure of α'_H - $Ca_{1.85}Na_{0.15}(SiO_4)_{0.85}(BO_3)_{0.15}$ has been worked out (Cuesta et al., 2012). It is also noteworthy that S.A.cement has high α'_H -belite content. This can be justified with the elemental composition (determined by XRF) containing a quite high amount of Na_2O (1.4 wt%).

iv) CS quantified in ALIPRE®, S.A.cement and CSA_trial is the high temperature polymorph, anhydrite-II (Kirfel and Will, 1980). So, this less reactive CS was produced during the clinkering process. It should be noted that gypsum, bassanite and less-soluble anhydrite-II can be easily distinguished and quantified by RQPA. However, bassanite and highly soluble anhydrite-III can only be distinguished in especial experimental conditions (Seufert et al., 2009) with high-quality LXRPD data.

v) The presence of ternesite (C_5S_2S , also known as sulphate-spurrite) is quite uncommon in CSA or BCSA clinkers. However, CSA_trial has a high amount of ternesite, 16.2(5) wt%. This is likely due to a very high SO_3 dosage in the raw materials. SO_3 value for this cement determined by XRF (16.7 wt%) is very high even taken into account the ~14 wt% of gypsum added. Overall SO_3 values range

approximately from 9 to 14 wt% for CSA clinkers and between 3 and 4 wt% for BCSA clinkers.

vi) Titanium is usually present in CSA and BCSA cements as it accompanies aluminium in bauxites. Furthermore, titanium may replace aluminium in some phases but the solubility limits are normally exceeded in CSA and BCSA clinkers. This is evident from the RQPA as the perovskite CaTiO_3 phase segregates. We have carried out the RQPA with this assumed stoichiometry, CaTiO_3 , however further studies are needed in order to establish the stoichiometry of the perovskite phase as it is well known that this phase forms extensive solid solutions with transition metals.

4.2.2. ACn content determination.

The ACn contents for the ye'elinite-containing samples were determined by two approaches: i) external standard procedure (G-factor method) with reflection geometry; ii) internal standard procedure (spiking method with ZnO), using $\text{CuK}\alpha_1$ radiation.

Table 6 in A#1 shows the RQPA results (wt%) including the ACn content for the studied ye'elinite-containing samples. The values obtained from reflection geometry using an external standard (G-factor method) are given in the first row, and those obtained from transmission geometry using ZnO as internal standard are given in the second row. In both cases, standard deviations are derived from three independent measurements.

The main conclusions drawn from the comparative study were: on the one hand, the G-factor method allows the measurement of both crystalline phases and ACn contents. The ACn contents obtained for CSA clinkers/cements are similar to those found in OPC cements, ~10 wt%. However, these contents are much higher in BCSAF clinkers, of the order of 25 wt%, in agreement with García-Maté et al. (2015b). On the other hand, the ACn values obtained by the internal standard showed the same trend obtained by the G-factor methodology, except for BELITH_CS10, which essentially showed a zero value.

The quantification of crystalline samples, taking into account ACn contents, obtained under these two methods matched quite well for four samples (S.A.cement, CSA_trial, BCSA_B0 and BCSAF_B2). However, for ALIPRE® and BELITH_CS10, the results are not that satisfactory. For the former, the differences in the quantification of $\text{c-C}_4\text{A}_3\text{S}$, β -belite and ACn are 5.7, 4.3 and 10.3 wt%. Three times the standard deviations is commonly used for a good level of confidence. So, the sum of 3σ for the two analyses (internal and external standard methods) was calculated giving 3.0, 5.1 and 9.6 wt% for $\text{c-C}_4\text{A}_3\text{S}$, β -belite and ACn values, respectively. Therefore, the quantification of $\text{c-C}_4\text{A}_3\text{S}$ for ALIPRE® is well out of the limits. For BELITH_CS10, the

differences in the quantification of α' -C₂S, β -belite and ACn are 4.3, 7.2 and 14.5 wt%, with the sum of 3σ for the two analyses giving 3.9, 3.9 and 5.7 wt%, respectively. In this case, the quantification of β -belite and ACn do not agree. García-Maté et al. (2015b) have recently published a comparative study of the amorphous determination in CSA and building related materials by these two methodologies. They reported that scale phase factors seem to be correlated to peak shape parameters or phenomena such as preferred orientation, which results in the overestimation of the ACn contents determined by G-factor method.

To finish this study, it is worth to highlight the importance of having accurate structural descriptions for every phase of the cements to be analysed. This is more important for major phases, and it will be illustrated for the RQPA of BC SAF_B2. If the 'old' published approximate crystal structure of α' -C₂S is used (Mumme et al., 1995), the Rietveld fit of the reflection data gave $R_{WP}=5.2\%$ and $R_F(\alpha'\text{-C}_2\text{S})=7.2\%$. The application of the G-method gave α' -C₂S and ACn contents of 35(1) and 33(1) wt%, respectively. A better Rietveld fit of the same pattern was achieved when a revised structural description was used, $\alpha'\text{-Ca}_{1.85}\text{Na}_{0.15}(\text{SiO}_4)_{0.85}(\text{BO}_3)_{0.15}$ (Cuesta et al., 2012). As a result lower disagreement factors were obtained: $R_{WP}=4.9\%$ and $R_F(\alpha'\text{-C}_2\text{S})=5.7\%$. This better fit gave a larger α' -C₂S scale factor (30.9(3) instead of 25.5(2)) and therefore, the α' -C₂S content was higher (41(1) wt%) and ACn content smaller, 28(1) wt%. So, the use of approximate crystal structures gives lower determined crystalline phase contents and higher ACn contents, as expected.

4.3. HYDRATION STUDY OF BC SAF CEMENTS.

The hydration and inter-relationship between phase composition and performance of the two laboratory-prepared BC SAF cements were studied. The presence of different polymorphs of ye'elimite and belite affects the hydration due to the different reactivity of those polymorphs. The aim of this section is to understand the influence of different types and amounts of calcium sulphate sources on the hydration of two laboratory-prepared BC SAF cements which contain different belite (β -C₂S or α' -C₂S) and ye'elimite (orthorhombic or pseudo-cubic) polymorphs (A#2, A#3 and A#5).

The methodology to prepare cement pastes was previously optimised. Initially, methacrylate sample holders (at $20\pm 1^\circ\text{C}$ and 99% relative humidity) covered with a plastic wrap were used to store the pastes until the corresponding measurements were performed (A#3); this procedure gave irreproducible results (due to carbonation problems) and segregations during early-age hydration. Finally, cement pastes were poured into hermetically closed PTFE cylinder shape moulds and

rotated at 15 rpm during the first 24 hours at $20\pm 1^\circ\text{C}$; after that, the samples were demoulded and stored within deionised water at $20\pm 1^\circ\text{C}$ until the age of study (A#5, submitted). With this procedure, we have achieved homogenous cement pastes, avoiding the undesired drying and carbonation effects during hydration.

Additionally, a methodology to stop hydration was established prior to LRPD characterisation (described in A#3). It is known that complete drying of sample without any chemical and/or physical effects is not possible in practice, so it is very important to select the appropriate methodology for water removal (Zhang and Scherer, 2011). One fraction of the pastes was milled to fine powder in an agate mortar prior to stopping hydration. The stopping procedure consisted on filtration in a Whatman system (90 mm diameter Whatman filter with a pore size of $2.5\ \mu\text{m}$ and a Teflon support) with acetone (Prolabo S.A.) twice and finally with diethyl ether (Prolabo S.A.). Although, the use of acetone may affect the specific surface area of the cements (Zhang and Scherer, 2011), we have not observed this effect in our experimental conditions. The stopped-hydration samples were stored in a desiccator to avoid further hydration and any possible carbonation/alteration.

All the cement hydration studies were performed on pastes prepared by mixing cement with water at $w/c = 0.55$. We are fully aware that lower w/c ratios give large mechanical strength developments, but we have chosen this ratio in this first study to avoid irreproducible local drying effects. Studies with variable w/c ratios are planned, but not for this Thesis.

4.3.1. Hydration of BCSAF cements with gypsum as setting regulator.

Two studies were carried out in our BCSAF cements to better understand their hydration behaviour. On the one hand, an *in-situ* SXRPD study for the first hours of hydration was carried out in the XRPD station of ALBA, the Spanish Synchrotron Radiation Facility (Barcelona, Spain). RQPA was used to establish the degree of reaction (α) of main crystalline phases. Kinetics of hydration and factors influencing the hydration reactions were established and correlated to calorimetric data. On the other hand, *ex-situ* studies at later ages of hydration (3, 7, 28 and 120 days) were performed to determine the influence of the amount of gypsum added to BCSAF cements on hydration behaviour through LRPD ($\text{CuK}\alpha_1$ radiation).

Moreover, an attempt to determine the possible composition of the ACn (sulphate, silicate, aluminate and iron-bearing groups) was performed; in addition, a comparative study of $\text{MoK}\alpha_1$ and synchrotron radiations for selected samples was also performed.

Sample preparation. For the *in-situ* study, the two BCSAF clinkers, BCSAF_B0 and BCSAF_B2, were used and mixed with 10 wt% of gypsum. Then, pastes (w/c=0.55) were immediately introduced into glass capillaries of 0.5 mm of diameter with a syringe. The capillaries were sealed with wax and grease to avoid any water loss. During data collection (Figure 4.7), the capillaries were rotated to improve diffracting particle statistics. The data acquisition time was ~15 min per pattern to attain very good signal-to-noise ratio over the angular range of 1–35° (2 θ) with $\lambda = 0.61984 \text{ \AA}$. The temperature inside the experimental hutch was 26(1)°C.

For *ex-situ* experiments, the optimisation of the sulphate source content was performed by adding different amounts of gypsum (5, 10 and 15 wt%) to both clinkers. Cements are labelled hereafter as GgBx, where g = 5, 10 or 15, and x = 0 or 2 (for non-active or active clinkers, respectively). These cement pastes were also prepared by mixing cement with water at w/c = 0.55 (mass ratio).

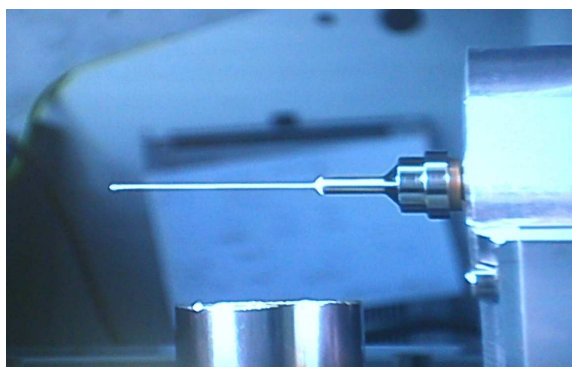


Figure 4.7. Cement paste in sealed capillary placed in the sample holder in the XRPD end station of MSPD beamline of ALBA synchrotron.

4.3.1.1. *In-situ* early hydration behaviour (< 24 h).

The early hydration of two BCSAF cements was studied and reported in A#2. Figure 4.8 gives selected ranges of SXPDP raw patterns of G10B0 (containing β -C₂S and orthorhombic ye'elimitite) and G10B2 (with α' -C₂S and pseudo-cubic ye'elimitite), at selected times of hydration. Figures 2 and 3 in A#2 give the extended range of these SXPDP raw patterns.

The first important difference in the hydration process is the dissolution kinetic of gypsum and ye'elimitite as reported in Li et al., 2007a. In G10B0, gypsum is completely dissolved after 5 h of hydration. However, in G10B2, gypsum is dissolved after 11 h (Figures 4.8.a and 4.8.c). Moreover, in non-active BCSA, ye'elimitite phase

dissolves at a higher pace than in active BCSA. For instance, ye'elimite is fully dissolved after 26 h in G10B0, but it is still present after 51 h of hydration for G10B2 (Figure 4.8.b and 4.8.d). In addition, the crystallisation rate of AFt is also different in both cements. At 1 h of hydration G10B0 contains 14.2(2) wt% of AFt while at the same hydration time, only 1.9(1) wt% was quantified for G10B2. Both clinkers present different ye'elimite crystal structures that may also justify the hydrating behaviours. Moreover, the SEM study performed on BCSAF_B0 and BCSAF_B2 clinkers, discussed in the previous section, revealed that ye'elimite average particle size in BCSAF_B0 was slightly smaller than that in BCSAF_B2. This observation may also partly justify the faster dissolution of ye'elimite in G10B0. The pH value of the pastes was measured to understand the difference in dissolution rates of ye'elimite and gypsum between both systems. To measure the pH, a fraction of the prepared G10B0 and G10B2 pastes was filtered in a Whatman filter (pore size of 8 μm) after 10 min of hydration. The pH of the filtration waters was measured by using standard digital pHmeter, giving a value of 12.4 ± 0.1 for G10B0 and 10.3 ± 0.1 for G10B2. It is known that the depletion of dissolved sulphate ions causes the increase of hydroxide concentration, and consequently a higher pH value (Winnefeld and Lothenbach, 2010). The fast sulphate consumption by crystalline ettringite precipitation in G10B0 paste is likely responsible for the higher pH value.

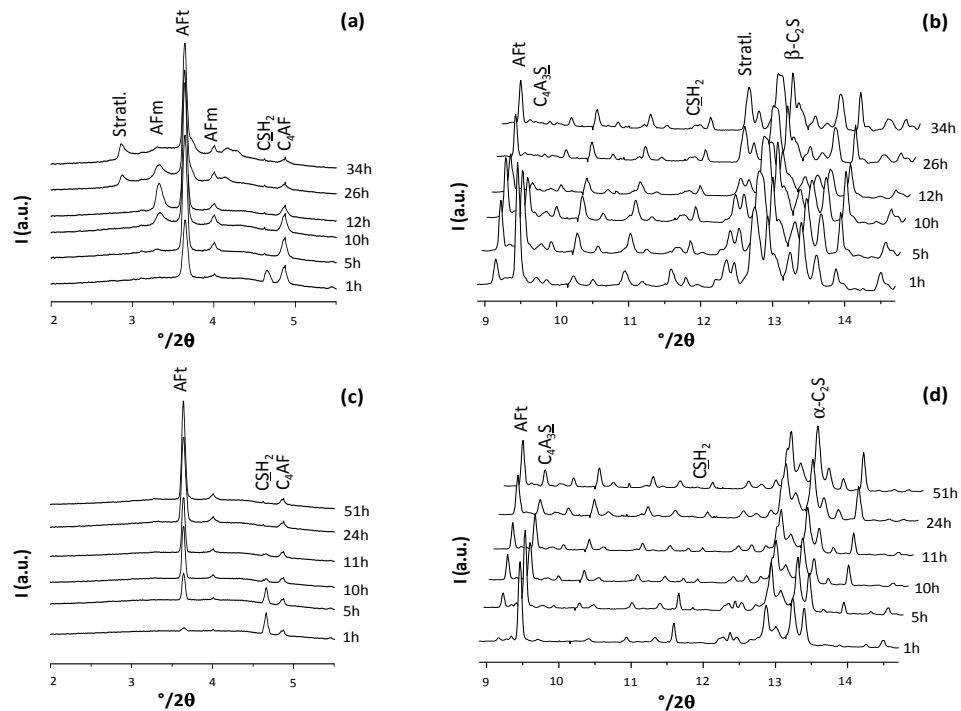


Figure 4.8. Selected ranges of SXPDP raw patterns for (a) and (b) G10B0; and (c) and (d) G10B2 cement paste at different ages of hydration ($\lambda = 0.61984 \text{ \AA}$).

The second most important difference between both hydration behaviours takes place after 1 day of hydration. On the one hand, in G10B0, the dissolution of β -C₂S and C₄AF starts after 24 h of hydration, with the consequent crystallisation of layered AFm type phases, such as stratlingite (see Figure 4.8.a). On the other hand, for G10B2, α' _H-C₂S percentage remains constant up to 51 h of hydration and C₄AF dissolves very slowly after 14 h. The difference in reactivity of both belite polymorphs is astonishing, i.e. β -C₂S reacts faster than α' _H-C₂S. This behaviour is in disagreement with the general accepted idea in the cement field: α -forms of belite are reported to have faster hydration kinetics than β -forms (Jelenic et al., 1978; Chatterjee, 1996). However, under our studied experimental conditions, β -C₂S reacts faster than α' _H-C₂S, to yield stratlingite, see equation [1.4] (introduction section). This behaviour may well be justified with the formation of high amounts of ettringite at early hours which implies a concomitant large quantity of amorphous aluminium hydroxide. The availability of amorphous AH₃ promotes the precipitation of stratlingite, C₂ASH₈, from belite reaction (equation [1.4]). In conclusion, the hydration behaviour of C₂S is likely more dependent on the chemical environment than on its polymorphism.

4.3.1.2. *Ex-situ* hydration behaviour at late ages (> 24 h), with different amounts of gypsum.

The influence of the amount of gypsum in BCSAF cements at late ages of hydration (> 24 h) was determined through LXRPD and published in A#3.

Three different amounts of gypsum were tested: 5, 10 and 15 wt%. The hydrated pastes, after stopping hydration, were characterised by LXRPD and Rietveld methodology at 3, 7, 28 and 120 days. The G-factor approach was used to obtain a full mineralogical phase assemblage including ACn contents. The FW content was also determined by the difference between the added water and the combined water determined by DTA-TGA. Figure 4.9 shows the degree of reaction of belite polymorphs, orthorhombic and pseudo-cubic ye'elimite, and ferrite as a function of hydration time and amount of added gypsum.

Several conclusions can be drawn of this study:

- *Effect of the activation of clinkers on hydration.* The most surprising result of the previous study at early ages was that β -belite in non-active clinker reacts at a higher pace than α' _H-belite in BCSAF_B2. That behaviour has been corroborated in this study at later ages, Figure 4.9.a. Thus, the reactivity of β -C₂S seems to be enhanced by an oversaturation of aluminate ions at early hours to yield stratlingite (Martín-Sedeño et al., 2010; Winnefeld and Lothenbach, 2010;). Moreover, ye'elimite reacts at a different pace for BCSA_B0 and BCSA_B2. Orthorhombic ye'elimite, in non-active cements, is completely hydrated after 3 days of hydration in GgB0, while pseudo-cubic ye'elimite in GgB2 reacts at slightly slower pace for the same gypsum

content and age of hydration, Figure 4.9.b. This effect was previously observed in the hydration study at early hours (A#2).

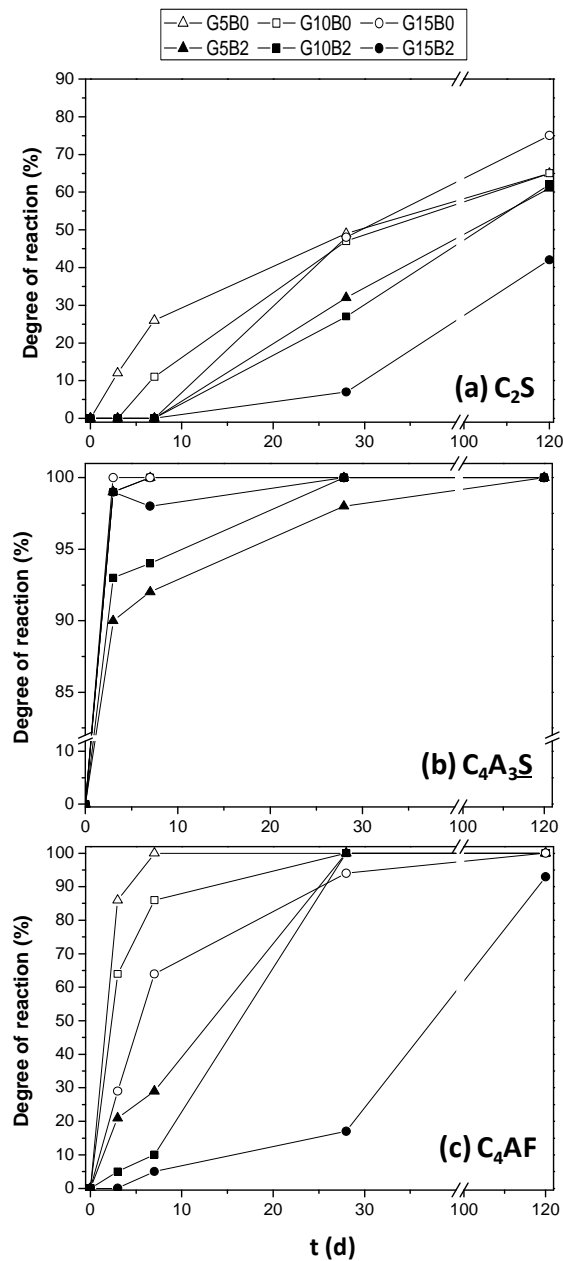


Figure 4.9. Hydration degree, α (%), for GgB0 and GgB2 pastes as a function of curing time and amount of gypsum added of (a) C_2S ; (b) C_4A_3S ; and (c) C_4AF . Solid lines are just guide3 to the eyes.

It must be underlined that although the phases in BCSAF_B0 react faster than in BCSAF_B2, the non-active cement develop much smaller mechanical strength, which clearly indicate the importance of the hydration chemistry/environment, as discussed previously.

- Effect of the amount of gypsum during hydration. Ye'elimite reaction kinetics show a small dependence on the amount of added gypsum, as there is a slight increase in hydration rate by increasing the gypsum content. This behaviour seems to be slightly more marked in pseudo-cubic ye'elimite. The final reaction degree of both polymorphs of dicalcium silicate is more affected by the addition of gypsum. On the one hand, β -C₂S reactivity (α) was enhanced by increasing the gypsum content (α rises from 65% to 75% by the addition from 5 to 15 wt% of gypsum). On the other hand, α' -C₂S reaction degree decreased from 62% to 42% for addition of 5 to 15 wt% of gypsum, respectively, Figure 4.9.a. The hydration of the ferrite phase was strongly retarded by increasing the gypsum content in both GgB0 and GgB2 cements, Figure 4.9.c, in agreement with previous studies (Wang, 2010).

- Concerning the hydration products. The main crystalline hydrated compounds were ettringite, stratlingite and katoite. Figure 4.10 shows, as a representative example, a selected range of Rietveld plots for two samples, G15B0 and G15B2, hydrated for 120 days. The main peaks of each phase are labelled. The amount of crystallised ettringite in GgB2 cements is higher than that in GgB0 cements, irrespective of gypsum content (see Tables 1 and 2 in A#3). Moreover, the crystallisation process of stratlingite is strongly affected by the amount of added gypsum; in fact, the amount of stratlingite decreases by increasing the gypsum content, Tables 1 and 2 in A#3. The crystallisation of stratlingite was confirmed by DTA measurements. DTA curves for G15B0, at all the studied ages, were plotted (see Figure 3 in A#3). The endothermic signal at $\sim 235^\circ\text{C}$, corresponding to the dehydration of AH₃, is present at 3 and 7 days. After 28 and 120 days, this signal disappears and two endothermic peaks related to stratlingite precipitation at $160\text{--}175^\circ\text{C}$ and $\sim 200^\circ\text{C}$ appear (arrows in figure 3 in A#3), thus confirming stratlingite formation by consumption of AH₃, according to reaction 1.4 given in the introduction.

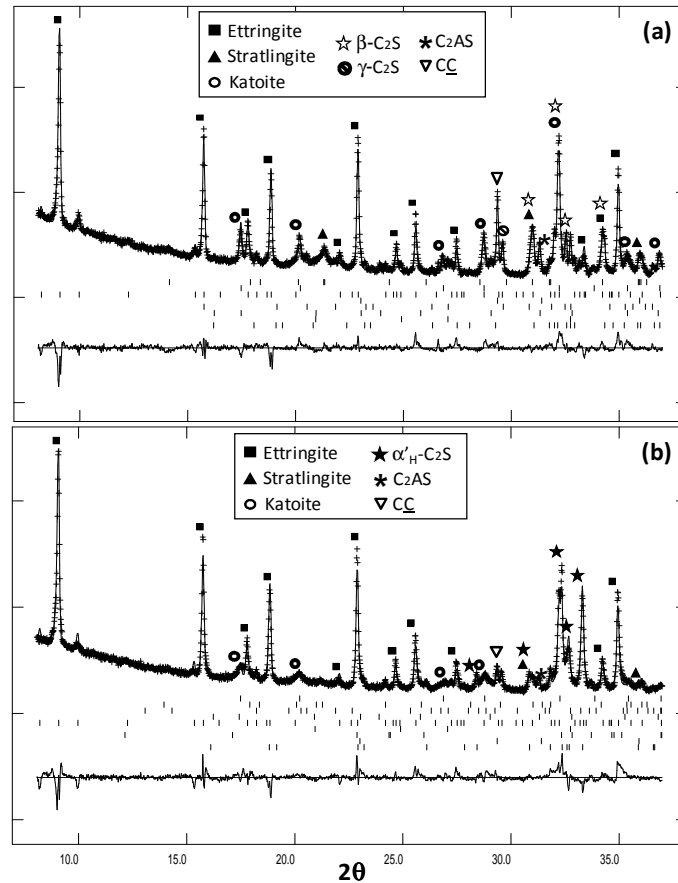


Figure 4.10. Selected range of Rietveld plots for two pastes, (a) G15B0 and (b) G15B2, cured for 120 days.

In addition, the amount of precipitated crystalline katoite seems to depend on C_4AF hydration, as significant amounts of this siliceous-hydrogarnet phase crystallises just after the dissolution of C_4AF (Tables 1 and 2 in A#3). This supports the hypothesis that katoite might contain a significant amount of iron as a substitute for aluminium. Consequently, the katoite solid solution, also known as hydrogarnet, may be expressed as $C_3A_{1-x}F_xSH_4$. The x values were determined by unit cell parameter inspection. Refined a unit cell parameters obtained in cubic katoites, for all cement pastes, were compiled. Then, according to the equation $a = 0.16x + 12.29$, obtained by assuming a linear variation of the unit cell (Taylor, 1997) the Al/Fe ratio in $C_3A_{1-x}F_xSH_4$ can be estimated. Figure 4.11 shows the theoretical values of a as a function of x (dotted line), and the corresponding values obtained for the different cement pastes. The average value of the refined unit cell parameters at different hydration ages was used in the cement pastes for which the standard deviation (σ_{n-1})

was lower than 0.009. When σ_{n-1} was higher, the average was not calculated. For G10B2 and G15B2 pastes two values of refined unit cell (a) were calculated. One at early hydration ages (3 and 7 days), marked with an asterisk in figure 4.11, and other at later ages of hydration (28 and 120 days).

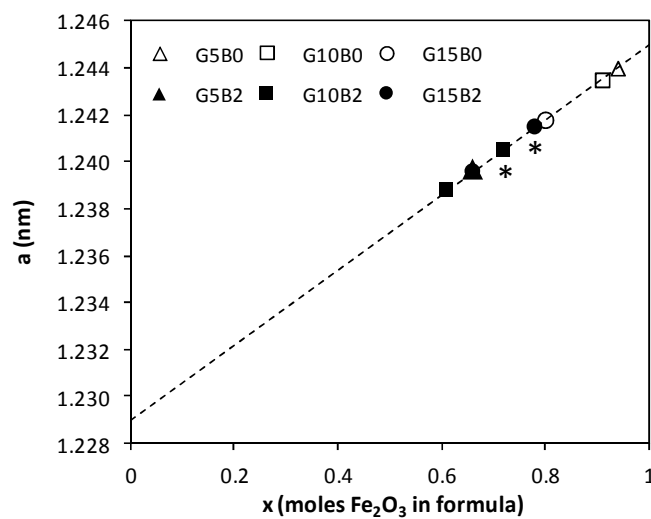


Figure 4.11. Values of the cell parameter (a) for katoite vs values of x (moles of Fe_2O_3 in formula $\text{C}_3\text{A}_{1-x}\text{F}_x\text{SH}_4$) for different GgBx pastes. (Dotted line stands for theoretical dependence of a as function of x).

4.3.1.3. Elemental composition of ACn.

It is not only important to quantify the amorphous content, also try to characterise and estimate its elemental composition to correlate it with the cement hydration behaviour and mechanical properties. As it was discussed in the introduction, it is not possible to determine the chemical composition of ACn directly by LXRPD. An attempt to find out the possible composition of the ACn (sulphate, silicate, aluminates and iron-bearing groups) was performed through RQPA combined with G-factor, which was published in A#3. For this purpose, the evolution of different ions-containing groups was studied with time:

i) Sulphate groups. The amount of reacted/dissolved sulphate was determined from the disappearance of ye'elimite and gypsum; and the amount of crystallised sulphate was calculated from the formation of ettringite. Figure 4.12 shows the evolution of sulphate content with time for G10B0 and G10B2 pastes as representative examples. The dotted line represents the maximum sulphate that can be hydrated and/or crystallised. As mentioned before, we can observe that the

crystallisation of Aft in BCSA_B2 is higher than that in BCSA_B0 pastes: ~76 wt% of the hydrated sulphates had crystallised for G10B2 against ~57 wt% for G10B0, meaning that, in this case, ~43 wt% of dissolved, but not crystallised, sulphate groups (Figure 4.12) were mainly incorporated into ACn phase(s) and/or in pore solution (Winnefeld and Lothenbach, 2010).

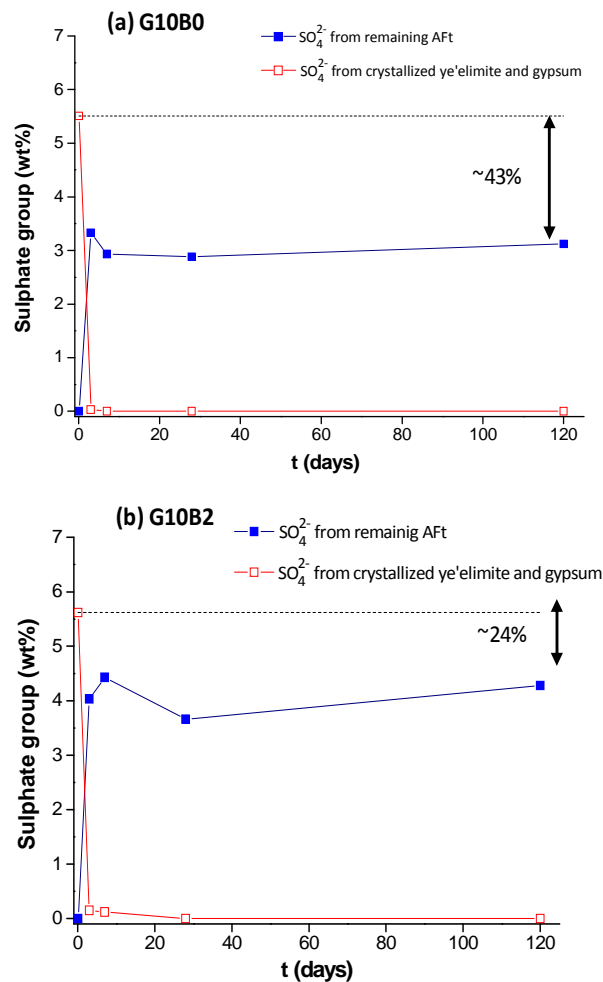


Figure 4.12. Hydration and crystallization rate of sulphate groups for (a) G10B0 and (b) G10B2 pastes. Dashed lines represent the maximum values of dissolved sulphate group.

ii) Silicate groups. The evolution of silicate contents (both dissolved and crystallised) in G10B0 and G10B2 pastes (as representative examples) during hydration is shown in Figure 4.13. On the one hand, hydrated silicate contents stand

for the amount of silicon-bearing phases that have reacted with water (calculated from belite consumption, Tables 1 and 2 in A#3). On the other hand, crystallised silicate contents mean the amount of silicon-containing crystalline hydrated phases that have precipitated and been quantified, that is, stratlingite and katoite (from Tables 1 and 2 in A#3). Dotted lines in Figure 4.13 stand for the maximum hydrated silicate content for G10Bx cement pastes. The amount of crystallised silicate is higher in G10B0 than in G10B2, where higher amounts of stratlingite were found. Thus, a higher amount of hydrated silicate remains in the amorphous phase(s) for G10B2 cement paste.

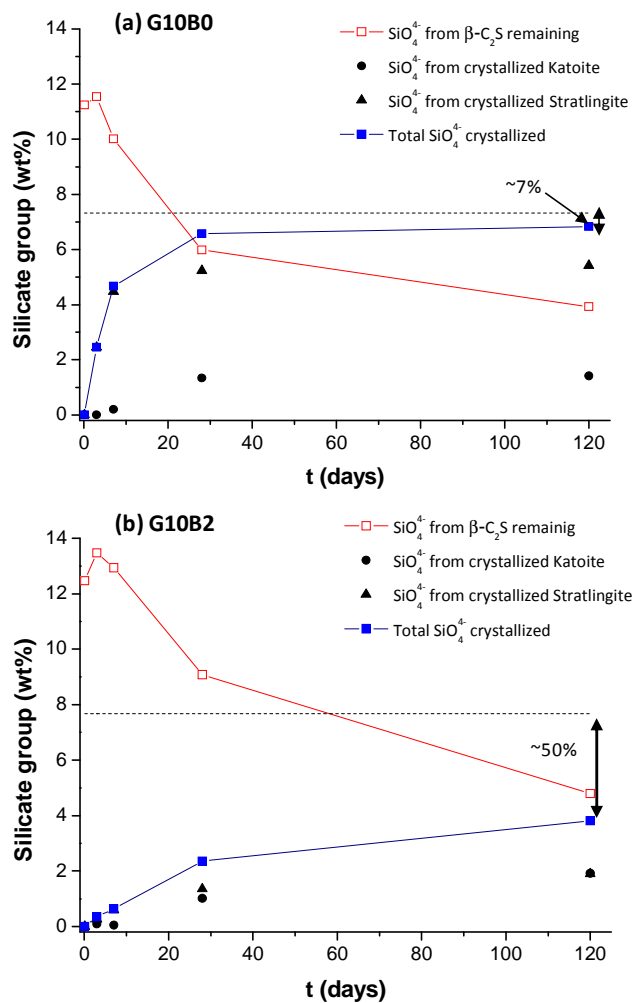


Figure 4.13. Hydration and crystallisation rate of silicate groups for (a) G10B0 and (b) G10B2 pastes. Dashed lines represent the maximum values of dissolved silicate group.

iii) Aluminate groups. The evolution of aluminium was also studied through the same methodology. Hydrated aluminate contents were obtained from C_4A_3S and C_4AF consumption, and crystallised aluminate amounts were calculated from the precipitated Aft, katoite, and stratlingite. Evolution of aluminate with hydration time, for G10Bx, G5Bx and G15Bx pastes, is given in Figures 4, S4 and S5 (Supporting Information) of A#3. The amount of crystallised aluminium-bearing phases was higher in GgB0 than in GgB2 cement pastes, matching in some cases the maximum, whereas more than 30 wt% of the aluminate content remained in the ACn phase(s) for GgB2 cement pastes, and/or to a minor extent in pore solution.

- **NMR study:** A NMR study was also performed on these samples (G10Bx) during my research stage at Instituto de Ciencias de los Materiales (ICMM-CSIC) in Madrid. Here, the complex heterogeneous molecular compositions and structures of anhydrous and hydrated cements have been followed by solid-state NMR. One-dimensional (1D) single-pulse NMR measurements are generally quantitative, allowing resolved species to be evaluated and their relative populations monitored over time, as the cement hydrates and solidifies. 1D single-pulse ^{29}Si and ^{27}Al NMR have been used to characterise the species in anhydrous and hydrated G10Bx cement.

It has been established that the primary silicate constituents of cements are so-called $Q0$ ^{29}Si silicate species that compose dicalcium silicate (C_2S) phase. (" Qn " refers to ^{29}Si atoms that are covalently bonded via bridging oxygen atoms to $n < 4$ other Si atoms; " $Qn(mAl)$ " similarly refers to a ^{29}Si atom bonded via bridging oxygen atoms to n other silicon or aluminium atoms, m of which are Al). During the hydration process, more condensed silicate species form disordered products, such as calcium-silicate hydrates or amorphous phases, are characterised by $Q1$ and $Q2$ ^{29}Si moieties with broad distributions of local environments that are typically not resolved by single-pulse ^{29}Si MAS NMR or other methods. In cements hydrated for longer times, $Q3$ and $Q4$ ^{29}Si silicate species are also prevalent, which indicates a more densely cross-linked silicate network, as expected. ^{29}Si NMR MAS spectra for G10B0 and G10B2 (anhydrous and hydrated) are shown in Figures 4.14 and 4.15, respectively. Similarly, solid-state 1D ^{27}Al NMR measurements show that aluminate species in anhydrous cements have principally 4-fold coordination (Al^{IV}). The initial anhydrous cement phases, containing aluminate, are C_4A_3S and C_4AF , and they are composed principally of Al^{IV} species. The ^{27}Al NMR signals are often extensively broadened by ferro- or paramagnetic iron components in close proximity. The iron components can be present in crystalline or disordered regions as cations, oxides, and/or hydroxides (e.g., Fe^{2+} , Fe^{3+} , Fe_2O_3 , Fe_3O_4 , $\text{Fe}(\text{OH})_3$, referred to broadly as "ferrites" within the cement literature) with indefinite compositions and distributions. During hydration, Al^{IV} species are thought to react with the calcium

silicate species and be partially incorporated into the amorphous phase, with some Al^{IV} species replacing four-coordinated ^{29}Si atoms. For these reasons, the quantification of the intensities in all the ^{27}Al MAS NMR spectra becomes very difficult.

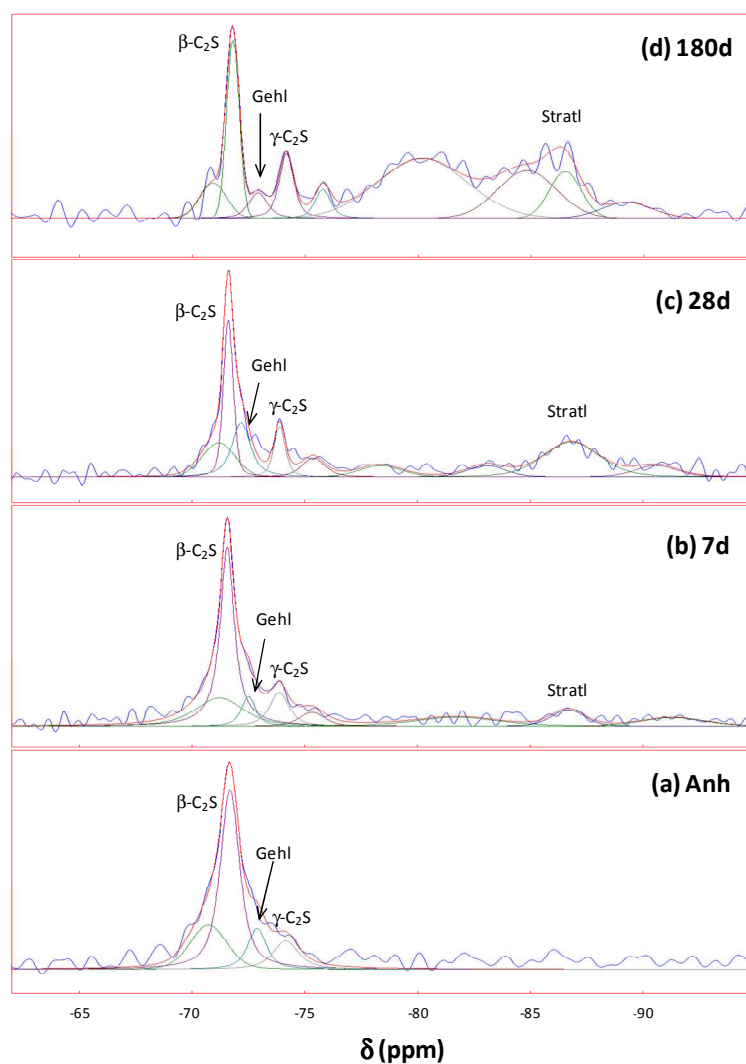


Figure 4.14. ^{29}Si NMR MAS spectra for G10B0 cement, (a) anhydrous, and hydrated at different curing times: (b) 7 days, (c) 28 days, and (d) 180 days.

The ^{29}Si signals, that are clearly resolved at -70.3, -71.4 and -73.5 ppm in Figures 4.14 and 4.15, are assigned to α , β and γ belite polymorphs, respectively. Other ^{29}Si signal was observed in two figures (Figures 4.14 and 4.15) at -72.5 ppm

related to the gehlenite phase. Hydrated cements are substantially more complicated than the anhydrous starting materials due to the presence of species with local environments without long-range order which exacerbates the ^{29}Si signals overlapping. ^{29}Si signals intensity over the range -67 to -76 ppm, decrease slightly with the hydration time, which indicates that the anhydrous silicate species have reacted to form hydration products. Additionally, at early hydration time (7 days) of G10B0, broad upfield ^{29}Si signal is observed at approx. -86.5 ppm, (Figure 4.14.b), which is attributed to $Q2(1Al)$ silicate species. This signal indicates that the stratlingite is formed in this paste (Santacruz et al., 2015) and it increases with the hydration time (Figures 4.14.c and d). Moreover the ^{29}Si signal intensity over -80 ppm increases with the hydration time, indicating that a condensed $Q2(2Al)$ silicate species are being formed, probably in the amorphous phase. In G10B2 the ^{29}Si signal corresponding to the formation of stratlingite is not observed until 28 days of hydration (Figure 4.15.c). In general the ^{29}Si signal for G10B2 is wider than the corresponding for G10B0, likely due to the higher amount of ACn content present in the G10B2. These results seem to be in accordance with that obtained in previous studies about the evolution of silicate groups in G10B0 and G10B2 samples.

The quantification of ^{29}Si NMR measurements is possible, but it is not an easy task. The lack of information about the ^{29}Si signals corresponding to different hydrated cement phases and the presence of an amorphous fraction, made difficult to perform an accurate quantification.

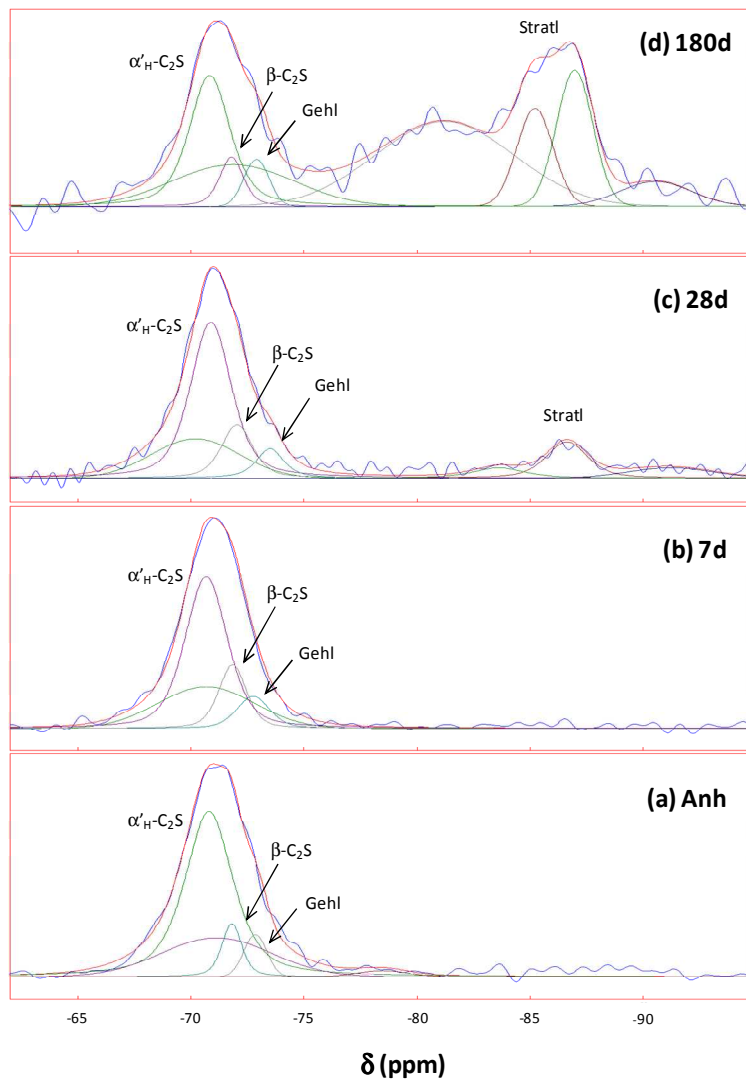


Figure 4.15. ^{29}Si NMR MAS spectra for G10B2 cement, (a) anhydrous, and hydrated at different curing times: (b) 7 days, (c) 28 days, and (d) 180 days.

^{27}Al MAS NMR spectra for G10B0 and G10B2 hydrated pastes show two chemical shift regions, Figure 4.16. Once for Al in tetrahedral coordination ($50 < \delta < 100$ ppm) that displays centre bands from the Al of ye'elimitite (~ 70 ppm) and gehlenite (~ 61 ppm). The other spectral region corresponds to octahedrally coordinated Al ($-10 < \delta < 20$ ppm). This region exhibits three distinct resonances: i) the first frequency peak ($\delta = 13.1$ ppm) assigned to ettringite (AFt); ii) the second resonance located at ~ 9 ppm, and reported for monosulphate (AFm phases); iii)

finally, a third resonance is observed at ~ 10 ppm corresponding to the octahedral Al in stratlingite. Figure 4.16 shows, as an example, the ^{27}Al MAS NMR spectrum for G10B0 and G10B2 at 28 days of hydration. The main difference observed in the figure is the ^{27}Al signals intensity corresponding to the AFt and AFm. These results are in concordance with the results obtained by RQPA

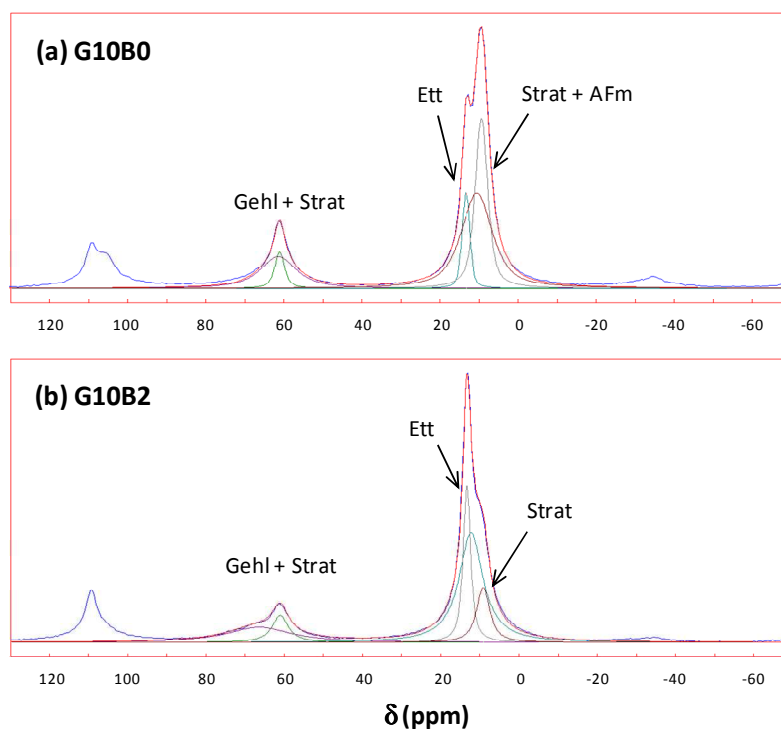


Figure 4.16. ^{27}Al NMR MAS spectra at 28 days of hydration for (a) G10B0, and (b) G10B2 cement paste.

4.3.1.4. A comparative study of $\text{MoK}\alpha_1$ and synchrotron radiations for selected samples.

Selected samples (G10B0, G5B2 and G10B2 at 28 days of hydration time) were also analysed under two different radiations: strictly monochromatic $\text{MoK}\alpha_1$ radiation with transmission geometry and also synchrotron, for the sake of comparison, included in A#4. These samples were selected as they presented a very complex phase assemblage when hydrated (see Table VII in A#4).

Irradiated volume in diffraction is a key issue since higher volume yields enhanced particle statistics. Therefore, the use of a high-energy radiation is

beneficial as the irradiated volume of sample can be increased, and absorption effects can be reduced. Figure 4.17 shows a graphical representation of the volumes that are bathed by X-ray radiations ($\text{MoK}\alpha$ and $\text{CuK}\alpha$) for two laboratory diffraction geometries (transmission and reflection). The total irradiated volume was calculated taking into account different parameters depending on the geometry used (the beam width, the thickness of the sample, the mass absorption coefficient, the density, the packing fraction, and so on). The values obtaining for the irradiated volume for flat sample holder in transmission mode using Mo-radiation is close to 100 mm^3 , whereas for Cu-radiation the value is not larger than 5 mm^3 . Unfortunately, the latter cannot be enlarged without decreasing the resolution and having strong absorption effects. For reflection geometry with Cu-radiation, the calculated irradiated volume is close to 2 mm^3 . Furthermore, the enlargement of this value is not possible as it only depends on the absorption factor of the sample.

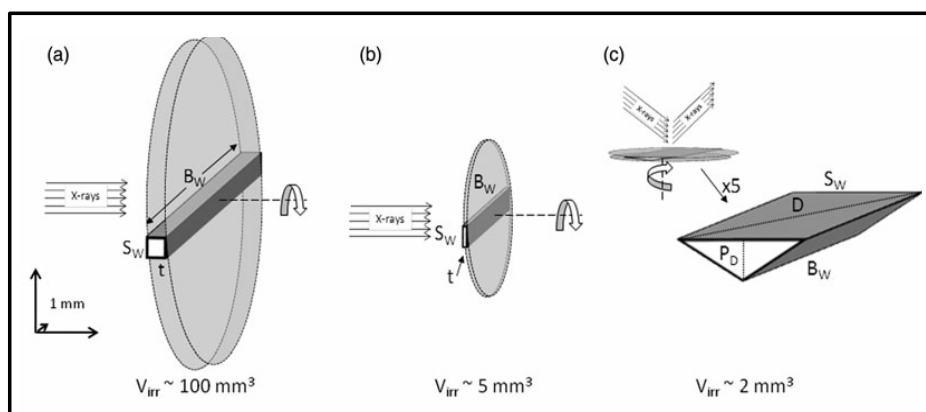


Figure 4.17. Irradiated volume for flat sample holder in the transmission mode using (a) Mo radiation and (b) Cu radiation; and (c) reflection mode using Cu radiation.

Moreover, to keep the angular resolution in powder diffraction is a key point since high-energy patterns are squeezed and therefore, if the appropriate optic elements are not present, peak overlap may become an important drawback. The instrumental contribution to peak broadening for LXRPD and SXRPD was determined with SRM LaB_6 and $\text{Na}_2\text{Ca}_3\text{Al}_2\text{F}_{14}$ (NAC) standards, respectively. Measured FWHM as a function of angle for different diffractometers and configurations was studied (Figure 1 in A#4). As expected, the SXRPD pattern yielded the narrowest diffraction peaks. On the other hand, the broadest diffraction peaks arisen from the $\text{CuK}\alpha_{1,2}$ transmission geometry with the focusing mirror. The most important outcome from this study was the observation of quite low FWHM values for strictly monochromatic $\text{MoK}\alpha_1$ radiation, implying that peak overlapping is not very important.

As a representative example, Figure 4.18 gives Rietveld plots for G10B0 paste ($\text{MoK}\alpha_1$ and synchrotron patterns). This figure highlights not only the complexity of the sample, but also the high resolution features of the $\text{MoK}\alpha_1$ pattern, where the diffraction peak overlapping is similar to that observed in the synchrotron pattern. The main conclusions derived from these RQPA results are: i) the carbonation effects are clearly observed in these patterns where calcium carbonate (calcite and vaterite phases) slightly evolves with time; ii) in spite of the carbonation effects and the complexity of the systems, the derived contents for the main crystalline phases agree relatively well with both radiations and optics setups.

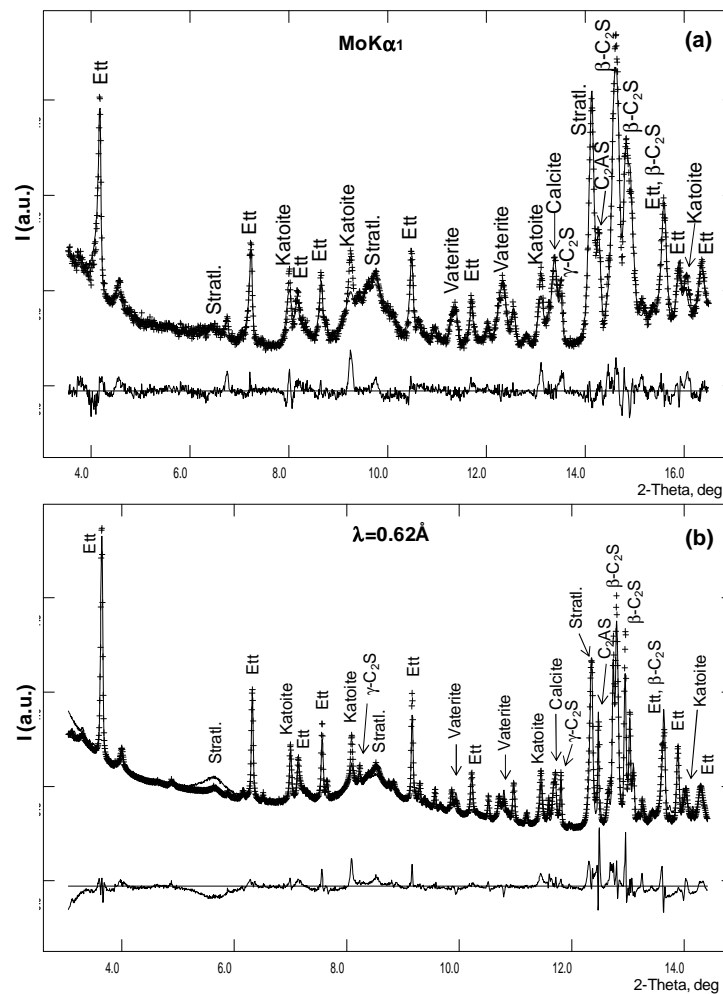


Figure 4.18. Rietveld plots for G10B0 hydrated sample patterns (a) strictly monochromatic $\text{MoK}\alpha_1$ radiation in transmission (flat sample), (b) synchrotron radiation in transmission (capillary) (Figure 5 in A#4).

It is also recommended to use high-energy radiation (Mo), and transmission geometry for better particle statistic distribution, which give more accurate results and, moreover, some effects such as the preferred orientation or micro-absorption are minimised. The results obtained combining high energy radiation and transmission geometry with internal standard seem to be the most appropriate approach for determining amorphous contents.

4.3.2. Hydration of BCSAF cements with different calcium sulphate source.

Bassanite, $\text{CSH}_{0.5}$, and anhydrite, CS , were previously synthesized by heating commercial gypsum at 90°C for 24 h in a stove and at 700°C for 1 h in a furnace, respectively. Cement pastes were prepared, at a $w/c = 0.55$, by mixing both BCSAF clinkers, BCSAF_B0 and BCSAF_B2, with 10 wt% of gypsum (G), bassanite (B) or anhydrite (A), hereafter G10Bx, B10Bx and A10Bx, respectively; where x can be either 0 or 2, for non-active and active clinkers.

4.3.2.1. Early hydration behaviour (< 24 h).

An *in-situ* SXRPD study was performed to determine the role of the type of calcium sulphate source (10 wt%) in the first hours of BCSAF hydration (A#2). Cement pastes were poured into glass capillaries. Tables 4.7, 4.8 and 4.9 give direct RQPA results as a function of hydration time for G10B2, A10B2 and B10B2, respectively. The reaction degrees of ye'elimite and ettringite for the three cements are given in Figure 4.19, and both normalised direct RQPA results and calorimetric curves are shown in Figure 4.20. The normalised data, calculated taking into account the theoretical data of the sample at 0.0 h of hydration, were: 28.0 wt% of ye'elimite and 10.0 wt% of gypsum/anhydrite or bassanite. Taking into account these values, the theoretical amount of dissolved and formed (ettringite) phases were calculated, assuming that the reaction degree of independent phases is the same. As an example, if we consider a reaction degree (α) of 10% for both ye'elimite and gypsum for G10B2, according to Eq. [1.1] (in the introduction section), that sample should contain 25.2 wt% of ye'elimite, 9.0 wt% of gypsum and 5.8 wt% of AFt. Then, these values were normalised to obtain the crystalline fraction at a reaction degree of $\alpha \sim 10\%$, using the percentages corresponding to three crystalline phases, i.e. ye'elimite, gypsum and AFt (63.1, 22.5 and 14.4 wt%, respectively). These latter data are now comparable to direct Rietveld results, without taking into account gibbsite. Thus, theoretical data were tabulated for all possible α values. Comparing these theoretical results with data reported in Table 4.7, we can conclude that, at 2 h of hydration, ye'elimite was dissolved at $\alpha \sim 11\%$ and the crystallisation of ettringite was $\sim 6\%$. These results are plotted in Figure 4.19 (α vs. time). For G10B2 paste, the AFt crystallisation process is parallel to ye'elimite dissolution, and the gypsum dissolution is very fast. Moreover, a passivation effect is observed, where gypsum showed a

degree of reaction of almost 100% and ye'elimite and ettringite over 80% after one day of hydration, Figures 4.19.a, and 4.20.a, and Table 4.7. In addition, G10B2 presented an induction period close to 6 h, when the dissolution and crystallisation of phases become significant. The calorimetric curve shows two broad signals mainly associated to first dissolution and precipitation processes, Figure 4.19.a. A10B2 RQPA results plotted in Figures 4.19.b and 4.20.b, demonstrated that the dissolution kinetic for anhydrite is much slower than that for gypsum or bassanite. For A10B2 paste, the precipitation of ettringite is limited by $C\bar{S}$ dissolution, which starts to be significant up to 7 h. Using these results we can also state that the predicted reactivity of ye'elimite with water to form AFm as main hydrated phase (Winnefeld and Barlag, 2010; Song and Young, 2002) has not taken place within the first 6 h of hydration. Our results state that ye'elimite dissolution yields ettringite in spite of the fact that anhydrite is not dissolved until 6 h, in agreement with a recent work (Cuesta et al., 2014a). This behaviour is in disagreement with chemical equation [1.2] although it is thermodynamically expected (Damidot and Glasser 1993) and it has been also previously described (Berger et al., 2011a; Andac and Glasser, 1999).

Table 4.7. Direct Rietveld quantitative phase analysis results (wt%) for G10B2 sample as a function of hydration time. Numbers between brackets are mathematical errors from Rietveld calculations.

Phases	t_0	2h	4h	6h	9h	11h	18h	24h
α'_H-C_2S	50.2(1.8)	47.6(2)	47.7(2)	48.0(2)	47.3(2)	47.4(2)	47.0(1)	47.0(2)
$C_4A_3\bar{S}$	27.5(1.7)	22.9(1)	19.9(1)	16.7(1)	10.8(1)	9.3(1)	3.8(1)	3.6(1)
C_4AF	8.9(6)	11.4(2)	11.3(2)	11.3(2)	10.5(2)	10.8(2)	8.5(1)	8.3(2)
C_2AS	1.4(2)	2.7(1)	2.8(1)	2.8(1)	2.8(1)	2.8(1)	1.4(1)	1.3(1)
CT	1.9(2)	1.6(1)	1.7(1)	1.8(1)	1.8(1)	1.8(1)	2.0(1)	1.9(1)
$C\bar{S}H_2$	10.0(-)	10.7(1)	8.0(1)	5.8(1)	1.8(1)	1.0(1)	-	-
Aft	-	3.1(1)	8.5(2)	13.7(2)	25.1(1)	26.9(1)	37.3(1)	37.9(1)

Table 4.8. Direct Rietveld quantitative phase analysis results (wt%) for A10B2 sample as a function of hydration time. Numbers between brackets are mathematical errors from Rietveld calculations.

Phases	t_0	2h	4h	6h	9h	11h	13h	24h
α'_H	50.2(1.8)	47.0(2)	48.9(2)	49.0(2)	48.7(2)	48.3(2)	48.2(2)	46.6(2)
C_2S								
C_4A_3S	27.5(1.7)	23.1(1)	20.3(1)	18.8(1)	14.7(1)	12.8(1)	11.3(1)	4.8(1)
C_4AF	8.9(6)	11.8(2)	11.5(2)	11.4(2)	11.3(2)	11.1(2)	11.1(2)	10.8(1)
C_2AS	1.4(2)	3.4(1)	2.6(1)	2.6(1)	2.7(1)	2.7(1)	2.7(1)	2.6(1)
CT	1.9(2)	1.6(1)	1.7(1)	1.7(1)	1.7(1)	1.7(1)	1.7(1)	1.6(1)
CS	10.0(-)	11.1(1)	9.8(1)	9.2(1)	7.2(1)	6.2(1)	5.5(1)	1.8(1)
Aft	-	2.0(1)	5.2(2)	7.2(2)	12.0(2)	17.2(1)	19.5(1)	31.7(1)

Table 4.9. Direct Rietveld quantitative phase analysis results (wt%) for B10B2 sample as a function of hydration time. Numbers between brackets are mathematical errors from Rietveld calculations.

Phases	t_0	1h	12h	24h
α'_H - C_2S	50.2(1.8)	46.7(2)	45.8(2)	44.9(2)
C_4A_3S	27.5(1.7)	20.0(1)	5.9(1)	5.1(1)
C_4AF	8.9(6)	11.4(2)	10.7(2)	10.2(2)
C_2AS	1.4(2)	3.2(1)	3.8(1)	3.7(1)
CT	1.9(2)	1.9(1)	1.6(1)	1.6(1)
$CSH_{0.5}$	10.0(-)	0.6(1)	0.5(1)	0.5(1)
CSH_2	-	11.3(2)	0.8(1)	0.6(1)
Aft	-	5.9(1)	30.8(1)	33.4(1)

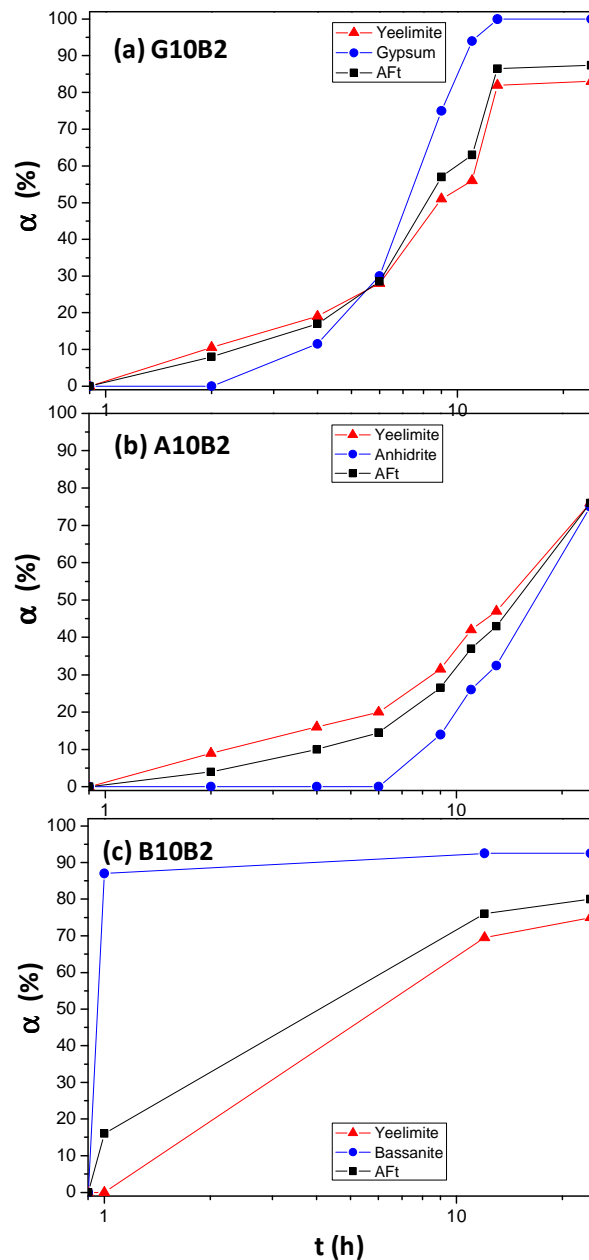


Figure 4.19. Degree of reaction [α] of ye'elimite, sulphate source and AFt as a function of time for (a) G10B2, (b) A10B2 and (c) B10B2. Solid lines are just guide to the eyes.

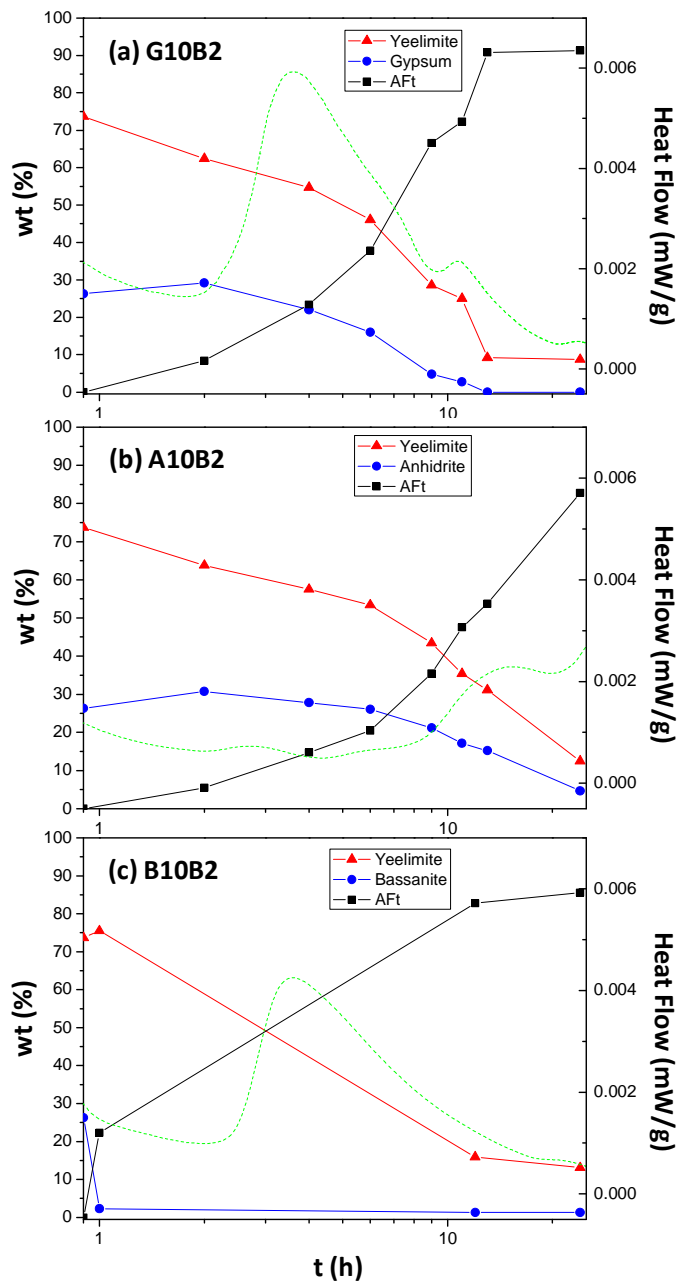


Figure 4.20. Normalised direct RQPA results and the calorimetric heat flow curve (dashed line) for (a) G10B2, (b) A10B2 and (c) B10B2. Solid lines are just guide to the eyes.

The slower kinetic of precipitation of AFt in A10B2 paste has allowed following the growth of the ettringite crystals by inspecting the FWHM of some diffraction peaks. For instance (010) diffraction peak at ~ 9.7 Å had FWHM values of 0.0494(3), 0.0439(6) and 0.0408(2)° for 1, 3 and 8 h of hydration, respectively. This sharpening of the diffraction peak is likely due to the growth of AFt crystals.

B10B2 was also analysed. Due to experimental requirements (sample loading in the capillaries, alignment and so on) it is not possible to measure the first ~ 40 min of hydration. The dissolution of bassanite and precipitation of gypsum are reported as very fast processes (Solberg and Hansen, 2001). Our measurements fully agree with this behaviour and after 1 h of hydration, bassanite was almost absent and gypsum had crystallised. In addition, the FWHM of (020) peak of gypsum in this sample after 1 h of hydration was 0.0495(3)°, and it was compared to the same peak of gypsum in G10B2 under same hydration conditions, 0.0457(4)°. These broader peaks are due, as expected, to smaller particle sizes for in-situ crystallised gypsum. Subsequent hydration reactions are similar to those already described for the gypsum-regulated cement, G10B2.

The very fast dissolution of bassanite with precipitation of gypsum, as well as the low dissolution rate of anhydrite were quantified, confirming the accurateness of the methodology reported in A#2.

4.3.2.2. Hydration with different sulphate sources at late ages (> 24 h).

In article a#5, the three systems, G10Bx, A10Bx and B10Bx, with 10 wt% of sulphate source at w/c = 0.55 were characterised through LXRPD and Rietveld methodology at 3, 7, 28, 120, 180 and 365 days, DTA-TGA, SEM and porosimetry after stopping hydration.

Rheological characterisation of the fresh pastes. Since bassanite in contact with water suffers from a fast grain decay (intergranular attack) which produces an increasing of the surface area of the sulphate carrier, and as a consequence, a high water demand (and high viscosity). In addition, a primary gypsum precipitation occurs, which will also affect the rheological behaviour of the paste. Thus, both parameters the high water demand and the gypsum precipitation increase the viscosity of bassanite-pastes. The viscosity curves of X10B2 pastes (Figure 4.21) show that the bassanite-containing pastes presents both the highest viscosity values and the largest rheopectic cycle, in agreement with previous studies (García-Maté et al., 2015a). Since our objective is to study the effect of the calcium sulphate source (including compressive strengths of the corresponding mortars) similar rheological

behaviour, and in particular, similar viscosity values at very early hydration ages are desired. When a small amount of a commercial polycarboxylate-based superplasticizer (SP) (0.05 wt% of active matter referred to total solids content), with 25 wt% of active matter, was added to water to prepare bassanite-containing pastes, it exhibited a considerable diminishing in viscosity, (Figure 4.21) and a similar rheological behaviour to those prepared with gypsum or anhydrite. The addition of that small amount of SP would not delay considerably the setting time or modify the phase assemblage (RQPA) of these pastes (García-Maté et al., 2012; 2015a; Ma et al., 2014b); the main effect is just related to the improvement of workability and homogeneity of the corresponding mortars.

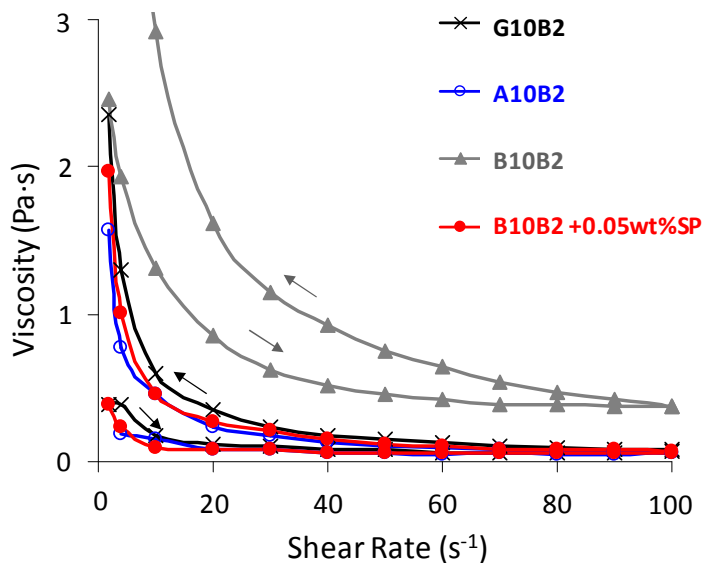


Figure 4.21. Viscosity curves of G10B2, A10B2, B10B2 and B10B2 with 0.05 wt% superplasticizer pastes.

- *Hydrating phase evolution.* The evolution of the phases during hydration was followed by RQPA. Tables 4.10-4.15 show the phase assemblage, including both ACn and FW contents, for both types of cement (active and non-active) prepared with 10 wt% of gypsum, anhydrite or bassanite. In all cases, the sulphate source was consumed before 3 days of hydration to form ettringite as the main crystalline hydrated phase. AFm and stratlingite were also found in all the studied pastes but in variable amounts. As found before, independently of the sulphate source, lower quantities of AFt were found and consequently, larger amounts of AFm were

quantified in non-active cements (X10B0) than in active cements (X10B2). This is related to the different ye'elimite polymorphs found in both clinkers (see Tables 4.10-4.15).

In addition, the presence of larger amounts of ettringite in X10B2 is very likely the responsible of the improved mechanical properties of this family when compared to the lower data for X10B0; this will be discussed below. Focusing on the belite reactivity, β -C₂S (present in X10B0) dissolves faster than α' -C₂S (present in X10B2) within the first 28 days, independently of the sulphate source. In addition, crystalline stratlingite is quantified in X10B0 just after 3 days of hydration, but it is not detected until 28 days in X10B2 pastes. However, X10B2 families showed lower amounts of FW at curing ages over 28 days, indicating higher degree of reaction.

To conclude this study devoted to the phase evolution from RQPA, the analysis of the data reported in Tables 4.10-4.15, indicate that the phase assemblage at latter ages are slightly sensitive to the initial sulphate source. AFt, stratlingite, katoite and AFm contents between 120 and 365 days are very similar for G10B2 and A10B2. When comparing the results for G10B0 and A10B0, some (minor) differences are detected, for instance larger amounts of AFm in G10B0 than in A10B0 were found.

Table 4.10. RQPA results for G10B0 cement paste, as a function of hydration time, including ACn calculated with G-method and free water content. Numbers between brackets are mathematical errors from Rietveld calculations.

Phase	t ₀	3d	7d	28d	120d	180d	365d
β -C ₂ S	17.5(3)	17.0(3)	15.7(3)	8.9(4)	5.2(3)	4.2(3)	4.0(4)
α -C ₄ A ₃ S	9.5(7)	2.2(1)	0.8(1)				
C ₄ AF	5.3(2)	4.1(2)	3.2(2)	1.1(2)			
C ₂ AS	3.7(2)	4.6(1)	4.3(1)	3.3(1)	3.3(1)	3.7(1)	3.4(1)
γ -C ₂ S	1.9(1)	1.8(1)	1.9(1)	1.5(1)	1.8(1)	1.7(1)	1.7(1)
CT	0.5(1)	0.4(1)	0.4(1)	0.2(1)	0.2(1)	0.2(1)	
CSH ₂	9.9(1)						
AFt		17.7(2)	15.9(2)	9.3(2)	9.6(3)	9.8(3)	10.6(3)
Stratlingite		4.1(6)	6.6(4)	12.5(2)	13.4(5)	10.6(5)	12.2(5)
AFm			2.3(1)	5.5(2)	8.8(2)	10.8(2)	9.6(2)
Katoite				2.3(4)	4.9(3)	4.6(2)	6.2(3)
CAH ₁₀		0.4(1)	0.6(1)				
Hemicarbo					0.7(1)	1.0(1)	1.0(1)
CC							0.8(1)
ACn	16.1(8)	28.8(8)	30.7(6)	41.9(7)	37.5(8)	40.6(7)	40.3(8)
FW	35.5(-)	18.9(-)	17.6(-)	13.5(-)	14.7(-)	12.9(-)	10.2(-)

Table 4.11. RQPA results for G10B2 cement paste, as a function of hydration time, including ACn calculated with G-method and free water content. Numbers between brackets are mathematical errors from Rietveld calculations.

Phase	t ₀	3d	7d	28d	120d	180d	365d
α' -C ₂ S	18.6(4)	20.5(4)	20.0(4)	13.6(5)	5.0(6)	4.3(4)	4.4(6)
β -C ₂ S	1.1(2)	1.2(3)	1.3(2)	1.5(2)	2.1(2)	2.0(2)	2.3(2)
c-C ₄ A ₃ S	10.5(1)	0.7(1)	0.2(1)				
C ₄ AF	5.1(2)	4.5(2)	4.4(2)	3.4(2)	1.1(2)	0.9(2)	0.9(2)
C ₂ AS	1.6(1)	2.5(1)	2.2(1)	2.1(1)	1.8(1)	1.8(1)	2.1(1)
CT	0.5(1)	0.7(1)	0.7(1)	0.5(1)			
CSH ₂	6.5(1)						
Aft		21.3(2)	21.8(2)	18.7(2)	19.1(2)	20.6(2)	20.8(2)
Stratlingite				10.2(4)	16.9(4)	17.4(4)	15.3(4)
AFm			0.2(1)	0.5(1)	1.8(1)	1.5(1)	1.0(1)
Katoite				0.5(1)	3.2(3)	3.9(3)	4.7(3)
AH ₃		0.4(1)	0.5(1)				
ACn	20.6(5)	30.7(6)	30.7(6)	35.8(7)	41.1(9)	44.9(7)	45.1(9)
FW	35.5(-)	17.5(-)	17.8(-)	13.1(-)	7.8(-)	2.6(-)	3.3(-)

Table 4.12. RQPA results for A10B0 cement paste, as a function of hydration time, including ACn calculated with G-method and free water content. Numbers between brackets are mathematical errors from Rietveld calculations.

Phase	t ₀	3d	7d	28d	120d	180d	365d
β -C ₂ S	17.3(3)	17.1(3)	13.3(3)	10.9(4)	5.9(4)	5.9(5)	5.4(5)
o-C ₄ A ₃ S	10.2(6)						
C ₄ AF	5.4(2)	3.3(2)	1.4(2)	1.2(2)	0.9(2)	1.0(2)	0.8(2)
C ₂ AS	2.9(2)	5.0(1)	4.6(1)	4.3(1)	4.6(2)	4.7(2)	4.6(2)
γ -C ₂ S	1.8(1)	1.4(1)	1.2(1)	1.4(1)	1.4(1)	1.4(1)	1.4(1)
CT	0.3(1)	0.3(1)	0.3(1)	0.3(1)			
CS	7.5(1)						
Aft		22.2(2)	16.5(2)	17.2(2)	14.5(2)	11.6(2)	13.6(3)
Stratlingite		6.0(7)	13.4(5)	12.6(5)	10.2(6)	12.8(7)	11.5(7)
AFm			2.9(1)	2.4(1)	5.2(1)	4.6(1)	5.3(1)
Katoite			0.9(1)	2.1(2)	3.0(2)	3.2(2)	3.2(2)
CAH ₁₀		0.3(1)					
Hemicarbo				0.5(1)	0.4(1)	0.6(1)	0.4(1)
CC							1.5(1)
ACn	19.1(7)	30.5(8)	33.9(7)	37.9(8)	43.5(8)	44.3(9)	46.2(1.0)
FW	35.5(-)	14.1(-)	11.6(-)	9.4(-)	10.5(-)	9.8(-)	6.2(-)

Table 4.13. RQPA results for A10B2 cement paste, as a function of hydration time, including ACn calculated with G-method and free water content. Numbers between brackets are mathematical errors from Rietveld calculations.

Phase	t ₀	3d	7d	28d	120d	180d	365d
α' -C ₂ S	19.2(4)	20.5(5)	17.1(5)	15.8(4)	6.6(6)	5.2(6)	5.9(6)
β -C ₂ S	0.8(1)	1.1(2)	0.9(3)	1.2(3)	2.3(5)	2.2(5)	2.4(5)
c- C ₄ A ₃ S	11.2(1)	0.1(1)	0.2(1)				
C ₄ AF	5.9(2)	4.4(2)	3.8(2)	3.5(2)	1.3(2)	1.0(2)	0.9(2)
CT	0.7(1)	0.6(1)	0.6(1)	0.7(1)			
C ₂ AS	1.6(1)	2.2(1)	2.1(1)	2.4(1)	2.0(1)	1.8(1)	1.6(1)
CS	6.8(1)						
Aft		24.1(2)	19.8(2)	25.0(2)	23.1(2)	22.3(2)	23.3(2)
Stratlingite				8.5(3)	16.3(4)	17.1(3)	13.6(4)
AFm				0.5(1)	1.2(1)	3.0(2)	1.1(1)
Katoite					2.5(4)	2.9(5)	3.5(5)
AH ₃		0.3(1)	0.2(1)				
CC							0.7(1)
ACn	18.3(5)	32.3(6)	36.6(7)	27.5(7)	41.2(1.0)	39.5(1.0)	42.4(1.1)
FW	35.5(-)	14.3(-)	18.4(-)	15.0(-)	3.5(-)	4.9(-)	4.8(-)

Table 4.14. RQPA results for B10B0 cement paste, as a function of hydration time, including ACn calculated with G-method and free water content. Numbers between brackets are mathematical errors from Rietveld calculations.

Phase	t ₀	3d	7d	28d	120d
β -C ₂ S	18.9(4)	14.1(3)	13.4(3)	10.2(3)	5.4(3)
o- C ₄ A ₃ S	9.4(7)	2.2(1)	1.2(1)		
C ₄ AF	5.0(2)	3.8(2)	3.6(2)	1.4(2)	0.9(2)
C ₂ AS	4.8(2)	3.9(1)	3.5(1)	3.6(1)	3.3(1)
γ -C ₂ S	1.4(1)	1.7(1)	1.6(1)	2.0(1)	1.8(1)
CT	0.4(1)	0.3(1)	0.2(1)	0.2(1)	0.2(1)
CSH _{0.5}	5.2(2)				
Aft		15.9(3)	14.9(3)	12.6(3)	13.3(3)
Stratlingite		3.6(6)	4.2(6)	15.4(5)	12.1(5)
AFm		0.8(1)	1.0(1)	4.8(1)	5.4(2)
Katoite				3.3(4)	5.1(3)
Hemicarbo				0.5(1)	
ACn	19.5(9)	32.5(8)	37.3(8)	31.3(8)	39.8(8)
FW	35.5(-)	21.3(-)	19.1(-)	14.6(-)	12.8(-)

Table 4.15. RQPA results for B10B2 cement paste, as a function of hydration time, including ACn calculated with G-method and free water content. Numbers between brackets are mathematical errors from Rietveld calculations.

Phase	t ₀	3d	7d	28d	120d
$\alpha'_H\text{-C}_2\text{S}$	20.8(4)	19.9(4)	20.6(5)	17.4(3)	4.0(5)
$\beta\text{-C}_2\text{S}$	0.4(1)	1.2(4)	1.1(3)	1.3(3)	2.1(3)
$c\text{-C}_4\text{A}_3\text{S}$	11.9(1)	0.3(1)	0.3(1)		
C_4AF	5.2(2)	4.2(2)	4.0(2)	3.5(2)	0.6(2)
C_2AS	2.2(1)	2.3(1)	2.1(1)	2.6(1)	1.9(1)
CT	0.7(1)	0.7(1)	0.7(1)	0.7(1)	
$\text{CSH}_{0.5}$	4.1(1)				
Af _t		20.7(2)	19.7(2)	23.3(2)	19.5(2)
Stratlingite				5.0(6)	9.6(6)
AF _m					1.1(2)
Katoite				0.9(2)	4.6(3)
AH ₃		0.4(1)	0.5(1)	0.4(1)	0.4(1)
ACn	19.3(5)	34.9(7)	36.2(7)	30.4(8)	47.7(9)
FW	35.5(-)	15.5(-)	14.9(-)	14.6(-)	8.6(-)

- **Thermal analysis.** DTA and TGA curves for G10B0 and G10B2 pastes (hydration stopped as described previously) at different curing ages were plotted as representative examples (Figure 4.22). G10B2 has a higher degree of reaction at 365 hydration days with a higher overall weight loss (~32 wt%) than the corresponding value for G10B0 (~26 wt%). Therefore, FW is large (at same hydration ages) for G10B0 than for G10B2. Moreover, Af_t, which is characterised by the weight loss at ~100°C, slightly increases with hydrating time for G10B2, see Figure 4.22.b, but it decreases with time for G10B0, see Figure 4.22.a. Two endothermic peaks at ~165 and ~200°C, are attributed to the stratlingite formation (Winnefeld and Barlag, 2010; Winnefeld and Lothenbach, 2010; Pelletier-Chaignat et al., 2010; 1011), however the second signal overlaps with the AF_m signals. The formation of stratlingite is much faster in G10B0 pastes (as reported in A#3), where is observed at 3 days of hydration, than in G10B2 pastes. The formation of stratlingite is delayed in G10B2, and its content is smaller than in the non-active paste. All these crystalline phases were quantified by powder diffraction and the results are fully consistent with those reported here. The same behaviour has been observed for the cements with bassanite and anhydrite.

The thermal characterisation is very suitable to identify poor crystalline phases that cannot be properly analysed by LXRPD, such as amorphous gibbsite or even AF_m. The decomposition of AF_m produces different peaks in the DTA-TGA

curves, where some are overlapped with other phases, so it is difficult to quantify; however, Figure 4.22.a shows how AFm appears in G10B0 paste just after 3 days of hydration. AH_3 is detected in G10B2 pastes at 3 and 7, however, after 28 days, this signal disappears and the peak related to stratlingite develops, thus confirming that stratlingite is formed by consuming AH_3 , according to reaction 1.4. Similar conclusions can be drawn from the corresponding curves of X10B0 and X10B2 pastes. In addition, amorphous gibbsite signal is almost not evident in G10B0 traces, at any age. This is explained as it rapidly reacts to yield stratlingite which shows a strong signal at ages later than 3 days of hydration.

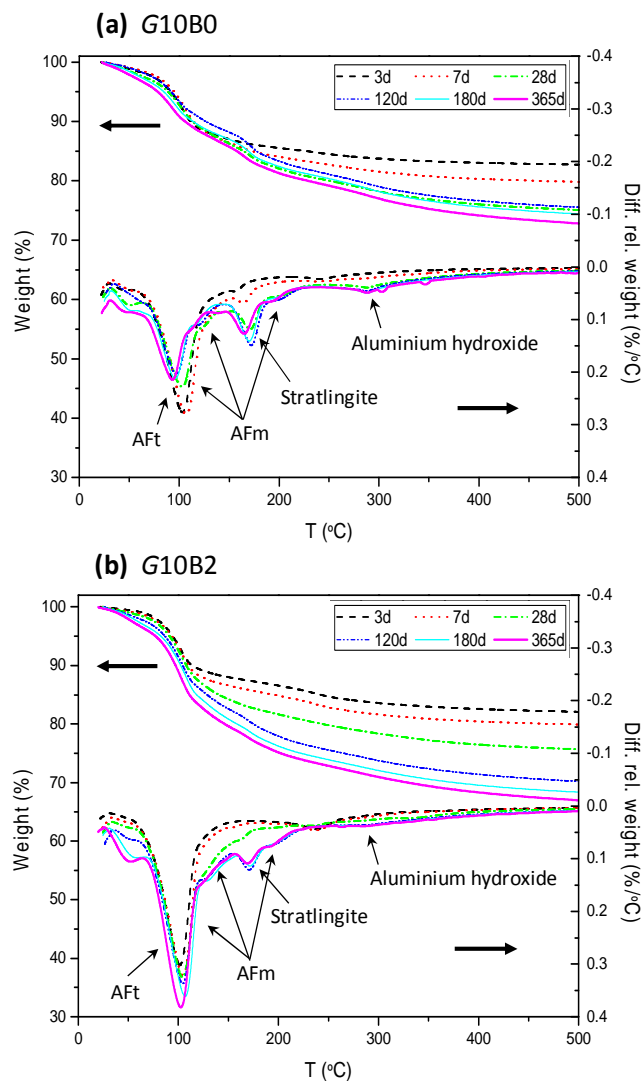
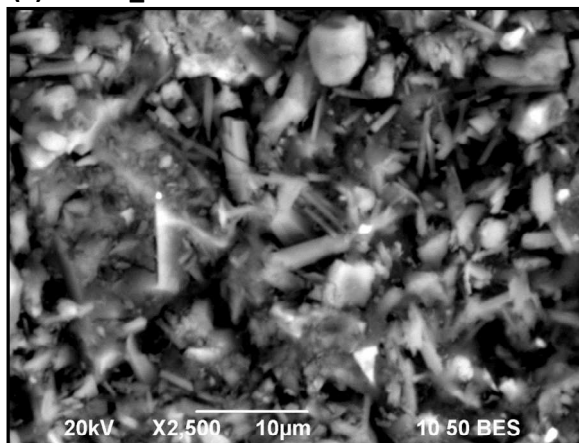


Figure 4.22. DTA-TGA curves for: (a) G10B0, and (b) G10B2 pastes after stopping hydration at 3, 7, 28, 120, 180 and 365 days (Figure 2 in A#5).

- **SEM-EDS characterisation.** A SEM-EDS study was performed to better characterise the chemical composition of each phase in the X10B2 pastes, especially for amorphous/ill-crystalline phases (A#5). This type of study helped to estimate the elemental composition (especially Si, Al and Fe) of new crystalline or amorphous phases with time of hydration, since this may affect the mechanical properties. Figure 4.23 shows two representative micrographs of A10B2 stopped-hydration pastes at different hydration time, 7 and 120 days.

(a) A10B2_7d



(b) A10B2_120d

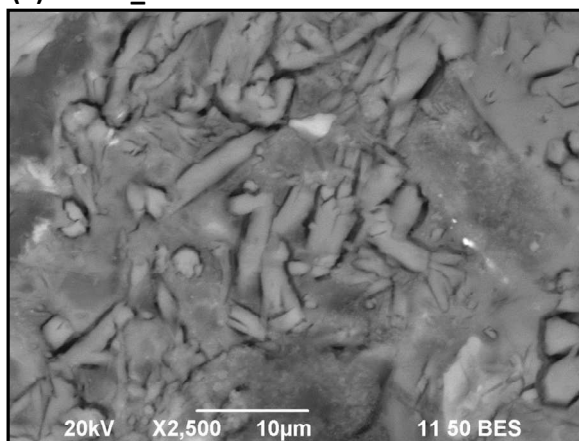


Figure 4.23. SEM micrographs of A10B2 stopped-hydration paste at different hydration time: (a) 7 days and (b) 120 days.

SEM-EDS analyses of these hydrated pastes reveal that the chemical composition of amorphous phase(s) in G10B2 and B10B2 at 120 days is very similar, but slightly richer in silicon and iron in A10B2. The chemical composition evolution with time may generate interesting information. Al/Ca vs. Si/Ca atomic ratios, for A10B2 paste at 7 and 120 days of hydration, were plotted in Figure 5 in A#5. Representative micrographs of the pastes are also provided in the figure. These results reveal that amorphous phases in A10B2 are rich in aluminium at 7 days, while they are enriched in silicon with time (120 days). The former is related to early hydration products (AFt and amorphous aluminium hydroxide) formed in these cements from the dissolution of ye'elimite and calcium sulphate; the latter, to the reactivity of belite. Moreover, hydration products which contain iron are difficult to be identified by LXRPD. Figure 6 in A#5, shows Al-Fe atomic ratio for A10B2 pastes at different ages (7 and 120 days). According to the results given in this figure, particles with a needle shape, which are identified as ettringite, contain some iron at both studied hydration ages, in agreement with previous reports (Möschner et al., 2009). In addition, A10B2 hydrated during 7 days shows some small bright particles with a chemical composition similar to that of stratlingite; the DTA thermograph of this sample showed a small shoulder at $\sim 170^\circ\text{C}$, which is related to stratlingite. However, these particles seem to have low crystallinity degree, and so they cannot be detected by LXRPD at that hydration age. The iron content in these bright particles increases from ~ 0.05 Fe/Ca atomic ratio at 7 days, to ~ 0.1 Fe/Ca atomic ratio at 120 days. These results yield us to propose two hypotheses: i) There is amorphous layers of FH_3 covering stratlingite particles, or ii) the following reaction [4.1] between belite and ferrite to give iron-bearing stratlingite is taking place:



If the second hypothesis is right, the study on iron evolution performed in A#3 (Figure 4a and 4b in article a#3) has to be considered as an approximation, since in that study, stratlingite is considered as an iron-free phase. However, this need more research.

4.4. MECHANICAL PROPERTIES OF BCSAF MORTARS.

Standard mortars were prepared with a cement/sand/water ratio of 1/3/0.55 in order to study the mechanical properties. Figure 4.24 summarises the compressive strengths of mortars studied in this PhD Thesis. We highlight that larger mechanical strengths could have been attained by decreasing the w/c ratio (to, for example, 0.35 or 0.40); however, following the chemical evolution may be tougher as local drying effects may start to appear. More studies are needed correlating variable w/c ratios

and curing conditions with phase evolutions and strength developments to understand the thorough hydrating behaviour for this emerging type of cements.

The most important result is that all mortars prepared with the aBCSAF cement developed higher compressive strengths than non-active mortars, independently of the type and amount of sulphate source (Figure 4.24). Consequently, it can be stated that the higher hydration rate of β -C₂S in BCSAF_B0 pastes does not imply higher mechanical strengths. In addition, by increasing the gypsum content from 5 to 10 wt%, the compressive strength increased in both systems. Furthermore, the addition of 15 wt% gypsum produced a slight decrease in the compressive strength, probably due to the slowdown of belite hydration rate. It should be noted that the size of the mortar specimens prepared to measure compressive strengths (30 x 30 x 30 mm³) is smaller than that of the mortar specimens prepared for length change measurements. Therefore it was possible to measure the compressive strength for G15B0 as the mortar prisms were not broken.

Setting times of mortars prepared with different amount of gypsum (see Table 4.16) were also measured. Gypsum mortars showed intermediate initial setting time values, comparing with values obtained for anhydrite and bassanite mortars (García-Maté, 2015). The different kinetic behaviours between BCSAF_B0 and BCSAF_B2 pastes, justify the differences in the measured initial and final setting times. For G10B0, these values are 2.8 and 5.5 h, respectively; whereas for G10B2, the values are 3.5 and 5.8 h, respectively. In general, GxB2 mortars presented higher initial setting time than that for GxB0 mortars, showing a higher plasticity which can better accommodate the precipitation of ettringite. However, G5Bx mortars showed the highest initial setting time, due probably to the small amount of gypsum added that cause at lowest ettringite formation.

Within the non-active mortars, A10B0 presented the highest values. This behaviour may be explained/justified by the higher amount of AFt present in that paste when compared to G10B0. In addition, García-Maté et al., (2015a) determined that, since the setting time of CSA pastes with anhydrite is longer than that for pastes/mortars with gypsum, anhydrite-mortars show higher plasticity that can better accommodate the precipitation of ettringite. Bassanite cement reacts very quickly with water showing a short setting time (García-Maté et al., 2015a) which leads to mortars with low degree of homogeneity. Due to this fact, the compressive strength values for B10B0 mortars were not measured. For B10B2, although the addition of a small amount of SP improved the workability of the mortar, the delay in the setting time was not enough to develop comparable mechanical strength values to gypsum and anhydrite mortars, see Figure 4.24.b.

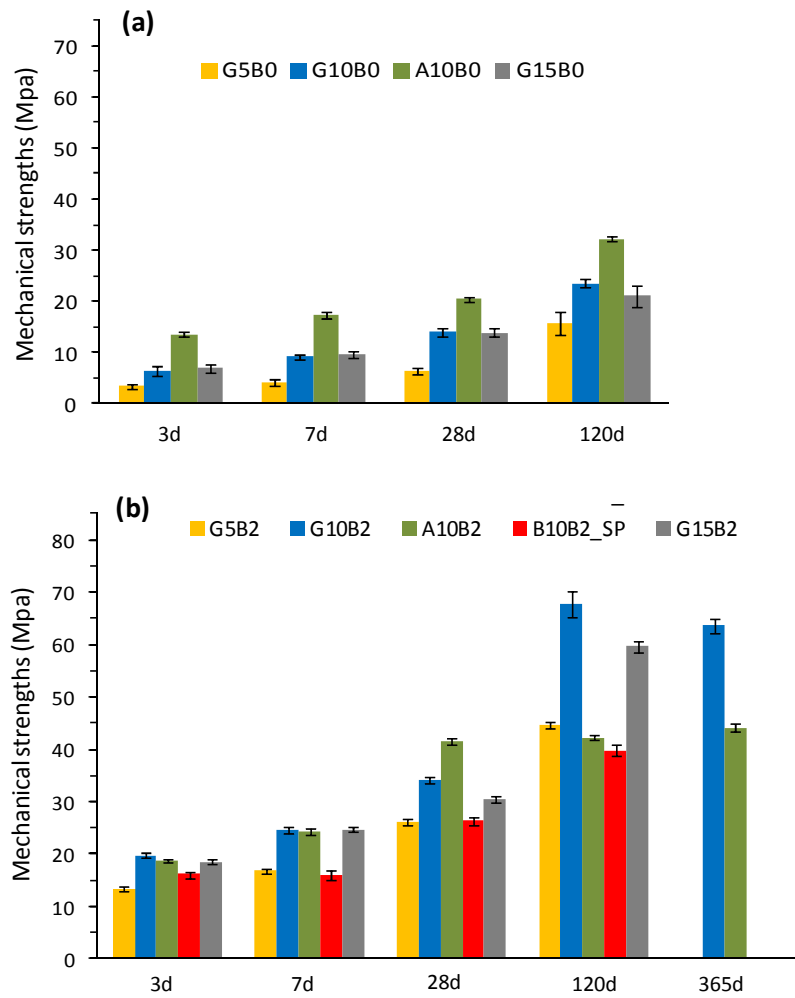


Figure 4.24. Compressive strength development at different hydration times for (a) non-active, and (b) active BCSAF mortars.

Table 4.16. Initial and final setting times of different G-mortars.

Mortar	Initial setting time	Final setting time
G5B0	350min	470min
G10B0	170min	330min
G15B0	160min	410min
G5B2	250min	330min
G10B2	210min	350min
G15B2	215min	385min

Within the active mortars, G10B2 and A10B2 present very similar compressive strengths values up to 7 days and their pastes also show similar ettringite contents. However, at 28 hydration days, A10B2 mortar shows slightly higher compressive strength values, which can be justified by a larger amount of ettringite (25 and 19 wt% for A and G-pastes, respectively). However, at 120 days, G10B2 mortar developed the highest mechanical strength value, even when the amount of ettringite in A-paste was slightly larger than that for G-paste (23 and 19 wt%, respectively). Therefore, we are forced to conclude that the amorphous contents (and the microstructure of the paste) are playing a key role for the strength development at late ages. The reaction degree of $\alpha'_H\text{-C}_2\text{S}$ in G10B2 (74%) is slightly higher than that in A10B2 (65%), which could help in improving the mechanical strengths. At a constant porosity, the strength increases by increasing the amount of hydrates being formed and a declining amount of non-hydrated material (Older, 2003). Since A and G-pastes contain similar ACn contents, the porosity of the pastes was measured. It is well known that the porosity of the paste has an adverse effect on strength development (Chen et al., 2012). The porosity of the three X10B2 cement pastes at 120 days of hydration was measured by mercury intrusion porosimetry (MIP), which could be extrapolated to the mortars. Bassanite-paste showed the highest percentage of porosity (16%), and the gypsum one showed the lowest value (10%) (see Figure 4.25); this behaviour helps to justify the measured mechanical strengths. Density/porosity can also be evaluated from the SEM micrographs of these three pastes (Figures 4.26.a, b, and c show the polished cross-section of gypsum, anhydrite and bassanite-pastes, respectively). Pores in the anhydrite paste are numerous and larger than those in the gypsum paste, and the bassanite paste shows large pores as can be appreciated in the inset of Figure 4.26.c, and some cracks.

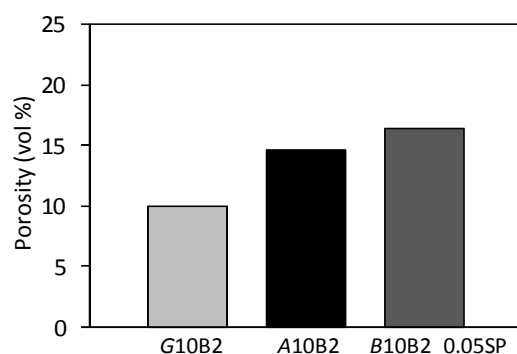


Figure 4.25. Open porosity percentage of X10B2 pastes at 120 days,

In conclusion, the **optimum amount and type of sulphate source** in these systems seems to be quite close to **10 wt% of gypsum**, as higher mechanical strengths are obtained.

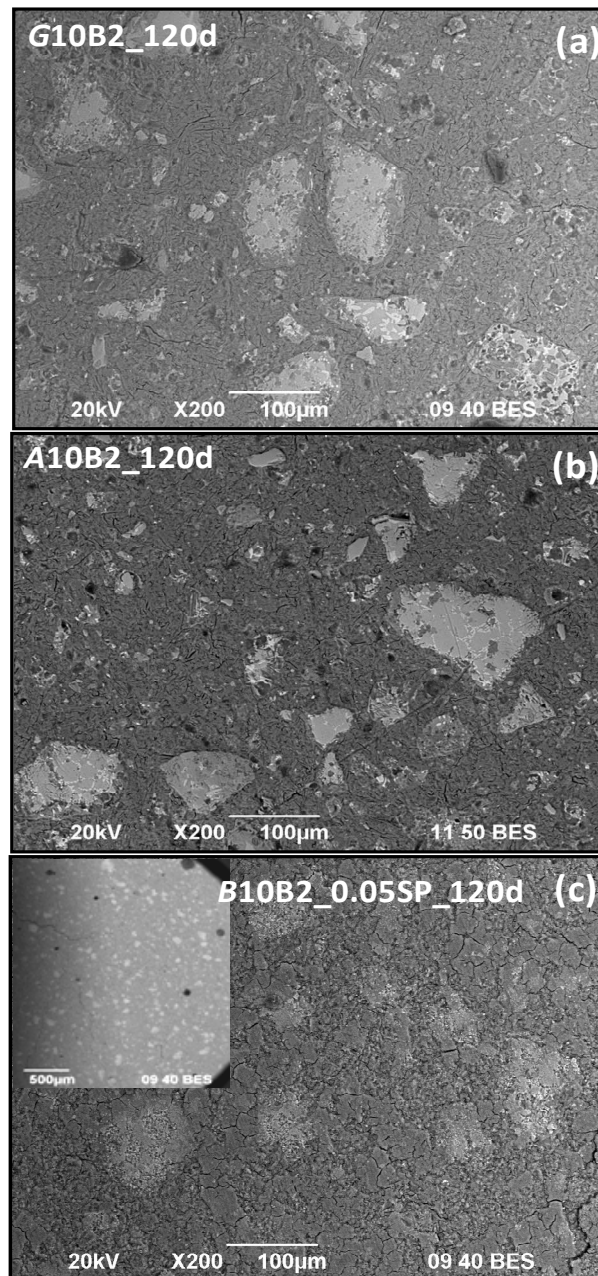


Figure 4.26. SEM micrographs of polished (a) G10B2, (b) A10B2 and (c) B10B2_0.05%SP pastes at 120 days of hydration time. The inset of figure (c) shows the B10B2 paste at a lower magnification.

Finally, the expansion/shrinkage of the mortars was also measured at different hydration ages and the data are shown in Figure 4.27. This figure represents the percentage of length change, ΔL (%), with respect to the initial value, L_0 . The latter was the measured length taken just after demoulding the standard prismatic samples and prior to immersion in water (24 h hydration). The expansion (or shrinkage) experienced by mortars is mainly related to the nature of the pore structure (which affects the mobility of ions) and the amount of space for reaction products to be formed. The low expansion values obtained for these mortars agree with previous studies (Chen et al., 2012).

Firstly, our study has revealed the effect of gypsum content on dimensional stability of BCSA mortars. The addition of 15 wt% of gypsum caused the highest expansion values for both systems due to the larger amounts of AFt formed, comparable, as expected, to commercial CSA. The expansion in G15B0 was so severe that the mortar prism appeared cracked after 3 hydration days. A photograph of the broken prism is shown in the inset of Figure 4.27, where a significant amount of ettringite crystals (white powder) is appreciable inside the crevice. According to Figure 4.27, G5B0 and G10B0 experienced low expansion values and almost negligible dimensional changes with time, likely due to the lower amounts of AFt formed compared to GgB2 mortars. In addition, G5B2 and G10B2 mortars showed a length variation roughly from -0.01% to 0.04% within 180 days.

Secondly, the effect of the sulphate source on dimensional stability was also studied. Mortars prepared with anhydrite presented high expansion in early hydration ages, similar than that in CSA mortars. However, the B10B2 mortar showed very low expansion values, similar to mortars prepared with 5 wt% of gypsum; this is in agreement with the results obtained in the hydrating behaviour study, as bassanite is completely dissolved before the first 45 minutes of hydration and gypsum precipitates. Consequently, bassanite-mortars behave similar to those made with gypsum at very early ages.

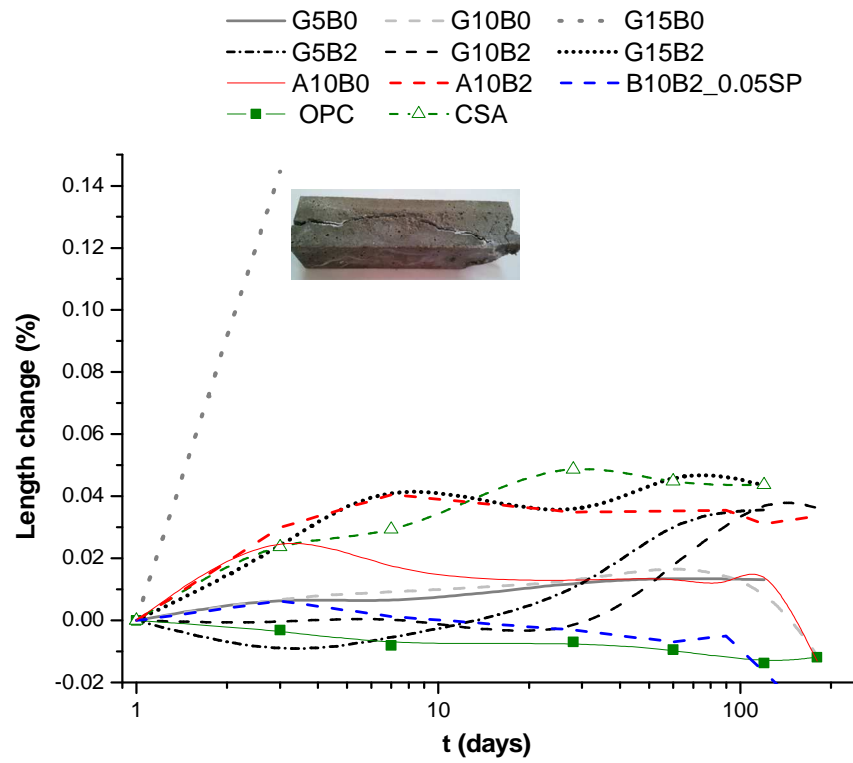


Figure 4.27. Length change measurements for mortars prepared with active and non-active BCSAF cement. Corresponding values for OPC and CSA mortars are also given for the sake of comparison.

CHAPTER 5

CONCLUSIONS

5. CONCLUSIONS.

The synthesis and hydration mechanisms of BCSAF cements have been studied. The effect of the polymorphism of the main phases of the clinkers, and type and amount of the sulphate source was thoroughly studied on hydrated pastes, and consequently on the corresponding mortars. X-ray diffraction combined with the Rietveld method have been used for the identification and quantification of phases of cement (anhydrous and hydrated). Data from various diffraction sources including laboratory X-ray (Cu and Mo radiations) and synchrotron X-ray were used in the investigations. It was shown that the reliability of Rietveld method is directly linked to the quality of data in terms of counting statistics and resolution, and the ability of the structural models used to correctly describe the phases present in the sample.

Several specific conclusions arisen from this PhD Thesis, and are numbered below:

i) Two BCSAF clinkers active and non-active ones, have been prepared in the laboratory at "medium scale" (~2 kg) using the same raw materials commonly used in cement plants. The non-active clinker contained β -C₂S and orthorhombic ye'elimite as main phases, meanwhile α' _H-C₂S and pseudo-cubic ye'elimite were stabilized in the active clinker due to the addition of borax to the raw mixture. The optimum clinking cycle for the two scaled-up clinkers was the following: 900°C/0.5 h - 1350°C/ 0.5 h, and forced air flow cooling.

ii) The crystalline phases present in the two BCSAF clinkers and other related materials (commercial CSA clinkers) were characterised and quantified through the combination of LXRPD and the Rietveld method. Moreover, the ACn content of these materials was measured by both external and internal standard methods. Overall, the analyses showed that commercial CSA clinkers have ACn contents quite similar to those of OPCs, ~10 wt%. Conversely, the ACn content of the BCSAF clinkers were higher, ~25 wt%.

iii) A reproducible methodology of processing and characterisation of hydrated BCSAF cement pastes has been established, including the quantification of ACn content and FW that enable to understand and control the behaviour of these cement pastes during hydration. Moreover, an initial characterisation of ACn has been performed to estimate its elemental composition and correlate it with the hydration behaviour and mechanical properties. The highest amount of dissolved sulphate groups incorporated into ACn phase(s) was found in non-active BCSAF cement pastes. However, aBCSAF cement pastes show the highest amounts of silicate and aluminate contents in their amorphous phase(s).

iv) Orthorhombic ye'elimite phase in non-active BCSAF cement dissolves at a higher pace than pseudo-cubic ye'elimite in active BCSAF cement for the same gypsum content (10 wt%). Different amounts of gypsum did not strongly affect the ye'elimite reactivity rate. Moreover, non-active cements showed larger amounts of AFm and consequently, lower quantities of ettringite during hydration when compared to active cements. In active cements, the formation of AFm from the reaction of ye'elimite with water was not observed.

v) The hydration behaviour of belite resulted more dependent on the chemical environment than on its polymorphism. In our hydration conditions, β -C₂S in non-active BCSAF reacted faster than α' -C₂S in active cement, independently of the amount and type of sulphate source to give stratlingite. The increase of gypsum addition to BCSAF cements caused a slowdown in hydration rate of belite (independently of the polymorphism). The sulphate source added (gypsum, bassanite or anhydrite) does not strongly affect the belite dissolution.

vi) Mortars prepared with active BCSAF cement developed higher compressive strengths than non-active ones, independently of the type and amount of sulphate source; it implies that the higher hydration rate of β -C₂S in BCSAF_B0 pastes does not mean higher mechanical strengths. By increasing the gypsum content from 5 to 10 wt%, the compressive strength increases in both systems, but the addition of 15 wt% gypsum produced a slight decrease in the compressive strengths.

In the case of non-active mortars, those prepared with anhydrite (A10B0) presented the highest compressive strength values (e.g. 32±1 MPa at 120 days). For B10B2, the addition of a small amount of SP improved the workability of the mortar, but it was not enough to develop comparable mechanical strength values to gypsum and anhydrite mortars.

In the case of active-mortars, those with gypsum or anhydrite (G10B2 and A10B2, respectively) showed very similar compressive strength values up to 7 days of hydration (~25±1 MPa). However, at 120 days, the G10B2 mortar developed the highest mechanical strengths (68±1 MPa), even when its amount of AFt was slightly lower than that for the A-sample. This is related to the highest BET area value of G10B2 and the porosity of these pastes (10 and 15 vol% for G and A-pastes, respectively).

Finally, **active mortars with 10 wt% of gypsum resulted as the best option** due to their higher mechanical strengths (**68±1 MPa at 120 days**).

vii) More researches varying w/c ratios and using supplementary cementitious materials (SCMs) are needed for a better characterisation of these emerging new eco-cements.

CHAPTER 5

CONCLUSIONES (In Spanish)

5. CONCLUSIONES.

En esta tesis doctoral se ha llevado a cabo el estudio de la síntesis y los mecanismos de hidratación de cementos BSACF. El efecto de los distintos polimorfos de las fases principales de los clínkeres, así como la influencia de la cantidad y el tipo de fuente de sulfato utilizados también han sido estudiados en las pastas de cemento y en consecuencia en los correspondientes morteros preparados. La difracción de rayos X combinada con el método de Rietveld se han utilizado como herramientas para la identificación y cuantificación de las fases del cemento (anhidro e hidratado). Para llevar a cabo esta investigación se han usado datos de diversas fuentes de radiación, incluyendo la difracción de rayos X de laboratorio (de Cu y Mo) y de rayos X sincrotrón. Se ha demostrado que la fiabilidad del método de Rietveld está directamente relacionada con la calidad de los datos, en términos de estadísticas de conteo y resolución, y con la capacidad de los modelos estructurales utilizados para describir correctamente las fases presentes en la muestra.

A continuación se enumeran varias conclusiones específicas surgidas de esta tesis doctoral:

i) Se han preparado dos clínkeres BSACF, uno activado y otro no, a "media escala" (~2 kg) en el laboratorio, utilizando las mismas materias primas utilizadas en las cementeras. El clinker no activado contiene β -C₂S y ye'elimita ortorrómbica como fases principales, mientras que la α' -C₂S y la ye'elimita pseudo-cúbica se estabilizaron en el clinker activado debido a la adición de borax en las materias primas del crudo. El proceso de clinkerización óptimo para la síntesis de los dos clínkeres ha sido 900°C/0.5 h -1350°C/ 0.5 h, y enfriamiento con una corriente de aire.

ii) Las fases cristalinas presentes en los dos clínkeres sintetizados y en otros materiales relacionados (clínkeres de CSA comerciales) han sido caracterizados y cuantificados mediante DRXPL y el método de Rietveld. Además, el contenido de ACn de estos materiales se ha determinado usando métodos de estándar interno y externo. En general, los análisis mostraron que los clínkeres comerciales de CSA presentan contenidos de ACn bastante similares a los de los OPC, ~10% en peso. Por el contrario, los contenidos de ACn presentes en los clínkeres BSACF fueron mayores, ~25% en peso.

iii) Se ha establecido una metodología reproducible para el procesado y la caracterización de las pastas de cemento BSACF hidratado, incluyendo la cuantificación del ACn y el FW, lo que permite comprender y controlar el comportamiento de estas pastas de cemento durante su hidratación. Además se ha

llevado a cabo una caracterización inicial del ACn mediante la estimación de su composición elemental para correlacionarlo con el comportamiento hidráulico de los cementos y las propiedades mecánicas de los morteros. Se ha encontrado que las pastas de cementos BSACF no activos presentan una mayor cantidad de grupos sulfatos en la fase(s) amorfa(s). Mientras que las pastas de cementos BSACF activos presentan una mayor cantidad de grupos silicatos y aluminatos disueltos en el ACn.

iv) La ye'elimita ortorrómbica presente en el cemento BSACF no activo se disuelve a una mayor velocidad que la ye'elimita pseudo-cúbica que se encuentra en el cemento BSACF activo para el mismo contenido de yeso (10% en peso). Diferentes cantidades de yeso no afectan a la reactividad de la ye'elimita. Por otro lado, los cementos no activos mostraron mayores cantidades de AFm y en consecuencia menores cantidades de etringita durante su hidratación, si los comparamos con los cementos activos. En los cementos activos no se observa la reacción de la ye'elimita con agua para formar AFm, como principal fase hidratada.

v) El comportamiento de la belita durante la hidratación depende más del ambiente químico que la rodea que de su polimorfismo. En nuestras condiciones de hidratación, la β -C₂S, presente en los cementos no activados, reacciona más rápidamente que la α' -C₂S, presente en los cementos activados independientemente de la cantidad y el tipo de fuente de sulfato añadida, para dar stratlingita. El aumento de la cantidad de yeso añadida a los cementos provoca una disminución de la velocidad de hidratación de belita (independientemente del polimorfismo). La fuente de sulfato añadida (yeso, anhidrita o basanita) no afectan demasiado a la disolución de la belita.

vi) Los correspondientes morteros preparados con los cementos aBSACF desarrollan mayores resistencias a la compresión que los morteros no activados, independientemente del tipo y de la cantidad de fuente de sulfato, lo que demuestra que la mayor velocidad de disolución de la β -C₂S en las pastas de BSACF_B0 no significa resistencias mecánicas más altas. El aumento del contenido de yeso del 5 al 10% en peso, produce un aumento en la resistencia en ambos sistemas, pero la adición de 15% en peso de yeso produce una ligera disminución de la resistencia.

Dentro de los morteros de cementos no activados, los preparados con anhidrita (A10B0) presentaron los valores más altos de resistencia (32 ± 1 MPa a 120 días). Para B10B2, la adición de una pequeña cantidad de aditivo superplastificante (SP) mejoró la trabajabilidad del mortero, pero no fue suficiente para desarrollar valores de resistencias comparables a los obtenidos para los morteros preparados con yeso y anhidrita.

En el caso de los morteros preparados con cementos activados, los morteros de yeso y anhidrita (G10B2 and A10B2, respectivamente) mostraron resistencias a la compresión muy similares a 7 días ($\sim 25 \pm 1$ MPa). Sin embargo, a los 120 días, el mortero G10B2 desarrolló el valor de resistencia más elevado (68 ± 1 MPa), aun cuando la cantidad de AFt fue ligeramente inferior a la de la muestra con anhidrita. Esto está relacionado con el mayor valor de área específica del cemento G10B2 y la porosidad de las pastas (10 y 15% en volumen para la pasta de yeso y anhidrita, respectivamente).

En conclusión, se ha determinado que los **morteros preparados con cementos BSACF y un 10% en peso de yeso, han resultado ser la mejor opción** porque son los que desarrollaron mayores resistencias mecánicas (**68+1 MPa a 120 días**).

vii) Se necesita más investigación utilizando distintas relaciones a/c y usando materiales cementantes suplementarios para caracterizar mejor estos nuevos eco-cementos.

CHAPTER 6

REFERENCES

A

- Abdul-Maula S and Older I, (1992). "SO₃-rich Portland cements: synthesis and strength development". *Mat Res Soc Symp Proceedings*, 245, 315-320.
- Adolfsson D, Menad N, Viggh E and Bjorkman B, (2007). "Hydraulic properties of sulfoaluminate belite cement based on steelmaking slags". *Adv Cem Res*, 19, 133-138.
- Allmann R, (1977). "Refinement of the hybrid layer structure [Ca₂Al(OH)₆].0.5(SO₄).3H₂O". *Neues Jb Miner Monat*, 136-144.
- Andac M and Glasser F P, (1999). "Pore solution composition of calcium sulfoaluminate cement". *Adv Cem Res*, 11, 23-26.
- Andersen M D, Jakobsen H J and Skibsted J, (2003). "Incorporation of aluminum in the calcium silicate hydrate (C-S-H) of hydrated Portland cements: a high-field Al-27 and Si-29 MAS NMR". *Inorganic Chemistry*, 42, 2280-2287.
- Aranda M A G, Cuberos A J M, Cuesta A, Álvarez-Pinazo G, De la Torre A G, Schollbach K and Pöllmann H, (2011). "Hydrating behaviour of activated belite sulfoaluminate cements". *Proceedings of the 13th International Congress on the Chemistry of Cement, Madrid, Spain*.
- Aranda M A G and De la Torre A G, (2013). "Sulfoaluminate cement" in *Eco-efficient Concrete*, Pacheco-Torgal F, Jalali S, Labrincha J and John V M (Eds.), Woodhead Publishing, Cambridge, 488-522.
- Aranda M A G, De la Torre A G and León-Reina L, (2012). "Rietveld quantitative phase analysis of OPC clinkers, cements and hydration products". *Rev Mineral Geochem*, 74, 169-209.
- Aranda M A G, De la Torre A G and León-Reina L, (2015). "Powder diffraction characterisation of cements". *International Tables for Crystallography. Volume H. Powder Diffraction*, in press.
- Arjunan P, Silsbee M R and Roy D M, (1999). "Sulfoaluminate-belite cement from lowcalcium fly ash and sulfur-rich and other industrial by-products". *Cem Concr Res*, 29, 1305-1311.

B

- Banfill P F G, (2006). "Rheology of fresh cement and concrete". *Rheology Reviews*, 61-130.
- Barcelo L, Kline J, Walenta G and Gartner E, (2014). "Cement and carbon emissions". *Mater Struct*, 47, 1055-1065.

- Barnes P and Bensted J, **(2002)**. "Structure and performance of cements", in Taylor and Francis, Spon Press, London, 565.
- Benarchid M Y, Diouri A, Boukhari A, Aride J, Rogez J and Castanet R, **(2004)**. "Elaboration and thermal study of iron-phosphorus-substituted dicalcium silicate phase". *Cem Concr Res*, 34, 1873-1879.
- Benhelal E, Zahedi G and Haslenda H, **(2012)**. "A novel design for green and economical cement manufacturing". *J Clean Prod*, 22, 60-66.
- Bensted J, **(1979)**. "Some hydration studies of α -dicalcium silicate". *Cem Concr Res*, 9, 97-101.
- Bentur A and Ish-Shalom M, **(1974)**. "Properties of Type K expansive cement and pure components". *Cem Concr Res*, 4, 709-721.
- Beretka J, Marroccoli M, Sherman N and Valenti G L, **(1996)**. "The Influence of C_4A_3S content and w/s ratio on the performance of calcium sulfoaluminate-based cements". *Cem Concr Res*, 26, 1673-1681.
- Berger S, Coumes C C D, Bescop P and Damidot D, **(2011a)**. "Influence of a thermal cycle at early age on the hydration of calcium sulphoaluminate cements with variable gypsum contents". *Cem Concr Res*, 41, 149-160.
- Berger S, Coumes C C D, Bescop P, Aouad G and Damidot D, **(2011b)**. "Leaching of calcium sulfoaluminate cement-based materials: experimental investigation and modelling". Proceedings of the 13th international Congress on the Chemistry of Cement, Madrid, Spain.
- Bernardo G, Telesca A and Valenti G L, **(2006)**. "A porosimetric study of calcium sulfoaluminate cement pastes cured at early ages". *Cem Concr Comp*, 36, 1042-1047.
- Bizzozero J, Gosselin C and Scrivener K L, **(2014)**. "Expansion mechanisms in calcium aluminate and sulfoaluminate systems with calcium sulfate". *Cem Concr Res*, 56, 190-202.
- Blaine R, **(1995)**. "Determination of calcium-sulfate hydrates in building-materials using thermal-analysis". *Am Lab*, 27, 24-28.
- Brown P W and Taylor H F W, **(1999)**. "The role of ettringite in external sulfate attack". *Am Ceram Soc*, 73-98.
- Brunet F, Charpentier T, Chao C N, Peycelon H and Nonat A, **(2010)**. "Characterization by solid-state NMR and selective dissolution techniques of anhydrous and hydrated CEM V cement pastes". *Cem Concr Res*, 40, 208-219.
- Bullerjahn F, Schmitt D and Haha M B, **(2014)**. "Effect of raw mix design and of clinkering process on the formation and mineralogical composition of

(ternesite) belite calcium sulfoaluminate ferrite clinker". *Cem Concr Res*, 59, 87–95.

C

- Calos N J, Kennard C H L, Whittaker A K and Davis R L, **(1995)**. "Structure of calcium aluminate sulfate $\text{Ca}_4\text{Al}_6\text{O}_{16}\text{S}$ ". *J Solid State Chem*, 119, 1-7.
- Campbell D H and Galehouse J S, **(1991)**. "Quantitative clinker microscopy with the light microscope". *Cem Concr Aggr*, 13, 94-96.
- Canonico F and Bernardo G, **(2006)**. "Microstructural investigation on hydrated high performance cements based on calcium sulfoaluminate". University of Basilicate, Potenza, Italy.
- Catti M, Gazzoni G and Ivaldi G, **(1984)**. "Order-disorder in the α' -(Ca,Sr) $_2$ SiO $_4$ solid solution: a structural and statistical-thermodynamic analysis". *Acta Cryst*, B40, 537-544.
- Cau Dit Coumes C, Courtois S, Peysson S, Ambroise J and Péra J, **(2009)**. "Calcium sulfoaluminate cement blended with OPC: a potential binder to encapsulate low-level radioactive slurries of complex chemistry". *Cem Concr Res*, 39, 740-747.
- Chatterjee A K, **(1996)**. "High belite cements-Present status and future technological options: Part I and Part II". *Cem Concr Res*, 26, 1213–1237.
- Chatterjee A K, **(2002)**. "Special Cements", in *Structure and Performance of Cements*, Edited by Bensted J, and Barnes P, Published by Spon Spress, 186.
- Chen C, Habert G, Bouzidi Y and Jullien A, **(2010)**. "Environmental impact of cement production: detail of the different processes and cement plant variability evaluation". *J Clean Prod*, 18, 478-485.
- Chen I A, Hargis C W and Juenger M C G, **(2012)**. "Understanding expansion in calcium sulfoaluminate-belite cements". *Cem Concr Res*, 42, 51-60.
- Chen Y L, Lin C J, Ko M S, Lai Y C and Chang J E, **(2011)**. "Characterization of mortars from belite-rich clinkers produced from inorganic wastes". *Cem Concr Com*, 33, 261-266.
- Cline J P, Von Dree R B, Winburn R, Stephens P W and Filliben J J, **(2011)**. "Addressing the amorphous content issue in quantitative phase analysis: the certification of NIST standard reference material 676a". *Acta Crystallogr*, A67, 357-367.
- Cohen M D, **(1983a)**. "Modeling of expansive cements". *Cem Concr Res*, 13, 519–528.
- Cohen M D, **(1983b)**. "Theories of expansion in sulfoaluminate-type expansive cements — Schools of thought". *Cem Concr Res*, 13, 809–818.

- Collier N C, Milestone N B, Hill J and Godfrey I H, **(2006)**. "The disposal of radioactive ferric floc". *Waste Manag*, 26, 769–775.
- Collier N C, Milestone N B, Hill J and Godfrey I H, **(2009)**. "Immobilisation of Fe floc: part 2, encapsulation of floc in composite cement". *J Nucl Mater*, 393, 92–101.
- Colville A A, **(1970)**. "The crystal structure of $\text{Ca}_2\text{Fe}_2\text{O}_5$ and its relation to the nuclear electric field gradient at the iron sites". *Acta Cryst*, B26, 1469-1473.
- Colville A A and G  ller S, **(1971)**. "The crystal structure of brownmillerite, $\text{Ca}_2\text{FeAlO}_5$ ". *Acta Cryst*, B27, 2311-2315.
- Crumbie A, Walenta G and Fuellmann T, **(2006)**. "Where is the iron? Clinker microanalysis with XRD Rietveld, optical microscopy/point counting, Bogue and SEM-EDS techniques". *Cem Concr Res*, 36, 1542-1547.
- Cuberos A J M, De la Torre A G,   lvarez-Pinazo G, Mart  n-Sede  o M C, Schollbach K, P  llmann H and Aranda M A G, **(2010)**. "Active Iron-Rich Belite Sulfoaluminate Cements: Clinkering and Hydration". *Env Sci Tech*, 44, 6855-6862.
- Cuesta A, Losilla E R, Aranda M A G and De la Torre A G, **(2012)**. "Reactive belite stabilization mechanisms by boron-bearing dopants". *Cem Concr Res*, 42, 598–606.
- Cuesta A, De la Torre A G, Losilla E R, Peterson V K, Rejmak P, Ayuela A, Frontera C and Aranda M A G, **(2013)**. "Structure, Atomistic Simulations, and Phase Transition of Stoichiometric Yeelimitite". *Chem Mater*, 25, 1680-1687.
- Cuesta A,   lvarez-Pinazo G, Sanf  lix S G, Peral I, Aranda M G A and De la Torre A G, **(2014a)**. "Hydration mechanisms of two polymorphs of synthetic ye'elimitite". *Cem Concr Res*, 63, 127-136.
- Cuesta A, Aranda M A G, Sanz J, De la Torre A G and Losilla E R, **(2014b)**. "Mechanism of stabilization of dicalcium silicate solid solution with aluminium". *Dalton Trans*, 43, 2176-2182.
- Cuesta A, De la Torre A G, Losilla E R, Santacruz I and Aranda M A G, **(2014c)**. "Pseudo-cubic crystal structure and phase transition in doped ye'elimitite". *Cryst Growth Des*, 14, 5158–5163.

D

- Damidot D and Glasser F P, **(1993)**. "Thermodynamic investigation of the $\text{CaO-Al}_2\text{O}_3\text{-CaSO}_4\text{-H}_2\text{O}$ system at 25   C and the influence of Na_2O ". *Cem Concr Res*, 23, 221–238.

- Dan E and Janotka I, **(2003)**. "Chemical Resistance of Portland Cement, Blast-Furnace Slag Portland Cement and Sulphoaluminate-Belite Cement in Acid, Chloride and Sulphate Solution: Some Preliminary Results." *Ceram Silikaty*, 47, 141-148.
- De la Torre A G, Bruque S and Aranda M A G, **(2001)**. "Rietveld quantitative amorphous content analysis". *J Appl Cryst*, 34, 196-202.
- De la Torre A G, Morsli K, Zahir M and Aranda M A G, **(2007)**. "In-situ belite Portland clinkerization study by X-ray synchrotron powder diffraction". *J App Cryst*, 40, 999-1007.
- De la Torre A G, Cuberos A J M, Álvarez-Pinazo G, Cuesta A and Aranda M A G, **(2011a)**. "In situ powder diffraction study of belite sulfoaluminate clinkering". *J Synch Rad*, 18, 506–514.
- De la Torre A G, Cuberos A J M, Álvarez-Pinazo G, Cuesta A and Aranda M A G, **(2011b)**. "In-Situ Clinkering Study of Belite Sulfoaluminate Clinkers by Synchrotron X-Ray Powder Diffraction". *Proceedings of the 13th International Congress on the Chemistry of Cement, Madrid, Spain*.
- Deng M and Tang M, **(1994)**. "Formation and expansion of ettringite crystals". *Cem Concr Res*, 24, 119-126.
- Dilnesa B Z, Lothenbach B, Renaudin G, Wichser A and Kulik D, **(2014)**. "Synthesis and characterization of hydrogarnet $\text{Ca}_3(\text{Al}_x\text{Fe}_{1-x})_2(\text{SiO}_4)_y(\text{OH})_{4(3-y)}$ ". *Cem Concr Res*, 59, 96–111.
- Dilnesa B Z, Lothenbach B, Renaudin G, Wichser A and Wieland E, **(2012)**. "Stability of monosulfate in the presence of iron". *J Am Ceram Soc*, 95, 3305–3316.
- Drabik M, Smrcok L, Stevula L and Kapralik I, **(1987)**. "Study of brownmillerite prepared at 1200°C". *Silikaty*, 31, 299-307.
- Dyson H M, Richardson I G and Brough A R, **(2007)**. "A combined 29Si MAS NMR and selective dissolution technique for the quantitative evaluation of hydrated blast furnace slag cement blends". *J Am Ceram Soc*, 90, 598-602.

E

- Ectors D, Neubauer J and Goetz-Neunhoeffler F, **(2013)**. "The hydration of synthetic brownmillerite in presence of low Ca-sulfate content and calcite monitored by quantitative in-situ-XRD and heat flow calorimetry". *Cem Concr Res*, 54, 61-68.

F

- Fauth F, Peral I, Popescu C and Knapp M, **(2013)**. “The new Material Science Powder Diffraction beamline at ALBA Synchrotron”. *Powder Diffr*, 28, S360-S370.
- Fierens P and Tirlocq J, **(1983)**. “Nature and concentration effect of stabilizing elements of Beta-dicalcium silicate on its hydration rate”. *Cem Concr Res*, 13, 267-276.
- Florian P, Veron E, Green T F G, Yates J R and Massiot D, **(2012)**. “Elucidation of the Al/Si Ordering in Gehlenite $\text{Ca}_2\text{Al}_2\text{SiO}_7$ by Combined ^{29}Si and ^{27}Al NMR Spectroscopy/Quantum Chemical Calculations”. *Chem Mater*, 24, 4068–4079.
- François M, Renaudin G and Evrad O, **(1998)**. “A cementitious compound with composition $3\text{CaO}\cdot\text{Al}_2\text{O}_3\cdot\text{CaCO}_3\cdot 11\text{H}_2\text{O}$ ”. *Acta Cryst*, C54, 1214-1217.
- Fukuda K and Ito S, **(1999)**. “Improvement in reactivity and grindability of belite-Rich cement by remelting reaction”. *J Am Cer Soc*, 82, 2177-2180.
- Fukuda K, Wakamatsu N and Ito S, **(2001)**. “Improvement in hydration reactivity of α -phase belite by remelting reaction”. *J Am Ceram Soc*, 84, 639-641.
- Fukuhara M, Goto S, Asage K, Daimon M and Kondo R, **(1981)**. “Mechanisms and kinetics of C_4AF hydration with gypsum”. *Cem Concr Res*, 11, 407–414.

G

- García-Lodeiro I, Fernández-Jiménez A, Sobrados I, Sanz J and Palomo A, **(2012)**. “CSH-Gels: Interpretation of ^{29}Si MAS-NMR Spectra”. *J Am Ceram Soc*, 95, 1440-1446.
- García-Maté M, Santacruz I, De la Torre A G, León-Reina L and Aranda M A G, **(2012)**. “Rheological and hydration characterization of calcium sulfoaluminate cement pastes”. *Cem Concr Comp*, 34, 684–691.
- García-Maté M, De la Torre A G, León-Reina L, Aranda M A G and Santacruz I, **(2013)**. “Hydration studies of calcium sulfoaluminate cements blended with fly ash”. *Cem Concr Res*, 54, 12–20.
- García-Maté M, **(2015)**. “Processing and characterisation of calcium sulphoaluminate (CSA) eco-cements with tailored performances”. Ph.D. Thesis, University of Malaga, Spain.
- García-Maté M, De la Torre A G, León-Reina L, Losilla E R, Aranda M A G and Santacruz I, **(2015a)**. “Effect of calcium sulfate source on the hydration of calcium sulfoaluminate eco-cement”. *Cem Concr Comp*, 55, 53–61.

- García-Maté M, Santacruz I, Cuesta A, León-Reina L, Aranda M A G, Baco I, Morin V, Walenta G, Gartner E and De la Torre A G, **(2015b)**. "Amorphous determination in calcium sulfoaluminate materials by external and internal methods". *Adv Cem Res*, (On-line). DOI: 10.1680/adcr.14.00026.
- Gartner E, **(2004)**. "Industrially interesting approaches to "low-CO₂" cements". *Cem Concr Res*, 34, 1489-1498.
- Gartner E and Li G, **(2006)**. "High-belite sulfoaluminate clinker: fabrication process and binder preparation", World Patent Application WO2006/018569 A2.
- Gartner E and Macphee D E, **(2011)**. "A physico-chemical basis for novel cementitious binders". *Cem Concr Res*, 41, 736-749.
- Gartner E M, Young J F, Damidot D A and Jawed I, **(2002)**. "Hydration of Portland Cement". In *Structure and Performance of Cements*, Edited by Bensted J, and Barnes P, Published by Spon Spress, 57-113.
- Georgin J F, Ambroise J, Péra J and Reynouard J M, **(2008)**. "Development of selfleveling screed based on calcium sulfoaluminate cement: Modelling of curling due to drying". *Cem Concr Comp*, 30, 769-778.
- Gies A and Knofel D, **(1987)**. "Influence of sulfur on the composition of belite-rich cement clinkers and the technological properties of the resulting cements". *Cem Concr Res*, 17, 317-328.
- Glasser F P and Zhang L, **(2001)**. "High-performance cement matrices based on calcium sulphoaluminate-belite compositions". *Cem Concr Res*, 31, 1881-1886.
- Ghosh S N, Rao P B, Paul A K and Raina K J, **(1979)**. "The chemistry of the dicalcium silicate mineral". *J Mater Sci*, 14, 1554-1566.
- Gobbo L, Sant' Agostino L and Garcez L, **(2004)**. "C₃A polymorphs related to industrial clinker alkalies content". *Cem Concr Res*, 34, 657-664.
- Goetz-Neunhoeffler F and Neubauer J, **(2006)**. "Refined ettringite (Ca₆Al₂(SO₄)₃(OH)₁₂·26H₂O) structure for quantitative X-ray diffraction analysis". *Powder Diffr*, 21, 4-11.
- Gualtieri A F, Riva V, Bresciani A, Maretta S, Tamburini M and Viani A, **(2014)**. "Accuracy in quantitative phase analysis of mixtures with large amorphous contents. The case of stoneware ceramics and bricks". *J Appl Cryst*, 47, 835-846.

H

- Halstead P and Moore A E J, **(1962)**. "The composition and crystallography of an anhydrous calcium aluminosulphate occurring in expanding cement". Appl Chem, 12, 413-417.
- Hargis C W, Moon J, Lothenbach B, Winnefeld F, Wenk H R and Monteiro J M, **(2014a)**. "Calcium Sulfoaluminate Sodalite ($\text{Ca}_4\text{Al}_6\text{O}_{12}\text{SO}_4$), Crystal Structure Evaluation and Bulk Modulus Determination". J Am Ceram Soc, 97, 892–898.
- Hargis C W, Telesca A and Monteiro P J M, **(2014b)**. "Calcium sulfoaluminate (Ye'elimite) hydration in the presence of gypsum, calcite, and vaterite". Cem Concr Res, 65, 15–20.
- Hasanbeigi A, Menke C and Price L, **(2010)**. "The CO₂ abatement cost curve for the Thailand cement industry". J Clean Prod, 18, 1509-1518.
- Herrick J, Scrivener K L and Pratt P L, **(1992)**. "The development of microstructure in calcium sulfoaluminate expansive cement". Mat Res Soc Symp Proceedings, Pittsburgh, USA, 277-282.
- Hesse C, Goetz-Neunhoeffler F and Neubauer J, **(2011)**. "A new approach in quantitative in-situ XRD of cement pastes: Correlation of heat flow curves with early hydration reactions". Cem Concr Res, 41, 123-128.

I

- IDB (Inter-American Development Bank), **(2010)**. Cement Manufacturing Plant Guidelines, An Approach to Reconciling the Financing of Cement Manufacturing Plants with Climate Change Objectives. idbdocs.iadb.org/wsdocs/getdocument.aspx?docnum=35601768 (accessed 02.04.12.).
- Idrissi M, Diouri A, Damidot D, Greneche J M, Alami T M and Taibi M, **(2010)**. "Characterisation of iron inclusion during the formation of calcium sulfoaluminate phase". Cem Concr Res, 40, 1314–1319.
- Idrissi M, Diouri A, Talbi M A, Sassi O, Taibi M and Damidot D, **(2012)**. "Hydration behavior of iron doped calcium sulfoaluminate phase at room temperature". MATEC Web of Conferences INVACO2, p. 01005.
- IEA (International Energy Agency) statistics, **(2010)**. CO₂ Emissions from Fuel Combustion Highlights. www.iea.org/co2highlights (accessed 12.11.10.).
- Il'inets A M and Bikbau M Y, **(1990)**. "Structural mechanism of polymorphic transformations of dicalcium silicate, Ca_2SiO_4 . Part II. Refinement of crystal structure of high temperature α'_1 modification of dicalcium silicate Ca_2SiO_4 ". Sov Phys Crystallogr, 35, 54-56.

J

- Janotka I and Krajci L, **(1999)**. "An experimental study on the upgrade of sulfoaluminate-belite cement systems by blending with Portland cement". *Adv Cem Res*, 11, 35-41.
- Janotka I, Krajci U and Mojumdar S C, **(2007)**. "Performance of sulphoaluminate-belite cement with high C_4A_3S content". *Cer Silik*, 51, 74-81.
- Jansen D, Bergold S T, Goetz-Neunhoeffler F and Neubauer J, **(2011b)**. "The hydration of alite: a time-resolved quantitative X-ray diffraction approach using the G-factor method compared with heat release". *J Appl Crystallogr*, 44, 895-901.
- Jansen D, Goetz-Neunhoeffler F, Lothenbach B and Neubauer J, **(2012a)**. "The early hydration of Ordinary Portland Cement (OPC): An approach comparing measured heat flow with calculated heat flow from QXRD". *Cem Concr Res*, 42, 134-138.
- Jansen D, Neubauer J, Goetz-Neunhoeffler F, Haerzschel R and Hergeth W D, **(2012b)**. "Change in reaction kinetics of a Portland cement caused by a superplasticizer – Calculation of heat flow curves from XRD data". *Cem Concr Res*, 42, 327-332.
- Jansen D, Stabler CH, Goetz-Neunhoeffler F, Dittrich S and Neubauer J, **(2011a)**. "Does ordinary Portland cement contain amorphous phase? A quantitative study using an external standard method". *Powder Diffr*, 26, 31-38.
- Jelenic I, Bezjak A and Bujan M, **(1978)**. "Hydration of B_2O_3 -stabilized α - and β -modifications of dicalcium silicate". *Cem Concr Res*, 8, 173-180.
- Jones D A, **(1996)**. "Principles and Prevention of Corrosion". 2nd. ed. Prentice Hall, Upper Saddle River, NJ.
- Jost K H, Ziemer B and Seydel R, **(1977)**. "Retermination of the structure of β -dicalcium silicate". *Acta Cryst*, B33, 1696-1700.
- Juenger M C G and Chen I, **(2011)**. "Composition–property relationships in calcium sulfoaluminate cements". *Proceedings of the 13th International Congress on the Chemistry of Cement*, Madrid, Spain, 2011.
- Juenger M C G, Winnefeld F, Provis J L and Ideker J H, **(2011)**. "Advances in alternative cementitious binders". *Cem Concr Res*, 41, 1232-1243.
- Jupe A C, Turrillas X, Barnes P, Colston S L, Hall C, Hausermann D and Handfland M, **(1996)**. "Fast in situ x-ray-diffraction studies of chemical reactions: A synchrotron view of the hydration of tricalcium aluminate". *Phys Rev*, B 53, 14697-14700.

K

- Kacimi L, Simon-Masseron A, Salem S, Ghomari A and Derriche Z, **(2009)**. "Synthesis of belite cement clinker of high hydraulic reactivity". *Cem Concr Res*, 39, 559–565.
- Kalogridis D, Kostogloudis G C, Ftikos C and Malami C, **(2000)**. "A quantitative study of the influence of non-expansive sulfoaluminate cement on the corrosion of steel reinforcement". *Cem Concr Res*, 30, 1731-1740.
- Kantro D L and Weise C H, **(1979)**. "Hydration of various beta-dicalcium silicate preparations". *J Am Cer Soc*, 62, 621-626.
- Kasselouri V, Tsakiridis P, Malami C, Georgali B and Alexandriou C A, **(1995)**. "Study on the hydration products of a non-expansive sulfoaluminate cement". *Cem Concr Res*, 25, 1725-1736.
- Katsioti M, Tsakiridis P E, Leonardou-Agatzini S and Oustadakis P, **(2006)**. "Examination of the jarosite–alunite precipitate addition in the raw meal for the production of sulfoaluminate cement clinker". *J Haz Mat*, B131, 187-194.
- Kirfel A and Will G, **(1980)**. "Charge density in anhydrite, CaSO_4 , from X-ray and neutron diffraction". *Acta Crystallogr B36*, 2881–2890.
- Klein A, **(1963)**. "Calcium aluminosulfate and expansive cements containing same", US Patent 3155526.
- Knapp M, Peral I, Nikitina L, Quispe M and Ferrer S, **(2011)**. "Technical concept of the materials science beamline at ALBA". *Z Kristallogr*, 1, 137–142.
- Kurokawa D, Takeda S, Colas M, Asaka T, Thomas P and Fukuda K, **(2014)**. "Phase transformation of $\text{Ca}_4[\text{Al}_6\text{O}_{12}]\text{SO}_4$ and its disordered crystal structure at 1073K". *J Solid State Chem*, 215, 265-270.
- Kwan S, LaRosa J and Grutzeck MW, **(1995)**. " ^{29}Si and ^{27}Al MAS NMR study of stratlingite". *J Am Ceram Soc*, 78, 1921-1926.

L

- Larson A C and Von Dreele R B, **(2000)**. "General structure analysis system (GSAS)". Los Alamos national laboratory report LAUR, 86-748.
- Leoni M, Scardi P, Pelosato R, Sora I N, Dotelli G, Stampino P G and Presti A L, **(2007)**. "Phase composition gradient in leached polluted cement monoliths". *Cem Concr Res*, 37, 1483-1495.
- Leon-Reina L, De la Torre A G, Porrás-Vázquez J M, Cruz M, Ordoñez L M, Alcobe X, Gispert-Guirado F, Larranaga-Varga A, Paul M, Fuellmann T, Schmidt R and

- Aranda M A G, (2009). "Round robin on Rietveld quantitative phase analysis of Portland cements". *J Appl Crystallogr*, 42, 906-916.
- Le Saout G, Lécolier E, Rivereau A and Zanni H, (2006). "Chemical structure of cement aged at normal and elevated temperatures and pressures: part I. Class G oilwell cement". *Cem Concr Res*, 36, 71–78.
- Li G S, Walenta G and Gartner E M, (2007a). "Formation and hydration of low-CO₂ cements based on belite, calcium sulfoaluminate and calcium aluminoferrite". Proceedings of the 12th International Congress of the Cements Chemistry, Montreal, Canada, p. TH3-15.3.
- Li J H, Ma H W and Zhao H W, (2007b). "Preparation of Sulphoaluminate-alite Composite Mineralogical Phase Cement Clinker from High Alumina Fly Ash". *Key Eng Mat*, Vols 334-335, 421-424.
- Lili R, Xiaocun L, Tao Q, Lian L, Deli Z and Yanjun L, (2009). "Influence of MnO₂ on the Burnability and Mineral Formation of Alite-sulphoaluminate Cement Clinker". *Sil Ind*, 74, 183-187.
- Liu X C, Li B L, Qi T, Liu X L and Li Y J, (2009). "Effect of TiO₂ on mineral formation and properties of alite-sulphoaluminate cement". *Mat Res Innov*, 13 92-97.
- Liu X and Li Y, (2005). "Effect of MgO on the composition and properties of alite sulphoaluminate cement". *Cem Concr Res*, 35, 1685-1687.
- Liu X, Li Y and Zhang N, (2002). "Influence of MgO on the formation of Ca₃SiO₅ and 3CaO·3Al₂O₃·CaSO₄ minerals in alite-sulphoaluminate cement". *Cem Concr Res*, 32, 1125-1129.
- Liu X, Liu T, Wu Y, Wang W and Li Y, (2013). "Effect of alkalis on the mineral formation and properties of alite-sulfoaluminate cement". *Adv Cem Res*, 25, 98–103.
- Locher F W, (1986). "Low energy clinker". Proceedings of 8th International Congress on the Chemistry of Cement, Rio de Janeiro, subtheme 1.3, I, 57.
- Lothenbach B, Matschei T, Möschner G and Glasser F P, (2008). "Thermodynamic modelling of the effect of temperature on the hydration and porosity of Portland cement". *Cem Concr Res*, 38, 1-18.

M

- Ma B, Li X, Shen X, Mao Y and Huang H, (2014a). "Enhancing the addition of fly ash from thermal power plants in activated high belite sulfoaluminate cement". *Constr Build Mater*, 52, 261–266.

- Ma B, Ma M, Shen X, Li X and Wu X, **(2014b)**. "Compatibility between a polycarboxylate superplasticizer and the belite-rich sulfoaluminate cement: Setting time and the hydration properties". *Constr Build Mater*, 51, 47–54.
- Ma S, Shen X, Gong X and Zhong B, **(2006)**. "Influence of CuO on the formation and coexistence of $3\text{CaO}\cdot\text{SiO}_2$ and $3\text{CaO}\cdot 3\text{Al}_2\text{O}_3\cdot\text{CaSO}_4$ minerals". *Cem Concr Res*, 36, 1784-1787.
- Ma S, Snellings R, Li X, Shen X and Scrivener K L, **(2013)**. "Alite-ye'elimitite cement: Synthesis and mineralogical analysis". *Cem Concr Res*, 45, 15–20.
- Madsen I C, Scarlett N V Y and Kern A, **(2011)**. "Description and survey of methodologies for the determination of amorphous content via X-ray powder diffraction". *Z Kristallogr*, 226, 944-955.
- Mahlia T M I, **(2002)**. "Emissions from electricity generation in Malaysia". *Renew Energ*, 27, 293-300.
- Marchi M and Costa U, **(2011)**. "Influence of the Calcium Sulphate and w/c ratio on the hydration of calcium sulfoaluminate cement". *Proceedings of 13th International Congress on the Chemistry of Cement, Madrid, Spain*.
- Marinoni N, Pavese A, Voltolini M and Merlini M, **(2008)**. "Long-term leaching test in concretes: an X-ray powder diffraction study". *Cem Concr Comp*, 30, 700-705.
- Martín-Sedeño M C, Cuberos A J M, De la Torre A G, Álvarez-Pinazo G, Ordóñez L M, Gateshki M and Aranda M A G, **(2010)**. "Aluminum-rich belite sulfoaluminate cements: clinkering and early age hydration". *Cem Concr Res*, 40, 359-369.
- Matkovic B, Carin V, Gacesa T, Halle R, Jelenic I and Young J F, **(1981)**. "Influence of BaSO_4 on the Formation and Hydration Properties of Calcium Silicates: I, Doped Dicalcium Silicates". *Am Ceram Soc Bull*, 60, 825-829.
- McCaffrey R, **(2002)**. "Climate change and the cement industry". *Global Cement and Lime Magazine Environmental Special Issue*, 15-19.
- Mechling J M, Lecomte R A and Le Rolland B, **(2013)**. "Sulphoaluminate cement behaviours in carbon dioxide, warm and moist environments". *Adv Cem Res*, 26, 52-61.
- Mehta P K, **(1973)**. "Mechanism of expansion associated with ettringite formation". *Cem Concr Res*, 3, 1-6.
- Mehta P K, **(1980)**. "Investigation on Energy-Saving Cements". *World Cement Technology*. 11, 167-177.
- Mehta P K and Hu F, **(1975)**. "Further evidence for expansion of ettringite by water absorption". *J Am Ceram Soc*, 61, 179-181.

- Mehta P K and Wang S, **(1982)**. "Expansion of ettringite by water adsorption". *Cem Concr Res*, 12, 121-122.
- Meller N, Hall C and Crawshaw J, **(2004a)**. "ESEM evidence for through-solution transport during brownmillerite hydration". *J Mat Sci*, 39, 6611-6614.
- Meller N, Hall C, Jupe A C, Colston S L, Jacques S D M, Barnes P and Phipps J, **(2004b)**. "The paste hydration of brownmillerite with and without gypsum: a time resolved synchrotron diffraction study at 30, 70, 100 and 150°C". *J Mater Chem*, 14, 428-435.
- Meredith P, Donald A M, Meller N and Hall C, **(2004)**. "Tricalcium aluminate hydration: Microstructural observations by in-situ electron microscopy". *J Mater Sci*, 39, 997-1005.
- Midgley C M, **(1952)**. "The crystal structure of β -dicalcium silicate". *Acta Cryst*, 5, 307-312.
- Mindess S, Young J F and Darwin D, **(2003)**. *Concrete*, 2nd. ed., Pearson Education, Inc., Upper Saddle River, NJ.
- Moore P B, **(1973)**. "Bracelets and Pinwheels: A topological-Geometrical approach to the calcium orthosilicate and alkali sulfate structures". *Am Mineral*, 58, 32-42.
- Morin V, Walenta G, Gartner E, Termkhajornkit P, Baco I and Casabonne J M, **(2011)**. "Hydration of a Belite-Calcium Sulfoaluminate- Ferrite cement: AetherTM". Proceedings of the 13th International Congress on the Chemistry of Cement, Madrid, Spain.
- Morsli K, De la Torre A G, Stöber S, Cuberos A J M, Zahir M and Aranda M A G, **(2007a)**. "Quantitative Phase Analysis of Laboratory Active Belite Clinkers by Synchrotron Powder Diffraction". *J Amer Cer Soc*, 90, 3205-3212.
- Morsli K, De la Torre A G, Zahir M and Aranda M A G, **(2007b)**. "Mineralogical Phase Analysis of Alkali and Sulfate Bearing Belite Rich Laboratory Clinkers". *Cem Concr Res*, 37, 639-646.
- Möschner G, Lothenbach B, Winnefeld F, Ulrich A, Figi R and Kretschmar R, **(2009)**. "Solid solution between Al-ettringite and Fe-ettringite ($\text{Ca}_6[\text{Al}_{1-x}\text{Fe}_x(\text{OH})_6]_2(\text{SO}_4)_3 \cdot 26\text{H}_2\text{O}$)". *Cem Concr Res*, 39, 482-489.
- Mumme W G, Hill R J, Bushnell-Wye G and Segnit E R, **(1995)**. "Rietveld crystal structure refinement, chemistry and calculated powder diffraction data for the polymorphs of dicalcium silicate and related phases". *N Jb Miner Abh*, 169, 35-68.

Mumme W, Cranswick L and Chakoumakos B, **(1996)**. "Rietveld crystal structure refinements from high temperature neutron powder diffraction data for the polymorphs of dicalcium silicate". *N Jb Miner Abh*, 170, 171-188.

N

Nettleship I, Slavick K G, Kim Y J and Kriven W M, **(1992)**. "Phase transformation in dicalcium silicate: I, Fabrication and phase stability of fine-grained β -phase". *J Am Cer Soc*, 75, 2400-2406.

Neuville N, Lécolier E, Aouad G, Rivereau A and Damidot D, **(2009)**. "Effect of curing conditions on oilwell cement paste behaviour during leaching: experimental and modeling approaches". *C R Chim*, 12, 511–520.

O

O'Connor B H and Raven M D, **(1988)**. "Application of the Rietveld refinement procedure in assaying powdered mixtures". *Powder Diffr*, 3, 2-6.

O'Daniel H and Tscheischwili L, **(1942)**. "Zur struktur von γ -Ca₂SiO₄ und Na₂BeF₄". *Z Kristallogr*, 104, 124-141.

Odler, I, **(1998)**. In *Lea's chemistry of cement & concrete*, ed. P C Hewlett, Butterworth-Heinemann, Oxford, pp. 195–240.

Odler I, **(2000)**. "Special inorganic cements" in Taylor and Francis Publisher, cap 4, 69-74.

Odler I, **(2003)**. "Hydration, setting and hardening of Portland cement", In *Lea's Chemistry of Cement and Concrete*, 4th ed., Hewlett P C, Elsevier: Oxford, U.K., and Burlington, MA, pp 241–297.

Odler I and Colan-Subauste J, **(1999)**. "Investigations on cement expansion associated with ettringite formation". *Cem Concr Res*, 29, 731-735.

Odler I and Zhang H, **(1996)**. "Investigations on high SO₃ Portland clinkers and cements I. Clinker synthesis and cement preparation". *Cem Concr Res*, 26, 1307-1313.

Ogawa K and Roy D M, **(1982)**. "C₄A₃S̄ Hydration, Ettringite Formation, and its Expansion Mechanisms: III. Effect of CaO, NaOH, and NaCl; Conclusions". *Cem Concr Res*, 12, 247-256.

P

- Paglia C, Wombacher F and Bohni H, **(2001)**. "The influence of alkali-free and alkaline shotcrete accelerators within cement systems I. Characterization of the setting behavior". *Cem Concr Res*, 31, 913-918.
- Palou M T and Majling J, **(1996)**. "Hydration in the System $C_4A_3S-C_2SH_2-CH-H$ ". *J Therm Anal*, 46, 557-563.
- Palou M T and Majling J, **(1997)**. "Hydration of the model sulfoaluminate-belite cements composed of blends of minerals with classified particle sizes". *Ceram Silikaty*, 41, 125-133.
- Palou M, Majling J, Dovál M, Kozanková J and Mojumdar S C, **(2005)**. "Formation and stability of crystallohydrates in the non-equilibrium system during hydration of SAB cements". *Cer Silik*, 49, 230-236.
- Park C K, **(2001)**. "Phase transformation and hydration of dicalcium silicate containing stabilizers". *J Cer Soc Jap*, 109, 380-386.
- Passaglia E and Rinaldi R, **(1984)**. "Katoite, a new member of the $Ca_3Al_2(SiO_4)_3-Ca_3Al_2(OH)_{12}$ series and a new nomenclature for the hydrogrossular group of minerals". *Bull Mineral*, 107, 605-618.
- Paul G, Boccaleri E, Buzzi L, Canonico F and Gastaldi F, **(2015)**. "Friedel's salt formation in sulfoaluminate cements: A combined XRD and ^{27}Al MAS NMR study". *Cem Concr Res*, 67, 93-102.
- Pelletier-Chaignat L, Winnefeld F and Lothenbach B, **(2010)**. "The ternary system Portland cement-calcium sulfoaluminate clinker-anhydrite: hydration mechanism and mortar properties". *Cem Concr Compos*, 32, 497-507.
- Pelletier-Chaignat L, Winnefeld F, Lothenbach B, Saout G L, Müller C J and Famy C, **(2011)**. "Influence of the calcium sulphate source on the hydration mechanism of Portland cement-calcium sulfoaluminate clinker-calcium sulphate binders". *Cem Concr Compos*, 33, 551-561.
- Pelletier-Chaignat L, Winnefeld F, Lothenbach B and Müller C J, **(2012)**. "Beneficial use of limestone filler with calcium sulfoaluminate cement". *Cons Build Mat*, 26, 619-627.
- Pera J and Ambroise J, **(2004)**. "New applications of calcium sulfoaluminate cement". *Cem Concr Res*, 34, 671-676.
- Pérez-Bravo R, Álvarez-Pinazo G, Compañá J M, Santacruz I, Losilla E R, Bruque S and De la Torre A G, **(2014)**. "Alite sulfoaluminate clinker: Rietveld mineralogical and SEM-EDX analysis". *Adv Cem Res*, 26, 10-20.
- Phair J W, **(2006)**. "Green chemistry for sustainable cement production and use". *Green Chem*, 8, 763-780.

Popescu C D, Muntean M and Sharp J H, **(2003)**. "Industrial Trial Production of Low Energy Belite Cement". *Cem Concr Comp*, 25, 689-693.

Poulsen S L, Kocaba V, Le Saout G, Jakobsen H J, Scrivener K L and Skibsted J, **(2009)**. "Improved quantification of alite and belite in anhydrous Portland cements by ^{29}Si MAS NMR: effects of paramagnetic ions". *Solid State NMR*, 36, 32-44.

Pritts M and Daugherty K E, **(1976)**. "The effect on stabilizing agents on the hydration rate of $\beta\text{-C}_2\text{S}$ ". *Cem Concr Res*, 6, 783-796.

Puertas F, Garcia-Diaz I, Palacios M, Gazulla M F, Gomez M P and Orduna M, **(2010)**. "Clinkers and cements obtained from raw mix containing ceramic waste as a raw material. Characterization, hydration and leaching studies". *Cem Concr Comp*, 32, 175-186.

Q

Quillin K, **(2001)**. "Performance of belite-sulfoaluminate cements". *Cem Concr Res*, 31, 1341-1349.

R

Rawal A, Smith B J, Athens G L, Edwards C L, Roberts L, Gupta V and Chmelka B F, **(2010)**. "Molecular Silicate and Aluminate Species in Anhydrous and Hydrated Cements". *J Am Chem Soc*, 132, 7321-7337.

Regourd M and Guinier A, **(1974)**. "The Crystal Chemistry of the Constituents of Portland Cement Clinker". VI Inter Symp on the Chem of Cements, Moscow, Russia.

Renaudin G, Kubel F, Rivera J P and Francois M, **(1999)**. "Structural phase transition and high temperature phase structure of Friedels salt, $3(\text{CaO})(\text{Al}_2\text{O}_3)(\text{CaCl}_2)\cdot 10(\text{H}_2\text{O})$ ". *Cem Concr Res*, 29, 1937-1942.

Rietveld H M, **(1967)**. "Line profiles of neutron powder-diffraction peaks for structure refinement". *Acta Crystallogr*, 22, 151-152.

Rietveld H M, **(1969)**. "A profile refinement method for nuclear and magnetic structures". *J Appl Crystallogr*, 2, 65-71.

Rinaldi R, Sacerdoti M and Passaglia E, **(1990)**. "Stratlingite: crystal structure, chemistry, and a reexamination of its polytype vertumnite". *Eur J Mineral*, 2, 841-849.

Rogers D E and Aldridge L P, **(1977)**. "Hydrates of calcium ferrites and calcium aluminoferrites". *Cem Concr Res*, 7, 399-410.

Roussel N (Ed.) (2012). "Understanding the rheology of concrete". Woodhead Publishing Limited.

S

Saalfeld H and Depmeier W, (1972). "Silicon-free compounds with sodalite structure". *Kristall Technik*, 7, 229-233.

Sahu S, Havlica J, Tomková V and Majling J, (1991). "Hydration behaviour of sulphoaluminate belite cement in the presence of various calcium sulphates". *Therm Act*, 175, 45–52.

Sahu S and Majling J, (1993). "Phase compatibility in the system $\text{CaO-SiO}_2\text{-Al}_2\text{O}_3\text{-Fe}_2\text{O}_3\text{-SO}_3$ referred to sulphoaluminate belite cement clinker". *Cem Concr Res*, 23, 1331-1339.

Santacruz I, De la Torre A G, Álvarez-Pinazo G, Cabeza A, Cuesta A, Sanz J and Aranda M A G, (2015). "Structure of stratlingite and effect of hydration methodology on microstructure". *Adv Cem Res*, in press.

Scarlett N V Y and Madsen I C, (2006). "Quantification of phases with partial or no known crystal structures". *Powder Diffr*, 21, 278-284.

Schreyer M, Guo L, Tjahjono M and Garland M, (2011). "Three approaches to total quantitative phase analysis of organic mixtures using an external standard". *J Appl Crystallogr*, 44, 17-24.

Scrivener K L, Fullmann T, Gallucci E, Walenta G and Bermejo E, (2004). "Quantitative study of Portland cement hydration by X-ray diffraction/Rietveld analysis and independent methods". *Cem Concr Res*, 34, 1541-1547.

Seluck N, Soner I and Seluck E, (2010). "Synthesis of special cement with fluidised bed combustion ashes". *Adv Cem Res*, 22, 107-113.

Seufert S, Hesse C, Goetz-Neunhoeffler F and Neubauer J, (2009). "Discrimination of bassanite and anhydrite III dehydrated from gypsum at different temperatures". *Z Kristallogr Suppl*, 30, 447–452.

Sharp J H, Lawrence C D and Yang R, (1999). "Calcium sulphoaluminate cements—Low-energy cements, special cements or what?". *Adv Cem Res*, 11, 3-13.

Shen Y, Qian J, Chai J and Fan Y, (2014). "Calcium sulphoaluminate cements made with phosphogypsum: Production issues and material properties". *Cem Concr Comp* 48, 67–74.

Skibsted J and Hall C, (2008). "Characterization of cement minerals, cements and their reaction products at the atomic and nano scale". *Cem Concr Res*, 38, 205-255.

- Skibsted J, Hall C and Jakobsen H J, **(2002)**. “Nuclear magnetic resonance spectroscopy and magnetic resonance imaging of cements and cement based materials”. *In: Structure and Performance of Cements*. 2nd Edition, Bensted J, Barnes P (ed), Spon Press, London, p 457-476.
- Smith D K, Johnson G G, Scheible A, Wims A M, Johnson J L and Ullmann G, **(1987)**. “Quantitative X-ray powder diffraction method using the full diffraction pattern”. *Powder Diffr*, 2, 73-77.
- Snellings R, Bazzoni A and Scrivener K, **(2014)**. “The existence of amorphous phase in Portland cements: Physical factors affecting Rietveld quantitative phase analysis”. *Cem Concr Res*, 59, 139-146.
- Solberg C and Hansen S, **(2001)**. “Dissolution of $\text{CaSO}_4 \cdot 1/2\text{H}_2\text{O}$ and precipitation of $\text{CaSO}_4 \cdot 2\text{H}_2\text{O}$: a kinetic study by synchrotron X-ray powder diffraction”. *Cem Concr Res*, 31, 641–646.
- Sokol E V, Kokh S N, Vapnik Y, Thiéry V and Korzhova S A, **(2014)**. “Natural analogous of belite sulfoaluminate cement clinkers from Negev Desert, Israel”. *Am Mineral*, 99, 1471-1487.
- Song J T and Young J F, **(2002)**. “Direct synthesis and hydration of calcium aluminosulfate ($\text{Ca}_4\text{Al}_6\text{O}_{16}\text{S}$)”. *J Am Ceram Soc*, 85, 535–539.
- Song F, Yu Z, Yang F, Lu Y and Liu Y, **(2015)**. “Microstructure of amorphous aluminum hydroxide in belite-calcium sulfoaluminate cement”. *Cem Concr Res*, 71, 1–6.
- Stark J, **(2011)**. “Recent advances in the field of cement hydration and microstructure analysis”. *Cem Concr Res*, 41, 666-678.
- Stark J, Müller A, Schrader R and Rümpler K, **(1981)**. “Existence conditions of hydraulically active belite cement”. *Zem-Kalk-Gips*, 34, 476.
- Strigac J, Palou M T, Kristin J and Majling J, **(2000)**. “Morphology and Chemical Composition of Minerals inside the Phase Assemblage $\text{C-C}_2\text{S-C}_4\text{A}_3\text{S-C}_4\text{AF-CS}$ Relevant to Sulphoaluminate Belite Cements”. *Ceramics-Silikaty*, 44, 26-34.
- Stutzman P, **(2011)**. “Direct Determination of Phases in Portland Cements by Quantitative X-Ray Powder Diffraction”. NIST Technical Note 1692, 59 pages.
- Stutzman P and Leigh S, **(2002)**. “Phase Composition Analysis of the NIST Reference Clinkers by Optical Microscopy and X-ray Powder Diffraction”. NIST Technical Note 1441, 44 pages.
- Suherman P M, Van Riessen A, O’ Connor B, Li D, Bolton D and Fairhurst H, **(2002)**. “Determination of amorphous phase levels in Portland cement clinker”. *Powder Diffr*, 17, 178-185.

Sun Q, Li J and Wang J, **(2011)**. "Effect of borate concentration on solidification of radioactive wastes by different cements". Nucl Engin Design, 241, 4341-4345.

T

Taylor H F W, **(1997)**. "Cement Chemistry", 2nd ed. Thomas Telford, UK.

Taylor J C and Zhu R, **(1992)**. "Simultaneous use of observed and calculated standard profiles in quantitative XRD analysis of minerals by the multiphase Rietveld method: the determination of pseudorutile in mineral and products". Powder Diffr, 7, 152-161.

Telesca A, Marroccoli M, Pace M L, Tomasulo M, Valenti G L and Monteiro P J M, **(2014)**. "A hydration study of various calcium sulfoaluminate cements". Cem Concr Comp, 53, 224–232.

Toby B H, **(2001)**. "EXPGUI, a graphical user interface for GSAS". J Appl Crystallogr, 34, 210-213.

Touzo B, Scrivener K L and Glasser F P, **(2013)**. "Phase compositions and equilibria in the CaO–Al₂O₃–Fe₂O₃–SO₃ system, for assemblages containing ye'elimite and ferrite Ca₂(Al,Fe)O₅". Cem Concr Res, 54, 77-86.

U

Udagawa S, Urabe K, Takada K and Natsume M, **(1979)**. "Studies on the dusting of Ca₂SiO₄. The crystal structure of α'-Ca₂SiO₄". Cem Assoc Jpn Rev, Gen Meet, Tech Sess, 33, 35-38.

Udagawa S, Urabe K, Natsume M and Yano T, **(1980)**. "Refinement of the crystal structure of γ-Ca₂SiO₄". Cem Concr Res, 10, 139-144.

U.S. Geological Survey, Mineral Commodity Summaries. January **2014**.

V

Viani A and Gualtieri A F, **(2013)**. "Recycling the product of thermal transformation of cement-asbestos for the preparation of calcium sulfoaluminate clinker". J Haz Mat, 260, 813– 818.

W

Walenta G and Comparet C, **(2011)**. "New Cements and Innovative Binder Technologies BCSAF cements-recent developments", ECRA-Barcelona-2011. Presentation available at <http://www.aether-cement.eu/press->

room/publications/aethercement-ecra-barcelona-presentation-2011-05-05.html.

Walsh C, Thornley P, (2012). "Barriers to improving energy efficiency within the process industries with a focus on low grade heat utilization". *J Clean Prod*, 23, 138-146.

Wang Y G, Ye H Q, Kuo K H, Feng X J, Lao G L and Long S Z, (1990). "Electron diffraction and HREM studies of the new phase and superstructures in $\text{Ca}_4\text{Al}_6\text{SO}_{16}$ ". *J Mater Sci*, 25, 5147-5156.

Wang J, (2010). "Hydration mechanism of cements based on low- CO_2 clinkers containing belite, ye' elimite and calcium alumino-ferrite". Ph.D. Thesis, University of Lille, France.

Wesselsky A and Jensen O M, (2009). "Synthesis of pure Portland cement phases". *Cem Concr Res*, 39, 973-980.

Westphal T, Fullmann T and Pollmann H, (2009). "Rietveld quantification of amorphous portions with internal standard-Mathematical consequences of the experimental approach". *Powder Diffr*, 24, 239-243.

Winnefeld F and Barlag S, (2010). "Calorimetric and thermogravimetric study on the influence of calcium sulfate on the hydration of ye'elimite". *J Therm Anal Calorim*, 101, 949-957.

Winnefeld F and Lothenbach B, (2010). "Hydration of calcium sulfoaluminate cements—Experimental findings and thermodynamic modelling". *Cem Concr Res*, 40, 1239-1247.

Y

Yang L, Yan Y, Hu Z and Xie X, (2013). "Utilization of phosphate fertilizer industry waste for belite-ferroaluminate cement production". *Constr Build Mater*, 38, 8-13.

Z

Zhang J and Li Z, (2007). "Comparison of early age resistivity development between ordinary Portland and calcium sulfoaluminate cement". Hongkong University of Science and technology, Clear Water Bay, Kowloon, Hong Kong, China.

Zhang J and Scherer G W, (2011). "Comparison of methods for arresting hydration of cement". *Cem Concr Res*, 41, 1024-1036.

- Zhang H and Odler I, **(1996)**. "Investigations on high SO₃ Portland clinkers and cements II. Properties of cements". *Cem Concr Res*, 26, 1315-1324.
- Zhang L, Su M Z and Wang Y M, **(1999)**. "Development of the use of sulfo-and ferroaluminate cements in China". *Adv Cem Res*, 11, 15-21.
- Zhang P, Chen Y, Shi L, Zhang G and Huang W W J, **(1992)**. "The crystal structure of C₄A₃S̄". Proceedings of the 9th International Congress on the Chemistry of Cement, New Delhi, India.
- Zhang X F, Zhang S Y, Hu Z Y, Yu G, Pei C H and Sa R N, **(2012)**. "Identification of connection units with high GHG emissions for low-carbon product structure design". *J Clean Prod*, 27, 118-125.
- Zhou Q, Milestone N B and Hayes M, **(2006)**. "An alternative to Portland cement or waste encapsulation-the calcium sulfoaluminate cement system". *J Haz Mater*, 136, 120-129.
- Ziemer B, Altrichter B and Jesenak V, **(1984)**. "Effect of SO₃ on formation and hydraulic reactivity of belite". *Cem Concr Res*, 14, 686-692.

ANNEX A

LICENSES AGREEMENTS

COPYRIGHT.

In order to use some figures and full articles in this Thesis, it has been necessary to request permission from each magazine. Licenses are listed below:

Article A#1:

5/8/2015 Rightslink® by Copyright Clearance Center




Home Account Info Help Live Chat



Title: Rietveld quantitative phase analysis of Yeelimitite-containing cements
Publication: Cement and Concrete Research
Publisher: Elsevier
Date: July 2012
 Copyright © 2012 Elsevier Ltd. All rights reserved.

Logged in as: Gema Alvarez
 LOGOUT

Order Completed

Thank you very much for your order.

This is a License Agreement between Gema Alvarez ("You") and Elsevier ("Elsevier"). The license consists of your order details, the terms and conditions provided by Elsevier, and the [payment terms and conditions](#).

[Get the printable license.](#)

License Number	3624120192411
License date	May 08, 2015
Licensed content publisher	Elsevier
Licensed content publication	Cement and Concrete Research
Licensed content title	Rietveld quantitative phase analysis of Yeelimitite-containing cements
Licensed content author	None
Licensed content date	July 2012
Licensed content volume number	42
Licensed content issue number	7
Number of pages	12
Type of Use	reuse in a thesis/dissertation
Portion	full article
Format	both print and electronic
Are you the author of this Elsevier article?	Yes
Will you be translating?	No
Title of your thesis/dissertation	Active sulpho-belite cements. Hydration mechanisms and mechanical properties
Expected completion date	Jul 2015
Estimated size (number of pages)	250
Elsevier VAT number	GB 494 6272 12
Permissions price	0.00 EUR
VAT/Local Sales Tax	0.00 EUR / 0.00 GBP
Total	0.00 EUR

ORDER MORE...

CLOSE WINDOW

Copyright © 2015 Copyright Clearance Center, Inc. All Rights Reserved. [Privacy statement](#), [Terms and Conditions](#).

Comments? We would like to hear from you. E-mail us at customercare@copyright.com

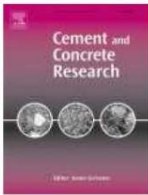
Article A#2:

5/8/2015 Rightslink® by Copyright Clearance Center



RightsLink®

[Home](#)
[Account Info](#)
[Help](#)

Title: In-situ early-age hydration study of sulfoelite cements by synchrotron powder diffraction

Publication: Cement and Concrete Research

Publisher: Elsevier

Date: February 2014

Copyright © 2013 Elsevier Ltd. All rights reserved.

Logged in as:
Gema Alvarez
Account #:
3000917257

LOGOUT

Order Completed

Thank you very much for your order.

This is a License Agreement between Gema Alvarez ("You") and Elsevier ("Elsevier"). The license consists of your order details, the terms and conditions provided by Elsevier, and the [payment terms and conditions](#).

[Get the printable license.](#)

License Number	3624120684355
License date	May 08, 2015
Licensed content publisher	Elsevier
Licensed content publication	Cement and Concrete Research
Licensed content title	In-situ early-age hydration study of sulfoelite cements by synchrotron powder diffraction
Licensed content author	None
Licensed content date	February 2014
Licensed content volume number	56
Licensed content issue number	n/a
Number of pages	8
Type of Use	reuse in a thesis/dissertation
Portion	full article
Format	both print and electronic
Are you the author of this Elsevier article?	Yes
Will you be translating?	No
Title of your thesis/dissertation	Active sulpho-belite cements. Hydration mechanisms and mechanical properties
Expected completion date	Jul 2015
Estimated size (number of pages)	250
Elsevier VAT number	GB 494 6272 12
Permissions price	0.00 EUR
VAT/Local Sales Tax	0.00 EUR / 0.00 GBP
Total	0.00 EUR

ORDER MORE...
CLOSE WINDOW

Copyright © 2015 [Copyright Clearance Center, Inc.](#) All Rights Reserved. [Privacy statement](#). [Terms and Conditions](#).
 Comments? We would like to hear from you. E-mail us at customercare@copyright.com

Article A#3:

5/8/2015 Rightslink® by Copyright Clearance Center

Copyright Clearance Center **RightsLink®** Home Create Account Help Live Chat

ACS Publications **Title:** Hydration Reactions and Mechanical Strength Developments of Iron-Rich Sulfo-belite Eco-cements

Author: Gema Álvarez-Pinazo, Isabel Santacruz, Laura León-Reina, et al

Publication: Industrial & Engineering Chemistry Research

Publisher: American Chemical Society

Date: Nov 1, 2013

Copyright © 2013, American Chemical Society

LOGIN
If you're a copyright.com user, you can login to RightsLink using your copyright.com credentials. Already a RightsLink user or want to learn more?

PERMISSION/LICENSE IS GRANTED FOR YOUR ORDER AT NO CHARGE

This type of permission/license, instead of the standard Terms & Conditions, is sent to you because no fee is being charged for your order. Please note the following:

- Permission is granted for your request in both print and electronic formats, and translations.
- If figures and/or tables were requested, they may be adapted or used in part.
- Please print this page for your records and send a copy of it to your publisher/graduate school.
- Appropriate credit for the requested material should be given as follows: "Reprinted (adapted) with permission from (COMPLETE REFERENCE CITATION). Copyright (YEAR) American Chemical Society." Insert appropriate information in place of the capitalized words.
- One-time permission is granted only for the use specified in your request. No additional uses are granted (such as derivative works or other editions). For any other uses, please submit a new request.

BACK

CLOSE WINDOW

Copyright © 2015 Copyright Clearance Center, Inc. All Rights Reserved. [Privacy statement](#). [Terms and Conditions](#).
Comments? We would like to hear from you. E-mail us at customercare@copyright.com

Article A#4:

"Ana Cuesta, Gema Álvarez-Pinazo, Marta García-Maté, Isabel Santacruz, Miguel A. G. Aranda, Ángeles G. De la Torre and Laura León-Reina. *"Rietveld quantitative phase analysis with molybdenum radiation"*, Powder Diffraction, Volume 30(1), pp 25-35, (2015)."

Cambridge University Press is pleased to grant non-exclusive permission to reproduce this article in this PhD thesis, for non-commercial publication, in print and electronic format.

Figure 1.9 and 1.10:

6/1/2015 Rightslink® by Copyright Clearance Center

Copyright Clearance Center RightsLink® Home Account Info Help Live Chat



Title: Synthesis and characterization of hydrogarnet
 $\text{Ca}_3(\text{Al}_x\text{Fe}_{1-x})_2(\text{SiO}_4)_y(\text{OH})_4(3-y)$

Author: Belay Zeleke Dilnesa, Barbara Lothenbach, Guillaume Renaudin, Adrian Wichser, Dmitrii Kulik

Publication: Cement and Concrete Research

Publisher: Elsevier

Date: May 2014

Copyright © 2014 Elsevier Ltd. All rights reserved.

Logged in as: Gema Alvarez
 Account #: 3000917257
 LOGOUT

Order Completed

Thank you very much for your order.

This is a License Agreement between Gema Alvarez ("You") and Elsevier ("Elsevier"). The license consists of your order details, the terms and conditions provided by Elsevier, and the [payment terms and conditions](#).

[Get the printable license.](#)

License Number	3640390473727
License date	Jun 01, 2015
Licensed content publisher	Elsevier
Licensed content publication	Cement and Concrete Research
Licensed content title	Synthesis and characterization of hydrogarnet $\text{Ca}_3(\text{Al}_x\text{Fe}_{1-x})_2(\text{SiO}_4)_y(\text{OH})_4(3-y)$
Licensed content author	Belay Zeleke Dilnesa, Barbara Lothenbach, Guillaume Renaudin, Adrian Wichser, Dmitrii Kulik
Licensed content date	May 2014
Licensed content volume number	59
Licensed content issue number	n/a
Number of pages	16
Type of Use	reuse in a thesis/dissertation
Portion	figures/tables/illustrations
Number of figures/tables/illustrations	2
Format	both print and electronic
Are you the author of this Elsevier article?	No
Will you be translating?	No
Original figure numbers	Figure 1 and Figure 2
Title of your thesis/dissertation	Active sulpho-belite cements. Hydration mechanisms and mechanical properties
Expected completion date	Jul 2015
Estimated size (number of pages)	250
Elsevier VAT number	GB 494 6272 12
Permissions price	0.00 EUR
VAT/Local Sales Tax	0.00 EUR / 0.00 GBP
Total	0.00 EUR

ORDER MORE... CLOSE WINDOW

Copyright © 2015 Copyright Clearance Center, Inc. All Rights Reserved. [Privacy statement](#). [Terms and Conditions](#).
 Comments? We would like to hear from you. E-mail us at customer@copyright.com

ANNEX B

OTHER PUBLICATIONS

OTHER PUBLICATIONS

AUTHORS: Santacruz, I.; De la Torre, A.G.; **Álvarez-Pinazo, G.**; Cabeza, A.; Cuesta, A.; Sanz, J.; Aranda, M.A.G.

TITLE: Structure of stratlingite and effect of hydration methodology on microstructure.

REF: *Advances in Cement Research*, accepted. **2015**, in press.

AUTHORS: Pérez-Bravo, R.; **Álvarez-Pinazo, G.**; Compañá, J.M.; Santacruz, I.; Losilla, E.R.; Bruque, S.; De la Torre, A.G.

TITLE: Alite Sulfoaluminate Clinker: Rietveld mineralogical and SEM-EDX analysis.

REF: *Advances in Cement Research*, **2014**, 63, 127-136.

AUTHORS: Cuesta, A.; **Álvarez-Pinazo, G.**; Sanf3lix, S. G.; Peral, I.; Aranda, M.A.G.; De la Torre, A. G.

TITLE: Hydration mechanisms of two polymorphs of synthetic ye'elimité.

REF: *Cement and Concrete Research*, **2014**, 63, 127-136.

AUTHORS: De la Torre, A.G.; Martín-Sedeño, M.C.; León-Reina, L.; Cuberos, A.J.M.; **Álvarez-Pinazo, G.**; Aranda, M.A.G.; Ordonez, L.M.; Gateshki, L.M.

TITLE: Hidratación de cementos de sulfoaluminato de calcio.

REF: *Cemento y Hormigón*, **2011**, nº 942, pp 10-22.

AUTHORS: De la Torre, A.G.; Cuberos, A.J.M.; **Álvarez-Pinazo, G.**, Cuesta, A., Aranda, M.A.G.

TITLE: In-situ powder diffraction study of belite sulfoaluminate clinkering.

REF: *Journal of Synchrotron Radiation*, **2011**, 18, 506-514.

AUTHORS: Martín-Sedeño, M.C.; Cuberos, A.J.M.; De la Torre, A.G.; **Álvarez-Pinazo, G.**; Ordonez, L.M.; Gateshki, M.; Aranda, M.A.G.

TITLE: Aluminum-rich belite sulfoaluminate cements. Clinkerization and early age hydration.

REF: *Cement and Concrete Research*, **2010**, 40, 359-369.

AUTHORS: Cuberos, A.J.M.; De la Torre, A.G.; **Álvarez-Pinazo, G.**; Martín-Sedeño, M.C.; Schollbach, K.; Pöllmann, H.; Aranda, M.A.G.

TITLE: Active iron-rich belite sulfoaluminate cements: Clinkering and Hydration.

REF: *Environmental Science & Technology*, **2010**, 44, 6855-6862.

Annex B

AUTHORS: De la Torre, A.G.; Martín-Sedeño, M.C.; León-Reina, L.; Cuberos, A.J.M.; **Álvarez-Pinazo, G.**; Aranda, M.A.G.; Ordonez, L.M.; Gateshki, L.M.

TITLE: Hidratación de cementos de sulfoaluminato de calcio.

REF: *Actas de VII Colóquios de Directores y Técnicos de Fábricas de Cemento*, ISBN: 978-84-613-5835-9, pp. 227-248, Madrid, **2009**.